

Planetary Science Meets Chemistry: Studying Potential Biosignature Gases in Terrestrial Exoplanet Atmospheres

by

Jingcheng Huang

Bachelor of Science in Chemistry, Tufts University (2017)
Bachelor of Science in Physics, Tufts University (2017)
Bachelor of Science in Mathematics, Tufts University (2017)

Submitted to the Department of Chemistry
in partial fulfillment of the requirements for the degree of

Doctor of Philosophy in Chemistry

at the

MASSACHUSETTS INSTITUTE OF TECHNOLOGY

September 2022

© Massachusetts Institute of Technology 2022. All rights reserved.

Author
Department of Chemistry
August 12, 2022

Certified by
Sara Seager
Department of Earth, Atmospheric and Planetary Sciences
Department of Physics
Department of Aeronautics and Astronautics
Class of 1941 Professor Chair
Thesis Supervisor

Accepted by
Adam Willard
Associate Professor
Graduate Officer

This doctoral thesis has been examined by a committee as follows:

Prof. Adam P. Willard.
Thesis Committee Chair
Associate Professor
Graduate Officer

Prof. Sara Seager
Thesis Supervisor
Department of Earth, Atmospheric and Planetary Sciences
Department of Physics
Department of Aeronautics and Astronautics
Class of 1941 Professor Chair

Prof. Susan Solomon.
Thesis Committee Member
Lee and Geraldine Martin Professor of Environmental Studies
Chair of the Program in Atmospheres, Oceans and Climate

Planetary Science Meets Chemistry: Studying Potential Biosignature Gases in Terrestrial Exoplanet Atmospheres

by

Jingcheng Huang

Submitted to the Department of Chemistry on August 12, 2022, in partial fulfillment of the requirements for the degree of Doctor of Philosophy in Chemistry

Abstract

As more and more exoplanets are discovered, searching for biosignature gases is becoming one of the crucial ways to find extraterrestrial life. Biosignature gases are gases produced by living organisms that can accumulate to detectable levels in the atmosphere. Once detected, it can be attributed to signs of life on the planet. So far, only a few molecules have been studied as potential biosignature gases. A recent paper proposes that we should systematically evaluate All Small Molecules (ASM) as possible biosignature gases. This thesis summarizes my work in identifying and studying three new potential biosignature gases in terrestrial exoplanet atmospheres. In my research, I use various approaches, from simple Henry's law to our comprehensive photochemistry code and transmission spectra model, to study the biosignature potential of ammonia (NH_3) and methanol (CH_3OH). I also developed a simplified chloride steady-state chemical model to examine whether hydrogen chloride (HCl) is a good bioindicator in an H_2 -dominated atmosphere. First, we find that NH_3 in a terrestrial planet's atmosphere is generally a good biosignature gas, primarily because terrestrial planets have no significant known abiotic NH_3 source. NH_3 can accumulate in the atmosphere only if life is a net source of NH_3 and produces enough NH_3 to saturate the surface sinks. Second, we consider CH_3OH a poor biosignature gas in terrestrial exoplanet atmospheres due to the enormous production flux required to reach its detection limit. Although CH_3OH can theoretically accumulate on exoplanets with CO_2 - or N_2 -dominated atmospheres, such planets' small atmospheric scale height and weak atmosphere signals put them out of reach for near-term observations. Finally, albeit HCl has many advantages of being a potential bioindicator, we find it is not a suitable bioindicator because it cannot accumulate to detectable levels on an exoplanet with an H_2 -dominated atmosphere orbiting an M5V dwarf star. The extremely high water solubility of HCl means that wet deposition can efficiently remove it from the atmosphere, preventing HCl from accumulating to detectable levels in the atmosphere. Overall, my thesis aims to improve our understanding of biosignature gases and provide more diverse research methods and a more comprehensive framework for future work.

Keywords: Planetary science, Biosignature gases, Bioindicator, Astrobiology, Atmospheric photochemistry, Exoplanet atmosphere modeling, Planetary habitability, Ammonia, Methanol, Hydrogen chloride

Thesis Supervisor: Sara Seager,
Title: Professor of Planetary Science
Professor of Physics, Professor of Aerospace Engineering
Class of 1941 Professor Chair

Acknowledgments

Being able to study and research at MIT has always been my dream since I was a kid. To this day, I still vividly remember the moment I received the email telling me that I was accepted into the MIT Chemistry Ph.D. program. Five years fly by. Soon I will graduate with a Ph.D. and begin my postdoc research at MIT. Looking back on my time at MIT, I have had the privilege of learning from an extremely talented advisor, working with a group of brilliant team members, and being supported by numerous dedicated administrative staff members and countless caring friends. But most of all, I am incredibly proud to have a family that has always supported me unconditionally and loved me unreservedly. Without all these truly exceptional individuals, my experience at MIT would not have been the same, and I would not have been able to accomplish what I have achieved today.

First and foremost, I would like to thank my Ph.D. advisor, Prof. Sara Seager. Without her guidance and training, I would never have become a qualified MIT Ph.D., let alone a good researcher. I clearly remember the day Prof. Seager told me that I officially became her Ph.D. student, and I will never forget how excited and relieved I was at that time. Before joining Prof. Seager's group, I knew very little about the field of planetary science, and I didn't know how to write good scientific papers. Since I became her student, Prof. Seager has patiently taught me how to write short and sweet papers, how to communicate effectively with colleagues and others in the scientific community, and most importantly, how to be an independent researcher. Prof. Seager often tells me that transitioning from a student to a researcher is like breaking a cocoon into a butterfly: a slow, painful and difficult process. Today I can proudly say that I have finally become the researcher she always wants me to be. From a rookie to a qualified MIT Ph.D., from a novice writer to being able to write a paper accepted by a journal without revision, all these changes are possible because I have such a good advisor as Prof. Seager. I am incredibly fortunate to be able to stay in Prof. Seager's group after I graduate and continue doing research as a postdoc. I look forward to making more contributions to planetary science with Prof. Seager in the foreseeable future.

I would like to thank my thesis committee members: Prof. Adam P. Willard and Prof. Susan Solomon, for giving thoughtful advice on my thesis and always inspiring me to go above and beyond. My thesis would not have been possible without their guidance.

I would like to thank the current and former members of the Seager Group with whom I have had the privilege of working. First of all, thanks to Janusz J. Petkowski. Whenever I encounter a problem with research or writing a paper, Janusz can always put forward his unique insights and give me valuable suggestions. Janusz's expertise in biochemistry and astrobiology always brings new insights into my research. It has been a great pleasure to work with Janusz. Thanks to Sukrit Ranjan for sharing his expertise in photochemistry and atmosphere modeling. Not only does he help me with photochemical code issues, but he also teaches me how to solve similar problems myself. I wouldn't be proficient in photochemical modeling without his help. Thanks to Zhuchang Zhan for his contributions to simulated spectra and molecular distinguishability. Zhuchang's expertise in programming is impressive. Zhuchang's SEAS code has become an essential part of our biosignature gas research. Thanks to Ana Glidden for her insights into atmospheric modeling. Whenever I discuss photochemistry code with Ana, I can always learn something new. Ana's attention

to detail in her papers is also very admiring. Thanks to Zifan Lin for supporting my research. I wish him success in his research on planetary interior and planets orbiting white dwarfs. I look forward to more cooperation opportunities with Zifan in the future. Thanks to Mihkel Pajusalu for his expertise in biochemistry experiments, image/video processing, and machine learning. Mihkel is a true experimentalist and a great engineer. Thanks to his dedication and hard work, our laboratory studies on the viability of life in H₂-dominated exoplanet atmospheres can be completed and published in Nature Astronomy. I would like to thank all my friends from the Seager Group, MIT, and beyond: Ziwei Li, Prajwal Niraula, William Bains, Daniel Koll, Maximilian N. Gunther, Tom Evans, Tansu Dylan, Mariona Badenas Agusti, Zahra Essack, Tajana Marie Schneiderman, Steven Smriga, Susan Mullen, Martin Wolf, Yuchen Sun, Michelle Kunimoto, Gen Li, Mengshan Ye, Benjamin Rackham, Artem Burdanov, Sammy Hasler, Peidong Wang, and many, many more. Thanks to their company and support, my life at MIT has been very enjoyable.

I would like to thank MIT Department of Chemistry and MIT Department of Earth, Atmospheric, and Planetary Sciences (EAPS). During my Ph.D. at MIT, I have had the privilege of learning from some outstanding faculties. I would like to thank Prof. Benjamin Weiss, Prof. Julien de Wit, Prof. Jack Wisdom, Prof. Ronald G. Prinn, Prof. Bin Zhang, Prof. Tyler Jacks, and Prof. Matt Vander Heiden. I have learned a lot from their classes. I would like to thank Prof. Andrew Babbin and Prof. Daniel Cziczo for their help with my experimental research. I would like to thank Nobel Laureate Prof. Richard Royce Schrock for letting me be his TA for his undergraduate chemistry class. I would like to thank Roberta Allard, Kayla Bauer, Megan Jordan, and Brandon Milardo for their excellent administrative work. I would like to thank all the staff members in the Chemistry Education Office and the EAPS Education Office. I especially want to thank Dr. Jennifer Weisman. Whenever I have a policy-related question, she always answers me right away. She can always give me constructive suggestions when I need her help. I would like to thank MIT Division of Student Life Office. I would like to thank MIT International Students Office for supporting our international students.

I would like to thank my undergraduate alma mater Tufts University for educating and nurturing me. I would like to thank Tufts president Anthony P. Monaco. I am so grateful that he has wished me a happy birthday every year for the past eight years. Every Halloween, I go to his house in Tufts and play trick or treat. I would also like to thank my three undergraduate advisors: Prof. Hugh Gallagher, Prof. Samuel Kounaves, and Prof. Bruce Boghosian. They make me passionate about science and dare to explore the unknown.

I would like to thank all my friends in Boston. I especially would like to thank Gabi Zambrano, Brigida Zambrano, and Emilia Iacono-Zambrano. Since I came to Boston about nine years ago, they have taken great care of me. They have added so much joy and happiness to my life in Boston. Because of them, Boston has become my second home. As I promised Gabi, I won't stop doing planetary science research until I find signs of life on other planets. In addition, I would like to thank Giorgio Di Costanzo's family, Giovanni Di Costanzo's family, Francisco Mauro Di Costanzo's family, Mario Di Costanzo's family, Silvano Di Costanzo's family, and many others, for taking care of me for so many years. I would also like to thank all my friends in Texas, New York, North Carolina, California, and the rest of the United States. Thank you all!

Most importantly, I would like to thank all of my family. I am very grateful to my parents, Xincan Huang and Ling Chen, and my grandparents. They have always supported me unconditionally in pursuit of my scientific dreams. The seeds of science they sowed in my childhood are now taking root. Their unreserved love, constant encouragement, and selfless devotion have made me who I am today. My family is my greatest motivator and warmest harbor, and I couldn't be more proud of them. My parents named me 'Jingcheng', which means 'where there's a will, there's a way' in Chinese. I will always remember their expectations of me and live up to my name.

Finally, I would like to conclude this acknowledgment section with my motto, a famous quote from Ralph Waldo Emerson: 'Do not go where the path may lead; go instead where there is no path and leave a trail.'

Table of Contents

Title page	1
Committee signature page	2
Abstract	4
Acknowledgments	6
1. Introduction	14
1.1 Introduction to exoplanets	14
1.2 Introduction to Biosignature Gases	16
1.3 The Motivations for My Research	17
1.4 Thesis Overview	18
2. Methods	22
2.1 Solubility and Henry's law	22
2.2 Simplified Chlorine Steady-state Chemical Model	24
2.3 In-depth Introduction to Our Photochemistry Model	27
3. Project I: Assessment of Ammonia as a Biosignature Gas in Exoplanet Atmospheres (Published in Astrobiology; https://doi.org/10.1089/ast.2020.2358)	35
Abstract	35
3.1 Introduction	35
3.2 Ammonia Sources and Sinks	36
3.2.1 Ammonia Sources on Earth	36
3.2.1.1 Anthropogenic NH ₃ Production	37
3.2.1.2 Biological NH ₃ Production	38
3.2.1.3 Minor NH ₃ Abiotic Sources	40
3.2.2 Ammonia Sinks on Earth	41
3.2.2.1 NH ₃ Atmospheric Sinks	42
3.2.2.2 NH ₃ Biological Sinks	43
3.3. Methods	43
3.3.1 Solubility and Henry's law	44
3.3.2 Ocean-NH ₃ Interaction Model	44
3.3.3 Photochemistry Model	45
3.3.4 Transmission Spectra Model and Simulated Observation	46
3.3.4.1 Simulated Exoplanet Atmosphere Spectra Model (SEAS)	46
3.3.4.2 Simulated Exoplanet Observation	47
3.3.4.3 Detection Assessment Metrics	48
3.4. Results	48
3.4.1 NH ₃ 's High Water Solubility Limits its Ability to Accumulate in the Atmosphere	49
3.4.2 NH ₃ Can Accumulate if Life Produces Enough NH ₃ to Saturate the Surface	49
3.4.3 Detectability of NH ₃ in Transmission Spectra	51

3.4.4 Variability of NH ₃ Atmospheric Accumulation in Various Planetary Scenarios	54
3.4.4.1 Conditions Required for NH ₃ to Accumulate with a Reasonable Surface Production Flux	54
3.4.4.2 Effects of NH ₃ Surface Deposition on Atmospheric NH ₃ Mixing Ratio	55
3.5. Discussion	57
3.5.1 Ammonia's High Water Solubility Compared to Other Atmospheric Gases	57
3.5.2 Horizontal Atmospheric Transport Limits NH ₃ Accumulation above Land	58
3.5.3 Implausibility of NH ₃ Formation by Lightning	59
3.5.4 Plausible Ocean-related Sinks of NH ₃ and NH ₄ ⁺	60
3.5.5 Volatile Amines are Good Biosignature Gases by Proxy with NH ₃	61
3.5.6 IR Absorbance Spectra of Amines	61
3.5.7 NH ₃ -Induced Hazes	62
3.5.8 NH ₃ as a greenhouse gas	63
3.5.9 NH ₃ Detectability with Future Telescopes	63
3.5.10 NH ₃ in Mini-Neptunes	64
3.6. Summary	64
Appendix A. Simulation Parameters for the Photochemistry Model	65
Appendix B. Dissociation Constants of Representative Amines at 25°C	73
Appendix C. Reaction Rates Between Life Produced Volatile Amines and O, OH Radicals	73
Appendix D. IR Spectra of Primary, Secondary and Tertiary Amines	74
Appendix E. NH ₃ Removal Rate in the Photochemistry Model	77
Appendix F. Photochemistry Model Sensitivity Tests	77
Appendix G. NH ₃ Condensation in the Atmosphere	80
Appendix H. NH ₃ Abiotic False-Positive Analysis	81
Appendix I. Detectability of TRAPPIST-1 Planets with JWST	82
4. Project II: Methanol - a Poor Biosignature Gas in Exoplanet Atmospheres (Published in The Astrophysical Journal; https://doi.org/10.3847/1538-4357/ac6f60)	84
Abstract	84
4.1 Introduction	84
4.2 CH ₃ OH Emission and Production Mechanisms	85
4.2.1 Earth's Atmospheric CH ₃ OH Concentrations and Lifetime	85
4.2.2 CH ₃ OH Production Flux on Earth	87
4.2.3 Biological CH ₃ OH Production	89
4.2.4 Minor CH ₃ OH Sources on Earth	90
4.3. CH ₃ OH Removal Mechanisms	91
4.3.1 CH ₃ OH Atmospheric Sinks	91
4.3.2 CH ₃ OH Deposition to Land and Ocean Uptake	93
4.4. Methods	94
4.4.1 Photochemistry Model	95
4.4.2 Transmission Spectra model and Simulated Observation	95
4.5 Results	96
4.5.1 Accumulation of CH ₃ OH on Exoplanets with H ₂ -dominated Atmospheres	97
4.5.2 The Detectability of CH ₃ OH with James Webb Space Telescope	102
4.6. Discussion	105

4.6.1 Alcohols' Solubility in Water	105
4.6.2 CH ₃ OH as an Antifreeze	106
4.6.3 CH ₃ OH on Exoplanets with CO ₂ - or N ₂ -dominated Atmospheres Orbiting M Dwarfs	107
4.6.4 Volatility of Alcohols and its Impact on Alcohols' Biosignature Potential	108
4.6.5 CH ₃ OH and Atmospheric Hazes	109
4.6.6 Plausibility of High Bioproduction Fluxes	110
4.7. Summary	110
Appendix J. Photochemical Simulation Parameters	112
5. Project III: Assessment of Hydrogen Chloride as a Bioindicator on Exoplanets with H ₂ -dominated Atmospheres	119
5.1 Introduction	119
5.2 The Abundance, Distribution, and Circulation of Chlorine on Earth	120
5.2.1 Abundance and Distribution of Chlorine on Earth	120
5.2.2 Overview of Earth's Natural Chlorine Cycle	124
5.3 Methods	128
5.3.1 Simplified Chlorine Steady-State Chemical Model	128
5.3.2 Photochemistry Model - Chlorine Chemical Network	129
5.4 Results	129
5.5 Discussion	134
5.5.1 Solubility of Chlorine-containing Gas Molecules	134
5.5.2 Acidity of Chlorine-containing Acids	135
5.5.3 Naturally Occurring Chloride Minerals	136
5.6 Summary	137
Appendix K. Chlorine Chemical Reaction Network for the Photochemistry Model	138
6. Summary and future work	144
List of Figures	152
List of Tables	155
Bibliography	158

Chapter 1

Introduction

Ever since humanity learned to look up at the stars in the sky, people have wondered if we are alone in this universe. Is there life similar to ours on other planets? Are there habitable planets other than Earth in our solar system or Milky Way? These questions, perhaps as old as human civilization itself, have been motivating people to create new tools and models to study the universe: from Nicolaus Copernicus put forward his heliocentric theory in 1543, ushering into the modern age of astronomy, to Johannes Kepler proposed his Kepler's laws of planetary motion in 1609, giving people a simple mathematical model to describe the motion of celestial bodies; from Galileo Galilei discovered the four moons of Jupiter in 1610 with his homemade telescope, confirming the existence of moons that orbit other planets, to Edwin Hubble discovered that the universe was expanding, revolutionizing modern astronomy and astrophysics. All these advancements not only give people a relatively comprehensive view of our universe but also bring people closer to being able to answer these millennia-old questions. Perhaps, one of the most impactful breakthroughs of the past few decades was the discovery in 1995 of a Jupiter-mass exoplanet orbiting a main-sequence star (51 Pegasi) by two astronomers, Michel Mayor and Didier Queloz. Their discovery marked the birth of an entirely new field of study, 'exoplanet research.' In this chapter, I first briefly describe what exoplanets are and how we can discover them (Chapter 1.1). I then introduce biosignature gases in Chapter 1.2. I discuss the motivations for my research in Chapter 1.3. Finally, I provide a general overview (i.e., outline) of my thesis in Chapter 1.4.

1.1 Introduction to exoplanets

Exoplanets, sometimes referred to as 'extrasolar planets,' are planets that orbit stars outside the solar system. Over the past decade, hundreds of new exoplanets have been discovered every year, thanks to advances in telescope technology. As of July 2022, the number of exoplanets confirmed by NASA exceeds 5,000. Exoplanets come in different sizes, and we can roughly group them into four categories. Terrestrial planets are rocky exoplanets with Earth-like masses and possibly iron-rich cores. Super-Earths, as the name suggests, are much more massive than Earth but smaller than Uranus or Neptune. Neptune-like exoplanets typically have thick H₂/He-dominated atmospheres similar to Neptune's and may have liquid oceans and ice deep in the atmospheres. We refer to those Neptune-like planets less massive than Neptune as 'mini-Neptunes.' Finally, gas giants are gas-dominated planets with a size similar to or much larger than Saturn or Jupiter. We call those gas giants that orbit very close to their stars, have short orbital periods, and have scorching surfaces 'hot Jupiters.' I summarize the characteristics of each type of exoplanet in the table below (Table 1-1). Data is collected from the NASA Exoplanet Archive.

Table 1-1. Different types of exoplanets and their respective characteristics.

	Size	Example	Note
Terrestrial	Between 0.5 and	TRAPPIST-1e	Bulk composition dominated by silicate

	Size	Example	Note
exoplanets	$2 R_{\text{Earth}}$		and/or carbon
Super-Earths	Between 2 and $10 R_{\text{Earth}}$	Kepler-186f	Can be very strange (e.g., water worlds, snowball planets)
Neptune-like exoplanets	Similar in size to Neptune	GJ 436 b	Typically have thick H ₂ /He-dominated atmospheres
Gas giants	Similar to or larger than Jupiter	Kepler-7b	Easy to detect using the radial velocity method

In general, there are four techniques we can use to find and study exoplanets: the transit method, the radial velocity method, microlensing, and direct imaging. The transit method is the most commonly used technique in our research. In recent years, more and more exoplanets have been discovered through the transit method. A transit occurs whenever an exoplanet passes in front of its host star. During transit, some of the light from the star is absorbed by the exoplanet's atmosphere, giving us clues about the atmosphere's chemical compositions and the planet's habitability. I summarize the advantages and disadvantages of each detection method in the table below (Table 1-2).

Table 1-2. Advantages and disadvantages of each detection method.

[1]. The transit method	
Pro 1	Can help us constrain the size of the exoplanet
Pro 2	Combined with the radial velocity method, we can estimate the planet's average density and composition.
Pro 3	We can study the exoplanet's atmosphere through transmission spectroscopy.
Con 1	Sensitive to planet size: the smaller the planet, the smaller the transit depth
Con 2	Exoplanet's orbit must be aligned with the observer's line of sight (i.e., sensitive to orbital inclination)
[2]. The radial velocity method	
Pro 1	Can help us constrain the mass of the exoplanet (i.e., minimum mass)
Pro 2	Good at detecting planets around low-mass stars (such as M dwarfs)
Con 1	This method does not work on planets with highly inclined orbits
[3]. Microlensing	
Pro 1	Can detect planets far from their host stars (i.e., planets with large semi-major axis)
Con 1	Since microlensing events are rare, repeated observations are virtually impossible.
[4]. Direct imaging	
Pro 1	The only method astronomers can directly 'see' the exoplanets
Pro 2	Can detect exoplanets with an orbital inclination of 90 degrees (i.e., face-on)
Con 1	This method doesn't work well when the planet is small (e.g., a terrestrial planet) or when the planet orbits close to its star.

1.2 Introduction to Biosignature Gases

Looking for biosignature gases is becoming one of the most promising methods of studying planetary habitability. Biosignature gases are gases produced by living organisms that can accumulate to detectable levels in the atmosphere. Once detected, it can be attributed to signs of life on the planet. A biosignature gas can be a by-product or a final product of biochemical metabolism. For a chemical to be a good biosignature gas, it must be detectable (i.e., it must be able to accumulate in the atmosphere) and distinguishable (i.e., we can distinguish it from other gases). So far, only a few molecules have been studied as potential biosignature gases. The most famous example has to be O₂ (e.g., Jeans, 1930; Meadows et al., 2018). Other biosignature gas candidates studied include methane (CH₄) (Leger et al., 1996; Des Marais et al., 2002; Kaltenecker et al., 2007; Dlugokencky et al., 2011), methyl chloride (CH₃Cl) (Segura et al., 2005), nitrous oxide (N₂O) (Des Marais et al., 2002; Segura et al., 2005; Tian et al., 2015; Rugheimer et al., 2018), methanethiol (CH₃SH) (Domagal-Goldman et al. 2011), DMS ((CH₃)₂S) (Domagal-Goldman et al., 2011; Seager et al., 2012; Arney et al., 2018), among others. I have listed some biosignature gases and their associated information in the table below (Table 1-3).

Table 1-3. Some biosignature gases that people have studied.

Oxygen (O ₂)	
Biological source	Photosynthesis
Abiotic sources	Can be produced by photolysis of H ₂ O and CO ₂
Related references	Jeans, 1930; Meadows et al., 2018
Methane (CH ₄)	
Biological source	Methanogenesis (a type of anaerobic respiration that reduces CO ₂ to CH ₄)
Abiotic sources	Geothermal; Outgassing of CH ₄ accumulated from planet formation
Related references	Kaltenecker et al., 2007; Dlugokencky et al., 2011
Nitrous oxide (N ₂ O)	
Biological source	Denitrification (A microbial process that reduces nitrate and nitrite to N ₂ O (or sometimes N ₂))
Abiotic sources	Chemodenitrification (the abiotic reaction between nitrite (NO ₂ ⁻) and Fe(II))
Related references	Tian et al., 2015; Rugheimer et al., 2018
Methanethiol (CH ₃ SH)	
Biological source	Most likely microbes
Abiotic sources	No known significant abiotic sources
Related references	Domagal-Goldman et al. 2011
Dimethyl sulfide DMS ((CH ₃) ₂ S)	
Biological source	Phytoplankton
Abiotic sources	No known significant abiotic sources

Related references	Seager et al., 2012; Arney et al., 2018
Methyl chloride CH ₃ Cl	
Biological source	Marine plants (e.g., seaweeds and phytoplankton), unicellular marine eukaryotes and tropical plants
Abiotic sources	No known significant abiotic sources
Related references	Segura et al., 2005

In a recent paper published by our group (Seager et al., 2016), we propose that we should systematically evaluate All Small Molecules (ASM) as possible biosignature gases. Of the millions of organisms living on Earth, only a tiny fraction has been studied for their production of gases. There are many more biologically produced gases yet to be identified and studied. Life on other planets may have different biochemistry than life on Earth and thus could produce a completely different set of chemicals than life on Earth. Inspired by this idea, in recent years, our group has studied some new and even exotic biosignature gases, such as phosphine (PH₃) (Sousa-Silva et al., 2020), isoprene (C₅H₈) (Zhan et al., 2021), and ammonia (NH₃) (Huang et al., 2022), to name a few (Table 1-4).

Table 1-4. Phosphine, isoprene, and ammonia as biosignature gases.

Phosphine (PH ₃)	
Biological source	Likely associated with anaerobic microbial processes
Abiotic sources	No known significant abiotic sources
Related references	Sousa-Silva et al., 2020; Greaves et al., 2020
Isoprene (C ₅ H ₈)	
Biological source	Almost the entire biosphere (plants, animals, bacteria)
Abiotic sources	No known significant abiotic sources
Related references	Zhan et al., 2021
Ammonia (NH ₃)	
Biological source	Biological nitrogen fixation by diazotrophic bacteria and Archaea; Bacterial and fungal ammonification of animal waste; Dissimilatory nitrate reduction to ammonium by prokaryotes
Abiotic sources	Volcanic eruptions; photochemically produced on iron-doped TiO ₂ containing sands (very minor); Lightning (very minor)
Related references	Seager et al., 2013; Huang et al., 2022

1.3 The Motivations for My Research

This thesis summarizes my work in identifying and characterizing potential biosignature gases. In my research, I use a variety of approaches, ranging from simple Henry's law to our comprehensive photochemistry code and transmission spectra model, to study the biosignature potential of ammonia (NH₃), methanol (CH₃OH), and hydrogen chloride (HCl).

I am motivated to study the biosignature potential of NH_3 since NH_3 plays a significant role in biochemistry. Due to its high bio-usability, plants and various microorganisms can easily absorb NH_3 . NH_3 is an ideal nitrogen source for life on Earth since it can be integrated into various amino acids and other organic molecules without life having to break the strong N_2 triple bond. Additionally, some life can use NH_3 as an energy source by oxidizing NH_3 . Furthermore, NH_3 stands out from all the previously studied biosignature gases because NH_3 has a very high solubility in water. NH_3 's high water solubility means the atmospheric accumulation of NH_3 is highly dependent on planetary conditions such as whether life produces a substantial amount of NH_3 and whether there are active NH_3 -removal sinks on the surface (including land and ocean). If life does not produce enough NH_3 to saturate the surface sinks, rain can much more efficiently remove NH_3 from the atmosphere than other atmospheric gases.

Atmospheric methanol (CH_3OH) is another exciting biosignature gas candidate I would like to study. CH_3OH is an important precursor molecule for life's biochemistry, as it is the building block of a diverse set of biochemicals such as acetic acid, methylamines, and methyl esters, to name a few. In the atmosphere, CH_3OH is a significant source of formaldehyde (CH_2O) and carbon monoxide (CO) (Tie et al., 2003; Solomon et al., 2005; Millet et al., 2008; Hu et al., 2011). CH_3OH stands out from other biosignature gas candidates because there is no significant known abiotic CH_3OH source on terrestrial planets. Furthermore, due to CH_3OH 's high water solubility, the limited amount of abiotic CH_3OH produced can be easily removed by rain, making it extremely difficult to accumulate. As a result, only when life generates a substantial amount of CH_3OH can it reach detectable levels in the atmosphere. People have not thoroughly studied CH_3OH as a biosignature gas before.

In the atmosphere, some biosignature gases do not survive photochemical destruction. These biosignature gases themselves cannot accumulate to detectable levels in the atmosphere. We can only infer the presence of biosignature gases by detecting their photochemical products. We refer to the final products of the chemical reactions of biosignature gases as bioindicators (Seager et al., 2013). I am motivated to study hydrogen chloride (HCl) for its many advantages as a bioindicator in H_2 -dominated atmospheres. In highly reducing atmospheres, many gases are converted to their most hydrogenated (i.e., reduced) form: dimethyl sulfide (DMS) will be turned into H_2S and CH_4 ; N_2O will be turned into H_2O and N_2 (Seager et al., 2013). Since the most reduced form of Cl element is HCl , atmospheric methyl chloride (CH_3Cl) and chlorine (Cl_2) gas will end up as HCl in H_2 -dominated atmospheres. In addition, there are very few abiotic sources of HCl , the only exception being volcanic activity. The high water solubility of HCl means that only when life converts enough non-volatile forms of Cl into HCl gas can HCl accumulate in the atmosphere to detectable levels. (Seager et al., 2013) very briefly mentions HCl as a potential bioindicator. In this work, I will take a closer look at the bioindicator potential of HCl .

1.4 Thesis Overview

My thesis aims not only to improve our understanding of biosignature/bioindicator gases,

but also to provide a more robust photochemical model and a more comprehensive framework for future work. In chapter 2, I describe in detail the various research methods I use in my research. In Chapter 2.1, I review the solubility of chemicals in water and introduce Henry's equation and Henry's law constant. I then briefly describe how Henry's law constants change with the temperature (the van't Hoff equation). In Chapter 2.2, I detail my simplified chloride steady-state chemical model. I start by describing why I develop this model. Then I compare the strengths and weaknesses of my simplified chloride steady-state chemical model compared to our full-fledged photochemistry code. I go on to describe the basic assumptions and ideas behind my model. Next, I thoroughly discuss several essential formulas in my simplified chloride steady-state chemical model and how I used these formulas to estimate chemical species' rainout and photolysis flux. In Chapter 2.3, I introduced our photochemical code, including how it differs from other open source simulation models and how we can use this valuable tool in planetary science research.

In Chapter 3, I present my work in accessing NH_3 as a biosignature gas in exoplanet atmospheres. To examine the biosignature potential of NH_3 , I first need to review how NH_3 is produced and destroyed on Earth. Therefore, I present in Chapter 3.2 the known production pathways and possible removal mechanisms of NH_3 on Earth. In Chapter 3.3, I introduce the various methods I used in this project, including solubility and Henry's law (Chapter 3.3.1), my ocean- NH_3 Interaction Model (Chapter 3.3.2), the photochemistry Model (Chapter 3.3.3), and our group's transmission spectra model (Chapter 3.3.4). I present our results in Chapter 3.4. In Chapter 3.5, I first compare NH_3 's solubility in water with other atmospheric gases (Chapter 3.5.1). Next, I discuss how horizontal atmospheric transport might limit NH_3 accumulation above land (Chapter 3.5.2). I also discuss other minor sources and sinks of ammonia, including NH_3 production by lightning (Chapter 3.5.3) and additional ocean-related sinks for dissolved NH_3 and NH_4^+ ions (Chapter 3.5.4). I discuss amines viability as biosignature gases by proxy with NH_3 (Chapter 3.5.4 and Chapter 3.5.6). Additionally, I briefly discuss NH_3 -induced hazes (Chapter 3.5.7), NH_3 's greenhouse effect (Chapter 3.5.8), and NH_3 detectability with future telescopes (Chapter 3.5.9). I end the discussion with a brief comparison of the significance of atmospheric NH_3 in mini-Neptunes vs. super-Earths (Chapter 3.5.10).

In Chapter 4, I present my work in exploring the biosignature potential of methanol (CH_3OH). Similar to Chapter 3, I first discuss CH_3OH sources and CH_3OH removal mechanisms. For CH_3OH emission and production mechanisms, I first discuss Earth's atmospheric CH_3OH concentrations and lifetime in Chapter 4.2.1. Then I review the CH_3OH production flux on Earth in Chapter 4.2.2. Next, I discuss biological CH_3OH production in Chapter 4.2.3 and minor CH_3OH sources on Earth in Chapter 4.2.4. For CH_3OH removal mechanisms: I look into CH_3OH atmospheric sinks in Chapter 4.3.1. We then explore CH_3OH 's deposition to land and ocean uptake in Chapter 4.3.2. I briefly describe the research methods I used in this project in Chapter 4.4. Next, I present our results in Chapter 4.5. Specifically, I discuss the possibility of accumulation of CH_3OH on exoplanets with H_2 -dominated atmospheres and the flux required to reach its detection level in the atmosphere. I also show that CH_3OH can experience a phenomenon called 'photochemical runaway' (Ranjan et al., 2022), albeit the condition is very stringent (Chapter 4.5.1). In Chapter 4.6, I first review alcohols' solubility in water (Chapter 4.6.1). I then examine the antifreeze properties of CH_3OH in Chapter 4.6.2. Next, I briefly discuss

CH₃OH as a biosignature gas on exoplanets with CO₂- and N₂-dominated atmospheres in Chapter 4.6.3. Additionally, in Chapter 4.6.4, I explore how volatility impacts the biosignature potential of alcohols. I comment on CH₃OH and atmospheric hazes in Chapter 4.6.5. Finally, I discuss the plausibility of high bioproduction fluxes in Chapter 4.6.6.

In chapter 5, I study whether hydrogen chloride (HCl) is a suitable bioindicator on exoplanets with H₂-dominated atmospheres. I provide a comprehensive literature review on chlorine's abundance, distribution, and circulation on Earth (Chapter 5.2). Of the 94 naturally-occurring elements, chlorine ranks in the top 20 in terms of abundance (Graedel et al., 1996; Öberg 2002; Sharp et al., 2013; Atashgahi et al., 2018; Svensson et al., 2021). However, chlorine is not evenly distributed on Earth but concentrated in its three major reservoirs: the mantle, the crust, and the ocean (Graedel et al., 1996; Sharp et al., 2013; Svensson et al., 2021) (Chapter 5.2.1). In Chapter 5.2.2, I go into detail about the natural transfer of chlorine between different reservoirs. I briefly mention my research methods in Chapter 5.3. In Chapter 5.4, I thoroughly discuss the results of my simplified chloride steady-state chemical model. Specifically, I explain in detail how I came to my conclusion, the approximations I made throughout my calculations, and how these approximations affect my calculations and overall conclusion (Chapter 5.4). In Chapter 5.5, I first review the solubility of chlorine-containing gas molecules (Chapter 5.5.1). I then discuss the acidity of chlorine-containing acids in Chapter 5.5.2. Finally, I explore naturally occurring chloride minerals and their properties in Chapter 5.5.3. Finally, I summarize the main conclusions of my thesis and discuss possible future work in Chapter 6.

Chapter 2

Methods

In this chapter, I will comprehensively review the various methods I have used in my research. Specifically, I will focus on the following three methods: Henry's law equation and Henry's law constants (Chapter 2.1), my simplified chlorine steady-state chemical model (Chapter 2.2), and our comprehensive photochemistry model (Chapter 2.3). Note that each of my three main chapters (Chapter 3, Chapter 4, and Chapter 5) also has its method section, where I briefly describe the methods I used in each project. Therefore, some of the content in this chapter will be repeated in subsequent chapters.

2.1 Solubility and Henry's law

In our study, we find that the solubility of a chemical species can profoundly affect whether it can accumulate in the atmosphere. Specifically, suppose a molecule has very high water solubility. In that case, this molecule can easily dissolve in cloud droplets and rainwater and fall back to the ground, making it difficult to accumulate to detectable levels in the atmosphere. Conversely, if a molecule has low water solubility, it will be difficult to remove the molecule from the atmosphere by rainout (i.e., wet deposition) alone.

We usually use Henry's law to describe the solubility of a substance. Henry's law was developed by the English chemist William Henry in the early 19th century to describe the amount of gas that can be absorbed by water. After research, he found that the amount of gas that can be dissolved in water is proportional to its (partial) pressure above the liquid, and the proportionality constant is Henry's law constant. We want to point out that, in reality, the amount of gas that can be dissolved in water is not only proportional to Henry's law constant but also related to some other factors, such as the ionic strength of the solution (i.e., the presence of other substances in the water), and temperature (which we'll get to later). Currently, many excellent review papers go into great detail about Henry's law and Henry's law constant (e.g., Mills et al., 1993; Gamsjäger et al., 2008; R. Sander, 2015; Gamsjäger et al., 2010). We recommend reading these papers if you want to know more details. Here in this section, I'll briefly address some key points.

There are many types (i.e., variants) of Henry's law constants, the most common and simplest of which is the physical Henry's law constant (also referred to as 'intrinsic Henry's law constant'). The physical Henry's law constant can be expressed as the ratio of the concentration of a substance in a solution to its partial pressure above the liquid.

$$H_{(X)}^{CP} = \frac{C_{(X)}}{P} \quad \text{Eq. 2-1}$$

Here $H_{(X)}^{CP}$ is Henry's law constant for a species X in $\text{mol Pa}^{-1}\text{m}^{-3}$. P is the partial pressure of that species in Pascal, and $C_{(X)}$ is the dissolved concentration (in mol m^{-3}) under the equilibrium condition. The larger H^{CP} , the more soluble the species is. In addition to being defined by the concentration of a substance (unit: $\text{mol Pa}^{-1}\text{m}^{-3}$), Henry's law constant can

also be defined by other quantities: for example, by the molality of a substance (unit: mol Pa⁻¹ kg⁻¹), or by the aqueous-phase mixing (i.e., mass) ratio (unit: Pa⁻¹). For unit conversions between variants of Henry's law constants, please see (R. Sander, 2015).

As the simplest method, in our research, we often compare Henry's law constants of the biosignature gas candidates we want to study with those of some common atmospheric gases. In this way, we can intuitively feel the impact of wet deposition on the biosignature gas and make preliminary predictions about whether it can accumulate in the atmosphere. Here, we compare the solubility of 30 molecules at 1 atm and 298 K (Table 2-1). The list includes 11 atmospheric gases, 4 studied biosignature gases, 5 representative amines, 4 representative alcohols, and 6 Cl-containing molecules. We collected the data from (R. Sander, 2015).

Table 2-1. Henry's law constants for some representative gases in water (R. Sander, 2015).

	Chemical	H ^{cp} [mol/(m ³ Pa)]	H ^{cp} (+)	H ^{cp} (-)
1	Tetrafluoromethane CF ₄	2.10×10 ⁻⁶	0.00×10 ⁰	0.00×10 ⁰
2	Helium He	3.83×10 ⁻⁶	6.67×10 ⁻⁸	3.33×10 ⁻⁸
3	nitrogen N ₂	6.43×10 ⁻⁶	6.67×10 ⁻⁸	3.33×10 ⁻⁸
4	hydrogen H ₂	7.75×10 ⁻⁶	5.00×10 ⁻⁸	5.00×10 ⁻⁸
5	Oxygen O ₂	1.30×10 ⁻⁵	0.00×10 ⁰	0.00×10 ⁰
6	methane CH ₄	1.41×10 ⁻⁵	8.57×10 ⁻⁷	1.43×10 ⁻⁷
7	Ethylene C ₂ H ₄	4.92×10 ⁻⁵	9.80×10 ⁻⁶	1.42×10 ⁻⁵
8	Phosphine PH ₃	7.00×10 ⁻⁵	1.10×10 ⁻⁵	1.10×10 ⁻⁵
9	Nitrogen dioxide NO ₂	1.20×10 ⁻⁴	2.03×10 ⁻⁵	2.08×10 ⁻⁵
10	Isoprene C ₅ H ₈	1.53×10 ⁻⁴	1.37×10 ⁻⁴	2.29×10 ⁻⁵
11	Nitrous oxide N ₂ O	2.40×10 ⁻⁴	0.00×10 ⁰	0.00×10 ⁰
12	Carbon dioxide CO ₂	3.36×10 ⁻⁴	4.44×10 ⁻⁶	5.56×10 ⁻⁶
13	Carbon tetrachloride CCl ₄	3.44×10 ⁻⁴	1.60×10 ⁻⁵	4.00×10 ⁻⁶
14	Acetylene C ₂ H ₂	4.10×10 ⁻⁴	0.00×10 ⁰	0.00×10 ⁰
15	Chlorine Cl ₂	9.20×10 ⁻⁴	0.00×10 ⁰	0.00×10 ⁰
16	Methyl chloride CH ₃ Cl	1.15×10 ⁻³	1.50×10 ⁻⁴	1.50×10 ⁻⁴
17	Chloroform CHCl ₃	2.52×10 ⁻³	8.00×10 ⁻⁵	2.00×10 ⁻⁵
18	Methylene chloride CH ₂ Cl ₂	3.66×10 ⁻³	2.40×10 ⁻⁴	6.00×10 ⁻⁵
19	Dimethyl sulfide CH ₃ SCH ₃	5.34×10 ⁻³	2.60×10 ⁻⁴	1.40×10 ⁻⁴
20	Sulfur dioxide SO ₂	1.27×10 ⁻²	1.33×10 ⁻³	6.67×10 ⁻⁴
21	1-butylamine C ₄ H ₉ NH ₂	4.41×10 ⁻¹	2.09×10 ⁻¹	2.21×10 ⁻¹
22	1-propylamine C ₃ H ₇ NH ₂	5.56×10 ⁻¹	2.24×10 ⁻¹	1.96×10 ⁻¹
23	Ethanamine C ₂ H ₅ NH ₂	5.80×10 ⁻¹	4.10×10 ⁻¹	2.80×10 ⁻¹
24	Ammonia NH ₃	5.90×10 ⁻¹	1.00×10 ⁻²	1.00×10 ⁻²
25	Methylamine CH ₃ NH ₂	6.00×10 ⁻¹	2.90×10 ⁻¹	2.50×10 ⁻¹
26	1-butanol C ₄ H ₉ OH	1.20×10 ⁰	1.00×10 ⁻¹	1.00×10 ⁻¹
27	1-propanol C ₃ H ₇ OH	1.38×10 ⁰	2.50×10 ⁻²	7.50×10 ⁻²
28	Ethanol C ₂ H ₅ OH	1.86×10 ⁰	1.40×10 ⁻¹	1.60×10 ⁻¹
29	Methanol CH ₃ OH	2.08×10 ⁰	1.25×10 ⁻¹	7.50×10 ⁻²
30	Hydrogen chloride HCl	1.50×10 ⁺¹	0.00×10 ⁰	0.00×10 ⁰

As we mentioned earlier, Henry's law constant is also a function of temperature, which can

be approximated by the van't Hoff equation.

$$\frac{d\ln(H^{CP})}{d(1/T)} = -\frac{\Delta H_{diss}}{R} \quad \text{Eq. 2-2}$$

Here T is the temperature in Kelvin, R is the universal gas constant in $\text{J}\cdot\text{K}\cdot\text{mol}^{-1}$, and ΔH_{diss} is the enthalpy change in dissolution. We can see from the van't Hoff equation that there is an inverse relationship between Henry's law constant and temperature. Therefore, unlike the solubility of solids, the solubility of gases in water decreases with increasing temperature. Here, we use five simple amines as examples to demonstrate the effect of temperature on Henry's law constant (Figure 2-1).

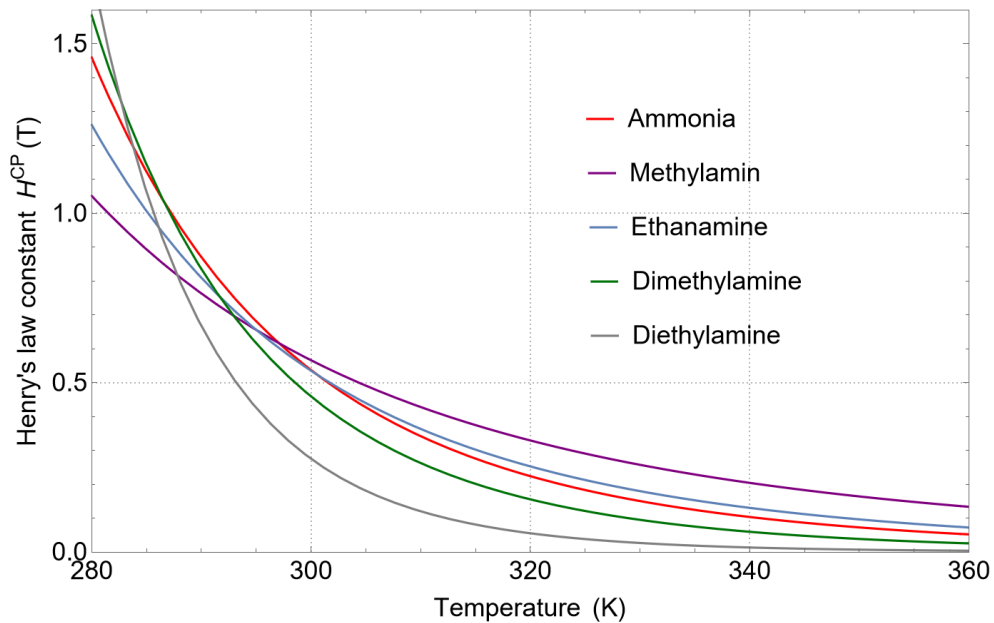


Figure 2-1. The effect of temperature on Henry's law constant. The y-axis shows Henry's law constant in $\text{mol Pa}^{-1}\text{m}^{-3}$, and the x-axis shows temperature in Kelvin. Henry's law constants of gases decrease as the temperature increases, and so does their solubility in water.

We want to point out that Henry's law constants we use in our research work best for dilute solutions and when the temperature is below 373 K and the pressure is below 1000 hPa (~ 1 atm). This is not a bad assumption for our studies, given that our research focuses on temperate terrestrial planets and the atmospheric concentrations of the biosignature gases we study are usually very low (\sim ppm levels).

2.2 Simplified Chlorine Steady-state Chemical Model

I developed a simplified chloride steady-state chemical model to study whether hydrogen chloride (HCl) is a good bioindicator in an H_2 -dominated atmosphere. Thanks to this simplified model, we can have a rough idea of whether HCl gas would accumulate to detectable levels in an H_2 -dominated atmosphere without running our complicated

photochemistry code. One advantage of my simplified chlorine steady-state chemical model is that it is easy to use (i.e., Excel will do). Compared to our full-fledged photochemistry model, which contains pages and pages of complex formulas and theorems, my simplified chlorine steady-state chemical model uses far fewer formulas and is therefore relatively easy to understand. It is worth pointing out in advance that my simplified chlorine steady-state chemical model is not meant to be a replacement for our photochemistry code. In fact, after we have upgraded our existing photochemistry code by adding a comprehensive Cl-reaction network, we plan to run our photochemistry code and quantitatively confirm our results here.

The question we want to answer with my simplified chloride steady-state chemical model is whether we can detect signs of life on an exoplanet with an H₂-dominated atmosphere by detecting HCl gas in the atmosphere. The idea is that life on such a planet produces CH₃Cl gas. In highly reducing atmospheres, many gases are converted to their most hydrogenated (i.e., reduced) form: dimethyl sulfide (DMS) will be turned into H₂S and CH₄; N₂O will be turned into H₂O and N₂ (Seager et al., 2013). Since the most reduced form of Cl element is HCl, atmospheric methyl chloride (CH₃Cl) gas will end up as HCl in H₂-dominated atmospheres. For my simplified chloride steady-state chemical model to work, I have to make two key assumptions. First, we assume that HCl and CH₃Cl are trace gases in the atmosphere, and their respective production flux is small. Therefore, their presence does not affect the concentration of other major chemical species in the atmosphere. Second, we assume that HCl and CH₃Cl are well-mixed in the atmosphere. In other words, their concentrations do not change with height (i.e., not a function of altitude). It's worth noting that these two assumptions/approximations are not physically accurate. The concentrations of the vast majority of the biosignature gases we've studied do change with altitude (pressure), and their presence also changes the concentrations of other chemicals in the atmosphere to a greater or lesser degree. However, these two assumptions are critical because they greatly simplify our calculations and effectively enable our simplified model to work. In this chapter, we use the symbol '[]' to denote a chemical's number density with a unit of molecules cm⁻³. Based on our two assumptions, we can get the concentration of oxygen radicals ([O]), H radicals ([H]), OH radicals ([OH]), and H₂O ([H₂O]) from our existing benchmark case (i.e., base scenario). We assume that HCl is in a steady state in the atmosphere. As a result, its production flux (in molecules cm⁻² s⁻¹) must equal its total removal flux (in molecules cm⁻² s⁻¹). Here, we consider three removal pathways for HCl: wet deposition, dry deposition, and photochemical destruction. In the following few paragraphs, I will explain how we roughly estimate the flux of each removal pathway.

First, to estimate the wet deposition flux of HCl, we have to calculate the rainout rate of HCl. We can use this formula (Giorgi et al., 1985; Hu et al., 2012):

$$k_R(z) = \frac{f_R \cdot [H_2O](z) \cdot k_{H_2O}}{55A_v \cdot [L \cdot 10^{-9} + (H'(T) \cdot R \cdot T(z))^{-1}]} \quad \text{Eq. 2-3}$$

Here, $K_R(z)$ is the rainout rate in s⁻¹. f_R is the rainout reduction factor that we can adjust. Since we assume that the exoplanet we are studying here has an Earth-like rainout intensity, we set f_R to 1. $[H_2O](z)$ is water number density as a function of altitude (in molecules cm⁻³). $K_{H_2O}(z)$ is the precipitation rate constant with a value of 2.0×10^{-6} s⁻¹ (Hu et al., 2012). A_v

is Avogadro's number in $\text{mL atm K}^{-1} \text{mol}^{-1}$. L is the liquid water content with a value of 1 g m^{-3} in the convective layer near the surface (Hu et al., 2012). $H'(T)$ is the temperature-dependent effective Henry's law constant. The most significant difference between the effective Henry's law constant used in this formula and the physical Henry's law constant is that the effective Henry's law constant takes into account the chemical equilibrium in the solution (Giorgi et al., 1985; Hu et al., 2012; R. Sander, 2015). For a chemical that can dissociate in water, its effective Henry's law constant might be larger than its physical Henry's law constant. Our photochemistry code uses both the physical Henry's law constant and the effective Henry's law constant (Hu et al., 2012). R is the universal gas constant in $\text{mL atm K}^{-1} \text{mol}^{-1}$, and $T(z)$ is the atmospheric temperature as a function of altitude, which we can get from our baseline scenario. To calculate $K_R(z)$ for HCl, we only need to find the temperature-dependent Henry's law constant for HCl. Since $K_R(z)$ is the rainout rate (in s^{-1}), to calculate the wet deposition flux (in $\text{molecule cm}^{-2} \text{s}^{-1}$), we need to multiply that by the width of each atmospheric bin (in cm), as well as the number density of HCl (i.e., $[\text{HCl}]$, in molecules cm^{-3}). HCl's dry deposition flux (in $\text{molecule cm}^{-2} \text{s}^{-1}$) is much easier to estimate than wet deposition flux. We can calculate HCl's dry deposition flux by multiplying HCl's dry deposition velocity (in cm s^{-1}) and the number density of HCl (in molecules cm^{-3}).

There are four items in photochemistry destruction, each of which corresponds to a photochemical reaction of HCl: the reaction between HCl and O ($\text{O} + \text{HCl} \rightarrow \text{OH} + \text{Cl}$), the reaction between HCl and H ($\text{H} + \text{HCl} \rightarrow \text{H}_2 + \text{Cl}$), the reaction between HCl and OH ($\text{OH} + \text{HCl} \rightarrow \text{H}_2\text{O} + \text{Cl}$), and the direct photolysis of HCl ($\text{HCl} \rightarrow \text{H} + \text{Cl}$). We can calculate the individual reaction rate between HCl and O, H, and OH (in $\text{molecules cm}^{-3} \text{s}^{-1}$) using this expression: $\text{Rate} = k \cdot [\text{HCl}] \cdot [\text{the other reactant}]$. We can get the number density of O, H, and OH (i.e., $[\text{O}]$, $[\text{H}]$, and $[\text{OH}]$) from our baseline scenario. Once we have the respective reaction rates between HCl and O, H, and OH only, we can multiply it by the width of each atmospheric bin (in cm) to get the corresponding reaction flux (in $\text{molecules cm}^{-2} \text{s}^{-1}$). To estimate the photolysis flux of HCl, we have to calculate its photolysis rate first using this formula (e.g., Hu et al., 2012; Brasseur et al., 2017):

$$J(z) = \frac{1}{2} \int q(\lambda) \cdot \sigma_a(\lambda) \cdot L(\lambda, z) d\lambda \quad \text{Eq. 2-4}$$

The $1/2$ factor accounts for diurnal variation (Hu et al., 2012). $q(\lambda)$ is the quantum yield, defined as the ratio between the yield of the photolysis product and the number of photons absorbed. $\sigma_a(\lambda)$ is the absorption cross-section of HCl, available from the JPL database. $L(\lambda, z)$ is the actinic flux with a unit of $\text{quanta cm}^{-2} \text{s}^{-1} \text{nm}^{-1}$. When UV hits the atmosphere, most short-wavelength radiation is absorbed in the upper atmosphere. Longer-wavelength UV can penetrate deeper into the atmosphere, which is why the actinic flux is a function of both the wavelength (λ) and height (z). Based on our assumption that the presence of HCl does not affect the concentration of other major chemical species in the atmosphere, we can get $L(\lambda, z)$ from our baseline scenario. It is worth noting that the unit of $J(z)$ is s^{-1} . To get photolysis flux (in $\text{molecules cm}^{-2} \text{s}^{-1}$), we need to multiply it by $[\text{HCl}]$ (i.e., the number density of HCl) and the width of each atmospheric bin (in cm).

Next, we need to estimate the production flux of HCl. As a reminder, one of our key assumptions in our model is that life produces CH_3Cl gas, which is later photochemically

converted to HCl in a high-reducing H₂-dominated atmosphere through this reaction: CH₃Cl + H → CH₃ + HCl. Hence, the production flux of HCl is equal to the reaction flux between CH₃Cl and H. To get the reaction flux between CH₃Cl and H (in molecules cm⁻² s⁻¹), we need to multiply the reaction rate (in molecules cm⁻³ s⁻¹) with the width of each atmospheric bin (in cm). We can express the reaction rate as: Rate = k · [H] · [CH₃Cl], where k is the reaction rate constant (in cm³ molecule⁻¹ s⁻¹). Then the question is, how do we estimate the number density of CH₃Cl (i.e., [CH₃Cl]) in the atmosphere. In short, we must repeat all the above calculations with CH₃Cl to get [CH₃Cl]. We assume that CH₃Cl is in a steady state, so its production flux must equal its total removal flux. The production flux of CH₃Cl (in molecules cm⁻² s⁻¹) is the input to our model (i.e., a free parameter). To simplify our model, for CH₃Cl, we only consider three of its dominant removal pathways: wet deposition, dry deposition, and direct photolysis, each of which can be calculated using the equations and methods already mentioned (e.g., Equation 2-3 and Equation 2-4). Combining all of the above, we can write the following equation:

$$\text{Bioproduction flux of CH}_3\text{Cl} = (k_R(z)_{\text{CH}_3\text{Cl}} \cdot [\text{CH}_3\text{Cl}] \cdot \text{width}_{\text{bin}}) + (V_{\text{dep_CH}_3\text{Cl}} \cdot [\text{CH}_3\text{Cl}]) + (J(z)_{\text{CH}_3\text{Cl}} \cdot [\text{CH}_3\text{Cl}] \cdot \text{width}_{\text{bin}}) \quad \text{Eq. 2-5}$$

There is only one unknown in this seemingly complicated equation: [CH₃Cl]. When we give our model an input value (i.e., the bioproduction flux of CH₃Cl), we can solve for [CH₃Cl]. Once we have [CH₃Cl], we can then use the following equation to solve for the number density of HCl in the atmosphere (i.e., [HCl]):

$$k_1 \cdot [\text{H}] \cdot [\text{CH}_3\text{Cl}] \cdot \text{width}_{\text{bin}} = (k_R(z)_{\text{HCl}} \cdot [\text{HCl}] \cdot \text{width}_{\text{bin}}) + (V_{\text{dep_HCl}} \cdot [\text{HCl}]) + (J(z)_{\text{HCl}} \cdot [\text{HCl}] \cdot \text{width}_{\text{bin}}) + (k_2 \cdot [\text{O}] \cdot [\text{HCl}] \cdot \text{width}_{\text{bin}}) + (k_3 \cdot [\text{H}] \cdot [\text{HCl}] \cdot \text{width}_{\text{bin}}) + (k_4 \cdot [\text{OH}] \cdot [\text{HCl}] \cdot \text{width}_{\text{bin}}) \quad \text{Eq. 2-6}$$

2.3 In-depth Introduction to Our Photochemistry Model

In this chapter, we will introduce our photochemistry code in detail, including how it differs from other open source simulation models and how we use this valuable tool in our planetary science research.

In our research, we often use our one-dimensional photochemistry model (Hu et al., 2012) to calculate the mixing ratio of the biosignature gas we want to study as a function of vertical altitude in an exoplanet atmosphere. Our photochemical code (Hu et al., 2012) can simulate various planetary atmospheres (e.g., reduced or oxidized) by calculating the steady-state chemical composition of the atmospheres. Our photochemistry model includes surface emission and formation, wet and dry deposition, and thermal escape of H, N, C, O, and S-containing molecules. Our model also has UV photolysis of atmospheric species and deposition of sulfur-bearing (both elemental sulfur and sulfuric acid) aerosols. Our model includes Rayleigh scattering, molecular absorption, and aerosol Mie scattering to determine the optical depth. Our model uses the delta-Eddington two-stream method to calculate

ultraviolet and visible radiation in the atmosphere. We have validated our photochemistry model by simulating the atmospheric compositions of modern Earth and Mars, matching observations of major trace gases in both cases. For applications of our photochemistry code, see (Hu et al., 2012; Seager et al., 2013; Hu et al., 2013; Sousa-Silva et al., 2020; Zhan et al., 2022; Huang et al., 2022; Ranjan et al., 2022).

The most prominent feature of our photochemistry code is that it is very flexible: we can use it to simulate different types of planets with different atmospheres orbiting a wide variety of host stars. First, we can simulate planets orbiting different stars by using different stellar radiation profiles as input to our code. The choice of the host star is crucial. For an active Sun-like star (i.e., a G-type main-sequence star), the accumulation of biosignature gases is extremely difficult due to the presence of UV-generated destructive species in the atmosphere. The accumulation of biosignature gases is relatively favorable if the central star is a UV-quiet M dwarf star (e.g., GJ 876 or TRAPPIST-1). We list some representative stars that our photochemistry code currently has in the table below (Table 2-2). Data are collected from the MUSCLES (Measurements of the Ultraviolet Spectral Characteristics of Low-mass Exoplanet host Stars) database. Generally speaking, G-type stars are brighter and hotter than K-type stars, which in turn are brighter than M-dwarf stars. The letter 'V' indicates that it is a variable star (i.e., a star that varies in brightness).

Table 2-2. Some representative stars and their respective spectral types.

Name	Spectral type	Mass [solar mass]	Radius [solar radius]
Sun	G2V	1.0	1.0
eps Eri	K2V	0.8	0.7
HD 85512	K6V	0.7	0.5
GJ 832	M1V	0.5	0.5
GJ 876	M5V	0.4	0.4
TRAPPIST-1	M8V	0.1	0.1

In our research, we often use GJ 876 as the host star for our simulated exoplanets because GJ 876 has the lowest near-ultraviolet (NUV) and far-ultraviolet (FUV) output of all the available stars. Therefore, exoplanets orbiting M dwarf stars (like GJ 876) represent the best opportunity for the accumulation and detection of potential biosignature gases. Our model currently doesn't include high-energy electrons or protons. Therefore, we might slightly underestimate the overall removal flux of chemicals in the atmosphere. Below we compare the stellar radiation spectrum of GJ 876 and our sun. Compared to our sun, the UV output of GJ 876 is much lower (Figure 2-2).

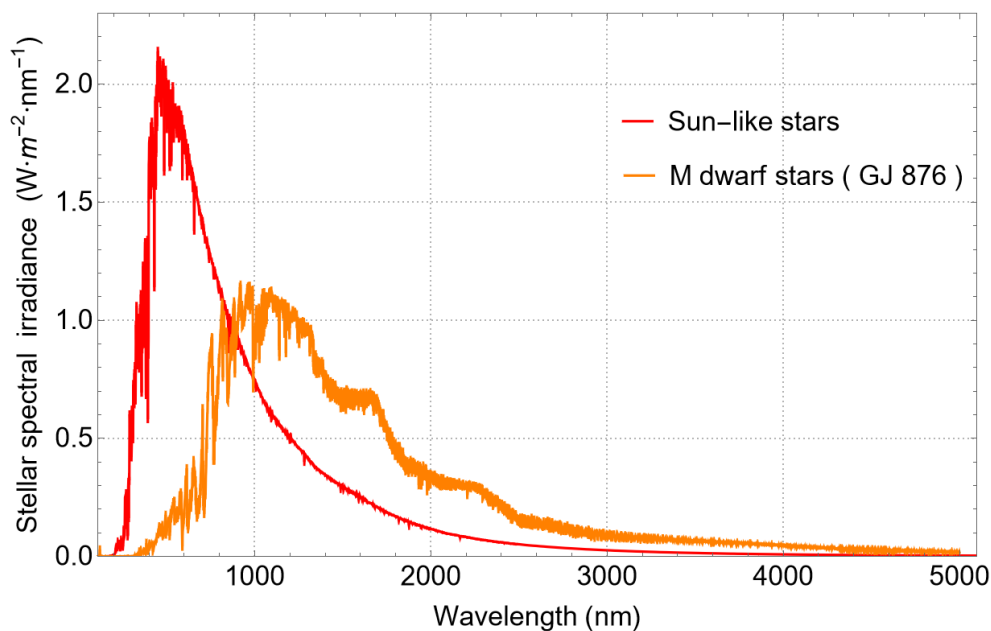


Figure 2-2. The synthetic stellar spectrum input of our photochemistry model (Loyd et al., 2016; France et al., 2016). The y-axis shows spectral irradiance in $\text{W}\cdot\text{m}^{-2}\cdot\text{nm}^{-1}$, and the x-axis shows wavelength in nm. Compared to our sun, the UV output of GJ 876 is much lower

We can also use photochemistry code to simulate a wide range of exoplanets with different types of atmospheres. In our studies, we often choose the following three atmospheres as our benchmark scenarios: CO_2 -dominated highly oxidizing atmospheres, N_2 -dominated weakly oxidizing atmospheres, and H_2 -dominated reducing atmospheres. Each atmosphere's main chemical compositions are different, and we summarize them in the table below (Table 2-3).

Table 2-3. Atmospheric compositions of our three benchmark scenarios (Hu et al., 2012).

Benchmark scenarios	Redox state	Main composition	Mean molecular weight
H_2 -dominated	reducing	90% H_2 + 10% N_2	4.6
N_2 -dominated	weakly oxidizing	>99% N_2	28.0
CO_2 -dominated	highly oxidizing	90% CO_2 + 10% N_2	42.4

Each atmosphere's dominant reactive species (i.e., radicals) are also different. In an H_2 -dominated atmosphere, the most dominant reactive species are H (hydrogen) radicals, followed by OH (hydroxyl) radicals. The primary source of H radicals and OH radicals is the direct photolysis of water vapor in the atmosphere. Another minor source of H radicals is the photodissociation of H_2 gas. Compared to the primary pathway, H production via H_2 photolysis is much less efficient due to the need for shorter UV (< 85 nm) (Hu et al., 2012). In an H_2 -dominated atmosphere, the abundance of H radicals is several orders of magnitude higher than that of OH radicals. The reason is that OH radicals can react with H_2 gas to form H and water vapor, thereby increasing the amount of H in the atmosphere (Hu et al., 2012). In an N_2 -dominated atmosphere, H radicals, OH radicals, and O (oxygen) radicals are all relatively abundant (Hu et al., 2012). In a CO_2 -dominated atmosphere, the dominant

reactive species are O radicals. The direct photolysis of atmospheric CO₂ can produce a series of products, such as O, CO, and O₂. Compared with O radicals, H and OH radicals are much less abundant since H can react with O₂ to form O and OH, which can further react with CO to form H and CO₂ (Hu et al., 2012).

We have different temperature-pressure profiles for exoplanets with different types of atmospheres. For each of the scenarios we study, we set the planet's surface pressure to 1 bar and temperature to 288 K. We divide the atmosphere into two layers: a lower convective layer and a higher radiative layer (Hu et al., 2012). We set the temperature of the convective layer to follow the dry adiabatic lapse rate. We set the stratospheric temperature in our model according to (Hu et al. 2012). We set the temperature above tropopause to 160K, 200K, and 175K for the H₂-dominated, N₂-dominated, and CO₂-dominated atmosphere. The temperature of the tropopause depends on the main chemical composition of the atmosphere. Since H₂ is a much better coolant than N₂ or CO₂, an H₂-dominated atmosphere has the lowest tropopause temperature. For an H₂-dominated atmosphere, we assume the stratosphere is very cold due to efficient radiative cooling from abundant H₂ (Birnbaum et al. 1996). Since we do not have a climate model coupled with our photochemistry code, we do not consider heating in the upper atmosphere. Hence, we assume the temperature to be constant (isothermal) in the radiative layer (Hu et al., 2012). The temperature profiles we set are consistent with significant greenhouse effects in the convective layer (Hu et al., 2012). It is worth noting that we currently include a cold trap in each of our existing photochemical simulations. The Earth's tropopause temperature is about 217 K (US Standard Atmosphere 1976). The tropopause temperatures we set for the H₂-dominated, N₂-dominated, and CO₂-dominated atmospheres are all lower than Earth's cold trap temperature. Please note that a cold trap does not require a thermal inversion. A cold trap is a part of the (upper) atmosphere where the temperature is low enough to condense volatiles like water (Wordsworth et al., 2013, Wordsworth et al., 2014). In our studies, we sometimes conduct sensitivity tests on the temperature-pressure profile (i.e., the strength of the cold trap) to verify the robustness of our photochemical simulation results. We choose the H₂-dominated atmosphere as our example here. To simulate an atmosphere with a reduced cold trap, we set the temperature above tropopause to 220 K. In this case, we assume the planet has a relatively hot stratosphere due to UV absorbers in the atmosphere. Here, we present the temperature-pressure profiles of the simulated exoplanets with H₂-dominated, CO₂-dominated, and N₂-dominated atmospheres (Figure 2-3).

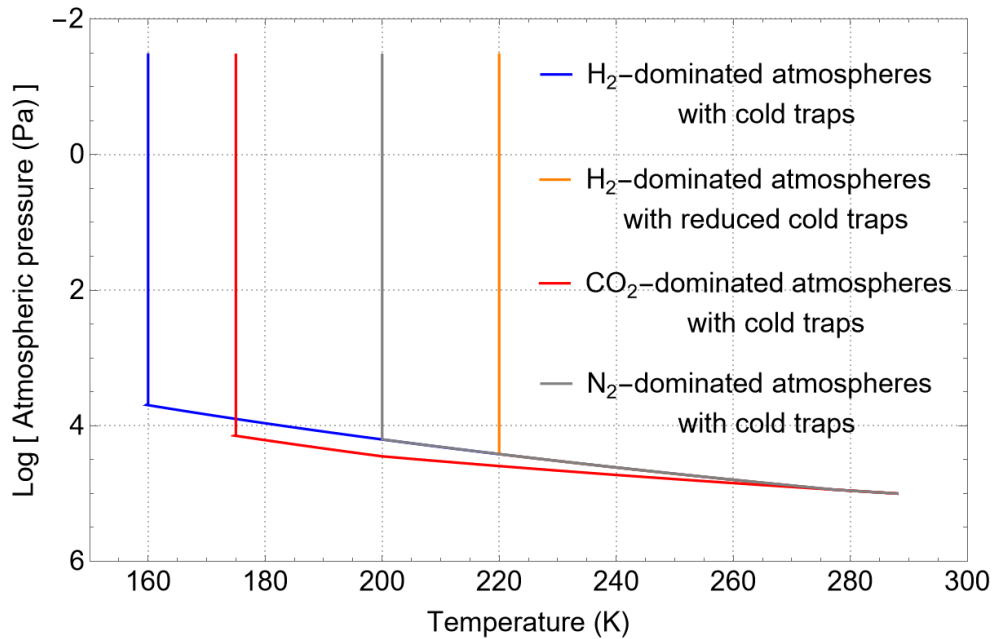


Figure 2-3. The temperature-pressure profiles of the simulated exoplanets with H₂-dominated, CO₂-dominated, and N₂-dominated atmospheres. The y-axis shows atmospheric pressure (Pa) on a log scale, and the x-axis shows temperature in Kelvin (K).

We also have different eddy diffusion profiles for exoplanets with different types of atmospheres. In our model, the vertical mixing processes are parameterized by the atmosphere's eddy diffusion coefficient (k_{zz}). The choice of eddy diffusion coefficient (K_{zz}) can impact whether the biosignature gas can accumulate in the atmosphere because photochemistry is most important in the upper atmosphere layers, whereas we assume that most biosignature gases are primarily produced at the planet's surface. In essence, the eddy diffusion coefficient (K_{zz}) reflects the atmosphere's diffusiveness. The larger K_{zz} , the more likely the biosignature gas will be transported to the upper atmosphere before being removed by wet or dry deposition. Compared to other parameters in our photochemistry code, k_{zz} is more speculative; hence, it is one of the major uncertainties in our model (Hu et al., 2012). K_{zz} is measured or inferred for solar system planets but is not known for exoplanets. In our studies, we often use the known Earth's eddy diffusion profile and scale it up to approximate the eddy diffusion profile of our simulated exoplanets. In our studies, we adopt the eddy diffusion scaling factor of 0.68 for the CO₂-dominated atmosphere, 1.0 for the N₂-dominated atmosphere, and 6.3 for the H₂-dominated atmosphere (Hu et al., 2012). We want to point out that this approximation is not physically accurate for exoplanets. The Earth's diffusion profile takes this shape because of the absorption of UV by O₃. The eddy diffusion profiles will likely have different shapes on exoplanets without ozone layers. We present our simulated exoplanets' eddy diffusion profiles in the figures below (Figure 2-4, Figure 2-5, and Figure 2-6).

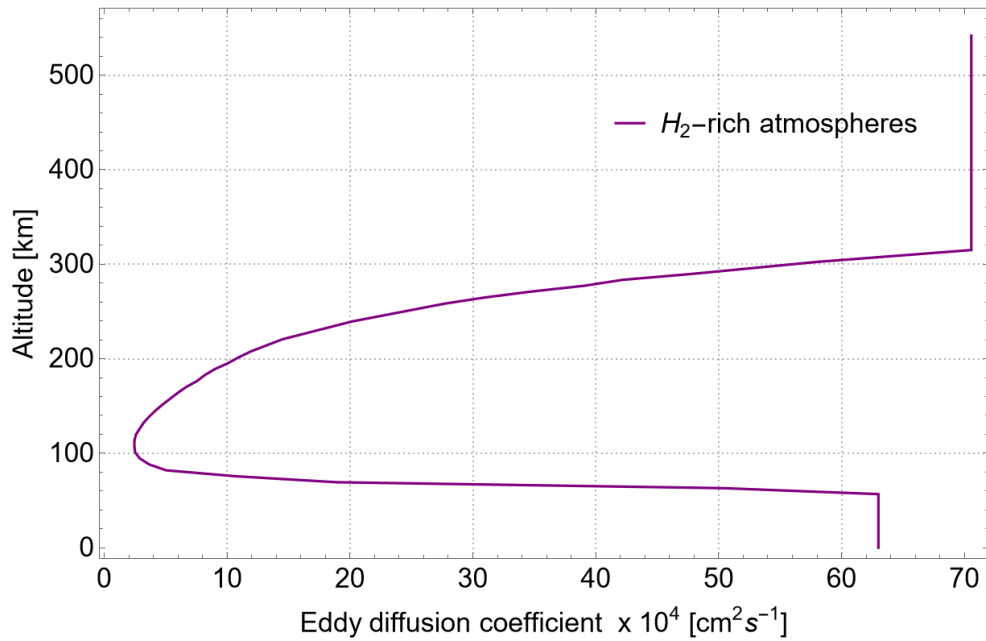


Figure 2-4. The eddy diffusion profile of the simulated exoplanets with H₂-dominated atmospheres. The y-axis shows altitude in km, and the x-axis shows the eddy diffusion coefficient in cm² s⁻¹.

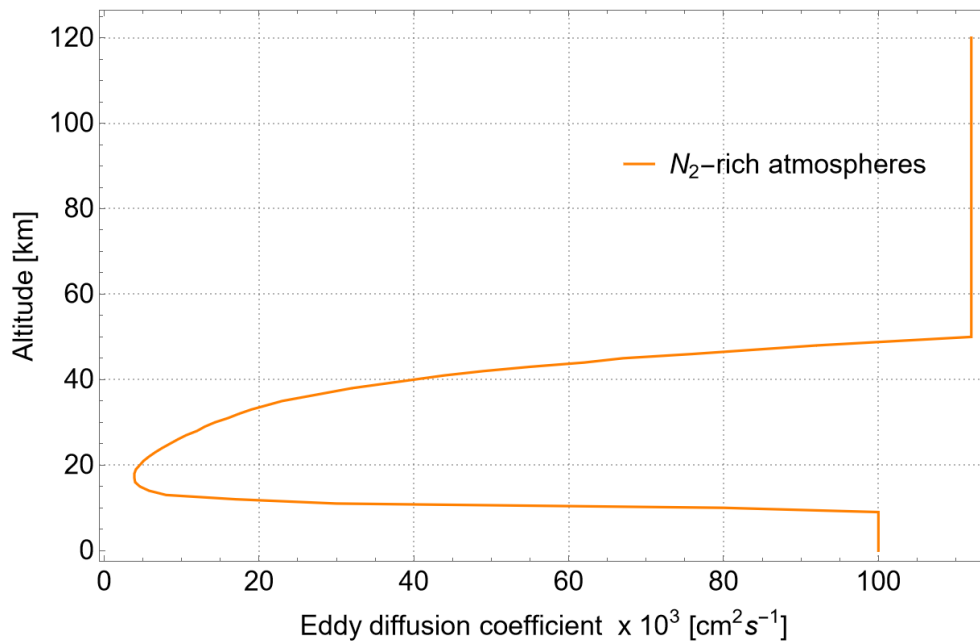


Figure 2-5. The eddy diffusion profile of the simulated exoplanets with N₂-dominated atmospheres. The y-axis shows altitude in km, and the x-axis shows the eddy diffusion coefficient in cm² s⁻¹.

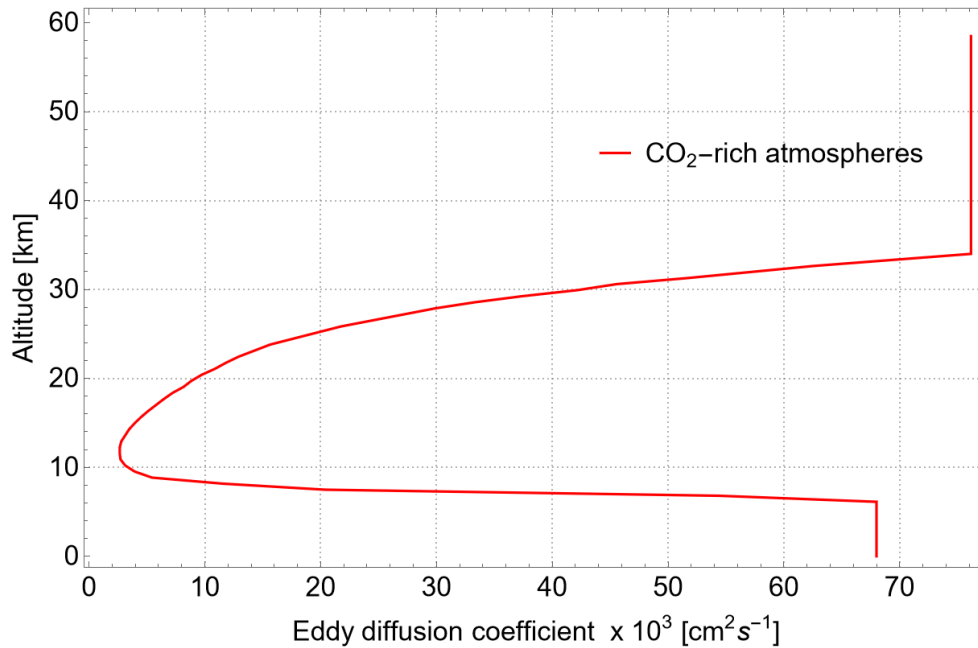


Figure 2-6. The eddy diffusion profile of the exoplanets with CO₂-dominated atmospheres. The y-axis shows altitude in km, and the x-axis shows the eddy diffusion coefficient in cm² s⁻¹.

Currently, our full photochemistry model encodes 111 species. Our photochemistry model demarcates chemical species into four types: type “X”, for species for which the full photochemical transport equation is solved, type “F” for species assumed to be in photochemical equilibrium (i.e., for which transport is neglected), type “C” for chemically inert species which are assumed not to react or transport and type “A” for aerosol species. In addition, for the lower boundary condition, we can either specify a fixed surface mixing ratio (type “1”) or a fixed emission/deposition velocity (type “2”) (Hu et al., 2012). Furthermore, our photochemistry code includes more than 800 chemical reactions. We classify them into four types: bimolecular reactions (‘R type’), termolecular reactions (‘M type’) (i.e., reactions depend on ambient pressure), thermal dissociation reactions (‘T type’) and direct photolysis (‘P type’) (Hu et al., 2012). In our simulations, we include all the reactions mentioned in (Hu et al., 2012) except for reactions that involve more than two carbon atoms (C>2-chem), HSO₂ thermal decay, and high-temperature reactions (Hu et al., 2012). Moreover, we set the surface deposition (including both rainout and dry deposition) of H₂, CO, CH₄, N₂, C₂H₂, C₂H₄, C₂H₆, and O₂ to zero to facilitate robust comparison with reference benchmark scenarios from (Hu et al., 2012). Such assumption corresponds to the situation where surface biology is not an efficient sink for these gases, which does not hold for modern Earth. However, our results are robust to this assumption as the main removal mechanisms of the biosignature gas we study are likely surface deposition and direct photolysis. It is worth pointing out that we did not include atmospheric escape in our simulations.

Chapter 3

Assessment of Ammonia as a Biosignature Gas in Exoplanet Atmospheres

The results presented in this chapter have been published in *Astrobiology* (<https://doi.org/10.1089/ast.2020.2358>). I would like to thank the following co-authors for their contributions to this project: Prof. Sara Seager, Dr. Janusz J. Petkowski, Dr. Sukrit Ranjan, and Dr. Zhuchang Zhan. Each of them played an essential role in the publication of the paper.

Abstract

Ammonia (NH₃) in a terrestrial planet atmosphere is generally a good biosignature gas, primarily because terrestrial planets have no significant known abiotic NH₃ source. The conditions required for NH₃ to accumulate in the atmosphere are, however, stringent. NH₃'s high water solubility and high bio-useability likely prevent NH₃ from accumulating in the atmosphere to detectable levels unless life is a net source of NH₃ and produces enough NH₃ to saturate the surface sinks. Only then can NH₃ accumulate in the atmosphere with a reasonable surface production flux.

For the highly favorable planetary scenario of terrestrial planets with H₂-dominated atmospheres orbiting M dwarf stars (M5V), we find a minimum of about 5 ppm column-averaged mixing ratio is needed for NH₃ to be detectable with JWST, considering a 10 ppm JWST systematic noise floor. When the surface is saturated with NH₃ (i.e., there are no NH₃-removal reactions on the surface), the required biological surface flux to reach 5 ppm is on the order of 10¹⁰ molecules cm⁻² s⁻¹, comparable to the terrestrial biological production of CH₄. However, when the surface is unsaturated with NH₃, due to additional sinks present on the surface, life would have to produce NH₃ at surface flux levels on the order of 10¹⁵ molecules cm⁻² s⁻¹ (~4.5×10⁶ Tg year⁻¹). This value is roughly 20,000 times greater than the biological production of NH₃ on Earth and about 10,000 times greater than Earth's CH₄ biological production.

Volatile amines have similar solubilities and reactivities to NH₃ and hence share NH₃'s weaknesses and strengths as a biosignature. Finally, to establish NH₃ as a biosignature gas, we must rule out mini-Neptunes with deep atmospheres, where temperatures and pressures are high enough for NH₃'s atmospheric production.

3.1 Introduction

A growing part of exoplanet research focuses on the search for biosignature gases with future telescopes. Biosignature gases are gases produced by living organisms either as final products or by-products from biochemical pathways. A viable biosignature gas must have spectral features that are both detectable and distinguishable from other molecular species

(e.g., Zhan et al., 2021). A growing number of gases have been proposed as biosignatures. The most well-known example is O_2 (e.g., Jeans, 1930; Meadows et al., 2018). Other biosignature gas candidates include DMS ($(CH_3)_2S$) (Domagal-Goldman et al., 2011; Seager et al., 2012; Arney et al., 2018), methane (CH_4) (Leger et al., 1996; Des Marais et al., 2002; Kaltenegger et al., 2007; Dlugokencky et al., 2011), nitrous oxide (N_2O) (Des Marais et al., 2002; Tian et al., 2015), ammonia (NH_3) (Seager et al., 2013), methyl chloride (CH_3Cl) (Segura et al., 2005), phosphine (PH_3) (Sousa-Silva et al., 2019), and isoprene (C_5H_8) (Zhan et al., 2021).

We are motivated to study the biosignature potential of NH_3 since NH_3 plays a significant role in biochemistry. Due to its high bio-usability, plants and various microorganisms can easily absorb NH_3 . NH_3 is an ideal nitrogen source for life on Earth since it can be integrated into various amino acids and other organic molecules without life having to break the strong N_2 triple bond. Additionally, some life can use NH_3 as an energy source by oxidizing NH_3 . Furthermore, NH_3 stands out from all the previously studied biosignature gases because NH_3 has a very high solubility in water. NH_3 's high water solubility means the atmospheric accumulation of NH_3 is highly dependent on planetary conditions such as whether life produces a substantial amount of NH_3 and whether there are active NH_3 -removal sinks on the surface (including land and ocean). If life does not produce enough NH_3 to saturate the surface sinks, rain can much more efficiently remove NH_3 from the atmosphere than other atmospheric gases.

NH_3 has been studied before. Early studies suggest NH_3 is unlikely to be present in an early Earth atmosphere because it is easily destroyed photochemically (Kasting et al., 1982; Sagan and Chyba, 1997). In a separate paper, we studied NH_3 as a biosignature gas for a specific, optimistic planetary scenario of a planet with an $H_2 - N_2$ atmosphere termed the 'cold Haber World' (Seager et al., 2013). On such a planet, life may have evolved catalytic machinery to break the N_2 triple bond and extract energy by fixing atmospheric H_2 and N_2 into NH_3 (Seager et al., 2013). A somewhat similar catalytic process occurs in the industry (the Haber process) at specific temperatures and pressures.

In this work, we reassess NH_3 as a biosignature gas by considering different planetary scenarios and surface conditions. We first summarize NH_3 's sources and sinks on Earth in Chapter 3.2. We then describe our models in Chapter 3.3. We present our results in Chapter 3.4. Finally, we conclude our paper with a discussion of our results and a description of limitations in Chapter 3.5.

3.2 Ammonia Sources and Sinks

To assess the biosignature potential of NH_3 , we first need to review how NH_3 is produced (Chapter 3.2.1) and destroyed (Chapter 3.2.2) on Earth. NH_3 sources on Earth are few and either anthropogenic (Chapter 3.2.1.1) or biological (Chapter 3.2.1.2), with limited abiotic sources (Chapter 3.2.1.3). In contrast, NH_3 has many destruction pathways. We discuss NH_3 atmospheric sinks in Chapter 3.2.2.1 and NH_3 biological sinks in Chapter 3.2.2.2.

3.2.1 Ammonia Sources on Earth

Ammonia is a trace gas (< 1 ppbv) in modern Earth's atmosphere, with a residence time of less than a day (Zhu et al., 2015). Current data on NH₃ emissions at a global level have significant uncertainties due to the lack of measurements in most parts of Earth's atmosphere (Olivier et al., 1998; Bouwman et al., 2002; Zhu et al., 2015; Van Damme et al., 2018). It is worth noting that anthropogenic NH₃ production is a significant NH₃ source on Earth (Söderlund et al., 1976; Dentener and Crutzen, 1994; Olivier et al., 1998).

3.2.1.1 Anthropogenic NH₃ Production

On Earth, most global NH₃ emissions are due to anthropogenic activities, especially agriculture (Behera et al., 2013). Large quantities of ammonia are directly applied on farm fields as fertilizer (anhydrous NH₃) or are used to produce secondary nitrogen fertilizers. Besides anhydrous NH₃, synthetic N fertilizers such as urea ((NH₂)₂CO) and ammonium bicarbonate (NH₄HCO₃) are also popular N fertilizers (Behera et al., 2013). Both applications result in very high localized NH₃ emissions from farmlands (e.g., Dong et al., 2009; Hou and Yu, 2020). NH₃ emissions from N fertilizers depend on many factors, including the type of fertilizers, local meteorological conditions, and soil properties (Behera et al., 2013). It has been estimated that up to 10% of N content is lost through NH₃ emission when anhydrous NH₃ fertilizer is used. This number rises to 18.7% for urea fertilizer (Behera et al., 2013). Animal husbandry also significantly contributes to global NH₃ emissions (through the microbial decomposition of animal waste, see Chapter 3.2.1.2 below). Coal-burning also produces NH₃, even though the quantity is relatively small (Soderlund et al., 1976, Behera et al., 2013).

Industrial NH₃ sources come from the production of nitric acid, fuel, explosives, and refrigerants. Other minor global NH₃ emissions include agriculture-related biomass decomposition and motor vehicles (Zhu et al., 2015). We summarize the major NH₃ sources and their flux in Table 3-1.

Table 3-1. Major anthropogenic NH₃ sources and their estimated flux (Soderlund et al., 1976).

Ammonia sources	Rate [Tg/year]
Domestic animals and human	20 - 35
Burning of coal	4 - 12
Wild animals	2 - 6
Total	26 - 53

Global NH₃ emission flux is extremely hard to estimate because most NH₃ measurements are local, and NH₃ abundance varies widely (Olivier et al., 1998; Zhu et al., 2015; Van Damme et al., 2018). It has been reported that global NH₃ emissions may have quadrupled in the past few years due to the increasing demand for food and other agricultural products (Lamarque et al., 2011 and Zhu et al., 2015). Global NH₃ emissions will likely keep growing in the near future (Moss et al., 2010, Behera et al., 2013). The fact that the NH₃ emission rate has a strong dependency on climate (Sutton et al., 2013) makes an accurate NH₃ emission estimate even more difficult. We summarize some estimates of global anthropogenic NH₃ emission from the past few decades in Table 3-2.

Table 3-2. A summary of global anthropogenic NH₃ emission estimates (Zhu et al., 2015).

Global NH ₃ emission rate [Tg/year]	Source
38.5	Moss et al., 2010
53	Soderlund et al., 1976
54	Bouwman et al., 1997
75	Schlesinger et al., 1992

As an aside, anthropogenic NH₃ is produced by the Haber-Bosch process. The Haber-Bosch process reduces unreactive atmospheric nitrogen (N₂) to ammonia with molecular hydrogen (H₂). This reaction requires a metal catalyst (e.g., iron and other catalysts), high temperatures (450 ~ 550 °C), and high pressures (250 ~ 350 bar).

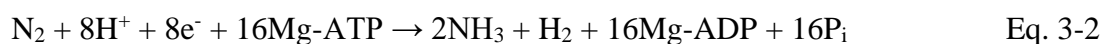


The Haber-Bosch reaction has a standard Gibbs free energy change (ΔG_f°) of -32.8 kJ/mol and standard enthalpy change (ΔH_f°) of -91.8 kJ/mol. Even though this reaction is thermodynamically favorable at room temperatures (~300 K), it is kinetically disfavored. The use of catalysts significantly lowers the activation energy required for breaking the triple bond in the N₂ gas. It is worth noting that the reaction becomes thermodynamically unfavorable at high temperatures (~550°C). Nevertheless, with high pressures, the forward reaction proceeds fast enough to give an industrially acceptable NH₃ yield.

3.2.1.2 Biological NH₃ Production

Three known biological processes generate ammonia (Figure 7). We briefly summarize them below.

Nitrogen fixation: Biological nitrogen fixation by diazotrophic bacteria and Archaea converts atmospheric N₂ to NH₃. The chemical reaction is catalyzed by a nitrogenase enzyme's metal cluster iron-molybdenum cofactor (FeMoco) (Burgess et al., 1996). The biosynthesis of NH₃ is highly energetically costly and is coupled to the hydrolysis of 16 ATP molecules.



Note that because the nitrogenase enzyme is susceptible to O₂, many nitrogen-fixing organisms inhabit strictly anaerobic conditions. Despite its complex catalytic mechanism, biological nitrogen fixation likely originated very early in the evolution of life on Earth. Nitrogen isotopic studies suggest that molybdenum-based nitrogenase arose earlier than 3.2 Gya (Stüeken et al., 2015).

Ammonification: Many microorganisms convert organic nitrogen within organic matter (e.g., animal and plant waste, etc.) into NH₃. Bacterial and fungal ammonification of animal

waste is one of the main processes contributing to the agricultural flux of atmospheric NH_3 (see section 2.1.1).

Dissimilatory nitrate reduction to ammonium (DNRA): Dissimilatory nitrate reduction to ammonium (DNRA; nitrate/nitrite ammonification) is a process of anaerobic chemoorganoheterotrophic respiration that uses nitrate (NO_3^-), instead of O_2 , as a final electron acceptor (Lam et al., 2011 and Kraft et al., 2011). As a result of DNRA, organic matter is oxidized anaerobically with a simultaneous reduction of nitrate to nitrite and subsequently to ammonia (or ammonium ion) ($\text{NO}_3^- \rightarrow \text{NO}_2^- \rightarrow \text{NH}_4^+$) (Lam et al., 2011). Dissimilatory nitrate reduction to ammonium is typically found in prokaryotes. However, eukaryotic microorganisms can also carry out DNRA (Kuypers et al., 2018; Preisler et al., 2007; and Stief et al., 2014). Note that in contrast to denitrification (the production of N_2 gas), the DNRA process conserves nitrogen, as soluble NH_4^+ can be efficiently utilized in biochemical processes (Marchant et al., 2014).

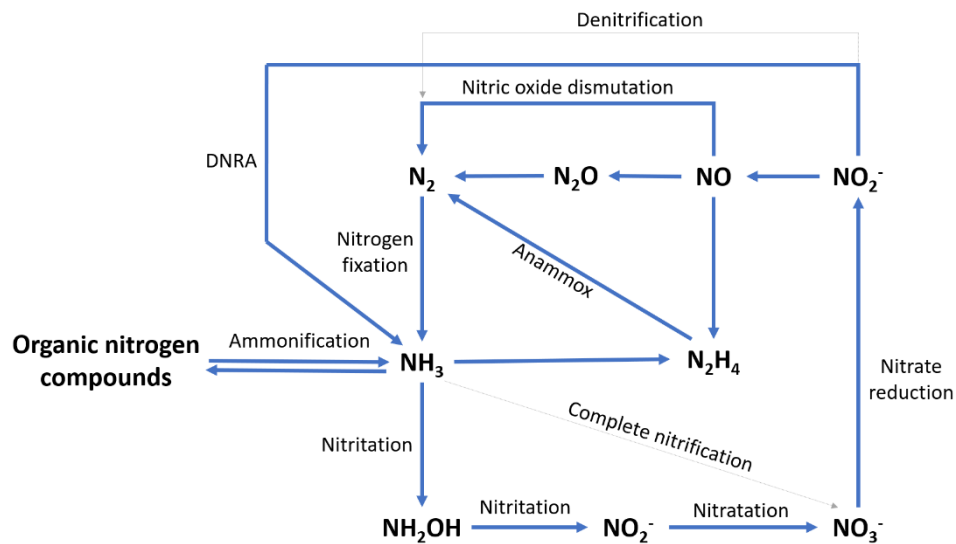


Figure 3-1. Interconversions between the main nitrogen species.

Of the three processes above (excluding ammonification that results from human industrialized agricultural activity (see Chapter 3.2.1.1)), biological nitrogen fixation at 200 Tg/year dominates the biological production of NH_3 (Rascio and Rocca 2013). We compare the annual biological production of ammonia (NH_3) to that of nitrogen gas (N_2), methane (CH_4), isoprene (C_5H_8), nitrous oxide (N_2O), and methyl chloride (CH_3Cl) in Figure 3-2.

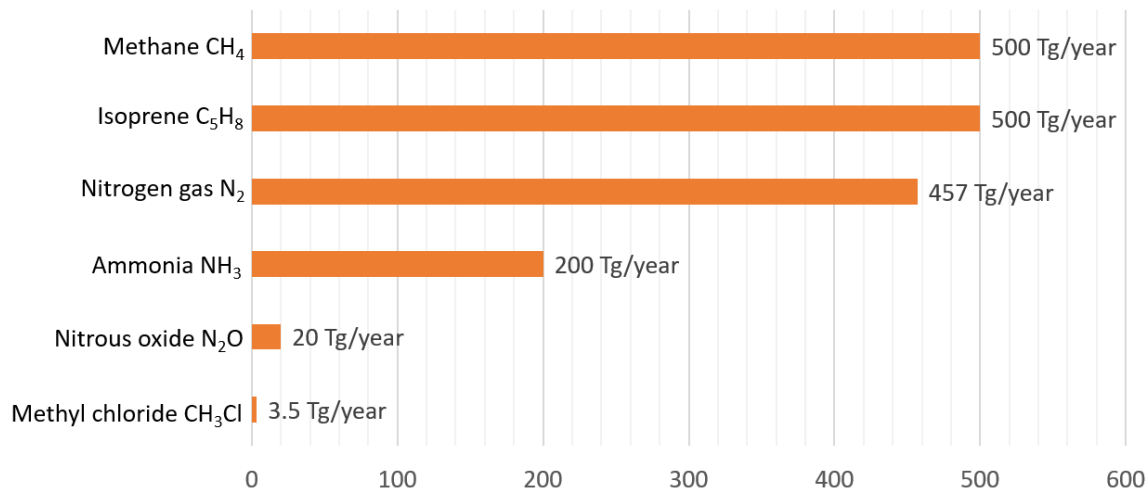


Figure 3-2. Biological production of six different gases in Tg year⁻¹. The biological production of ammonia is significantly smaller than that of methane or isoprene. Specifically, the bioproduction of ammonia is only about half of that of biologically produced nitrogen gas. References: Isoprene (Zhan et al., 2021); methane (Guenther et al., 2006); nitrogen gas (Yeung et al., 2019); ammonia (Rascio and Rocca, 2013); nitrous oxide and methyl chloride: (Tian et al., 2015), (Yokouchi et al., 2015) and (Korhonen et al., 2008).

3.2.1.3 Minor NH₃ Abiotic Sources

There are very few minor abiotic NH₃ sources on Earth¹. We briefly summarize them below.

NH₃ is a trace component of volcanic gases erupted by some, but not all, volcanoes on Earth (see (Möller 2014) and their Table 2.38). For example, (Uematsu et al., 2004) reported an emission of volcanic NH₃ from the Miyake-jima volcano that reached 5 ppb locally. The volcanic NH₃ is likely emitted due to the thermal breakdown of organic matter of biological origin (Sigurdsson et al., 2015), rather than the reduction of more oxidized N species, like N₂. Due to Earth's oxidizing conditions, volcanic outgassing includes some oxidized nitrogen species such as NO and HNO₃ (Mather et al., 2004, Martin et al., 2007, Gaillard & Scaillet, 2014). In contrast to Earth, on a planet with a reducing upper mantle condition, nitrogen would be predominately in the form of NH₄⁺ in the fluids and could be degassed as NH₃ (Mikhail et al., 2014 and Mikhail et al., 2017). Detailed modeling is required to explore the plausibility of this scenario further.

NH₃ can be photochemically produced on iron-doped TiO₂ containing sands without microorganisms' aid (Kasting et al., 1982; Schrauzer et al., 1983). When exposed to sunlight or UV, TiO₂ containing sands can reduce N₂ to NH₃ and trace N₂H₄. However, only up to 10⁷ tons (or 10 Tg) of NH₃ can be photochemically produced on desert sands every year (Schrauzer et al. 1983). Furthermore, this abiotic N₂ photo-fixation is only significant in arid and semiarid regions but not in areas with abundant rainfall and covered

¹ See Appendix H for our NH₃ abiotic false-positive analysis.

by vegetation, where biological N₂ fixation dominates (Schrauzer et al. 1983).

In the presence of dissolved Ni₃Fe, NiFe, Ni⁰, and Fe⁰ in the ocean, N₂, NO₂⁻ and NO₃⁻ can be converted to NH₃/NH₄⁺ (Smirnov et al. 2008). This potential abiotic NH₃/NH₄⁺ synthesis can happen in anaerobic (oxygen-depleted) conditions or reducing (H₂-rich) environments. Such conditions can potentially be present around the Hadean submarine hydrothermal vents (Smirnov et al. 2008). However, this reduction process is strongly temperature-dependent and only becomes efficient at high temperatures (~200°C and above).

NH₃ is very unlikely to be produced in hydrothermal vents on modern Earth, and even if it were, NH₃ would dissolve in Earth's ocean. The hydrothermal vents are not known to reach conditions for net NH₃ synthesis. There may be one extreme exception: the Piccard hydrothermal field. The Piccard hydrothermal system is the deepest known seafloor hot-spring (4957 ~ 4987 m) with pressures (~500 bar), temperatures (~500 °C), and H₂ gas abundances (from serpentinization) to enable some limited N₂ reduction (McDermott et al., 2018) if a suitable catalyst is present.

Lightning might produce NH₃ in the Earth's atmosphere, but only in tiny amounts if at all (see Section 5.3 for further discussion). In Earth's atmosphere, most of NH₃ is generated (or 'recycled') from NH₂ radicals, which likely originate from the photolysis of NH₃ itself (see Table 2-3). Hence, we do not consider Earth's atmospheric chemistry as a net source of NH₃. For completeness, we include the high-temperature reactions in Table 3-3 even though the rates are extremely low at Earth temperatures.

Table 3-3. NH₃-producing reactions. The reaction rates are in units of cm³·molecule⁻¹·s⁻¹.

Chemical Reaction	Rate at 298K	Rate law	Source
H ₂ + NH ₂ → NH ₃ + H	High temp reaction	6.75 · 10 ⁻¹⁴ · (T/298) ^{2.6} · exp[-3006.8/T]	NIST
NH ₂ + C ₂ H ₂ → C ₂ H + NH ₃	High temp reaction	8.2 · 10 ⁻¹³ · exp[-2780/T]	NIST
NH ₂ + C ₂ H ₄ → C ₂ H ₃ + NH ₃	4.07 × 10 ⁻¹⁶	3.42 · 10 ⁻¹⁴ · exp[-1320.6/T]	NIST
NH ₂ + C ₂ H ₄ O → C ₂ H ₃ O + NH ₃	5.28 × 10 ⁻¹⁵	3.50 · 10 ⁻¹³ · exp[-1250/T]	NIST
NH ₂ + C ₂ H ₆ → C ₂ H ₅ + NH ₃	2.13 × 10 ⁻¹⁸	2.74 · 10 ⁻¹⁴ · (T/298) ^{3.46} · exp[-2820/T]	NIST
NH ₂ + CH ₄ → CH ₃ + NH ₃	6.90 × 10 ⁻¹⁸	8.77 · 10 ⁻¹⁵ · (T/298) ³ · exp[-2130/T]	NIST
NH ₂ + H ₂ O → OH + NH ₃	9.52 × 10 ⁻²²	2.1 · 10 ⁻¹³ · (T/298) ^{1.9} · exp[-5725/T]	NIST
NH ₂ + HO ₂ → NH ₃ + O ₂	3.40 × 10 ⁻¹¹	3.4 · 10 ⁻¹¹	JPL
N ₂ H ₃ + N ₂ H ₃ → 2NH ₃ + N ₂	High temp reaction	5.0 · 10 ⁻¹²	NIST
NH ₂ + OH → NH ₃ + O	1.43 × 10 ⁻¹³	3.32 · 10 ⁻¹³ · (T/298) ^{0.4} · exp[-250.2/T]	NIST
H + NH ₂ → NH ₃	3.00 × 10 ⁻³⁰	3.00 · 10 ⁻³⁰	NIST

3.2.2 Ammonia Sinks on Earth

Compared to NH₃'s few formation pathways on Earth, there are numerous routes through which NH₃ can be removed. This section focuses on NH₃ atmospheric sinks (Section

3.2.2.1) and biological sinks (Section 3.2.2.2).

3.2.2.1 NH₃ Atmospheric Sinks

NH₃ is highly reactive in Earth's atmosphere and is destroyed by direct photolysis and reactions with UV-generated radicals. In Earth's oxic atmosphere, OH is the dominant radical. In exoplanet atmospheres with different bulk compositions, other radicals may become dominant. In particular, for an H₂-dominated (highly reducing) atmosphere, the most abundant reactive species are H radicals, produced by photolysis of atmospheric water vapor (Hu et al., 2012). In N₂ or CO₂-dominated atmospheres, O may also be important, though this needs to be further explored (Hu et al., 2012; Ranjan et al., 2020). We list the reactions between NH₃ and O, H, and OH radicals in Table 3-4.

Table 3-4. Reactions between NH₃ and H, O and OH radicals in the atmosphere. The reaction rates have units of cm³·molecule⁻¹·s⁻¹. (Reference: NIST)

Reactions	Rate at 298K	Rate law
NH ₃ + H· → H ₂ + NH ₂	8.27 × 10 ⁻²⁰	4.27 · 10 ⁻¹⁴ · (T/298) ^{3.87} · exp[-32.59/RT]
NH ₃ + O· → ·OH + NH ₂	4.37 × 10 ⁻¹⁷	2.87 · 10 ⁻¹³ · (T/298) ^{2.10} · exp[-21.78/RT]
NH ₃ + ·OH → H ₂ O + NH ₂	1.57 × 10 ⁻¹³	3.50 · 10 ⁻¹² · exp[-7.69 ± 1.66/RT]

NH₃ can also photodissociate under UV conditions. The photolysis rate coefficient J_A can be quantified by (e.g., Brasseur et al., 2017):

$$J_A = \int q_\lambda \cdot I_\lambda \cdot \sigma_\lambda \cdot e^{-\tau_\lambda} d\lambda \quad \text{Eq. 3-3}$$

Here q_λ is the quantum yield of NH₃ photolysis. I_λ is the solar intensity at the top of the atmosphere, τ_λ is the optical depth, and σ_λ is the absorption cross-section of NH₃. Ammonia photolysis has two pathways, which we summarize in Table 3-5. Reaction rates are computed in (Hu et al., 2012).

Table 3-5. Photolysis reactions of NH₃ (Hu et al., 2012).

Reaction	Quantum yields	Reaction rate at 295 K [s ⁻¹]
NH ₃ + hν → NH ₂ + H	<106nm: 0.3 106-165 nm: linear interpolation >165nm: 1.0	6.89 × 10 ⁻⁵
NH ₃ + hν → NH + H ₂	<106nm: 0.7 106-165 nm: linear interpolation >165nm: 0	1.55 × 10 ⁻⁶

Atmospheric NH₃ will react with nonradical molecules in the atmosphere. In total, we identified five other reactions that can remove NH₃ (Table 2-6), and this list is complete for reactions that remove NH₃, according to the NIST database (Manion et al., 2008). As in Table 3-6, we include the high-temperature reactions for completeness.

Table 3-6. NH₃-removing reactions. The reaction rates are in units of cm³·molecule⁻¹·s⁻¹.

Chemical Reaction	Rate at 298K	Rate law	Source
NH + NH ₃ → NH ₂ + NH ₂	High temp reaction	$5.25 \cdot 10^{-10} \cdot \exp[-13470/T]$	NIST
NH ₃ + CH → HCN + H ₂ + H	2.50×10^{-11}	$7.24 \cdot 10^{-11} \cdot \exp[-317/T]$	NIST
NH ₃ + CH ₃ → CH ₄ + NH ₂	High temp reaction	$9.55 \cdot 10^{-14} \cdot \exp[-4895/T]$	NIST
NH ₃ + CN → HCN + NH ₂	1.66×10^{-11}	$1.66 \cdot 10^{-11}$	NIST
NH ₃ + CNO → CO + N ₂ H ₃	1.20×10^{-14}	$6.29 \cdot 10^{-14} \cdot (T/298)^{2.48} \cdot \exp[-493/T]$	NIST

3.2.2.2 NH₃ Biological Sinks

On Earth, life is a significant sink for NH₃. Three biological processes are critical for NH₃ depletion by life: nitrification, anammox, and direct assimilation of NH₃ into nitrogen-containing organic building blocks of life (i.e., amino acids) (Figure 3-1). We discuss nitrification and anammox briefly below.

Nitrification is a process of oxidation of ammonia (NH₃) to nitrate (NO₃⁻) (Wendeborn 2020). NH₃ oxidizing bacteria and archaea harvest energy by aerobic oxidation of NH₃ to NO₃⁻ via a two-step process (Schimel et al., 2004). In the first step NH₃ is oxidized to NO₂⁻ by chemoautotrophs according to the following formula: $\text{NH}_3 + \text{O}_2 + 2\text{e}^- + 2\text{H}^+ \rightarrow \text{NO}_2^- + 4\text{e}^- + 5\text{H}^+$ ($\Delta G^\circ = -275 \text{ kJ mol}^{-1}$) (Daims et al., 2015, Caranto et al., 2017). In the second step NO₂⁻ is further oxidized to nitrate: $\text{NO}_2^- + \text{H}_2\text{O} \rightarrow \text{NO}_3^- + 2\text{H}^+ + 2\text{e}^-$ ($\Delta G^\circ = -74 \text{ kJ mol}^{-1}$) (Schimel et al., 2004; Daims et al., 2015). Nitrification is performed primarily by soil bacteria (e.g., *Nitrosomonas* sp., *Nitrospira* sp.).

The second major biological sink of NH₃ is called anammox. Anammox is a process of anaerobic oxidation of NH₃. Obligately anaerobic chemolithoautotrophs can perform anammox. (Kartal et al., 2011; Van Niftrik et al., 2012). According to the following formula, anammox-capable bacteria convert nitrite and ammonia directly to N₂ gas: $\text{NH}_4^+ + \text{NO}_2^- \rightarrow \text{N}_2 + 2\text{H}_2\text{O}$ ($\Delta G^\circ = -357 \text{ kJ} \cdot \text{mol}^{-1}$). Anammox is especially prominent in the oceans, even around hydrothermal vents along the Mid-Atlantic Ridge (Byrne 2009). Anammox is responsible for 50% of marine N₂ production (Strous et al., 2006; Devol, 2004).

3.3. Methods

We now describe our methods for assessing NH₃ as a biosignature gas. To study the biosignature potential of NH₃, we have to determine under which conditions can NH₃ accumulate in the atmosphere, considering NH₃'s high water solubility and high bio-usability. We first review solubility and Henry's law (Chapter 3.3.1). We then introduce our simplified ocean-NH₃ interaction model (Chapter 3.3.2), followed by a description of our one-dimensional photochemistry model (Chapter 3.3.3) and our transmission spectra model (Chapter 3.3.4).

3.3.1 Solubility and Henry's law

We use Henry's law to study the solubility of NH_3 . There are multiple ways to define Henry's law constant (R. Sander 2015). We choose the following form.

$$H_{(X)}^{CP} = \frac{C_{(X)}}{P} \quad \text{Eq. 3-4}$$

Here $H^{CP}(X)$ is Henry's law constant for a species X in $\text{mol}\cdot\text{Pa}^{-1}\cdot\text{m}^{-3}$. $C(X)$ is the dissolved concentration in the solution with units of $\text{mol}\cdot\text{m}^{-3}$. P is the partial pressure in Pascal ($1 \text{ atm} \cong 101325 \text{ Pa}$). Henry's law constant is also a function of temperature, which can be approximated by the van't Hoff equation.

$$\frac{d\ln(H^{CP})}{d(1/T)} = -\frac{\Delta H_{diss}}{R} \quad \text{Eq. 3-5}$$

Here T is the temperature in Kelvin, R is the universal gas constant in $\text{J}\cdot\text{K}\cdot\text{mol}^{-1}$, and ΔH_{diss} is the enthalpy change in dissolution. Since there is an inverse relationship between Henry's law constant and temperature, NH_3 will be more soluble as temperature decreases.

3.3.2 Ocean- NH_3 Interaction Model

To show that NH_3 can accumulate in the atmosphere when life is a net source of NH_3 and produces enough NH_3 to saturate the surface sinks, we use a simplified ocean- NH_3 interaction model. Specifically, we study the partitioning between the atmosphere and the ocean, assuming equilibrium chemistry.

Our model has two variables: the ocean pH and the planet's total NH_3 reserve maintained through biological production. We assume the exoplanet has an Earth-sized ocean, roughly $1.335 \times 10^{21} \text{ L}$ (Amante et al., 2009). Additionally, we assume there are no biological or geochemical sinks on the surface. In this case, the ocean is a reservoir. Once NH_3 dissolves in the ocean, it will react with water to form NH_4^+ and OH^- ions. We calculate the dissolved ammonia concentration ($[\text{NH}_3]$) and the ammonium ion concentration ($[\text{NH}_4^+]$) by using the Henderson-Hasselbalch equation.

$$\text{pH} = \text{pK}_a + \log_{10}\left(\frac{[\text{NH}_3]}{[\text{NH}_4^+]}\right) \quad \text{Eq. 3-6}$$

Ammonia has a pK_a (acid dissociation constant at log scale) of about 9.25 (David R. Lide et al., 2005). We can derive $[\text{NH}_3]$ by solving the system of equations,

$$\frac{[NH_3]}{[NH_4^+]} = 10^{(pH-9.25)} \quad \text{Eq. 3-7}$$

$$[NH_3] + [NH_4^+] = \frac{T_{NH_3}}{V_{Ocean-E}} \quad \text{Eq. 3-8}$$

Here pH is the ocean's overall pH, T_{NH_3} is the planet's total NH_3 reserve in mol, and $V_{Ocean-E}$ is the volume of the Earth's ocean in liters. We solve $[NH_3]$ and express it as a function of pH and the planet's total NH_3 reserve.

$$[NH_3] = \frac{T_{NH_3} \cdot 10^{pH}}{(1.77828 \times 10^9 + 1 \times 10^{pH}) \cdot V_{Ocean-E}} \quad \text{Eq. 3-9}$$

Using Henry's law (Eq. 3-1), we calculate NH_3 partial pressure from $[NH_3]$ and plot NH_3 volume mixing ratio as a function of pH and T_{NH_3} .

3.3.3 Photochemistry Model

We use our photochemistry code (Hu et al., 2012) to calculate the NH_3 mixing ratio as a function of vertical altitude in exoplanet atmospheres. In this section, we briefly describe how we use this computational approach to explore atmospheric NH_3 accumulation.

Our photochemistry code (Hu et al., 2012) can simulate a wide variety of planetary atmosphere scenarios by calculating the atmosphere's steady-state chemical composition. Our full photochemistry model encodes more than 800 chemical reactions and UV photolysis of atmospheric molecules. Our model also includes both wet and dry depositions, thermal escape of O, C, H, N, and S containing molecules, surface emission, and formation and deposition of sulfur-bearing (both elemental sulfur and sulfuric acid) aerosols. The one-dimensional chemical transport model has been validated by simulating modern Earth's and Mars' atmospheric composition, matching observations of major trace gases in both scenarios. We can flexibly implement this model to simulate oxidized, oxic, and reduced atmospheres. Both ultraviolet and visible radiation in the atmosphere is computed by the delta-Eddington two-stream method. This model also includes molecular absorption, Rayleigh scattering, and aerosol Mie scattering to compute the optical depth. For applications of our photochemistry code, see (Hu et al., 2012, Seager et al., 2013(a)(b), Hu et al., 2013, Sousa-Silva et al., 2020, Zhan et al., 2021).

In this work, we consider an exoplanet orbiting an M dwarf star (M5V). We use the stellar radiation model of GJ 876 (Lloyd et al., 2016; France et al., 2016). We study three different atmospheric scenarios: N_2 -dominated weakly oxidizing atmospheres, CO_2 -dominated highly oxidizing atmospheres, and H_2 -dominated reducing atmospheres. For exoplanets with N_2 -dominated, CO_2 -dominated, and H_2 -dominated atmospheres, the semi-major axes are 0.026 AU, 0.034 AU, and 0.042 AU, respectively. We choose the semi-major axes to ensure the surface temperature is maintained at 290 K across all scenarios. We model

massive super-Earths with $10 M_{\text{Earth}}$ and $1.75 R_{\text{Earth}}$ because these large planets are more likely to retain an H_2 -dominated atmosphere than Earth-mass planets due to a higher escape velocity.

In each atmosphere scenario, we consider two cases: one with NH_3 deposition (both dry deposition and rainout included) and one without NH_3 deposition (dry deposition and rainout are both set to 0). In both cases, we assume the atmospheric NH_3 is maintained through biological production (i.e., life is a net source of NH_3). The case with NH_3 deposition corresponds to active NH_3 -removal sinks on the surface, where the surface is not saturated with NH_3 . The case without NH_3 deposition corresponds to conditions in which life produces enough NH_3 to saturate the surface sinks. In this case, the ocean is a reservoir of NH_3 , and NH_3 is only removed by photochemistry.

For each of the scenarios we study, we set the planet's surface pressure to 1 bar and temperature to 288 K. We divide the atmosphere into two layers: a lower convective layer and a higher radiative layer (Hu et al., 2012). We set the temperature of the convective layer to follow the dry adiabatic lapse rate. We set the stratospheric temperature in our model according to (Hu et al. 2012). We set the temperature above tropopause to 160K, 200K, and 175K for the H_2 -dominated, N_2 -dominated, and CO_2 -dominated atmosphere. For an H_2 -dominated atmosphere, we assume the stratosphere is very cold due to efficient radiative cooling from abundant H_2 (Birnbaum et al. 1996). Since we do not have a climate model coupled with our photochemistry code, we do not consider heating in the upper atmosphere. Hence, we assume the temperature to be constant (isothermal) in the radiative layer (Hu et al., 2012). The temperature profiles we set are consistent with significant greenhouse effects in the convective layer (Hu et al., 2012).

To study NH_3 as a biosignature gas, we only use 735 reactions in our simulations. Specifically, we include all the reactions mentioned in (Hu et al., 2012), except for reactions that involve more than 2 carbon atoms ($\text{C}_{>2\text{-chem}}$), high-temperature reactions (Hu et al., 2012), and HSO_2 thermal decay. Furthermore, we do not consider rainout and biological sinks for H_2 , CO , CH_4 , N_2 , C_2H_2 , C_2H_4 , C_2H_6 , and O_2 . We make the assumptions mentioned above to facilitate robust comparison to our reference benchmark scenarios from (Hu et al., 2012). We present our simulation parameters (including the stellar spectrum input, atmospheric temperature-pressure profiles, the eddy diffusion profiles, and the planetary surface boundary information) in Appendix A.

3.3.4 Transmission Spectra Model and Simulated Observation

To assess future possibilities for the detection of NH_3 in each of the exoplanet atmospheric scenarios, we simulate transmission spectra for each scenario using our "Simulated Exoplanet Atmosphere Spectra" (SEAS) code (Zhan et al., 2021). We simulate atmospheric detection using the community JWST exposure time calculator and noise simulator Pandexo (Batalha et al., 2017) and assess the confidence in detecting NH_3 for each given scenario via a reduced chi-squared test.

3.3.4.1 Simulated Exoplanet Atmosphere Spectra Model (SEAS)

The SEAS transmission code takes in the output of the photochemistry code (temperature-pressure profiles and mixing ratio profiles) and calculates the optical depth along the limb path (Seager et al., 2013(a)(b); Zhan et al., 2021). The SEAS transmission code has been validated by reproducing Earth’s atmosphere spectra by comparing the SEAS simulated results with data from the Atmospheric Chemistry Experiment database (Bernath et al., 2005). Currently, our SEAS code does not have refraction. Hence our transmission spectra model works best for M dwarf planets, where refraction has a minimum impact on observations (Misra et al., 2014, B  tr  mieux et al., 2014). Details of the code are described in (Zhan et al., 2021). Here we provide a very brief description of the transmission code.

We divide the entire atmosphere (from the surface to the top of the atmosphere) into layers, and the width of each layer is one atmospheric scale height. Within each layer, we assume the atmosphere is in local thermodynamic equilibrium (LTE). The stellar radiation will penetrate along each layer's limb path, which we approximate as stellar radiation passing through multiple LTE chunks. We calculate the absorption along each beam path by using the following equation.

$$A = n_{i,j} \times \sigma_{i,j} \times l_i \quad \text{Eq. 3-10}$$

Here A is absorption, n is number density, σ is absorption cross-section, and l is the path length. The subscript i denotes each chunk, and subscript j denotes each molecule. We then compute the transmittance (T) of each beam by using the Beer-Lambert law. The amount of flux attenuated along each beam's path is determined by multiplying the absorbance (1-T) by each base chunk's scale height. Finally, we calculate the transit depth of the atmosphere by summing all the attenuated fluxes.

3.3.4.2 Simulated Exoplanet Observation

We assess an exoplanet atmospheres' detectability by using the metrics described in (Seager et al., 2013(a)(b)), (Batalha et al., 2017), and (Zhan et al., 2021). We calculate the signal-to-noise ratio (SNR) of an atmosphere using the following equation.

$$SNR = \frac{|F_{out} - F_{in}|}{\sqrt{\sigma_{F_{out}}^2 + \sigma_{F_{in}}^2}} \quad \text{Eq. 3-11}$$

F_{in} is the flux density within the absorption feature, F_{out} is the flux density of the surrounding continuum of the feature, and $\sigma_{F_{out}}$ and $\sigma_{F_{in}}$ is the respective uncertainty. More specifically, we calculate the uncertainty using the Pandexo JWST instrumental noise calculator using the NIRSspec (G140M, G235M, G395M) and MIRI (LRS) observation modes. The two instruments combined provided a spectral coverage from 1 to about 13 μm .

To analyze the transmission detectability of weakly oxidizing (N_2 -dominated), highly oxidizing (CO_2 -dominated), and reducing (H_2 -dominated) atmospheres (Chapter 3.3.3), we

consider a $10 M_{\text{Earth}}$, $1.75 R_{\text{Earth}}$ Super-Earth orbiting a host star with a visual magnitude of 10. The central star can be either a Sun-like (G) star or a $0.2 R_{\text{Sun}}$ M dwarf star. To observe a terrestrial exoplanet's atmosphere, we explore a total integration time between 10 transits and 100 transits (which may be impractical for G stars, but we include it for comparison).

3.3.4.3 Detection Assessment Metrics

We compare the difference in SNR to assess whether it is possible to distinguish between an H_2 -dominated atmosphere with and without a significant NH_3 surface flux (Chapter 3.4.4). We assess whether the models are good fits for the simulated observational data. We use the following equation to compute the reduced chi-square statistics between the data with several different models.

$$\chi_v^2 = \frac{\chi^2}{v} = \frac{1}{v} \cdot \left[\sum_i \frac{(O_i - C_i)^2}{\sigma_i^2} \right] \quad \text{Eq. 3-12}$$

Here χ_v^2 is the reduced chi-square, v is the degree of freedom (or the number of wavelength bins), χ^2 is the chi-square, O_i is simulated observational data, C_i is the simulated model, σ_i is the variance (or error as calculated from Pandexo noise simulator for a specific instrument), and finally i denotes each wavelength bin. We note that binning the spectra reduces the variance at the expense of reducing the degree of freedom. Due to NH_3 containing multiple broadband spectral features (peaks around $1.5 \mu\text{m}$, $2 \mu\text{m}$, $2.3 \mu\text{m}$, $3 \mu\text{m}$, $6 \mu\text{m}$, and $10 \mu\text{m}$), in practice, we find bin the spectra to a resolution of $R = 10 \sim 20$ is a good balance between maximizing SNR and preserving spectral information.

More specifically, we first apply a null-hypothesis test to see if the data can be explained by a straight line (i.e., no atmosphere can be detected). If the null hypothesis can be ruled out, we then compare the data for models with a variety of NH_3 (column-averaged mixing ratio from 0.1 ppm to 100 ppm) and assess which model best fits the data.

3.4. Results

In this section, we assess the possibility of NH_3 accumulation to detectable levels in various planetary scenarios. In brief, we find that NH_3 can theoretically accumulate the JWST detectable level in the atmosphere with a reasonable surface production flux (i.e., comparable to the terrestrial biological production of CH_4) only when life is a net source of NH_3 and produces enough NH_3 to saturate the surface sinks.

We first illustrate NH_3 's high water solubility by comparing NH_3 's Henry's law constant with other representative gases (Chapter 3.4.1). Using our simplified ocean- NH_3 interaction model and considering the atmosphere-ocean partitioning of NH_3 , we demonstrate that NH_3 can theoretically accumulate if there are no NH_3 -removal sinks on the surface (Chapter 3.4.2). Utilizing our transmission spectra model, we learn that detection of NH_3 is possible for exoplanets with H_2 -dominated atmospheres using JWST if the NH_3 column-averaged

mixing ratio reaches 5 ppm (Chapter 3.4.3). Finally, we run our photochemistry code to quantify the NH₃ flux needed to reach the 5 ppm detection limit under various planetary atmosphere conditions (Chapter 3.4.4).

3.4.1 NH₃'s High Water Solubility Limits its Ability to Accumulate in the Atmosphere

NH₃ is highly water-soluble, at least two orders of magnitude more soluble than other planetary atmospheric gases. NH₃'s high water solubility means that atmospheric accumulation of NH₃ is highly dependent on whether there are active NH₃-removal sinks on the surface (i.e., whether the surface is saturated with NH₃). When life does not produce enough NH₃ to saturate the surface sinks, rain (wet deposition) can much more efficiently remove NH₃ from the atmosphere than other gases, limiting NH₃'s ability to accumulate in the atmosphere.

We can quantitatively compare the solubility of different gases to each other based on Henry's law constants. Since Henry's law constant is a measure of solubility in water, the larger Henry's law constant, the more water-soluble the gas is. We summarize Henry's law constants for some representative gases at standard temperature and pressure (T = 298.15K and P ≈ 1atm) in Table 3-7 (R. Sander, 2015).

Table 3-7. Henry's law constant for some representative gases in water (R. Sander et al., 2015).

Chemical species	H ^{CP} [$\frac{\text{mol}}{\text{Pa}\cdot\text{m}^3}$]
Ammonia NH ₃	5.90×10^{-1}
Dimethyl Sulfide CH ₃ SCH ₃	5.34×10^{-3}
Methyl Chloride CH ₃ Cl	1.15×10^{-3}
Carbon dioxide CO ₂	3.36×10^{-4}
Isoprene C ₅ H ₈	1.53×10^{-4}
Nitrogen dioxide NO ₂	1.20×10^{-4}
Phosphine PH ₃	7.00×10^{-5}
Methane CH ₄	1.41×10^{-5}
Oxygen O ₂	1.30×10^{-5}
Hydrogen H ₂	7.75×10^{-6}
Nitrogen N ₂	6.43×10^{-6}
Helium He	3.83×10^{-6}

The high solubility of NH₃ and other amines (especially aliphatic amines) in water is due to their ability to form hydrogen bonds with water molecules and themselves. Even tertiary amines (three substituents are connected to N) can form hydrogen bonds between the lone pair of electrons carried by the central nitrogen atom and the H in a water molecule that carries a partial positive charge. As a result, NH₃ and other volatile amines are much more soluble than any previously studied biosignature gas candidates (Figure 8).

3.4.2 NH₃ Can Accumulate if Life Produces Enough NH₃ to Saturate the Surface

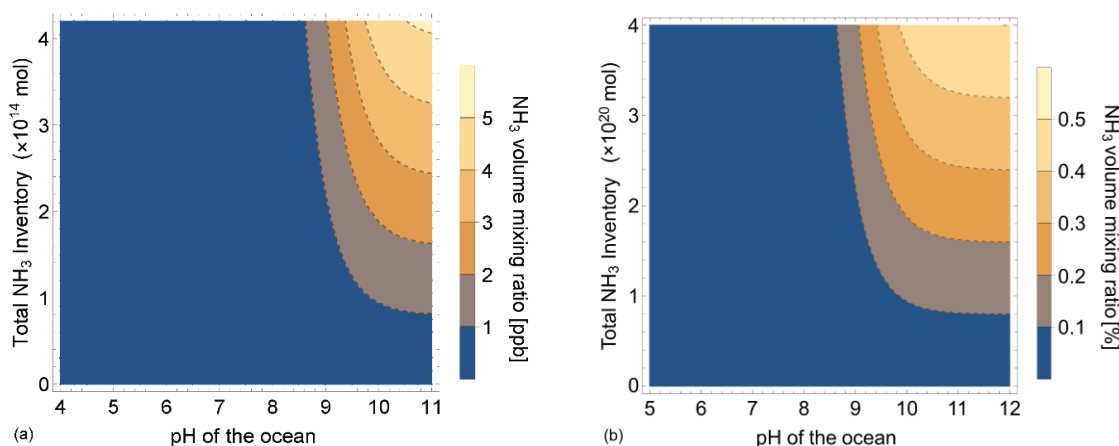
Using our simplified ocean-NH₃ interaction model, we find that NH₃ can theoretically

accumulate to a detectable level in the atmosphere when life is a net source of NH_3 and produces enough NH_3 to saturate the surface sinks. By detectable level, we mean a volume mixing ratio of 5 ppm (see Chapter 3.4.3 for a detailed assessment of detectability of NH_3).

To reach this conclusion, we assess how ocean-atmosphere equilibrium NH_3 partial pressure changes with the planet's total NH_3 reserve and ocean pH. As a reminder, we assume the atmospheric NH_3 is maintained through biological production (as postulated by Seager et al., 2013). We also assume no NH_3 -removal sinks on the land and in the ocean (see Chapter 3.3.2).

We find that life must produce enough NH_3 to maintain an NH_3 inventory of 6×10^{18} mol to reach a detectable level (5 ppm) in the atmosphere. This inventory is 10,000 times that of Earth's (1×10^{14} mol). One might ask if there is enough N to support such a sizeable NH_3 inventory. The answer is yes, compared with Earth's total N reservoir estimated at 4×10^{20} mol (Ranjan et al., 2019, Johnson et al., 2015). About $\sim 1.5\%$ of such a total N reservoir would be needed. Life on such planets² can theoretically maintain this NH_3 inventory by breaking down N_2 and H_2 gas to form NH_3 , analogous to the Haber–Bosch process (Seager et al., 2013(b)).

In our model, the planet's total NH_3 reserve is limited by the planet's total N reservoir. Unfortunately, the upper bound of the total N reservoir cannot be known for an exoplanet. Here, we assume the planet has an Earth-sized total N reservoir of 4×10^{20} mol. In an extreme situation where life manages to convert almost all of the planetary N reservoir into NH_3 , the NH_3 volume mixing ratio can reach 0.5% (Figure 3-3). In this case, NH_3 becomes one of the major chemical species in the atmosphere, and the ocean becomes basic. However, if life cannot produce a substantial amount of NH_3 and only maintain an Earth-like NH_3 inventory ($\sim 10^{14}$ mol), NH_3 will not be detectable regardless of the ocean's pH levels (Figure 3-3).



² We note that H_2 -dominated atmospheres are not detrimental for life and that life can survive and thrive in an H_2 -dominated environment (Seager et al., 2020).

Figure 3-3. Equilibrium volume mixing ratio of NH_3 as a function of the planet's total NH_3 reserve and ocean pH. The x-axis is the ocean pH, and the y-axis is the planet's total NH_3 reserve in mol. The contours are NH_3 volume mixing ratios. We assume the planet has an Earth-sized total N reservoir (4×10^{20} mol) and an Earth-sized ocean (1.335×10^{21} L). (a): If life cannot produce a substantial amount of NH_3 and only maintain an Earth-like NH_3 inventory ($\sim 10^{14}$ mol), the NH_3 volume mixing ratio is extremely low regardless of the ocean pH level ($4 \leq \text{pH} \leq 11$). (b): If life manages to convert almost all of the planetary N reservoir into NH_3 ($\sim 10^{20}$ mol), NH_3 will become one of the major chemical species in the atmosphere.

3.4.3 Detectability of NH_3 in Transmission Spectra

We study the detectability of NH_3 in transmission spectra using our ‘Simulated Exoplanet Atmosphere Spectra’ (SEAS) code. For exoplanets with H_2 -dominated atmospheres orbiting M dwarf stars (M5V), we find that a minimum of about 5 ppm column-averaged mixing ratio is needed to detect NH_3 with JWST, considering NH_3 's $1.5 \mu\text{m}$ feature and a 10 ppm JWST systematic noise floor (Figure 10). Furthermore, we find that exoplanets with high molecular-weight atmospheres (i.e., CO_2 -dominated and N_2 -dominated atmospheres) and those orbiting Sun-like stars have atmosphere signals too weak to be detected by JWST.

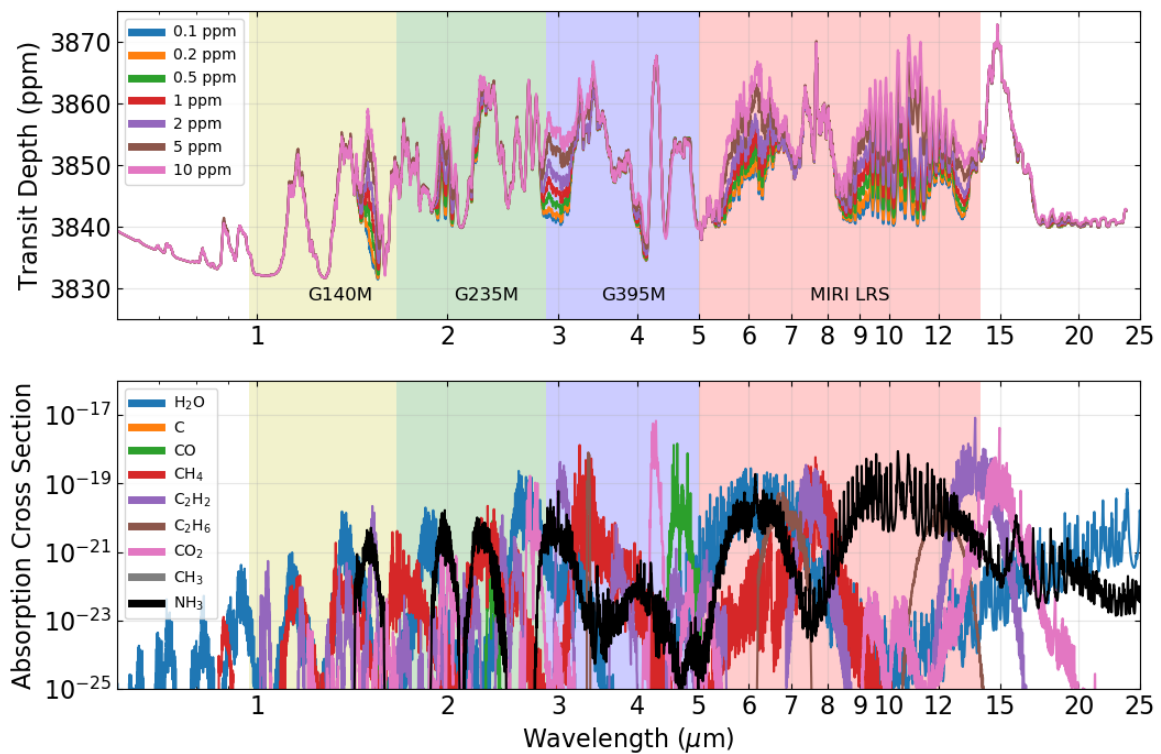


Figure 3-4. Simulated spectra of an exoplanet with an H₂-dominated atmosphere transiting an M5V star for a range of NH₃ column-averaged mixing ratios. The y-axis shows transit depth (ppm), and the x-axis shows wavelength (μm). The spectra are simulated from 0.3 - 23 μm, covering the wavelength span of most of JWST’s observation modes. The yellow, green and blue region shows the spectral coverage of NIRSpec, and the red region shows that of MIRI LRS. We simulate the spectra with varying NH₃ column-averaged mixing ratios from 0 (no NH₃) to 10 ppm. We calculate the NH₃ mixing ratio as a function of vertical altitude using our photochemistry code (Chapter 3.3.3). At lower surface mixing ratios, the NH₃ spectral features are not prominent as NH₃ is mostly concentrated near the surface and rapidly decays as a function of altitude. Increasing the abundance of NH₃ amplifies the spectral feature of NH₃, as more NH₃ can accumulate in the upper part of the atmosphere.

For exoplanets with high molecular-weight atmospheres (i.e., CO₂-dominated and N₂-dominated atmospheres), the transit depth resulting from the small atmosphere scale height is too small compared to the assumed 10 ppm JWST observational noise floor. Similarly, for exoplanets orbiting Sun-like stars, the transit depth (around 2 ~ 3 ppm for H₂-dominated atmospheres) is too small given the size of the host star. To support this argument, we conduct a null hypothesis test. We check whether our model is a better fit than a flat line. We find that only exoplanets with H₂-dominated atmospheres orbiting M5V stars pass this test³.

To demonstrate that a minimum of about 5 ppm is needed for NH₃ to be detected, we simulate JWST observations using the Pandexo JWST noise simulator with a detection noise floor of 10 ppm and a realistic noise model for JWST instrumentation (Batalha et al., 2017). We compare a simulated spectrum with 5 ppm of NH₃ and a spectrum with no NH₃ (Figure 3-5). We find that the spectrum with 5 ppm of NH₃ has spectral features 10 ~ 40 ppm larger than the spectrum with no NH₃. The inclusion of detection noise is the main reason why our 5 ppm detection limit is higher than the 0.1 ppm value stated in (Seager et al., 2013).

³ Except for TRAPPIST-1 planets (details see Appendix I)

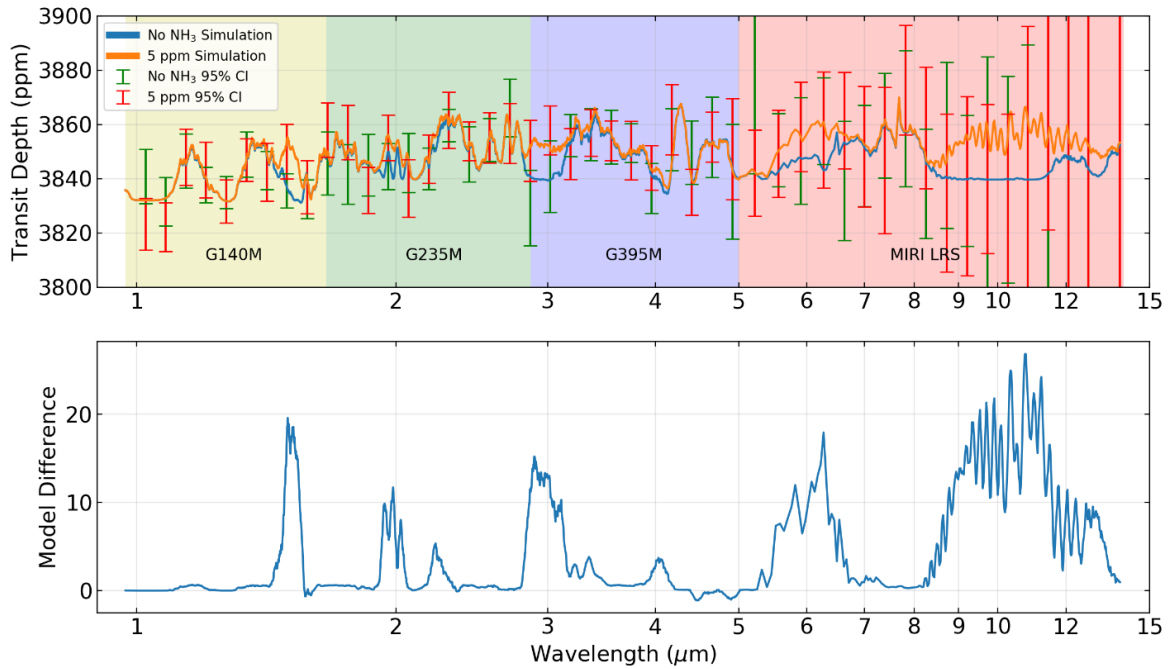


Figure 3-5. Upper Panel: Simulated JWST exoplanet atmosphere observation for a $10 M_{\text{Earth}}$, $1.75 R_{\text{Earth}}$ super-Earth with an H_2 -dominated atmosphere transiting an M5V star given 20 transit per instrument (80 transits in total), and comparing a model with no surface NH_3 (blue line) and a model with a column average mixing ratio of 5 ppm (orange line), which we also show in Figure 4. The y-axis shows transit depth (ppm), and the x-axis shows wavelength (μm). The simulated observation spans the wavelength range of the NIRSpec and MIRI instruments. The error bars are 95% confidence interval for each model with 5 ppm NH_3 (red) and green for no NH_3 (green) uniformly binned to a spectral resolution of $R=10$. We show that the difference between the two models achieves statistical significance within each instrument, indicating a confident simulated detection of NH_3 . **Lower Panel:** Model difference in ppm between the two simulated spectra showing the spectral feature of NH_3 peaks around 1.5 μm , 2 μm , 3 μm , 6 μm , and 10 μm . Negative values denote that the increase of NH_3 caused a decrease of CH_4 in the atmosphere.

Even though we find that a minimum of about 5 ppm is needed for NH_3 to be detected, with one JWST instrument (e.g., NIRSpec) and one mode (i.e., G395M, which encompasses the NH_3 's 3 μm feature), constraining the amount of NH_3 will be challenging. A better quantification is possible with more modes covered. We have analyzed an ideal case with observations of all NH_3 spectral features in the wavelength range of 1.6 to 10 μm (three modes of NIRSPEC and MIRI LRS, i.e., 80 transits). In this case, we can further constraint the NH_3 mixing ratio to 1 ~ 10 ppm.

For illustration purposes, we also show an instance of a simulated observation of an exoplanet with H_2 -dominated atmospheres transiting an M5V star, with both a reasonable number of transits (20 transits; Figure 3-5) and the maximum theoretical observation time possible (200 transits; Figure 3-6). The maximum observation time means considering nearly every visible transit for an orbital period corresponding to the habitable zone of an M5V star (i.e., one transit every 10 days for five years based on Kepler's 3rd law). While such a 200 transit-observation is unrealistic (due to the competitive nature of JWST), Figure 12 illustrates what quality of data 200 transits would provide.

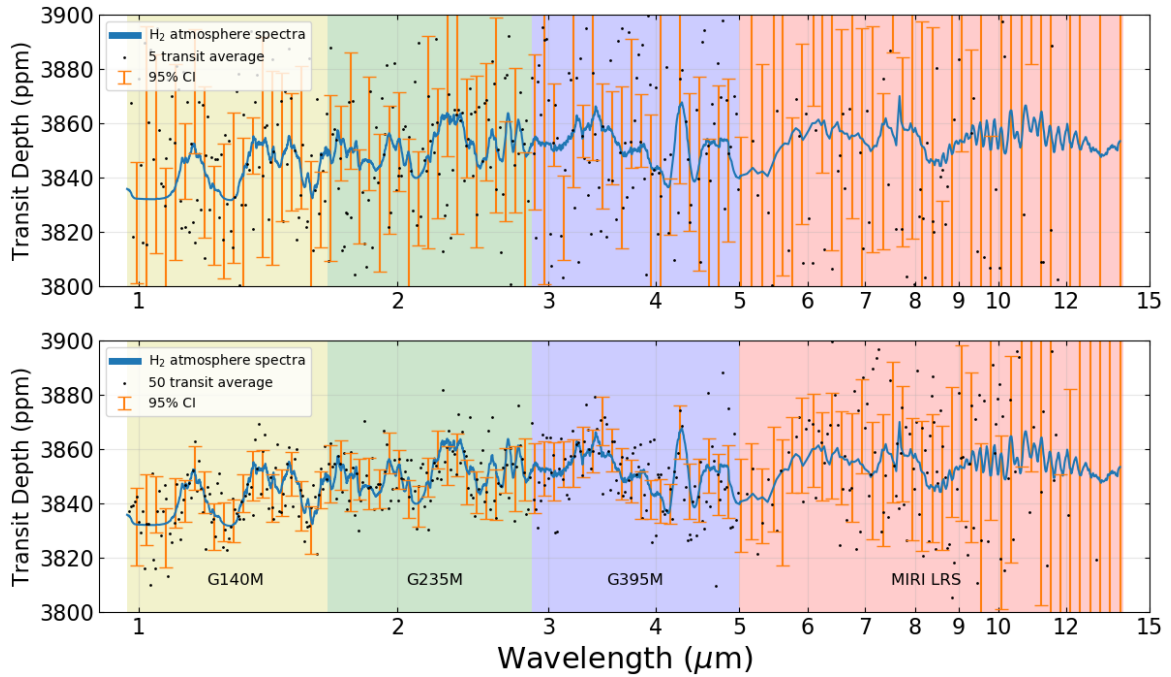


Figure 3-6. Comparison between 20 and 200 transits for simulated JWST exoplanet atmosphere observations for a $10 M_{\text{Earth}}$, $1.75 R_{\text{Earth}}$ super-Earth with H_2 -dominated atmosphere transiting an M5V star. Similar to Figure 3-5, the model shows a planet with a 5 ppm column-averaged mixing ratio of NH_3 . **Upper panel:** simulation for 20 transit observations (5 transits per instrument modes) and $R = 20$. The y-axis shows transit depth (ppm), and the x-axis shows wavelength (μm). The simulated observation focuses on the wavelength span of NIRSpec G140M (yellow), G235M (green), G395M (blue), and MIRI LRS (red), respectively. The blue line is the simulated transmission spectra, and the black dots are the average of all transits. The orange error bars represent the 95% confidence interval of the observation. **Lower panel:** same as the upper panel but for 200 transits (50 per mode). This simulation assumes the maximum observation time possible with JWST (200 transits, spanning across 5 years), and spectral features of various molecules can be characterized to high confidence.

3.4.4 Variability of NH_3 Atmospheric Accumulation in Various Planetary Scenarios

We use our photochemistry model to simulate the NH_3 mixing ratio as a function of vertical altitude in various planetary atmosphere scenarios. We first demonstrate that NH_3 can accumulate in the atmosphere with a reasonable surface production flux only when life produces enough NH_3 to saturate the surface sinks (Chapter 3.4.4.1). We also show the effect of the NH_3 surface deposition on atmospheric NH_3 mixing ratio given a fixed NH_3 surface production flux (Chapter 3.4.4.2).

3.4.4.1 Conditions Required for NH_3 to Accumulate with a Reasonable Surface Production Flux

We find that NH_3 can accumulate to the 5 ppm JWST-detectable level in the atmosphere with a reasonable surface production flux only if life is a net source of NH_3 and produces

enough NH₃ to saturate the surface sinks. In this case, there are no NH₃-removal sinks on the surface, and NH₃ is only removed by photochemistry (i.e., no dry deposition or rainout).

Specifically, for an exoplanet with H₂-dominated atmospheres orbiting an M dwarf star, when the surface is saturated with NH₃ (i.e., there are no NH₃-removal sinks on the surface), the required biological surface flux to reach 5 ppm is on the order of 10¹⁰ molecules cm⁻² s⁻¹, comparable to the terrestrial biological production of CH₄. However, when the surface is unsaturated with NH₃, due to additional sinks present on the surface, life would have to produce NH₃ at surface flux levels on the order of 10¹⁵ molecules cm⁻² s⁻¹ (~4.5×10⁶ Tg year⁻¹). This value is roughly 20,000 times greater than the biological production of NH₃ on Earth and about 10,000 times greater than Earth's CH₄ biological production.

Table 3-8. Simulated mixing ratios and surface fluxes for exoplanets with H₂-dominated, CO₂-dominated, and N₂-dominated atmospheres orbiting M dwarf stars (M5V).

Atmospheric scenarios	NH ₃ column-averaged mixing ratio	NH ₃ surface flux needed [molecules cm ⁻² s ⁻¹]	
		With NH ₃ deposition	Without NH ₃ deposition
H ₂ -dominated	5.0 × 10 ⁻⁶ (5 ppm)	6.40 × 10 ¹⁵	1.44 × 10 ¹⁰
CO ₂ -dominated	5.0 × 10 ⁻⁶ (5 ppm)	3.60 × 10 ¹⁴	8.49 × 10 ⁸
N ₂ -dominated	5.0 × 10 ⁻⁶ (5 ppm)	7.10 × 10 ¹⁴	6.77 × 10 ¹⁰

As a reminder, we assume the atmospheric NH₃ is maintained through biological production in our simulations. The case with NH₃ deposition corresponds to active NH₃-removal sinks on the surface, where the surface is not saturated with NH₃. The case without NH₃ deposition corresponds to conditions in which life produces enough NH₃ to saturate the surface sinks (see Chapter 3.3.3). We include the N₂- and CO₂-dominated scenario for completeness even though we show exoplanets with high molecular-weight atmospheres (i.e., CO₂-dominated and N₂-dominated atmospheres) have atmosphere signals too weak to be detected by JWST (see Chapter 3.4.3 for more details).

Additionally, we find that the dominant photochemical removal pathway for NH₃ is direct photolysis, followed by reactions with OH radicals. Except in CO₂-dominated atmospheres, the second dominant removal pathway is reactions with excited O radicals. We compile the top three loss rates for NH₃ in Table 3-15 (see Appendix E).

To test our photochemistry results' robustness, we perform various sensitivity tests (including the presence of a cold trap, the choice of eddy diffusion coefficient, and Henry's law constant for NH₃). We find that our results are not sensitive to any of these variables (see Appendix F). Furthermore, we find that NH₃ is insufficiently abundant to condense in our simulated atmospheres (see Appendix G).

3.4.4.2 Effects of NH₃ Surface Deposition on Atmospheric NH₃ Mixing Ratio

Given a fixed NH₃ surface production flux, the presence of NH₃ surface deposition has a significant effect on the atmospheric NH₃ mixing ratio. Specifically, the atmospheric mixing ratio of NH₃ is several orders of magnitude lower with deposition than without

(Figure 3-7).

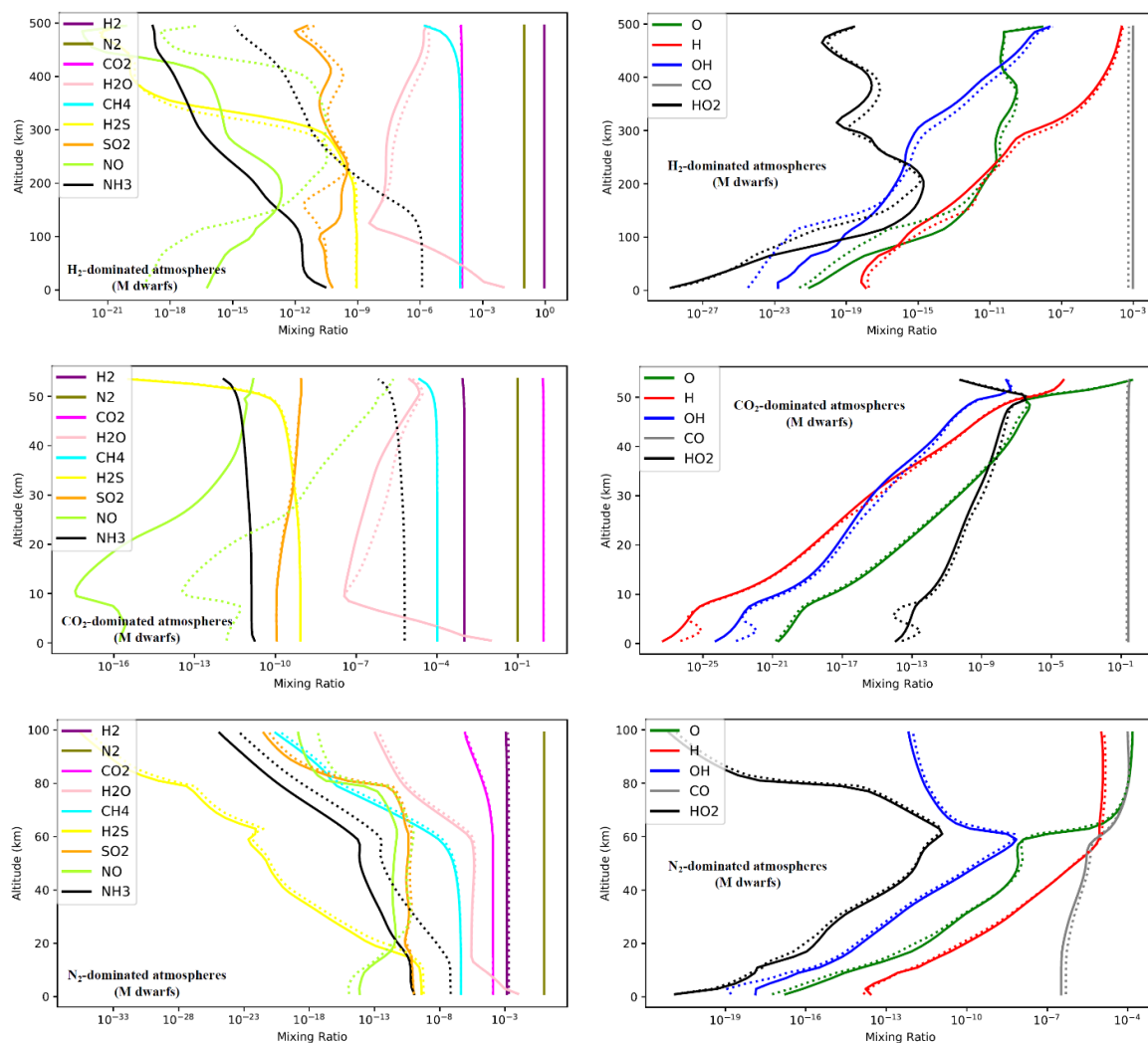


Figure 3-7. The volume mixing ratio of various atmospheric species on planets with H₂-dominated, CO₂-dominated, and N₂-dominated atmospheres orbiting active M dwarfs. The NH₃ surface production flux is 1.0×10^{10} molecule·cm⁻²·s⁻¹ for the H₂- and N₂-dominated atmospheres. For the CO₂-dominated case, the flux is 1.0×10^9 molecule·cm⁻²·s⁻¹. The y-axis shows altitude in km, and the x-axis shows the mixing ratio. Note that each row of figures has a different x-axis scale. Each color denotes one particular species. The dotted lines for NH₃ deposition absent, and solid lines for NH₃ deposition present. The figures in the left panel show molecular concentrations, and the figures in the right panel show radical concentrations under different atmospheric scenarios. In each of the three atmospheric scenarios we simulate, the solid black curve (NH₃ mixing ratio with deposition) is shifted further to the left (smaller mixing ratio) compared to the dotted black curve (NH₃ without deposition) since NH₃ deposition suppresses atmospheric NH₃ concentration. Note that the solid curves for species other than NH₃ show the effects of NH₃ deposition on the atmospheric concentration of other species.

When life cannot produce a substantial amount of NH₃, the surface remains unsaturated with NH₃. Hence, surface deposition (both rainout and dry deposition) effectively removes NH₃ from the atmosphere. If life produces enough NH₃ to saturate the surface, surface

deposition no longer plays a role, and NH_3 is only removed by photochemistry.

The effect of surface deposition on NH_3 mixing ratio differs between the H_2 -, N_2 - and CO_2 -dominated atmospheres. Specifically, we find that rainout (i.e., wet deposition) is most effective in H_2 -dominated atmospheres compared to N_2 - or CO_2 -dominated atmospheres. The difference in atmospheric NH_3 mixing ratio with and without surface deposition⁴ can reach six orders of magnitude. The effect of rainout is most significant in H_2 -dominated atmospheres due to the thermodynamics of H_2 . The tropospheric lapse rate is lower in H_2 -dominated atmospheres than either CO_2 - or N_2 -dominated atmospheres, driving higher temperatures, higher water content, and higher rainout rates.

Even though surface deposition (particularly rainout) is not as effective in CO_2 -dominated atmospheres as H_2 -dominated atmospheres, surface deposition can make a massive difference in the NH_3 mixing ratio in CO_2 -dominated atmospheres. In the absence of surface deposition, NH_3 concentrations are the lowest in the relatively oxidizing CO_2 -dominated atmospheres (compared to the N_2 - and H_2 -dominated atmospheres), as one might naively expect on the grounds of simple thermodynamics. With the presence of surface deposition, NH_3 concentrations are the highest in the CO_2 -dominated atmospheres. The reason is that the wet deposition rate decreases as temperature and atmospheric water content decreases (Giorgi & Chameides 1985; Hu et al., 2012, Equation 21). The relatively high lapse rate of CO_2 -dominated atmospheres suppresses both temperature and atmospheric water content, reducing rainout and enhancing NH_3 concentrations relative to the N_2 - and H_2 -dominated atmospheric scenarios.

3.5. Discussion

We first compare NH_3 's solubility in water with other atmospheric gases, particularly several previously studied biosignature gases (Chapter 3.5.1). We next discuss how horizontal atmospheric transport might limit NH_3 accumulation above land (Chapter 3.5.2). We also discuss other minor sources and sinks of ammonia, including NH_3 production by lightning (Chapter 3.5.3) and additional ocean-related sinks for dissolved NH_3 and NH_4^+ ions (Chapter 3.5.4). We discuss amines viability as biosignature gases by proxy with NH_3 (Chapter 3.5.4 and Chapter 3.5.6). Additionally, we briefly discuss NH_3 induced hazes (Chapter 3.5.7), NH_3 's greenhouse effect (Chapter 3.5.8), and NH_3 detectability with future telescopes (Chapter 3.5.9). We end our discussion with a brief comparison of the significance of atmospheric NH_3 in mini-Neptunes vs. super-Earths (Chapter 3.5.10).

3.5.1 Ammonia's High Water Solubility Compared to Other Atmospheric Gases

We compare ammonia's solubility to that of 27 other gases, a list that includes common atmosphere gases, biosignature gases, and a group of volatile amines (Figure 3-8).

⁴ NH_3 dry deposition velocity is the same for all the scenarios.

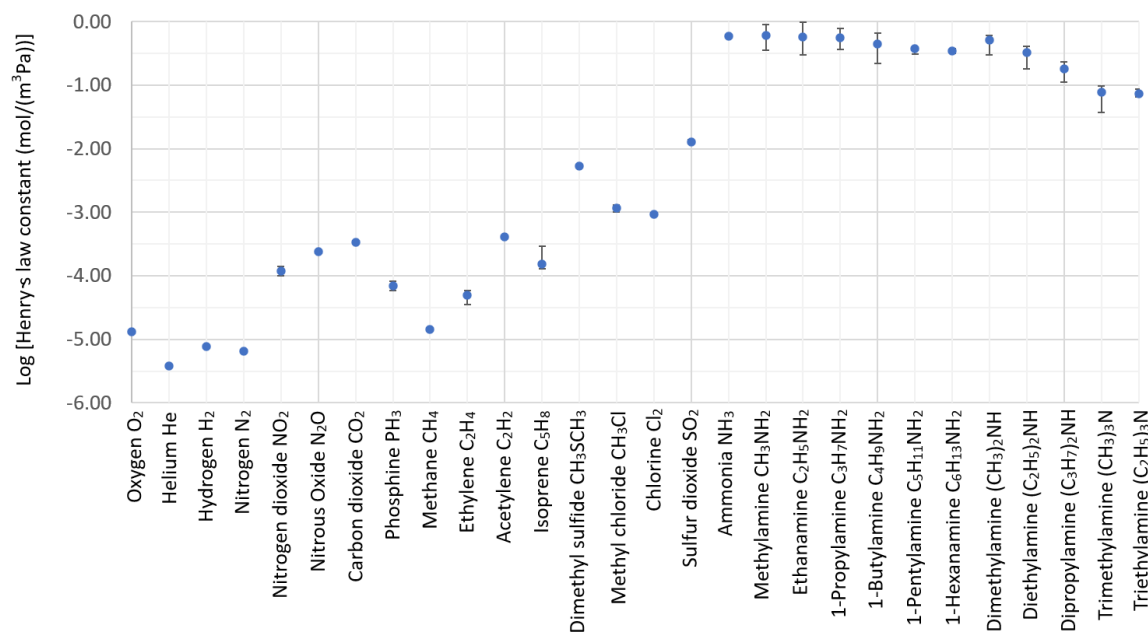


Figure 3-8. The solubility of common molecules on a log scale. The x-axis shows the chemical species' name, and the y-axis shows Henry's law constant on a log scale. Ammonia and other amines are at least two orders of magnitude more soluble than other chemicals in the list, including several biosignature gas candidates that have already been studied.

In contrast to ammonia and volatile amines, previously studied biosignature gases such as isoprene (Zhan et al., 2021), DMS (Domagal-Goldman et al., 2011, Seager et al., 2012, and Arney et al., 2018), CH₄ (Dlugokencky et al., 2011), N₂O (Tian et al., 2015), CH₃Cl (Segura et al., 2005) and phosphine (Sousa-Silva et al., 2019) have very low solubilities in water. Therefore, molecule water solubility has not needed to be emphasized as a reservoir in exoplanet atmosphere characterization studies.

Sulfur dioxide (SO₂) has a much higher solubility in water than other common atmospheric gases (but not as high as NH₃). Many studies show that both SO₂ molecules and their associated aerosols (H₂SO₄-H₂O) can potentially be detected in exoplanets' atmospheres (Hu et al., 2013, Lincowski et al., 2018, Loftus et al., 2019). However, Earth does not sustain a detectable level of sulfur aerosols in the atmosphere, possibly due to the presence of a global ocean (McCormick et al., 1995 and Loftus et al., 2019). Furthermore, it has been shown that SO₂ accumulation in an Earth-like environment requires an unreasonably high source flux (Hu et al., 2013). Therefore, (Loftus et al., 2019) propose that detection of atmospheric SO₂ (or sulfate haze) can infer the lack of surface water oceans on a rocky exoplanet.

3.5.2 Horizontal Atmospheric Transport Limits NH₃ Accumulation above Land

Horizontal wind transport might limit NH₃ accumulation above land when the planet's surface is unsaturated with NH₃ (i.e., there are NH₃ biological or geochemical sinks on the surface). In this case, if land-based life produces NH₃, it can be transported over the ocean,

where NH_3 can rain out and dissolve in the ocean, thereby removing NH_3 from the atmosphere. Since Earth's NH_3 is produced by land-based life (soil bacteria (Chapter 3.2.1)), horizontal wind transport is important.

So far, our models have neglected wind transport because they are limited to one dimension (the vertical dimension). Horizontal wind transport is a sink through which NH_3 is removed from the atmosphere above land. An improved model would consider an NH_3 land-ocean transport cycle (Figure 3-9) that includes horizontal winds. After NH_3 is produced from land surfaces, it will either be transported horizontally by wind or move up to the upper atmosphere, where NH_3 will be photochemically destroyed. Once entering the atmosphere above the ocean, ammonia can rain out, followed by quick diffusion into the ocean due to its high solubility. As a result, wind transport limits NH_3 's ability to accumulate to a detectable level in the atmosphere. A numerical model for such atmospheric wind transport of NH_3 is very challenging since it's extremely sensitive to the geophysical conditions we assume for the exoplanets.

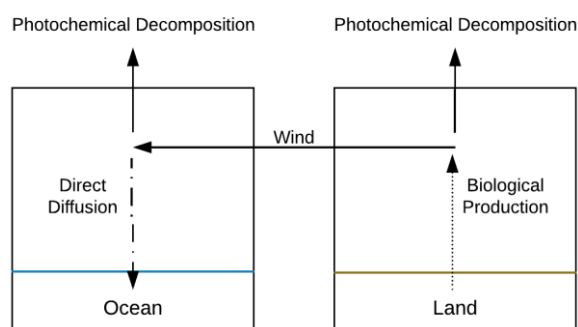


Figure 3-9. A simplified NH_3 land-ocean transport cycle. We assume that the planet's surface (land and ocean) is unsaturated with NH_3 , meaning there are NH_3 biological or geochemical sinks on the surface. Right panel: Ammonia is biologically produced from land surfaces and enters the atmosphere. Ammonia leaves the land area by traveling to the upper atmosphere, where it is photochemically destroyed. NH_3 can also be carried away by horizontal wind transport. Left panel: Once entering the atmosphere above the ocean, ammonia is removed through direct diffusion into the ocean, where NH_3 readily dissolves due to its high solubility. NH_3 can also fall back to the ground with rain, which is not shown in this figure.

3.5.3 Implausibility of NH_3 Formation by Lightning

In principle, the formation of NH_3 from N_2 is possible during lightning strikes. However, the reduction of N_2 to NH_3 by lightning is unlikely in oxidized atmospheres due to the very low concentration of H-containing reductants (e.g., H_2). N species' well-studied formation by lightning strikes on Earth (N_2 - O_2 atmosphere) favors the formation of nitrates and nitrites, not the thermally less stable reduced forms of N like ammonia (Ardaseva et al., 2017; Mancinelli and McKay 1988; Rakov and Uman 2003). Similarly, in oxidized N_2 - CO_2 atmospheres, lightning-induced N_2 transformation primarily leads to HNO but not NH_3 (Navarro-González et al., 2001; Holloway et al., 2002; Hawtof et al., 2019).

In an H₂-dominated atmosphere, NH₃ may form through lightning by breaking apart the N₂ bond and subsequent recombination of N atoms with H. Unfortunately, there are no laboratory studies on the formation of ammonia in N₂-H₂ atmospheres. Several studies focusing on the lightning-induced formation of PH₃ conclude it is possible, though extremely low efficiency. Specifically, simulated lightning discharges in laboratory conditions produce traces of PH₃, at very low efficiency, from discharges onto phosphate salt solutions (Glindemann et al., 1999; Glindemann et al., 2004). By analogy with PH₃, we infer that lightning is not likely an efficient source of NH₃ in exoplanet atmospheres.

3.5.4 Plausible Ocean-related Sinks of NH₃ and NH₄⁺

There are active NH₃-removal sinks on the surface (including land and ocean) that can maintain a surface unsaturated with NH₃. We summarize three chemical processes that can remove dissolved NH₃ or NH₄⁺ ions from the ocean: abiotic and biotic ammanox, marine photochemistry, and the formation of NH₄-containing sediments and minerals in the ocean.

The first process, called anammox (anaerobic ammonium oxidation), is a process that combines NH₄⁺ and NO₂⁻ to form N₂ and water. Such a process can occur biotically with marine anammox bacteria such as species belonging to the genus *Scalindua* (Jetten et al., 2009). Abiotic anammox is also possible. The rate of abiotic reaction of NH₃ with nitrite is sensitive to pH and temperature, with the reaction proceeding substantially faster at low pH and high temperature (Nguyen et al., 2003). NH₃ may also react with NO₃⁻, but this reaction is slower than reaction with NO₂⁻, by analogy with similar reduction reactions (Ranjan et al., 2019).

The second process is marine photochemistry. UV radiation in the wavelength range of 300-400 nm can effectively penetrate the first few centimeters of the surface ocean water⁵ before it is attenuated (Fleischmann 1989). Therefore, dissolved NH₃ and NH₄⁺ ions might be photochemically destroyed by the incident UV light close to the ocean surface. The bond dissociation energy for an N-H single bond is about 314 kJ·mol⁻¹ (T. L. Cottrell, 1966). Photons with wavelengths between 300 and 400 nm have 299 ~ 399 kJ·mol⁻¹ of energy. Therefore, it is not implausible for UV to break the N-H bond, effectively removing NH₃ or NH₄⁺ ions from the ocean surface.

The third process is the formation of NH₄-containing sediments and minerals in the ocean, whereby dissolved NH₄⁺ ions are deposited into the lithosphere. There are a wide variety of NH₄-containing minerals in nature (Table 3-9). NH₄-containing minerals like Lecontite, Ammonian fluorapophyllite, and Tobelite can form by substitution of ammonium for potassium. High concentrations of NH₄⁺ ions have been detected in the mineralizing fluids at the bottom of the ocean, specifically around the southwest pacific regions (Ridgway et al., 1990). Organic matter embedded in the sediments and rocks can break down to yield

⁵ The UV irradiance at the surface of an anoxic planet can be substantially greater than that of present-day Earth, due to the much more efficient penetration of the shorter UV wavelengths (Cockell, 1999).

NH_4^+ . Since NH_4 can easily replace K, Na, and other alkali metals in crystal lattices, K-containing rocks and sediments are particularly susceptible to the formation of NH_4 haloes and incursions (Ridgway et al., 1990). Both surface and subsurface rocks can have high NH_4 content (Ridgway et al., 1990). As a result, dissolved NH_3 and NH_4^+ ions can, in principle, be removed from the ocean environment through this mineralogical process.

Table 3-9. Naturally occurring NH_4 -containing minerals (Reference: Holloway et al., 2002).

Name of the mineral	Chemical formula
Ammoniojarosite	$(\text{NH}_4)\text{Fe}_3^+(\text{SO}_4)_2(\text{OH})_6$
Boussingaultite	$(\text{NH}_4)_2\text{Mg}(\text{SO}_4)_2 \cdot 6\text{H}_2\text{O}$
Letovicite	$(\text{NH}_4)_3\text{H}(\text{SO}_4)_2$
Mascagnite	$(\text{NH}_4)_2\text{SO}_4$
Sal-ammoniac	$(\text{NH}_4)\text{Cl}$
Mundrabillaite	$(\text{NH}_4)_2\text{Ca}(\text{HPO}_4)_2 \cdot \text{H}_2\text{O}$
Ammonioleucite	$(\text{NH}_4)\text{AlSi}_2\text{O}_6$
Lecontite	$(\text{NH}_4, \text{K})\text{Na}(\text{SO}_4) \cdot 2\text{H}_2\text{O}$
Ammonian fluorapophyllite	$(\text{NH}_4, \text{K})\text{Ca}_4\text{Si}_8\text{O}_{20}(\text{F}, \text{OH}) \cdot 8\text{H}_2\text{O}$
Tobelite	$(\text{NH}_4, \text{K})\text{Al}_2(\text{Si}_3\text{Al})\text{O}_{10}(\text{OH})_2$

3.5.5 Volatile Amines are Good Biosignature Gases by Proxy with NH_3

Volatile amines have similar solubilities and reactivities to NH_3 and hence are also suitable biosignature gases. Only when life produces enough volatile amines that can saturate the surface sinks can volatile amines accumulate in the atmosphere. Otherwise, volatile amines, just like NH_3 , can be removed from the atmosphere due to their high water solubility and high bio-useability.

Amines can be considered NH_3 derivatives, where an organic functional group replaces at least one H atom. There is some difference in solubility amongst volatile amines. In general, amine solubility decreases with an increasing length or number of hydrocarbon chains. Furthermore, like NH_3 , volatile amines will form basic solutions in water (see Appendix B).

The reactivity of volatile amines is also similar to NH_3 (see Appendix C), further allowing us to use NH_3 as a proxy for volatile amines. Here, we compare radical reaction rates⁶ for volatile amines to NH_3 in NIST (Manion et al., 2008). The few volatile amines with radical reaction rates at room temperature have reaction rates two to three orders of magnitude higher than that of NH_3 (see Appendix C). As a result, if NH_3 cannot accumulate in the atmosphere unless life produces a substantial amount of NH_3 that can saturate the surface sinks, neither can other volatile amines under similar planetary conditions.

3.5.6 IR Absorbance Spectra of Amines

⁶ H radicals do not destroy NH_3 or other volatile amines.

We can organize amines into three groups: primary, secondary, and tertiary amines, despite the amines' wide variety of molecular structures. Amines in each group will show similar features in their IR spectra. We use IR absorbance data from NIST to plot the spectra. We find 15 primary amines, 9 secondary amines, and 2 tertiary amines with available absorbance data in NIST. We overlay them onto a single graph to demonstrate the presence of shared IR features (Figure 3-10). We present the details of those amines and their raw (unnormalized) plots in Appendix D.

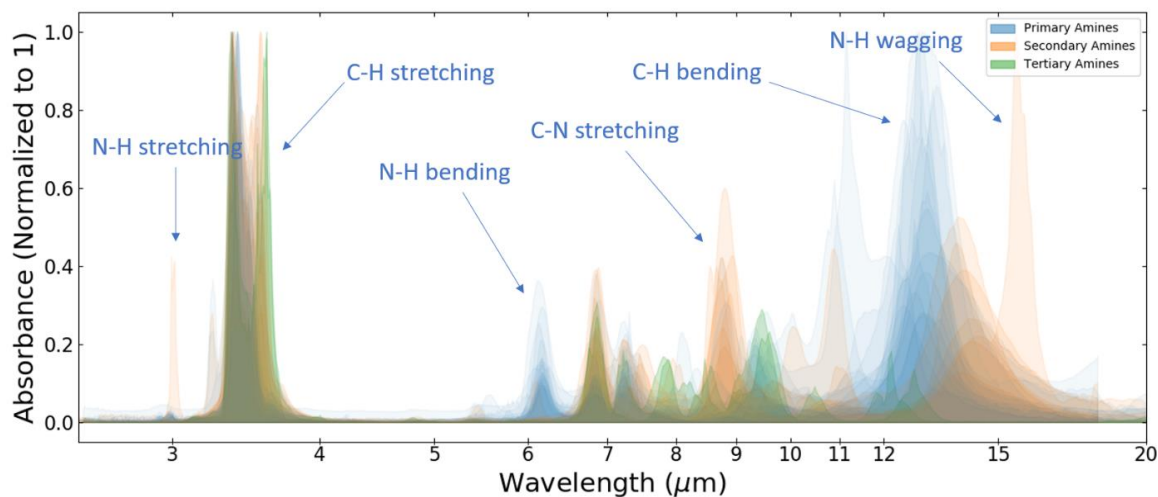


Figure 3-10. Spectral features of primary, secondary and tertiary amines in NIST (Manion et al., 2008). The x-axis shows wavelength in microns, and the y-axis shows absorbance that is normalized to 1. Amines in each group show similar IR absorbance features⁷.

3.5.7 NH₃-Induced Hazes

On an exoplanet with an H₂-dominated atmosphere, NH₃ haze generation processes have not yet been worked out in detail. In contrast to the formation of hydrocarbon and sulfur-based hazes that have been extensively studied (Domagal-Goldman et al., 2011; Arney et al., 2017; He et al., 2020), there is very little work on nitrogen-based hazes in H₂-dominated atmospheres. NH₃, on its own, does not participate in haze formation in reduced atmospheres. Hence, we do not focus on the formation and impact of NH₃-induced haze in our analysis. If hydrocarbons are present in the atmosphere and form hazes (Arney et al., 2017), NH₃ might participate in haze formation. In the presence of hydrocarbons, UV photolysis of NH₃ could form complex nitrogen-containing organics. This process is similar to the formation of organophosphine hazes (Sousa-Silva et al., 2020). However, contrary to the formation of organophosphine hazes, UV photolysis of NH₃ could reduce hydrocarbon hazes. The nitrogen-containing organics formed from UV photolysis of NH₃ are amines in nature. They are highly soluble and are susceptible to atmospheric precipitation.

⁷ Some peaks remain undiagnosed.

It's worth noting that on Earth, NH_3 plays a vital role in haze formation, especially $\text{PM}_{2.5}$ (i.e., fine particulate matter with diameter $<2.5 \mu\text{m}$) (Ye et al., 2011; Wei et al., 2015; Chen et al., 2016; Liu et al., 2019). In Earth's oxidized atmosphere, one way that atmospheric NH_3 can induce haze formation is by reacting with other pollutants such as sulfur dioxide (SO_2) and nitrogen oxides (NO_x). These reactions form fine airborne particles such as ammonium nitrate (NH_4NO_3), ammonium bisulfate (NH_4HSO_4), and ammonium sulfate ($(\text{NH}_4)_2\text{SO}_4$). The airborne particles can then form $\text{PM}_{2.5}$ by mixing with dust and other air pollutants (Chen et al., 2016). Furthermore, it has been shown that NH_3 can facilitate oxidation-reduction between NO_2 and SO_2 to form atmospheric nitrous acid (HONO) (Ge et al., 2019). Under UV conditions, atmospheric HONO can undergo photolysis to yield OH radicals, further facilitating haze formation (Ge et al., 2019; Wang et al., 2020).

3.5.8 NH_3 as a greenhouse gas

Ammonia is a greenhouse gas, given that it is a good IR absorber. However, its greenhouse effect is negligible on Earth due to its high reactivity and short atmospheric lifetime.

For exoplanets, we show in a separate paper that an increase in atmospheric NH_3 concentration does not lead to a considerable increase in surface temperature (Ranjan et al. Submitted). Specifically, in an H_2 -dominated atmosphere, the surface temperature only increases by about 10 K with 100 ppm of atmospheric NH_3 due to NH_3 - H_2 collision-induced absorption. In contrast, for an N_2 -dominated atmosphere, the temperature increase is roughly 40 K with 100 ppm of NH_3 (Ranjan et al. Submitted).

In an implausible scenario where NH_3 does accumulate to extremely high concentrations on exoplanets, NH_3 can indeed heat the surface significantly, particularly for N_2 - and CO_2 -dominated atmospheres. NH_3 -induced heating on H_2 -dominated atmospheres is minimal because NH_3 absorption is degenerate with H_2 - H_2 collision-induced absorption. Such high concentrations of NH_3 might also heat the stratosphere due to NH_3 UV absorption.

3.5.9 NH_3 Detectability with Future Telescopes

We assess the detectability of NH_3 with the premise of using a JWST-like telescope, which has a 6.5-meter diameter primary mirror, an estimated systematic noise floor of 10 ppm, and an estimated service time of 5 years (cryogenic lifetime). As discussed in Section 4.3, for exoplanets transiting M5V stars and orbiting in the habitable zone, we find that JWST can characterize only those with an H_2 -dominated atmosphere with reasonable observation time. However, not all terrestrial exoplanets can retain H_2 -dominated atmospheres.

To explore the potential for detecting NH_3 in a non- H_2 -dominated atmosphere, we assume observation using more capable telescopes that are currently in design or development, such as missions like The Origins Space Telescope (OST) (Battersby et al., 2018) and the 30-meter class of ground telescopes (Johns et al., 2012; Tamai and Spyromilio 2014; Skidmore et al., 2015). Since these telescopes' instrumental details may change with mission development, we generalize those details into two abstract categories: (1) a 10-meter space

telescope with broad spectral coverage. (2) a 30-meter ground-based telescope constrained by Earth's atmosphere observing windows. In both scenarios, we assume a 1 ppm noise floor. We computed the new noise estimate by scaling the JWST noise simulator Pandexo output with lower noise floor input.

For a 10-meter space telescope with a lower noise floor, characterization of CO₂-dominated or N₂-dominated atmospheres for exoplanets transiting an M5V star (which have an atmospheric transit-depth of 10 ~ 20 ppm) are possible with 20 transits per observation mode. However, for exoplanets transiting a Sun-like star, even H₂-dominated atmospheres are not accessible (atmospheric transit-depth of 2 ~ 3 ppm). The fundamental constraint here is $(R_{\text{planet}}/R_{\text{star}})^2$. While it is arguably possible to characterize such H₂-dominated atmospheres with a 30-meter ground-based telescope, the only NH₃ IR spectral features observable in Earth's atmosphere window are the 2.3 μm and the 10 μm features.

3.5.10 NH₃ in Mini-Neptunes

Super-Earths and mini-Neptunes discovered by future direct imaging programs may not be distinguishable from each other, lacking a mass and/or a size measurement. In this situation, any NH₃ detected should not be considered a possible biosignature gas. The reason is that NH₃ should exist to some level in mini-Neptune atmospheres without production by life, as NH₃ can be generated deep in the mini-Neptune envelope where temperature and pressure are high enough for NH₃'s atmospheric production. More work is needed to explore mini-Neptunes, including photochemistry, where NH₃ might be a marker for identifying a directly imaged planet as a mini-Neptune instead of a super-Earth.

3.6. Summary

In this paper, we examine the potential of NH₃ as a biosignature gas. We use various approaches, ranging from comparing Henry's law constants for different atmospheric gases to our simplified ocean-NH₃ interaction model to applications of our comprehensive photochemistry code and transmission spectra model.

In brief, NH₃ in a terrestrial planet atmosphere is generally a good biosignature gas, primarily because terrestrial planets have no significant known abiotic NH₃ source. NH₃'s high water solubility and high bio-useability likely prevent NH₃ from accumulating in the atmosphere to detectable levels unless life is a net source of NH₃ and produces enough NH₃ to saturate the surface sinks. Only then can NH₃ accumulate in the atmosphere with a reasonable surface production flux.

Specifically, for the favorable scenario of exoplanets with H₂-dominated atmospheres orbiting M dwarf stars (M5V), we find that a minimum of about 5 ppm column-averaged mixing ratio is needed for NH₃ to be detectable with JWST, considering a 10 ppm JWST systematic noise floor.

Additionally, volatile amines share NH₃'s weaknesses and strengths as a biosignature since

volatile amines have similar solubilities and reactivities to NH_3 . Finally, to establish NH_3 as a biosignature gas, we must rule out mini-Neptunes with deep atmospheres, where temperatures and pressures are high enough for NH_3 's atmospheric production.

We thank William Bains for the valuable discussions. We thank Thomas Evans, Ana Glidden, and Zahra Essack for helpful discussion to establish the detection metric. We acknowledge funding from the Heising-Simons Foundation (grant number #2018-1104) and NASA (grant numbers 80NSSC19K0471 and NNX15AC86G). S.R. gratefully acknowledges support from the Simons Foundation, grant no. 495062.

Appendix A. Simulation Parameters for the Photochemistry Model

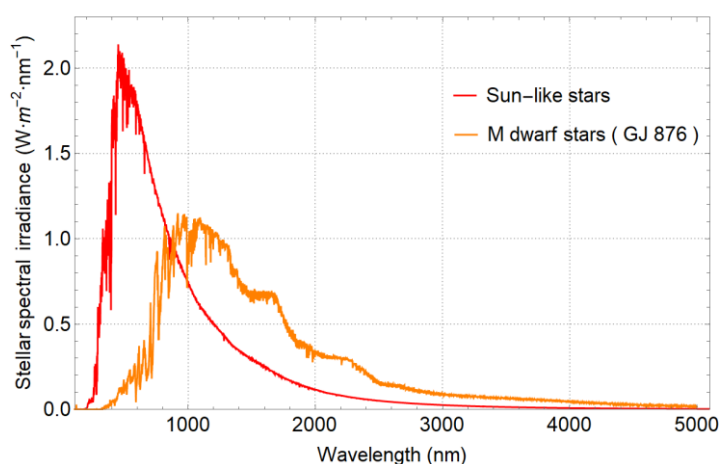


Figure 3-11. The synthetic stellar spectrum input of our photochemistry model (Loyd et al., 2016; France et al., 2016). The y-axis shows spectral irradiance in $\text{W}\cdot\text{m}^{-2}\cdot\text{nm}^{-1}$, and the x-axis shows wavelength in nm.

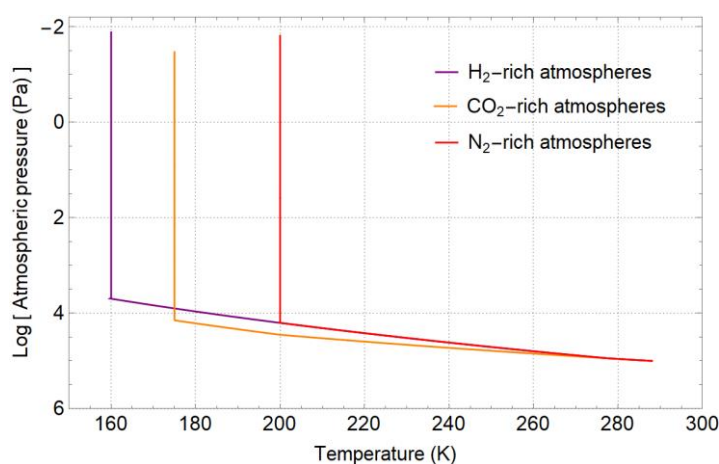


Figure 3-12. The temperature-pressure profiles of the simulated exoplanets with H₂-dominated, CO₂-dominated, and N₂-dominated atmospheres. The y-axis shows atmospheric pressure (Pa) on a log scale, and the x-axis shows temperature in Kelvin (K).

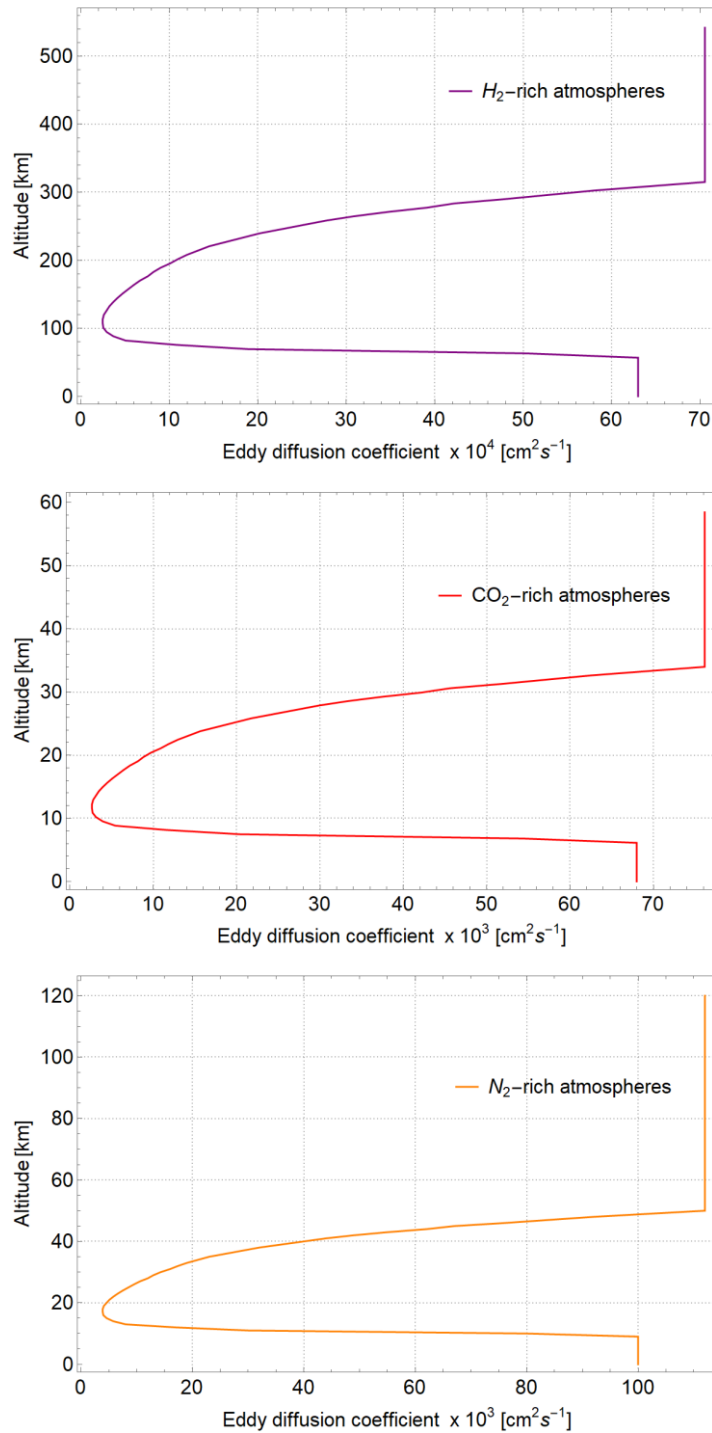


Figure 3-13. The eddy diffusion profiles of the simulated exoplanets with H₂-dominated (top panel), CO₂-dominated (middle panel), and N₂-dominated (bottom panel) atmospheres. The y-axis shows altitude in km, and the x-axis shows the eddy diffusion coefficient in cm²·s⁻¹.

Our photochemistry model demarcates chemical species into 4 types: type “A” for aerosol species, type “C” for chemically inert species which are assumed not to react or transport, type “F” for species assumed to be in photochemical equilibrium (i.e., for which transport is neglected), and type “X”, for species for which the full photochemical transport equation is solved. For the lower boundary condition, our model allows us to either specify a fixed surface mixing ratio (type “1”) or the surface emission flux and dry deposition velocity (type “2”) (Hu et al., 2012).

Table 3-10. Surface boundary conditions for exoplanets with CO₂-dominated atmospheres.

Name	Type	Initial Mixing Ratio	Upper Boundary Flux Beside Escape (Upwards) [molecule/(cm ² s)]	Lower Boundary Type	Dry Deposition Velocity [cm/s]	Lower Boundary Flux (Upwards) [molecule/(cm ² s)]
H	X	0	0	2	1	0
H ₂	X	1.60×10 ⁻³	0	2	0	3.00×10 ¹⁰
O	X	0	0	2	1	0
O(1D)	X	0	0	2	0	0
O ₂	X	0	0	2	0	0
O ₃	X	0	0	2	0.4	0
OH	X	0	0	2	1	0
HO ₂	X	0	0	2	1	0
H ₂ O	X	2.00×10 ⁻⁶	0	1	0	0.01
H ₂ O ₂	X	0	0	2	0.5	0
CO ₂	X	0.9	0	1	0	0.9
CO	X	0	0	2	1.00×10 ⁻⁸	0
CH ₂ O	X	0	0	2	0.1	0
CHO	X	0	0	2	0.1	0
C	X	0	0	2	0	0
CH	X	0	0	2	0	0
CH ₂	X	0	0	2	0	0
CH ₂ ₁	X	0	0	2	0	0
CH ₃	X	0	0	2	0	0
CH ₄	X	0	0	2	0	3.00×10 ⁸
CH ₃ O	X	0	0	2	0.1	0
CH ₄ O	X	0	0	2	0.1	0
CHO ₂	X	0	0	2	0.1	0
CH ₂ O ₂	X	0	0	2	0.1	0
CH ₃ O ₂	X	0	0	2	0	0
CH ₄ O ₂	X	0	0	2	0.1	0
C ₂	X	0	0	2	0	0
C ₂ H	X	0	0	2	0	0
C ₂ H ₂	X	0	0	2	0	0
C ₂ H ₃	X	0	0	2	0	0
C ₂ H ₄	X	0	0	2	0	0

C ₂ H ₅	X	0	0	2	0	0
C ₂ H ₆	X	0	0	2	1.00×10 ⁻⁵	0
C ₂ HO	X	0	0	2	0	0
C ₂ H ₂ O	X	0	0	2	0.1	0
C ₂ H ₃ O	X	0	0	2	0.1	0
C ₂ H ₄ O	X	0	0	2	0.1	0
C ₂ H ₅ O	X	0	0	2	0.1	0
S	X	0	0	2	0	0
S ₂	X	0	0	2	0	0
S ₃	X	0	0	2	0	0
S ₄	X	0	0	2	0	0
SO	X	0	0	2	0	0
SO ₂	X	0	0	2	1	3.00×10 ⁹
SO ₂₁	X	0	0	2	0	0
SO ₂₃	X	0	0	2	0	0
SO ₃	X	0	0	2	1	0
H ₂ S	X	0	0	2	0.015	3.00×10 ⁸
HS	X	0	0	2	0	0
HSO	X	0	0	2	0	0
HSO ₂	X	0	0	2	0	0
HSO ₃	X	0	0	2	0.1	0
H ₂ SO ₄	X	0	0	2	1	0
H ₂ SO ₄ A	A	0	0	2	0.2	0
S ₈	X	0	0	2	0	0
S ₈ A	A	0	0	2	0.2	0
N ₂	C	0.1	0	1	0	0.1
N	X	0	0	2	0	0
NH ₃	X	0	0	2	1	1.0×10 ⁹
NH ₂	X	0	0	2	0	0
NH	X	0	0	2	0	0
N ₂ O	X	0	0	2	0	0
NO	X	0	0	2	0.02	0
NO ₂	X	0	0	2	0.02	0
NO ₃	X	0	0	2	1	0
N ₂ O ₅	X	0	0	2	4	0
HNO	X	0	0	2	0	0
HNO ₂	X	0	0	2	0.5	0
HNO ₃	X	0	0	2	4	0
HNO ₄	X	0	0	2	4	0
HCN	X	0	0	2	0.01	0
CN	X	0	0	2	0.01	0
CNO	X	0	0	2	0	0
HCNO	X	0	0	2	0	0
CH ₃ NO	X	0	0	2	0.01	0

2

CH ₃ NO	X	0	0	2	0.01	0
³ CH ₅ N	X	0	0	2	0	0
C ₂ H ₂ N	X	0	0	2	0	0
C ₂ H ₅ N	X	0	0	2	0	0
N ₂ H ₂	X	0	0	2	0	0
N ₂ H ₃	X	0	0	2	0	0
N ₂ H ₄	X	0	0	2	0	0
OCS	X	0	0	2	0.01	0
CS	X	0	0	2	0.01	0
CH ₃ S	X	0	0	2	0.01	0
CH ₄ S	X	0	0	2	0.01	0

Table 3-11. Surface boundary conditions for exoplanets with H₂-dominated atmospheres.

Name	Type	Initial Mixing Ratio	Upper Boundary Flux Beside Escape (Upwards) [molecule/(cm ² s)]	Lower Boundary Type	Dry Deposition Velocity [cm/s]	Lower Boundary Flux (Upwards) [molecule/(cm ² s)]
H	X	0	0	2	1	0
H ₂	C	0.9	0	1	0	0.9
O	X	0	0	2	1	0
O(1D)	X	0	0	2	0	0
O ₂	X	0	0	2	0	0
O ₃	X	0	0	2	0	0
OH	X	0	0	2	1	0
HO ₂	X	0	0	2	1	0
H ₂ O	X	2.00×10 ⁻⁶	0	1	0	1.00×10 ⁻²
H ₂ O ₂	X	0	0	2	0.5	0
CO ₂	X	0	0	2	1.00×10 ⁻⁴	3.00×10 ¹¹
CO	X	0	0	2	1.00×10 ⁻⁸	0
CH ₂ O	X	0	0	2	0.1	0
CHO	X	0	0	2	0.1	0
C	X	0	0	2	0	0
CH	X	0	0	2	0	0
CH ₂	X	0	0	2	0	0
CH ₂₁	X	0	0	2	0	0
CH ₃	X	0	0	2	0	0
CH ₄	X	0	0	2	0	3.00×10 ⁸
CH ₃ O	X	0	0	2	0.1	0
CH ₄ O	X	0	0	2	0.1	0
CH ₂ O ₂	X	0	0	2	0.1	0
CH ₃ O ₂	X	0	0	2	0	0
CH ₄ O ₂	X	0	0	2	0.1	0
C ₂	X	0	0	2	0	0
C ₂ H	X	0	0	2	0	0
C ₂ H ₂	X	0	0	2	0	0

C ₂ H ₃	X	0	0	2	0	0
C ₂ H ₄	X	0	0	2	0	0
C ₂ H ₅	X	0	0	2	0	0
C ₂ H ₆	X	0	0	2	1.00×10 ⁻⁵	0
C ₂ HO	X	0	0	2	0	0
C ₂ H ₂ O	X	0	0	2	0.1	0
C ₂ H ₃ O	X	0	0	2	0.1	0
C ₂ H ₄ O	X	0	0	2	0.1	0
C ₂ H ₅ O	X	0	0	2	0.1	0
N ₂	C	0.1	0	1	0	0.1
S	X	0	0	2	0	0
S ₂	X	0	0	2	0	0
S ₃	X	0	0	2	0	0
S ₄	X	0	0	2	0	0
SO	X	0	0	2	0	0
SO ₂	X	0	0	2	1	3.00×10 ⁹
SO ₂₁	X	0	0	2	0	0
SO ₂₃	X	0	0	2	0	0
SO ₃	X	0	0	2	0	0
H ₂ S	X	0	0	2	0.015	3.00×10 ⁸
HS	X	0	0	2	0	0
HSO	X	0	0	2	0	0
HSO ₂	X	0	0	2	0	0
HSO ₃	X	0	0	2	0	0
H ₂ SO ₄	X	0	0	2	1	0
H ₂ SO ₄ A	A	0	0	2	0.2	0
S ₈	X	0	0	2	0	0
S ₈ A	A	0	0	2	0.2	0
CHO ₂	X	0	0	2	0.1	0
N	X	0	0	2	0	0
NH ₃	X	0	0	2	1	1.0×10 ¹⁰
NH ₂	X	0	0	2	0	0
NH	X	0	0	2	0	0
N ₂ O	X	0	0	2	0	0
NO	X	0	0	2	0.02	0
NO ₂	X	0	0	2	0.02	0
NO ₃	X	0	0	2	1	0
N ₂ O ₅	X	0	0	2	4	0
HNO	X	0	0	2	0	0
HNO ₂	X	0	0	2	0.5	0
HNO ₃	X	0	0	2	4	0
HNO ₄	X	0	0	2	4	0
HCN	X	0	0	2	0.01	0
CN	X	0	0	2	0.01	0
CNO	X	0	0	2	0	0

HCNO	X	0	0	2	0	0
CH ₃ NO	X	0	0	2	0.01	0
² CH ₃ NO	X	0	0	2	0.01	0
³ CH ₃ NO	X	0	0	2	0.01	0
CH ₅ N	X	0	0	2	0	0
C ₂ H ₂ N	X	0	0	2	0	0
C ₂ H ₅ N	X	0	0	2	0	0
N ₂ H ₂	X	0	0	2	0	0
N ₂ H ₃	X	0	0	2	0	0
N ₂ H ₄	X	0	0	2	0	0
OCS	X	0	0	2	0.01	0
CS	X	0	0	2	0.01	0
CH ₃ S	X	0	0	2	0.01	0
CH ₄ S	X	0	0	2	0.01	0

Table 3-12. Surface boundary conditions for exoplanets with N₂-dominated atmospheres.

Name	Type	Initial Mixing Ratio	Upper Boundary Flux Beside Escape (Upwards) [molecule/(cm ² s)]	Lower Boundary Type	Dry Deposition Velocity [cm/s]	Lower Boundary Flux (Upwards) [molecule/(cm ² s)]
H	X	0	0	2	1	0
H ₂	X	0	0	2	0	3.00×10 ¹⁰
O	X	0	0	2	1	0
O(1D)	X	0	0	2	0	0
O ₂	X	0	0	2	0	0
O ₃	X	0	0	2	0.4	0
OH	X	0	0	2	1	0
HO ₂	X	0	0	2	1	0
H ₂ O	X	2.00×10 ⁻⁶	0	1	0	1.00×10 ⁻²
H ₂ O ₂	X	0	0	2	0.5	0
CO ₂	X	0	0	2	1.00×10 ⁻⁴	3.00×10 ¹¹
CO	X	0	0	2	1.00×10 ⁻⁸	0
CH ₂ O	X	0	0	2	0.1	0
CHO	X	0	0	2	0.1	0
C	X	0	0	2	0	0
CH	X	0	0	2	0	0
CH ₂	X	0	0	2	0	0
CH ₂₁	X	0	0	2	0	0
CH ₃	X	0	0	2	0	0
CH ₄	X	0	0	2	0	3.00×10 ⁸
CH ₃ O	X	0	0	2	0.1	0
CH ₄ O	X	0	0	2	0.1	0
CHO ₂	X	0	0	2	0.1	0
CH ₂ O ₂	X	0	0	2	0.1	0
CH ₃ O ₂	X	0	0	2	0.1	0

CH ₄ O ₂	X	0	0	2	0.1	0
C ₂	X	0	0	2	0	0
C ₂ H	X	0	0	2	0	0
C ₂ H ₂	X	0	0	2	0	0
C ₂ H ₃	X	0	0	2	0	0
C ₂ H ₄	X	0	0	2	0	0
C ₂ H ₅	X	0	0	2	0	0
C ₂ H ₆	X	0	0	2	1.00×10 ⁻⁵	0
C ₂ HO	X	0	0	2	0.1	0
C ₂ H ₂ O	X	0	0	2	0.1	0
C ₂ H ₃ O	X	0	0	2	0.1	0
C ₂ H ₄ O	X	0	0	2	0.1	0
C ₂ H ₅ O	X	0	0	2	0.1	0
N ₂	C	1	0	1	0	1
S	X	0	0	2	0	0
S ₂	X	0	0	2	0	0
S ₃	X	0	0	2	0	0
S ₄	X	0	0	2	0	0
SO	X	0	0	2	0	0
SO ₂	X	0	0	2	1	3.00×10 ⁹
SO ₂₁	X	0	0	2	0	0
SO ₂₃	X	0	0	2	0	0
SO ₃	X	0	0	2	1	0
H ₂ S	X	0	0	2	0.015	3.00×10 ⁸
HS	X	0	0	2	0	0
HSO	X	0	0	2	0	0
HSO ₂	X	0	0	2	0	0
HSO ₃	X	0	0	2	0.1	0
H ₂ SO ₄	X	0	0	2	1	0
H ₂ SO ₄ A	A	0	0	2	0.2	0
S ₈	X	0	0	2	0	0
S ₈ A	A	0	0	2	0.2	0
N	X	0	0	2	0	0
NH ₃	X	0	0	2	1	1.0×10 ¹⁰
NH ₂	X	0	0	2	0	0
NH	X	0	0	2	0	0
N ₂ O	X	0	0	2	0	0
NO	X	0	0	2	0.02	0
NO ₂	X	0	0	2	0.02	0
NO ₃	X	0	0	2	1	0
N ₂ O ₅	X	0	0	2	4	0
HNO	X	0	0	2	0	0
HNO ₂	X	0	0	2	0.5	0
HNO ₃	X	0	0	2	4	0
HNO ₄	X	0	0	2	4	0

HCN	X	0	0	2	0.01	0
CN	X	0	0	2	0.01	0
CNO	X	0	0	2	0	0
HCNO	X	0	0	2	0	0
CH ₃ NO	X	0	0	2	0.01	0
² CH ₃ NO	X	0	0	2	0.01	0
³ CH ₃ N	X	0	0	2	0	0
C ₂ H ₂ N	X	0	0	2	0	0
C ₂ H ₅ N	X	0	0	2	0	0
N ₂ H ₂	X	0	0	2	0	0
N ₂ H ₃	X	0	0	2	0	0
N ₂ H ₄	X	0	0	2	0	0
OCS	X	0	0	2	0.01	0
CS	X	0	0	2	0.01	0
CH ₃ S	X	0	0	2	0.01	0
CH ₄ S	X	0	0	2	0.01	0

Appendix B. Dissociation Constants of Representative Amines at 25°C

Table 3-13. The pK_a values of some representative amines at 25°C (David R. Lide et al., 2005).

Chemical species	pK _a values
Ammonia NH ₃	9.25
Methylamine CH ₅ N	10.66
Ethylamine CH ₇ N	10.65
Propylamine C ₃ H ₉ N	10.54
Isopropylamine C ₃ H ₉ N	10.63
Butylamine C ₄ H ₁₁ N	10.60
sec-Butylamine C ₄ H ₁₁ N	10.56
tert-Butylamine C ₄ H ₁₁ N	10.68
Dimethylamine C ₂ H ₇ N	10.73
Diethylamine C ₄ H ₁₁ N	10.84
Diisopropylamine C ₆ H ₁₅ N	11.05
Trimethylamine C ₃ H ₉ N	9.80
Triethylamine C ₆ H ₁₅ N	10.75
Diethylmethylamine C ₅ H ₁₃ N	10.35

Appendix C. Reaction Rates Between Life Produced Volatile Amines and O, OH Radicals

Table 3-14. Reactions between life produced volatile amines and OH radicals. Reaction rates are at 298K. Second-order reactions have units of [cm³ molecule⁻¹ s⁻¹] (Reference:

NIST).

Chemical	Reaction with OH radicals	Reaction rate	Reaction Order
Ammonia (NH ₃)	NH ₃ + ·OH → ·NH ₂ + H ₂ O	1.60 × 10 ⁻¹³	2
Ethanamine (C ₂ H ₅ NH ₂)	C ₂ H ₅ NH ₂ + ·OH → C ₂ H ₅ NH + H ₂ O	2.77 × 10 ⁻¹¹	2
2-methylpropan-2-amine (tert-C ₄ H ₉ NH ₂)	tert-C ₄ H ₉ NH ₂ + ·OH → C ₄ H ₉ NH + H ₂ O	1.20 × 10 ⁻¹¹	2
Trimethylamine (C ₃ H ₉ N)	C ₃ H ₉ N + ·OH → C ₃ H ₈ N + H ₂ O	6.11 × 10 ⁻¹¹	2

Table 3-15. Reactions between life produced volatile amines and O radicals. Reaction rates are at 298K. Second-order reactions have units of [cm³ molecule⁻¹ s⁻¹] (Reference: NIST).

Chemical	Reaction with O radicals	Reaction rate	Reaction Order
Ammonia (NH ₃)	NH ₃ + ·O → ·OH + ·NH ₂	4.37 × 10 ⁻¹⁷	2
Methylamine (CH ₃ NH ₂)	CH ₃ NH ₂ + ·O → ·OH + CH ₃ NH	5.56 × 10 ⁻¹³	2
Ethylamine (C ₂ H ₅ NH ₂)	C ₂ H ₅ NH ₂ + ·O → ·OH + C ₂ H ₅ NH	3.87 × 10 ⁻¹²	2
Dimethylamine ((CH ₃) ₂ NH)	(CH ₃) ₂ NH + ·O → ·OH + (CH ₃) ₂ N·	6.00 × 10 ⁻¹²	2
Trimethylamine (C ₃ H ₉ N)	C ₃ H ₉ N + ·O → ·OH + C ₃ H ₈ N	7.54 × 10 ⁻¹²	2

Appendix D. IR Spectra of Primary, Secondary and Tertiary Amines

We list the IUPAC names of the 15 primary amines, 9 secondary amines, and 2 tertiary amines with absorbance data in NIST (Manion et al., 2008) in Table 3-16.

Table 3-16. Primary (15), Secondary (9) and Tertiary (2) Amines in NIST

Primary amines	2-methylpropan-2-amine, 2-methylbutan-2-amine, propan-2-amine, pentan-2-amine, methylamine, 2-methylprop-2-en-1-amine, 2-methylbutan-1-amine, ethanamine, prop-2-en-1-amine, propan-1-amine, butan-1-amine, pentan-1-amine, butane-1,4-diamine, (3-aminopropyl)(methyl)amine, (2-aminoethyl)(ethyl)amine
Secondary amines	diethylamine, ethyl(prop-2-en-1-yl)amine, [(1R)-1-(naphthalen-1-yl)ethyl]({3-[3-(trifluoromethyl)phenyl]propyl})amine, methyl(prop-2-en-1-yl)amine, methyl(2-methylpropyl)amine, methyl(prop-2-en-1-yl)amine, methyl[2-(methylamino)ethyl]amine, (3-aminopropyl)(methyl)amine, (2-aminoethyl)(ethyl)amine
Tertiary amines	trimethylamine, ethyldimethylamine

Here we show the overlaid IR spectra of the primary, secondary and tertiary amines.

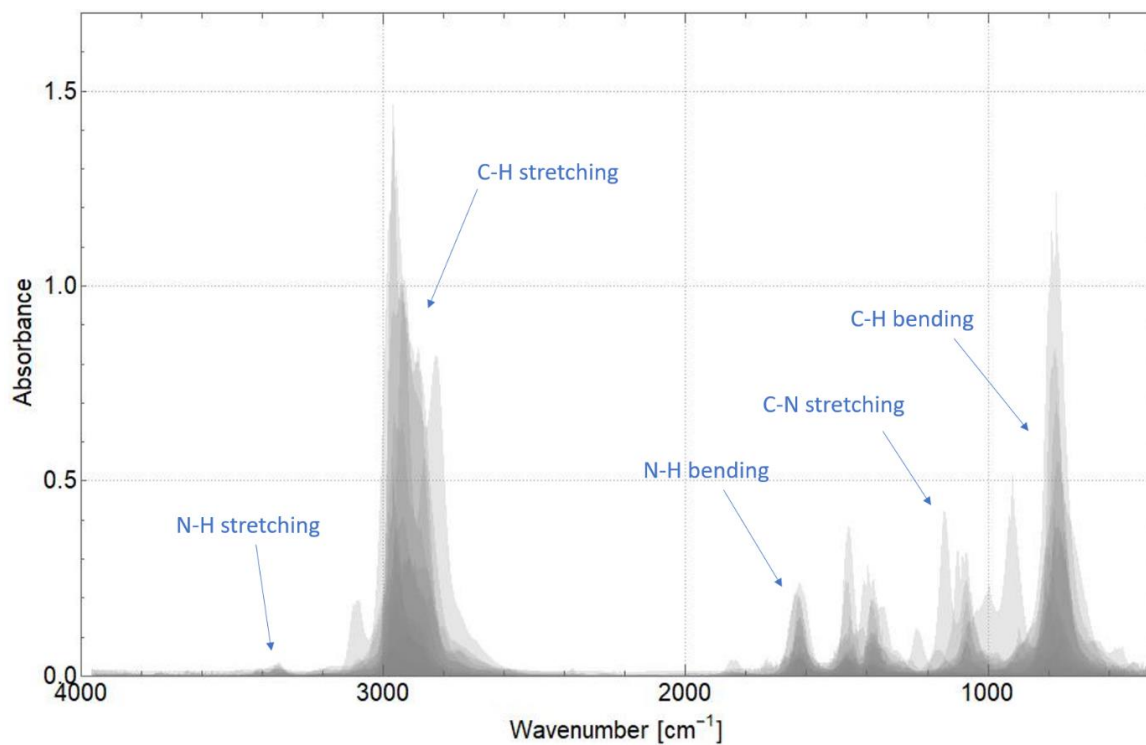


Figure 3-14. IR absorbance spectra of primary amines. Included are the fifteen are in the NIST database (Manion et al., 2008). The x-axis is the wavenumber, and the y axis is absorbance. Although only two of the amines contain nitrogen (N-H bending and C-N stretching), there are several distinctive peaks.

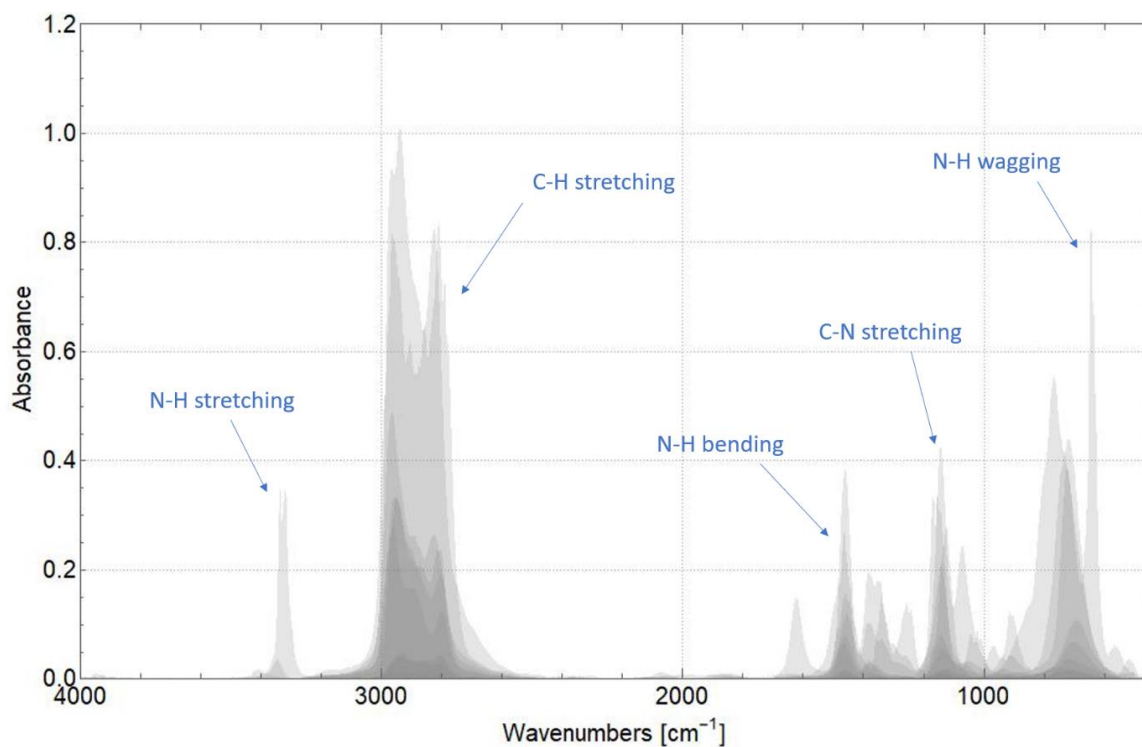


Figure 3-15. IR absorbance spectra of secondary amines. Nine species are present in the NIST database (Manion et al., 2008). The x-axis is the wavenumber, and the y axis is absorbance. Although only two of the amines contain nitrogen (N-H bending and C-N stretching), there are several distinctive peaks. The secondary amines have an N-H stretching feature not present in primary or tertiary amine spectra.

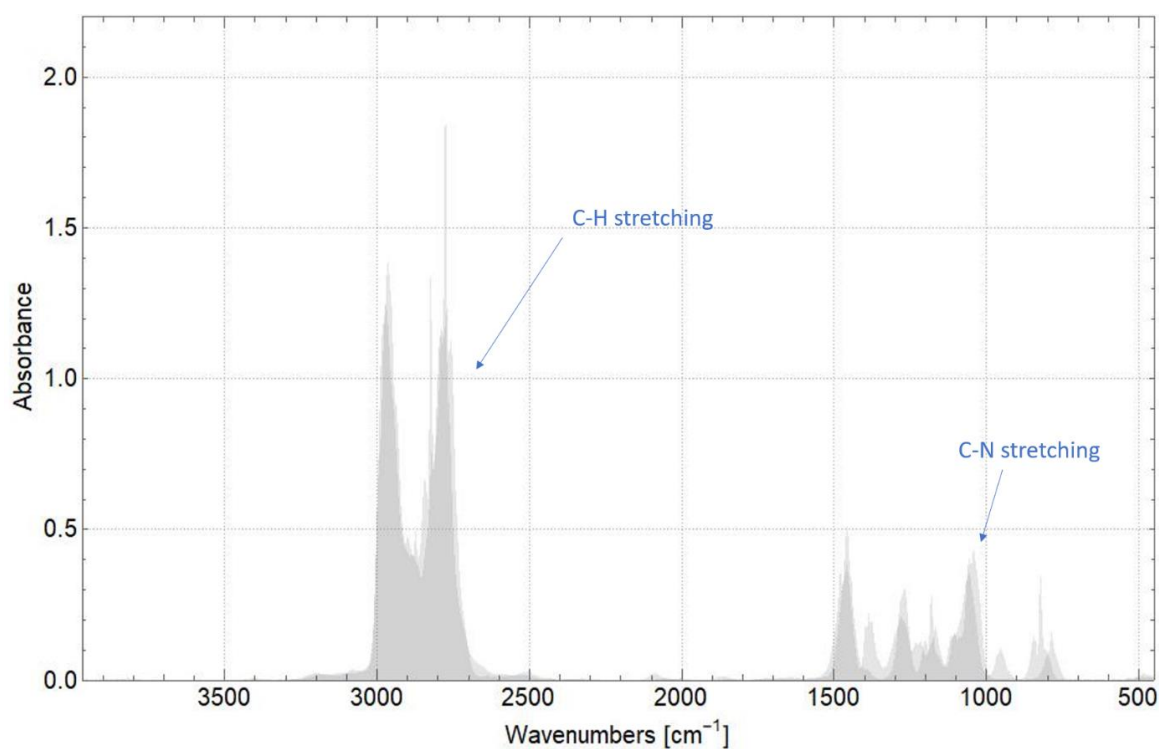


Figure 3-16. IR absorbance spectra of tertiary amines. Only two are present in the NIST database (Manion et al., 2008). The x-axis is the wavenumber, and the y-axis is absorbance. Tertiary amines lack N-H bonds, so they lack the N-H stretch feature found in primary and secondary amines.

Appendix E. NH₃ Removal Rate in the Photochemistry Model

Table 3-17. The top three photochemical removal mechanisms for NH₃ on exoplanets with H₂-dominated, CO₂-dominated, and N₂-dominated atmospheres orbiting M dwarf stars (M5V).

	Atmospheric scenarios	The top three loss reactions	Loss rate [molecule cm ⁻² s ⁻¹]
With NH ₃ deposition	H ₂ -dominated	NH ₃ → NH ₂ + H	1.54 × 10 ¹⁰
		OH + NH ₃ → H ₂ O + NH ₂	1.27 × 10 ⁴
		H + NH ₃ → H ₂ + NH ₂	4.99 × 10 ²
	CO ₂ -dominated	NH ₃ → NH ₂ + H	8.35 × 10 ⁸
		O(1D) + NH ₃ → OH + NH ₂	3.30 × 10 ⁶
		NH ₃ → NH + H ₂	1.34 × 10 ⁶
	N ₂ -dominated	NH ₃ → NH ₂ + H	9.01 × 10 ¹⁰
		OH + NH ₃ → H ₂ O + NH ₂	1.85 × 10 ⁸
		NH ₃ → NH + H ₂	5.60 × 10 ⁵
Without NH ₃ deposition	H ₂ -dominated	NH ₃ → NH ₂ + H	2.00 × 10 ¹⁰
		OH + NH ₃ → H ₂ O + NH ₂	2.78 × 10 ⁴
		NH ₃ + CH → HCN + H ₂ + H	1.34 × 10 ³
	CO ₂ -dominated	NH ₃ → NH ₂ + H	8.79 × 10 ⁸
		O(1D) + NH ₃ → OH + NH ₂	3.54 × 10 ⁶
		NH ₃ → NH + H ₂	1.44 × 10 ⁶
	N ₂ -dominated	NH ₃ → NH ₂ + H	9.64 × 10 ¹⁰
		OH + NH ₃ → H ₂ O + NH ₂	1.96 × 10 ⁸
		NH ₃ → NH + H ₂	1.08 × 10 ⁶

Appendix F. Photochemistry Model Sensitivity Tests

To test the robustness of our photochemistry results, we decide to run various sensitivity tests. We choose the H₂-dominated atmosphere as our example here since it is the most favorable scenario for detecting NH₃. Here we present our results.

I. The presence of a cold trap: Our results are not sensitive to the presence of a cold trap. To first order, the presence of a cold trap does not affect NH₃ rainout or dry deposition. Instead, whether a cold trap is present only influences the NH₃ photochemical production and loss rate. Here, we simulate an atmosphere with a reduced cold trap (compared to the

existing cold trap we set for the H₂-dominated atmosphere) (see Figure 3-17). In this case, the planet has a hot stratosphere due to UV-absorbers present in the upper atmosphere. We choose the H₂-dominated atmosphere as our example here since it is the most favorable scenario for detecting NH₃. To simulate an exoplanet with a reduced cold trap, we set the temperature above tropopause to 220K (see Figure 3-17)

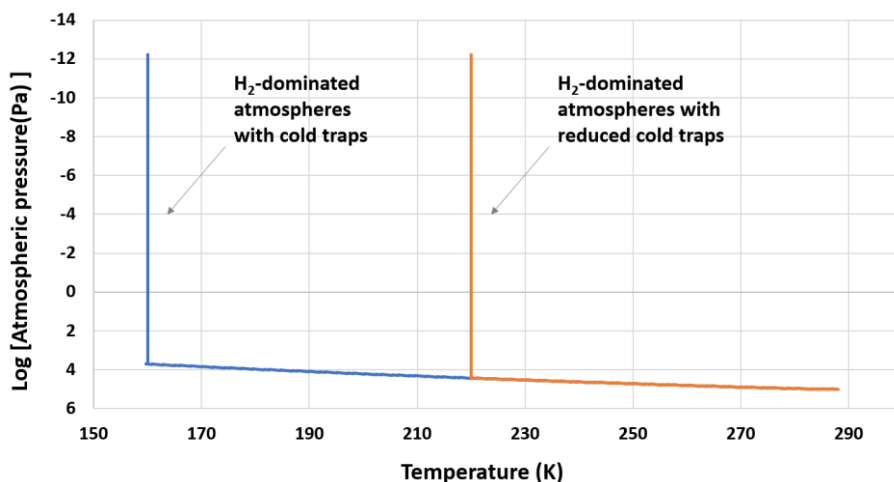


Figure 3-17. The temperature-pressure profiles of the simulated exoplanets with ‘standard’ and ‘reduced’ cold traps. The y-axis shows atmospheric pressure (Pa) on a log scale, and the x-axis shows temperature in Kelvin (K).

Our results show that when a cold trap is reduced, the photochemical production of NH₃ from NH₂ becomes more efficient due to more H radicals being present in the H₂-dominated atmosphere. As a result, with the same surface production flux, NH₃ column-averaged mixing ratio increases slightly from 5.0 ppm to 5.1 ppm (see Table 3-16).

Table 3-18. Simulated mixing ratios and reaction rates for exoplanets with H₂-dominated atmospheres orbiting M dwarf stars (M5V).

	With a cold trap	Without a cold trap
NH ₃ outgassing [molecule/(cm ² s)]	6.40×10^{15}	6.40×10^{15}
NH ₃ column-averaged mixing ratio	5.0 ppm	5.1 ppm
Chemical production [molecule/(cm ² s)]	4.90×10^9	1.20×10^{10}
Chemical loss [molecule/(cm ² s)]	1.54×10^{10}	1.21×10^{10}
Dry deposition [molecule/(cm ² s)]	4.16×10^{14}	4.16×10^{14}
Wet deposition [molecule/(cm ² s)]	5.98×10^{15}	5.98×10^{15}

We currently include a cold trap in each of our existing photochemical simulations. To simulate cold traps, we set the temperature above tropopause to 160 K, 200 K, and 175 K for the H₂-dominated, N₂-dominated, and CO₂-dominated atmosphere. In comparison, the Earth's tropopause temperature is about 217 K (US Standard Atmosphere 1976). Please note that a cold trap does not require a thermal inversion. A cold trap is a part of the (upper) atmosphere where the temperature is low enough to condense volatiles like water

(Wordsworth et al., 2013, Wordsworth et al., 2014).

II. The choice of eddy diffusion coefficient (K_{zz}): The choice of K_{zz} can affect NH_3 concentration because photochemistry is most important in the upper atmosphere layers, whereas NH_3 is primarily produced at the planet's surface. K_{zz} is measured or inferred for solar system planets but is not known for exoplanets. The K_{zz} variation does not change our main conclusion, as explained below.

The K_{zz} as a function of altitude (i.e., the eddy diffusion profile) is an input to our code. Each simulated atmospheric scenario has its own fixed eddy diffusion profile. Here, we perform a sensitivity test to a changing K_{zz} for the H_2 -dominated atmosphere scenario (see Table 3-17).

Table 3-19. Steady-state simulation outputs as a function of eddy diffusion magnitude, NH_3 surface flux, and presence/absence of wet and dry deposition of NH_3 for exoplanets with H_2 -dominated atmospheres orbiting M dwarf stars (M5V).

With NH_3 deposition			
Eddy diffusion coefficient scaling factor	0.1	1	10
NH_3 outgassing [molecule/(cm^2s)]	6.40×10^{15}	6.40×10^{15}	6.40×10^{15}
NH_3 column-averaged mixing ratio	3.3 ppm	5.0 ppm	12 ppm
Chemical production [molecule/(cm^2s)]	1.78×10^9	4.90×10^9	6.05×10^9
Chemical loss [molecule/(cm^2s)]	1.79×10^9	1.54×10^{10}	2.44×10^{10}
Dry deposition [molecule/(cm^2s)]	4.26×10^{14}	4.16×10^{14}	3.93×10^{14}
Wet deposition [molecule/(cm^2s)]	5.97×10^{15}	5.98×10^{15}	6.01×10^{15}
Without NH_3 deposition			
Eddy diffusion coefficient scaling factor	0.1	1	10
NH_3 outgassing [molecule/(cm^2s)]	1.44×10^{10}	1.44×10^{10}	1.44×10^{10}
NH_3 column-averaged mixing ratio	9.8 ppm	5.0 ppm	1.9 ppm
Chemical production [molecule/(cm^2s)]	5.76×10^9	5.52×10^9	6.37×10^9
Chemical loss [molecule/(cm^2s)]	2.02×10^{10}	2.00×10^{10}	2.08×10^{10}
Dry deposition [molecule/(cm^2s)]	0	0	0
Wet deposition [molecule/(cm^2s)]	0	0	0

We find that the K_{zz} variation does not affect rainout or dry deposition. In a more diffusive atmosphere (i.e., larger K_{zz}), the photochemical recycling of NH_3 becomes more efficient. Specifically, as K_{zz} increases, the photochemical loss of NH_3 becomes larger, mainly due to enhanced NH_3 direct photolysis ($\text{NH}_3 \rightarrow \text{NH}_2 + \text{H}$). Simultaneously, the reproduction of NH_3 from NH_2 also increases ($\text{H}_2 + \text{NH}_2 \rightarrow \text{NH}_3 + \text{H}$) since there are more NH_2 radicals in the atmosphere. Our findings are consistent with (Kasting et al., 1982).

The effect of K_{zz} variation on NH_3 atmosphere abundance depends on whether there are NH_3 -removal sinks on the surface. When NH_3 deposition is present (i.e., the surface is not saturated with NH_3), the column-averaged mixing ratio of NH_3 scales with K_{zz} . Compared

to chemical loss, wet and dry deposition can remove NH_3 much more efficiently than chemical loss (see Table S6-3). As K_{zz} increases, more NH_3 is transported to the upper atmosphere before NH_3 can be removed by deposition. In this case, larger K_{zz} suppresses the efficacy of NH_3 deposition, leading to an increase in atmospheric NH_3 concentration. However, when the surface is saturated with NH_3 (i.e., without NH_3 deposition), NH_3 column-averaged mixing ratio is inversely proportional to K_{zz} . In a more stagnant atmosphere (i.e., smaller K_{zz}), more NH_3 can accumulate at low altitudes since there is no wet or dry deposition. This local accumulation of NH_3 at low altitudes causes NH_3 surface mixing ratio and NH_3 column-averaged mixing ratio to increase. As K_{zz} increases, the NH_3 that could have accumulated locally at low altitudes is now transported to the upper atmosphere, where NH_3 photochemical removal dominates. Hence, when there is no deposition, NH_3 column-averaged mixing ratio decreases when the atmosphere becomes more diffusive.

Overall, the K_{zz} variation does not change our main conclusion as NH_3 column-averaged mixing ratio stays roughly at the same order of magnitude in our sensitivity test.

III. Henry's law constant for NH_3 : The effect of pH on NH_3 Henry's law constant is minimal. Even under high pH conditions (pH~14), NH_3 Henry's law constant will only decrease by up to 10% (Shi et al., 1999).

What might conceivably be quite different is the effective Henry's law constant invoked in the rainout calculation, which assumes a raindrop pH of 5 (Giorgi et al., 1985; Hu et al., 2012). At such acidic pH, the effective Henry's law constant (including partitioning of N(-III) into NH_4^+) is much higher than Henry's law constant alone. As raindrop becomes basic (pH>7), the effective Henry's law constant will converge with Henry's law constant. Hence, rainout would be much less efficient (though not ineffective, as even the 'regular' Henry's law constant for NH_3 is very high). In this case, we expect results intermediate to our NH_3 deposition on and off cases.

Appendix G. NH_3 Condensation in the Atmosphere

We find that NH_3 does not condense in our simulated atmospheres. At even the highest NH_3 flux considered in our study, NH_3 is insufficiently abundant anywhere in the atmosphere to condense. Here we plot the scenario with the highest NH_3 surface flux (i.e., H_2 -dominated atmosphere, with NH_3 deposition), and we superimpose the NH_3 saturation curve (equilibrium with both the liquid and solid phase) on top of it (see Figure SI.8). The black curve is the NH_3 volume mixing ratio on planets with H_2 -dominated atmospheres orbiting M dwarfs. The red curve is the NH_3 saturation curve (Stull, 1947). The NH_3 surface production flux is 6.4×10^{15} molecule $\text{cm}^{-2} \text{s}^{-1}$ (see Table 4-1).

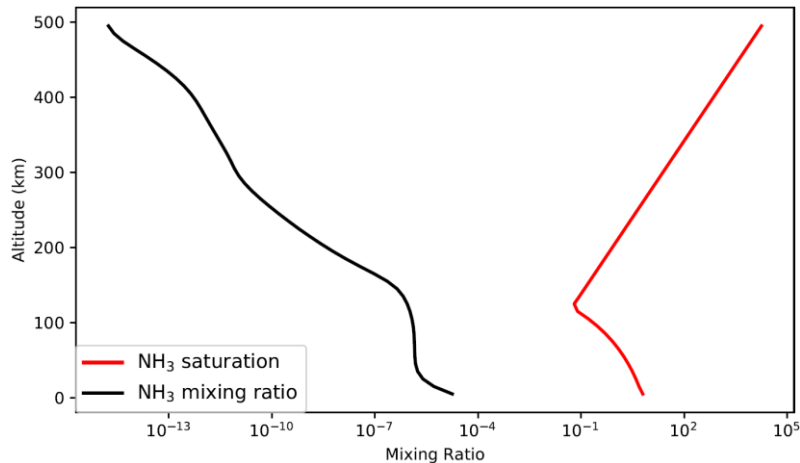


Figure 3-18. The volume mixing ratio of NH_3 on planets with H_2 -dominated atmospheres orbiting active M dwarfs. The NH_3 surface production flux is 6.4×10^{15} molecules $\text{cm}^{-2} \text{s}^{-1}$. The y-axis shows altitude in km, and the x-axis shows the mixing ratio. At even the highest NH_3 flux considered in our study, NH_3 is insufficiently abundant anywhere in the atmosphere to condense.

This figure clearly shows that our simulated NH_3 is not concentrated enough to condense in the atmosphere. Therefore, the stratospheric mixing ratio of NH_3 will never decouple from the surface mixing ratio (or the surface production flux). As a result, we do not consider upper atmosphere NH_3 condensation in our study.

Appendix H. NH_3 Abiotic False-Positive Analysis

I. Volcanic NH_3 outgassing: We can estimate the flux at which NH_3 can be degassed on an exoplanet based on Earth's N_2 volcanic outgassing flux. (Catling et al., 2017) estimates the N_2 volcanic outgassing on Earth is roughly 0.9×10^{11} mol/year. If all the nitrogen comes out as NH_3 instead, the NH_3 outgassing flux can be as high as 6.7×10^8 molecules $\text{cm}^{-2} \text{s}^{-1}$. For an exoplanet with H_2 -dominated atmospheres, to generate an NH_3 false positive from volcanic outgassing, the exoplanet's mantle conditions need to favor $\text{NH}_3/\text{NH}_4^+$ production, and the volcanic outgassing of N needs to be at least 100 times greater than Earth's (assuming there is no NH_3 -removal sink on the planet's surface). Hence, it is unlikely for volcanic NH_3 outgassing alone to generate a detectable false positive.

II. Nitrogen photoreduction on TiO_2 containing sands: We can estimate the upper limit of the amount of NH_3 this abiotic N_2 photo-fixation can produce. Suppose there is an Earth-sized exoplanet orbiting an M dwarf. The planet is arid, and the surface is covered by TiO_2 containing sands. We assume the planet has an Earth-sized desert (about 1.9×10^7 square miles) (Schrauzer et al., 1983). We also assume the planet's total surface area is the same as Earth's (roughly 1.97×10^8 square miles). Since M dwarf planets receive roughly 100 ~1000 times less UV than Sun-like star planets do (Ranjan et al., 2017), we assume this abiotic pathway is only 1% effective on the M dwarf planets. Hence, this abiotic N_2 fixation can produce up to 1 Tg of NH_3 every year (about 2.0×10^8 molecules $\text{cm}^{-2} \text{s}^{-1}$), roughly 2 orders of magnitude smaller than the flux needed to generate a detectable NH_3 false positive

(assuming there is no NH_3 -removal sink on the surface). (Kasting et al., 1982) reports that this abiotic N_2 photo-fixation can generate NH_3 at a rate of 2.8×10^{10} to 2.8×10^{11} molecules $\text{cm}^{-2} \text{s}^{-1}$ locally on Earth. Assuming this reaction is 1% effective on the M dwarf planets, we estimate that this abiotic N_2 fixation could produce NH_3 at a rate of up to 2.8×10^9 molecules $\text{cm}^{-2} \text{s}^{-1}$. Even in the most optimum case where NH_3 is emitted globally at this rate on exoplanets, the NH_3 production flux is still about an order of magnitude smaller than the flux needed to generate a detectable false positive. Overall, it is unlikely for nitrogen photoreduction on TiO_2 containing sands alone to generate a detectable false positive.

III. Abiotic $\text{NH}_3/\text{NH}_4^+$ synthesis around Hadean submarine hydrothermal vents: Suppose there is an Earth-sized exoplanet orbiting an M dwarf star. We assume the planet's total heat flow is the same as modern Earth's (roughly 4.3×10^{13} W) (Elderfield et al., 1996; Smirnov et al., 2008). Assuming the most favorable scenario with 80% of the planet's heat flow released via hydrothermal activity and 10% conversion of N_2 to NH_4^+ , the annual NH_4^+ production can be as high as 1.9×10^{12} mol/year (Smirnov et al. 2008). If we further assume all the NH_4^+ produced in the ocean is released into the atmosphere as NH_3 , this abiotic $\text{NH}_3/\text{NH}_4^+$ synthesis can produce up to 32 Tg of NH_3 every year (about 7×10^9 molecules $\text{cm}^{-2} \text{s}^{-1}$). Even in this most optimum case, the NH_3 production flux is not large enough to generate a detectable NH_3 false positive.

Appendix I. Detectability of TRAPPIST-1 Planets with JWST

Recently, some papers (e.g., Fauchez et al., 2019; Lustig-Yaeger et al., 2019) claim that gases like CH_4 , H_2O , CO_2 , and SO_2 might be detectable for TRAPPIST-1 planets with JWST (Lustig-Yaeger et al., 2019). Depends on the assumptions of the atmosphere (i.e., CO_2 -, N_2 - or H_2O -dominated atmospheres) and the signal-to-noise (S/N) ratio, the number of transits required to detect those gases on TRAPPIST-1 planets could range from 10 transits to more than 100 transits. What they claim is not contradictory to our statement here. TRAPPIST-1, an ultra-cooled M8V dwarf star, is rare and unique. TRAPPIST-1's small stellar radius and relatively low temperature are beneficial for trace gas detection because the transit depth scales with $(R_{\text{planet}}/R_{\text{star}})^2$. Furthermore, neither (Fauchez et al., 2019) or (Lustig-Yaeger et al., 2019) assumes a fixed systematic noise floor as we do in our analysis. Lastly, the detectability of gases on exoplanets depends on more than a dozen parameters - the presence of clouds and hazes, scattering, atmospheric refraction, to name a few. Different assumptions for those parameters can lead to very different conclusions. It is beyond the scope of this paper to go through every parameter to assess detectability.

Chapter 4

Methanol - a Poor Biosignature Gas in Exoplanet Atmospheres

The results presented in this chapter have been published in *The Astrophysical Journal* (<https://doi.org/10.3847/1538-4357/ac6f60>). I would like to thank the following co-authors for their contributions to this project: Prof. Sara Seager, Dr. Janusz J. Petkowski, Dr. Zhuchang Zhan, and Dr. Sukrit Ranjan. Each of them played an essential role in the publication of the paper.

Abstract

Biosignature gas research has been growing in recent years thanks to next-generation space and ground-based telescopes. Methanol (CH_3OH) has many advantages as a biosignature gas candidate. First, CH_3OH 's hydroxyl group (OH) has a unique spectral feature compared to other anticipated gases in rocky exoplanets atmospheres. Second, there are no significant known abiotic CH_3OH sources on terrestrial planets in the solar system. Third, life on Earth produces CH_3OH in large quantities. However, despite CH_3OH 's advantages, we consider CH_3OH a poor biosignature gas in terrestrial exoplanet atmospheres due to the enormous production flux required to reach its detection limit. CH_3OH 's high water solubility makes it very difficult to accumulate in the atmosphere. For the highly favorable planetary scenario of an exoplanet with an H_2 -dominated atmosphere orbiting an M5V dwarf star, we find that only when the column-averaged mixing ratio of CH_3OH reaches at least 10 ppm can we detect it with JWST. CH_3OH bioproduction flux required to reach the 10 ppm JWST detection threshold must be on the order of 10^{14} molecules $\text{cm}^{-2} \text{s}^{-1}$, which is roughly three times the annual O_2 production on Earth. Considering that such an enormous flux of CH_3OH is essentially a massive waste of organic carbon - a major building block of life, we think this flux, while mathematically possible, is likely biologically unattainable. Although CH_3OH can theoretically accumulate on exoplanets with CO_2 - or N_2 -dominated atmospheres, such planets' small atmospheric scale height and weak atmosphere signals put them out of reach for near-term observations.

4.1 Introduction

In planetary science, the search for biosignature gases is anticipated to become a pivotal way to uncover signs of extraterrestrial life. Thanks to the development of space telescopes (e.g., JWST), more and more gases have been proposed as biosignature gases in recent years. Biosignature gases are gases produced by living organisms that accumulate in the atmosphere to detectable levels. A biosignature gas can either be a by-product or a final product of biochemical metabolism. Among the known biosignature gases, oxygen (O_2) is the most famous (e.g., Jeans, 1930; Meadows et al., 2018). Other biosignature gases that people have studied include methane (CH_4) (Leger et al., 1996; Des Marais et al., 2002; Kaltenecker et al., 2007; Dlugokencky et al., 2011; Guzmán-Marmolejo et al., 2015), methyl chloride (CH_3Cl) (Segura et al., 2005), nitrous oxide (N_2O) (Des Marais et al., 2002;

Segura et al., 2005; Tian et al., 2015; Rugheimer et al., 2018), methanethiol (CH_3SH) (Domagal-Goldman et al., 2011), phosphine (PH_3) (Sousa-Silva et al., 2020), isoprene (C_5H_8) (Zhan et al., 2021) and ammonia (NH_3) (Seager et al., 2013; Huang et al., 2022).

We are motivated to study atmospheric CH_3OH as part of our program to assess all potential biosignature gases (Seager et al., 2016). CH_3OH is an important precursor molecule for life's biochemistry, as it is the building block of a diverse set of biochemicals such as acetic acid, methylamines, and methyl esters, to name a few. In the atmosphere, CH_3OH is a significant source of formaldehyde (CH_2O) and carbon monoxide (CO) (Tie et al., 2003; Solomon et al., 2005; Millet et al., 2008; Hu et al., 2011). CH_3OH stands out from other biosignature gas candidates because there is no significant known abiotic CH_3OH source on terrestrial planets (see Chapter 4.2). Furthermore, due to CH_3OH 's high water solubility (see Chapter 4.6.1), the limited amount of abiotic CH_3OH produced can be easily removed by rain, making it extremely difficult to accumulate. As a result, only when life generates a substantial amount of CH_3OH can it reach detectable levels in the atmosphere. People have not thoroughly studied CH_3OH as a biosignature gas before.

We first discuss CH_3OH sources (Chapter 4.2) and CH_3OH removal mechanisms (Chapter 4.3). We then describe our photochemistry model (Chapter 4.4.1) and our transmission spectra model (Chapter 4.4.2). We present our results in Chapter 4.5. We discuss our results and limitations in Chapter 4.6. Finally, we conclude with a summary (Chapter 4.7).

4.2 CH_3OH Emission and Production Mechanisms

In this section, we first discuss Earth's atmospheric CH_3OH concentrations and lifetime in Chapter 4.2.1. Then we review CH_3OH production flux on Earth in Chapter 4.2.2. Next, we discuss biological CH_3OH production in Chapter 4.2.3 and minor CH_3OH sources on Earth in Chapter 4.2.4.

4.2.1 Earth's Atmospheric CH_3OH Concentrations and Lifetime

Methanol is the second most abundant organic gas in the Earth's atmosphere, second only to CH_4 (Millet et al., 2008; Hu et al., 2011). Overall, atmospheric CH_3OH concentrations range from approximately 600 ppt in the upper troposphere to roughly 10 ppb near the surface (Heikes et al., 2002; Solomon et al., 2005; Hu et al., 2011; Stavrakou et al., 2011). CH_3OH surface concentrations can reach 47 ~ 55 ppb in some urban areas (Heikes et al., 2002; Solomon et al., 2005). Current data on atmospheric CH_3OH concentrations at a global level are scarce and have considerable uncertainties (Tie et al., 2003; Solomon et al., 2005; Hu et al., 2011; Stavrakou et al., 2011). In many parts of the world, long-term observations and measurements of CH_3OH are still unavailable and remain poorly constrained (Tie et al., 2003; Solomon et al., 2005; Hu et al., 2011; Stavrakou et al., 2011). Existing limited measurements show strong regional variability in atmospheric CH_3OH levels (Tie et al., 2003; Millet et al., 2008) (Figure 4-1).

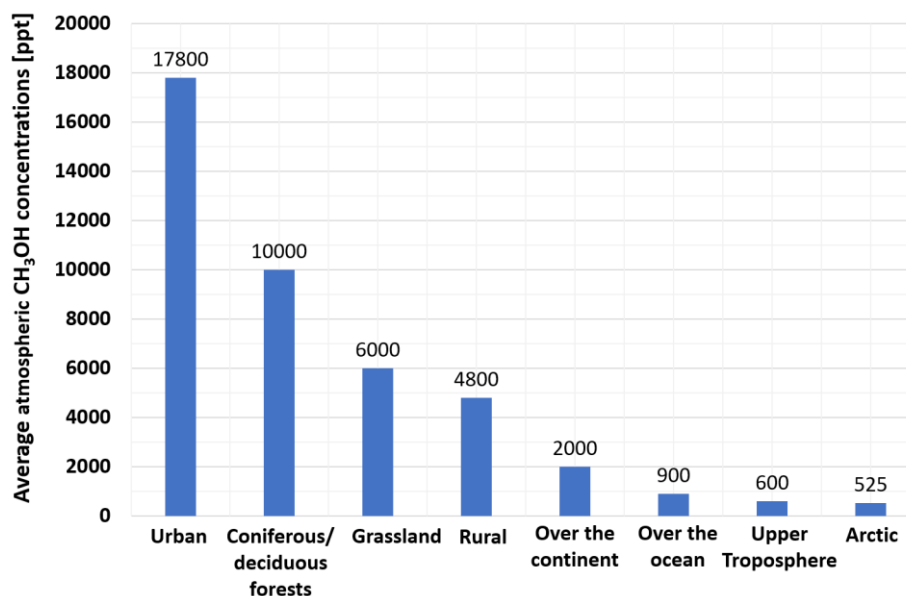


Figure 4-1. Average atmospheric CH₃OH concentrations over/in some representative regions. The y-axis is the atmospheric CH₃OH concentrations in ppt (parts-per-trillion). The x-axis shows the names of the regions. Atmospheric CH₃OH concentrations are the highest for urban areas and the lowest over the arctic. Atmospheric CH₃OH is relatively abundant above forests, especially during growing seasons (Stavrakou et al., 2011). Data from Heikes et al., 2002.

The atmospheric CH₃OH concentrations also have pronounced seasonal patterns (Tie et al., 2003; Hu et al., 2011). CH₃OH concentrations are highest in summer and lowest in winter (Hu et al., 2011). As the ambient temperature rises during summer, atmospheric CH₃OH levels increase. The seasonality of CH₃OH concentrations is mainly driven by variations in biogenic CH₃OH emissions (Hu et al., 2011). On hot summer days, plants proliferate. The rapid growth of plants and leaves results in much higher CH₃OH emissions (Chapter 4.2.3), leading to a significant (up to threefold) increase in atmospheric CH₃OH concentrations (Hu et al., 2011). In autumn and winter, old and mature leaves cannot produce as much CH₃OH as those newly-grown leaves, so overall biogenic CH₃OH emissions decrease (Hu et al., 2011). The impact of human activities on the seasonality of CH₃OH is minimal. Even in winter, the contribution of anthropogenic emissions to atmospheric CH₃OH concentrations is only about 40% on average (Hu et al., 2011). The atmospheric CH₃OH concentrations also exhibit consistent diurnal variations. CH₃OH concentrations at night are slightly higher than those during the day (Galbally et al., 2002; Solomon et al., 2005). The main reason for the increase in CH₃OH concentrations at night is the reduction of turbulent mixing in the boundary layer rather than the change in emission flux (Solomon et al., 2005).

The estimated overall lifetime of CH₃OH in Earth's atmosphere is roughly 5~12 days (Galbally et al., 2002; Heikes et al., 2002; Tie et al., 2003; Singh et al., 2004; Millet et al., 2008; Hu et al., 2011). However, depending on the altitude, the CH₃OH lifetime may vary considerably. In the surface boundary layer, the chemical lifetime of CH₃OH is only about 3~6 days (Galbally et al., 2002; Heikes et al., 2002; Tie et al., 2003). In the upper troposphere, CH₃OH lifetime is much longer, ranging from 16 days to a few weeks (Galbally et al., 2002; Heikes et al., 2002; Tie et al., 2003). The atmospheric lifetime of

CH₃OH is longer than that of isoprene (~ a few hours) and formaldehyde (~1 day) but much shorter than the atmospheric lifetime of CH₄ (8 ~ 10 years) (Heikes et al., 2002; Tie et al., 2003). Therefore, unlike isoprene, which is limited to the source regions due to its short lifetime, CH₃OH can be transported from the surface to the upper troposphere. However, CH₃OH's shorter lifetime than CH₄ means that CH₃OH cannot be as long-lived and widely spread in the upper troposphere as CH₄ (Tie et al., 2003).

4.2.2 CH₃OH Production Flux on Earth

The global CH₃OH emissions are huge, accounting for nearly half of the total annual oxygenate (i.e., chemicals that have oxygen in their molecules) production (Guenther et al., 1995; Heikes et al., 2002). Estimates of global CH₃OH source range from less than 100 Tg/year to roughly 350 Tg/year (Heikes et al., 2002; Tie et al., 2003; Singh et al., 2004; Millet et al., 2008; Hu et al., 2011; Stavrakou et al., 2011). In comparison, the estimated biological production of methane (CH₄), nitrogen gas (N₂), and ammonia (NH₃) on Earth is about 500 Tg/year, 457 Tg/year, and 200 Tg/year, respectively (Guenther et al., 2006; Rascio et al., 2013; Yeung et al., 2019). Different researchers have tried to come up with estimates of global CH₃OH fluxes, but the uncertainty in their estimates remains large (Table 4-1).

Table 4-1. Estimates of the global CH₃OH emission flux.

Estimated range (most probable value)	Reference
122 ~ 340 Tg/year (280 Tg/year)	Heikes et al., 2002
70 ~ 350 Tg/year (312 Tg/year)	Tie et al., 2003
75 ~ 490 Tg/year (110 Tg/year)	Singh et al., 2004
123 ~ 343 Tg/year (242 Tg/year)	Millet et al., 2008
100 ~ 320 Tg/year (187 Tg/year)	Stavrakou et al., 2011

The largest source of atmospheric CH₃OH is the terrestrial biosphere, specifically plant growth (Chapter 4.2.3). According to literature estimates, CH₃OH produced by plant growth can account for up to 80% of the global CH₃OH emissions (Galbally et al., 2002; Heikes et al., 2002; Tie et al., 2003; Millet et al., 2008; Hu et al., 2011; Stavrakou et al., 2011). Other CH₃OH sources include degradation of plant matter, industrial and urban activities, biomass and biofuel burning, and atmospheric production (Chapter 4.2.4) (Galbally et al., 2002; Heikes et al., 2002; Singh et al., 2004; Millet et al., 2008). So far, there has been no report claiming volcanic emission of CH₃OH. The figure below is a simplified schematic diagram of the global CH₃OH biogeochemical cycle (Figure 4-2).

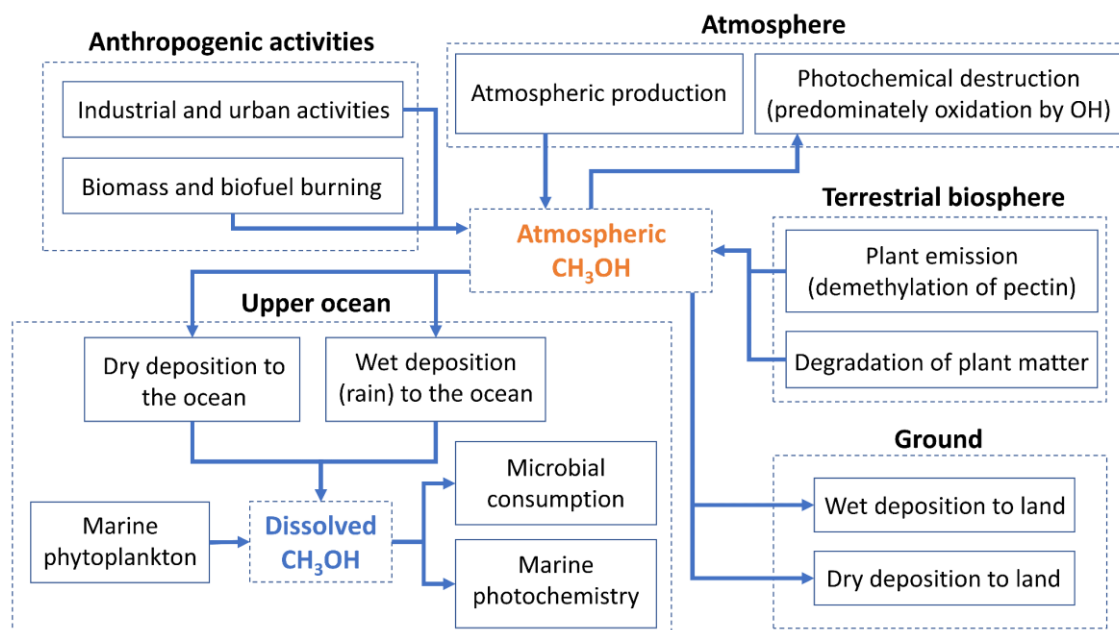


Figure 4-2. A simplified schematic diagram of the global CH₃OH biogeochemical cycle. The largest source of atmospheric CH₃OH is the terrestrial biosphere, accounting for up to 80% of the global CH₃OH emissions. In contrast, CH₃OH produced by anthropogenic activities (particularly industry) only makes up a tiny fraction ($\leq 5\%$) of the total annual CH₃OH emission flux (Galbally et al., 2002; Heikes et al., 2002; Millet et al., 2008; Hu et al., 2011; Stavrakou et al., 2011).

Some papers hypothesize that the marine biosphere might also be an essential source of CH₃OH (Galbally et al., 2002; Heikes et al., 2002; Millet et al., 2008; Hu et al., 2011; Stavrakou et al., 2011). In the upper ocean, where nutrient levels are high, marine phytoplankton can convert algal carbohydrates into CH₃OH. Since marine phytoplankton is one of the most abundant species on Earth, theoretically, it can produce considerable CH₃OH every year (Heikes et al., 2002; Millet et al., 2008). However, this source is exceeded by a much bigger oceanic sink (Galbally et al., 2002; Millet et al., 2008; Hu et al., 2011; Stavrakou et al., 2011). Therefore, on a global scale, the ocean acts as a net sink for CH₃OH (Chapter 4.3.2). We have summarized the estimated global CH₃OH sources in Table 4-2.

Table 4-2. Estimated global CH₃OH sources⁸ in Tg/yr.

Description	Estimated CH ₃ OH sources Tg/year: value (range)				
	Ref 1	Ref 2	Ref 3	Ref 4	Ref 5
Terrestrial plant growth	100 (37 - 212)	280 (50 - 280)	128 (37 - 280)	80 (75 - 312)	
Plant decay	13 (5 - 31)	20 (10 - 40)	23 (5 - 40)	23 (13 - 23)	100 (100 - 151)
Industry and urban	4 (3 - 5)	8 (5 - 11)	9 (2 - 11)	5 (2 - 8)	
Biomass/biofuel burning	13 (6 - 19)	12 (2 - 32)	12 (2 - 32)	12 (6 - 15)	9.3 (9.3)
Atmospheric production	19 (14 - 24)	30 (18 - 30)	37 (12 - 37)	37 (18 - 38)	31 (30.7 - 31.1)

[1]. Galbally et al., 2002; [2]. Heikes et al., 2002; [3]. Singh et al., 2004; [4]. Millet et al., 2008; [5]. Stavrakou et al., 2011.

⁸ We only include net CH₃OH sources in this table.

4.2.3 Biological CH₃OH Production

Plants are the largest source of CH₃OH in the Earth's atmosphere. Most plants can produce CH₃OH through the demethylation of pectin during leaf growth (Galbally et al., 2002; Heikes et al., 2002; Tie et al., 2003; Millet et al., 2008; Stavrakou et al., 2011). Pectin is a complex polysaccharide widely found in plant cell walls. As an essential tissue firming agent, pectin can strengthen the cell wall, protecting and supporting the intracellular structures. During cell growth, pectin is demethylated through the action of pectin methylesterase (PME), an enzyme involved in plant growth (Fall et al., 1996; Stavrakou et al., 2011). As a by-product of pectin demethylation, CH₃OH is released through stomata during transpiration (Galbally et al., 2002; Millet et al., 2008; Stavrakou et al., 2011) (Figure 4-3). The CH₃OH leaf emissions depend on light, temperature, and stomatal conductance (Stavrakou et al., 2011). As a result, CH₃OH emissions from leaves significantly decrease at night due to the stomatal control (Millet et al., 2008).

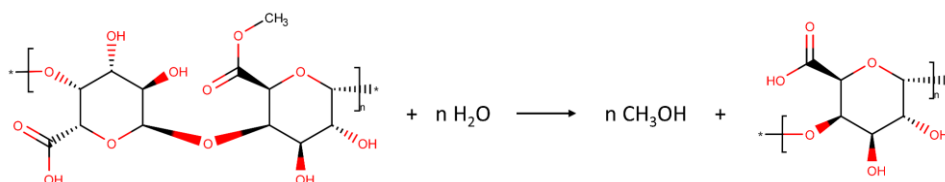


Figure 4-3. Through the action of pectin methylesterase (PME), pectin demethylation produces CH₃OH as a by-product.

In general, CH₃OH emissions are inversely proportional to leaf age (Stavrakou et al., 2011). Young and growing leaves can produce more methanol than old and senescing leaves (Heikes et al., 2002; Millet et al., 2008; Stavrakou et al., 2011). Different types of plants have different CH₃OH emission rates. Conifers have lower methanol emissions than broad-leaf plants. In addition, when leaves are wounded, CH₃OH emissions will increase (Heikes et al., 2002). Since leaf CH₃OH emissions depend on numerous parameters, most of which can change substantially during the growing seasons, estimating a global CH₃OH emission factor without considerable uncertainties is extremely difficult (Chapter 4.2.2). However, not all CH₃OH produced in leaves ends up in the atmosphere (Galbally et al., 2002; Millet et al., 2008). Plants can store a small amount of CH₃OH in their tissues. Plants can also metabolize (oxidize) some methanol to formaldehyde with the help of methanol oxidase (Galbally et al., 2002).

Even though plant growth and development is the dominant biological CH₃OH production mechanism on Earth, other biological processes can also generate CH₃OH at a much lower rate (Millet et al., 2008; Stavrakou et al., 2011). (Fall et al., 1996) reports that root and fruit growth can produce CH₃OH. Degradation of dead plants can also yield a small amount of CH₃OH either through the action of residual enzymes or with the help of microorganisms (Millet et al., 2008). During the fungal decomposition of wood, lignin demethylation can produce a limited amount of CH₃OH (Millet et al., 2008). For completeness, we note that methanotrophic bacteria (also called methanotrophs) can also produce CH₃OH. With the

help of methane monooxygenase (MMO), an enzyme that can oxidize the C-H bond in methane, methanotrophs can oxidize CH₄ to CH₃OH (Hanson et al., 1996; Basch et al., 1999). However, MMO-mediated CH₃OH production is insignificant compared to other biological production pathways. Due to the lack of research on these minor biological CH₃OH production pathways mentioned above, their respective contributions to global CH₃OH production, albeit extremely small, remain unknown.

4.2.4 Minor CH₃OH Sources on Earth

There are a few minor CH₃OH sources on Earth. One of the sources is anthropogenic activity, particularly industry (Galbally et al., 2002; Millet et al., 2008; Hu et al., 2011; Stavrou et al., 2011). CH₃OH has a wide range of industrial applications, including as a solvent, an antifreeze, fuel and fuel additives, and sewage treatment agent (Galbally et al., 2002; Millet et al., 2008). In industry, people also use CH₃OH to produce other compounds such as formaldehyde, acetic acid, methyl tertiary-butyl ether (MTBE), methylamines, and methyl esters (Galbally et al., 2002). Overall, global emission of industrially-produced CH₃OH is about 4 Tg/year, which makes up a tiny fraction ($\leq 5\%$) of the total annual CH₃OH emission flux (Galbally et al., 2002; Heikes et al., 2002; Millet et al., 2008; Hu et al., 2011; Stavrou et al., 2011).

In addition to industry, biomass burning is also a key contributor to atmospheric CH₃OH (Galbally et al., 2002; Stavrou et al., 2011). Every year, biomass burning related to deforestation, shifting cultivation, and agricultural waste disposal (e.g., stubble burning) can release considerable CH₃OH (Crutzen et al., 1990; Galbally et al., 2002). People also use wood or charcoal as fuel (for cooking and heating). During the combustion process (particularly in the smoldering phase), pyrolysis of hemicellulose polymers and lignin present in the biomass yields CH₃OH (McKenzie et al., 1995; Galbally et al., 2002). (Andreae et al., 2001) estimated that biomass burning can produce up to 12.7 Tg of CH₃OH per year.

In the atmosphere, CH₃OH can be chemically regenerated from CH₃O radicals, which likely originate from the photochemical decomposition of CH₃OH itself (Table 4-3). Hence, we do not consider Earth's atmospheric chemistry as a net source of CH₃OH. Our photochemistry model currently has 14 CH₃OH-producing reactions, including two low-temperature reactions.

Table 4-3. CH₃OH-producing reactions in the atmosphere.

Reaction	Reaction rate [cm ³ molecule ⁻¹ s ⁻¹]	Valid temp range [K]	Source
CH ₃ O + C ₂ H ₅ → C ₂ H ₄ + CH ₄ O	4.0 · 10 ⁻¹²	300 - 2500	NIST
CH ₃ O + C ₂ H ₆ → C ₂ H ₅ + CH ₄ O	4.0 · 10 ⁻¹³ · exp(-3570.0/T)	300 - 2500	NIST
CH ₃ O + CH ₂ O → CH ₄ O + CHO	1.7 · 10 ⁻¹³ · exp(-1500.0/T)	300 - 2500	NIST
CH ₃ O ₂ + CH ₃ O ₂ → CH ₄ O + CH ₂ O + O ₂	3.6 · 10 ⁻¹⁴ · exp(390.0/T)	200 - 300 *	JPL
CH ₄ + CH ₃ O → CH ₄ O + CH ₃	2.61 · 10 ⁻¹³ · exp(-4450.0/T)	300 - 2500	NIST
CHO + CH ₃ O → CH ₄ O + CO	1.5 · 10 ⁻¹⁰	300 - 2500	NIST
H + CH ₃ NO ₂ → CH ₄ O + NO	2.0 · 10 ⁻¹³ · exp(-956.2/T)	223 - 398 *	NIST
H + CH ₃ O → CH ₄ O	2.89 · 10 ⁻¹⁰ · (T/298.0) ^{0.04}	300 - 2500	NIST

$\text{H}_2 + \text{CH}_3\text{O} \rightarrow \text{CH}_4\text{O} + \text{H}$	$9.96 \cdot 10^{-14} \cdot (\text{T}/298.0)^2 \cdot \exp(-6720.0/\text{T})$	300 - 2500	NIST
$\text{H}_2 + \text{CH}_3\text{O}_2 \rightarrow \text{CH}_4\text{O}_2 + \text{H}$	$5.0 \cdot 10^{-11} \cdot \exp(-13110.0/\text{T})$	300 - 2500	NIST
$\text{H}_2\text{O}_2 + \text{CH}_3\text{O} \rightarrow \text{CH}_4\text{O} + \text{HO}_2$	$5.0 \cdot 10^{-15} \cdot \exp(-1300.0/\text{T})$	300 - 2500	NIST
$\text{HNO} + \text{CH}_3\text{O} \rightarrow \text{CH}_4\text{O} + \text{NO}$	$5.0 \cdot 10^{-11}$	298	NIST
$\text{OH} + \text{CH}_3\text{O}_2 \rightarrow \text{CH}_4\text{O} + \text{O}_2$	$1.0 \cdot 10^{-10}$	300 - 2500	NIST
$\text{OH} + \text{CH}_3 \rightarrow \text{CH}_4\text{O}$	$3.69 \cdot 10^{-29} \cdot \exp(1280.0/\text{T})$	300 - 700	NIST

(* : Low-temperature reaction)

4.3. CH₃OH Removal Mechanisms

In this section, we review CH₃OH removal mechanisms. We first look into CH₃OH atmospheric sinks in Chapter 4.3.1. The main CH₃OH removal pathway in Earth's atmosphere is oxidation by OH. Next, we explore deposition to land and ocean uptake in Chapter 4.3.2. While less significant than atmospheric destruction, surface deposition can still impact the accumulation of CH₃OH in the atmosphere.

4.3.1 CH₃OH Atmospheric Sinks

Of all the known CH₃OH removal mechanisms on Earth, photochemical oxidation by hydroxyl radicals (OH) dominates (Galbally et al., 2002; Heikes et al., 2002; Millet et al., 2008; Stavrou et al., 2011). In Earth's oxidizing atmosphere, OH is the most abundant radical (e.g., Seinfeld et al., 2008). The reaction between CH₃OH and gas-phase OH has two possible pathways: 1) abstraction of the H atom from the hydroxyl group to form CH₃O and H₂O; or 2) abstraction of H from the methyl group to yield CH₂OH and H₂O (Hagele et al., 1983; Hess et al., 1989; Dillon et al., 2005; Atkinson et al., 2006). At or below room temperature, H abstraction at the methyl site dominates. At 298K, the probability of the reaction to proceed according to the second pathway to form CH₂OH is about 85% (i.e., with a branching ratio of 0.85), and this ratio will increase as the temperature decreases (Dillon et al., 2005; Atkinson et al., 2006). In Earth's atmosphere, the final products of these two reaction pathways are the same: CH₂OH and CH₃O will react almost immediately with O₂ to give formaldehyde (CH₂O) and HO₂ radicals (Hagele et al., 1983; Heikes et al., 2002; Tie et al., 2003; Dillon et al., 2005). We compiled the temperature-dependent reaction rate coefficient in Table 4-4.

Table 4-4. CH₃OH photochemical oxidation by OH.

Reaction pathway	$\text{CH}_3\text{OH} + \cdot\text{OH} \rightarrow \cdot\text{CH}_2\text{OH} + \text{H}_2\text{O}$ (rate = k_1)	
	$\text{CH}_3\text{OH} + \cdot\text{OH} \rightarrow \text{CH}_3\text{O}\cdot + \text{H}_2\text{O}$ (rate = k_2)	
Overall reaction rate ($k = k_1 + k_2$) [cm ³ molecule ⁻¹ s ⁻¹]	Valid temp range [K]	Source
$3.6 \cdot 10^{-12} \cdot \exp(-415/\text{T})$	235 - 360	Jimenez et al., 2003
$6.67 \cdot 10^{-18} \cdot \text{T}^2 \cdot \exp(140/\text{T})$	210 - 350	Dillon et al., 2005
$3.82 \cdot 10^{-19} \cdot \text{T}^{2.4} \cdot \exp(300/\text{T})$	200 - 870	Dillon et al., 2005
$2.85 \cdot 10^{-12} \cdot \exp(-345/\text{T})$	210 - 300	Atkinson et al., 2006
$6.38 \cdot 10^{-18} \cdot \text{T}^2 \cdot \exp(144/\text{T})$	210 - 866	Atkinson et al., 2006

CH₃OH is the fourth largest sink for tropospheric OH in Earth's atmosphere, after CH₄, CO,

and isoprene (Galbally et al., 2002; Stavrakou et al., 2011). The CH₂O produced can further react with O, H, or OH radicals to form CO. Hence, CH₃OH is a significant source of CO in the troposphere and plays a vital role in tropospheric oxidant chemistry (Heikes et al., 2002; Solomon et al., 2005; Millet et al., 2008; Stavrakou et al., 2011). CH₂O can also react with HO₂ radicals in cloud water to yield formic acid (HCOOH) (Jacob, 1986; Heikes et al., 2002). Therefore, even if CH₃OH itself is not acidic, it can indirectly affect the acidity of rain and clouds (Jacob, 1986; Heikes et al., 2002).

CH₃OH can also react with H and O radicals in an exoplanet's atmosphere. In an H₂-dominated, high-reducing atmosphere, the H radical is the dominant reactive species (Hu et al., 2012). The importance of O radicals in a CO₂- or an N₂-dominated atmosphere still needs to be further explored (Hu et al., 2012; Ranjan et al., 2020). Our photochemistry model currently has 14 CH₃OH-removing reactions (in addition to the photochemical oxidation by OH listed in Table 4-5). Note that there is one high-temperature reaction and two low-temperature reactions in Table 4-5. We include both the high- and low-temperature reactions in our table for completeness even though the rates are extremely low at Earth-like temperatures.

Table 4-5. CH₃OH removal reactions in the atmosphere.

Reaction	Reaction rate [cm ³ molecule ⁻¹ s ⁻¹]	Valid temp range [K]	Source
C ₂ H + CH ₄ O → C ₂ H ₂ + CH ₃ O	2.0 · 10 ⁻¹²	300 - 2500	NIST
CH ₂ + CH ₄ O → CH ₃ + CH ₃ O	1.12 · 10 ⁻¹⁵ · (T/298.0) ^{3.1} · exp(-3490.0/T)	300 - 2500	NIST
CH ₃ + CH ₄ O → CH ₄ + CH ₃ O	1.12 · 10 ⁻¹⁵ · (T/298.0) ^{3.1} · exp(-3490.0/T)	300 - 2500	NIST
CH ₃ O ₂ + CH ₄ O → CH ₄ O ₂ + CH ₃ O	3.0 · 10 ⁻¹² · exp(-6900.0/T)	300 - 2500	NIST
CH ₄ O + CN → HCN + CH ₃ O	1.2 · 10 ⁻¹⁰	294	NIST
CHO + CH ₄ O → CH ₂ O + CH ₃ O	2.41 · 10 ⁻¹³ · (T/298.0) ^{2.9} · exp(-6600.0/T)	300 - 2500	NIST
H + CH ₄ O → CH ₃ + H ₂ O	3.32 · 10 ⁻¹⁰ · exp(-2670.0/T)	1370 - 1840 #	NIST
H + CH ₄ O → CH ₃ O + H ₂	2.42 · 10 ⁻¹² · (T/298.0) ² · exp(-2270.0/T)	300 - 2500	NIST
HO ₂ + CH ₄ O → CH ₃ O + H ₂ O ₂	1.6 · 10 ⁻¹³ · exp(-6330.0/T)	300 - 2500	NIST
N + CH ₄ O → CH ₃ + HNO	4.0 · 10 ⁻¹⁰ · exp(-4330.0/T)	309 - 409 *	NIST
NO ₃ + CH ₄ O → CH ₃ O + HNO ₃	9.4 · 10 ⁻¹³ · exp(-2646.0/T)	258 - 367 *	NIST
O + CH ₄ O → CH ₃ O + OH	1.66 · 10 ⁻¹¹ · exp(-2360.0/T)	300 - 1000	NIST
O(1 ^D) + CH ₄ O → CH ₃ O ₂ + H	9.0 · 10 ⁻¹¹	300	NIST
O(1 ^D) + CH ₄ O → CH ₃ O + OH	4.2 · 10 ⁻¹⁰	300	NIST

(#: High-temperature reaction; *: Low-temperature reaction)

CH₃OH can also undergo photolysis under UV radiation. We can express the photolysis rate coefficient J_A at the top of the atmosphere as $J_A = \int q_\lambda \cdot I_\lambda \cdot \sigma_\lambda \cdot e^{-\tau_\lambda} d\lambda$ (e.g., Brasseur et al., 2017). Here λ is the wavelength, τ_λ is the optical depth, σ_λ is the absorption cross-section of CH₃OH, I_λ is the solar intensity at the top of the atmosphere, and q_λ is the quantum yield of CH₃OH photolysis. We summarize the relevant parameters of CH₃OH photolysis in Table 4-6.

Table 4-6. Photolysis reactions of CH₃OH (Hu et al., 2012).

Reaction pathway	CH ₄ O → CH ₃ O + H
Reaction rate at 295 K [s ⁻¹]	5.97 × 10 ⁻⁶ ; computed in (Hu et al., 2012)
Cross Sections	16 - 106 nm: (Burton et al., 1992); 106 - 165 nm: (Nee et al., 1985); 165 - 220 nm: (Cheng et al., 2002)

Additionally, at high temperatures, CH₃OH will thermally decompose. We compile the thermal decomposition reactions of CH₃OH in Table 4-7, even though they do not occur at Earth-like temperatures.

Table 4-7. Thermal decomposition of CH₃OH (NIST).

Reaction	Reaction rate [cm ³ molecule ⁻¹ s ⁻¹]	Valid temp range [K]
CH ₄ O → CH ₃ O + H	$2.16 \cdot 10^{-8} \cdot \exp(-33556.0/T)$	1400 - 2500
CH ₄ O → CH ₃ + OH	$1.1 \cdot 10^{-7} \cdot \exp(-33075.0/T)$	1000 - 2000
CH ₄ O → CH ₂ O + H ₂	$2.12 \cdot 10^{13} \cdot (T/298.0)^{1.22} \cdot \exp(-43539.0/T)$	300 - 2500
CH ₄ O → CH ₂ + H ₂ O	$9.51 \cdot 10^{15} \cdot (T/298.0)^{-1.02} \cdot \exp(-46185.0/T)$	1000 - 3000

4.3.2 CH₃OH Deposition to Land and Ocean Uptake

Deposition to land and ocean uptake are two CH₃OH sinks in addition to atmospheric chemistry. Although less significant than atmospheric removal, they can still affect CH₃OH accumulation in the atmosphere.

There are significant uncertainties in CH₃OH dry deposition velocity on soil surfaces (Galbally et al., 2002; Millet et al., 2008). Due to the higher atmospheric temperature and more substantial convection/turbulence during the day, CH₃OH dry deposition velocity is higher during the day than at night (Millet et al., 2008). The decomposition of dead plants at night also slows down nighttime CH₃OH dry deposition (Millet et al., 2008). Several field studies claim that the CH₃OH dry deposition velocity is about 0.15 cm/s and can reach 0.5 cm/s locally (Karl et al., 2004; Mao et al., 2006; Millet et al., 2008). In general, CH₃OH dry deposition velocity adopted by most studies is in the range of 0.1-0.2 cm/s (Galbally et al., 2002; Millet et al., 2008). We use 0.1 cm/s as the estimated CH₃OH dry deposition velocity in our photochemistry model. Once deposited onto the soil, most⁹ CH₃OH is permanently removed through biological degradation (Galbally et al., 2002). Methylotrophs first oxidize CH₃OH to formaldehyde (CH₂O) in the soil through methanol dehydrogenase (Lehninger et al., 1993; Yurimoto et al., 2005), and then either further oxidize CH₂O to CO₂ for energy or convert CH₂O to a three-carbon compound (C₃) for biomass buildup (Galbally et al., 2002, Yurimoto et al., 2005).

Due to CH₃OH's extremely high water solubility (Chapter 4.6.1), atmospheric CH₃OH can dissolve in rainwater and fall to the ground or the sea with the rain. This process is called wet deposition (or 'rainout'), another CH₃OH removal mechanism. Compared to CH₃OH dry deposition, CH₃OH wet deposition is a much smaller sink (Galbally et al., 2002; Heikes et al., 2002; Tie et al., 2003; Stavrou et al., 2011). In this work, we collectively refer to CH₃OH dry and wet deposition to the ocean as ocean uptake. The atmosphere/ocean exchange rate of CH₃OH is very fast (Galbally et al., 2002). CH₃OH's high deposition rate is mainly limited by the gas-phase resistance to the exchange of CH₃OH between the atmosphere and the ocean's surface layer (i.e., the ocean mixed layer) (Galbally et al.,

⁹ A tiny amount of CH₃OH is absorbed by the soil materials (Barker et al., 1992).

2002). Due to the high efficiency of ocean uptake, atmospheric CH₃OH can reach equilibrium with CH₃OH in the ocean surface layer within approximately two weeks (Galbally et al., 2002). Some papers estimate that the CH₃OH concentration in the ocean mixed layer is between 0.1 and 0.6 μM, with CH₃OH concentration in the northern hemisphere (0.2 ~ 0.6 μM) slightly higher than that in the southern hemisphere (0.1 ~ 0.4 μM) (Galbally et al., 2002; Millet et al., 2008).

The ocean is a net sink of CH₃OH almost anywhere (Millet et al., 2008; Hu et al., 2011; Stavrakou et al., 2011), with only a few exceptions, such as the Persian Gulf and the Red Sea (Millet et al., 2008). Those areas are generally hot all year round, which dramatically reduces CH₃OH's water solubility. Even so, the ocean in those areas is only predicted as a weak source of CH₃OH (Millet et al., 2008). In most parts of the world, the net flux of CH₃OH is always into the ocean, with the strongest uptake near continental coasts where CH₃OH concentrations are high (Heikes et al., 2002; Millet et al., 2008; Stavrakou et al., 2011). Generally, ocean uptake is weaker during the day than at night (Heikes et al., 2002; Millet et al., 2008). This observed diurnal cycle likely reflects a competition between daytime CH₃OH production from marine phytoplankton and ocean uptake (Heikes et al., 2002; Millet et al., 2008).

After CH₃OH is deposited into the ocean, both microbial consumption and marine photochemistry will consume it and eventually remove most of it from the ocean (Heikes et al., 2002; Millet et al., 2008). Some papers suggest that marine methylotrophs can use CH₃OH as an energy and carbon source, similar to the methylotrophs in the soil (Kiene 1993; Heikes et al., 2002; Neufeld et al., 2007; McCarren et al., 2010). Dissolved CH₃OH can also react with OH in the aqueous phase to form formaldehyde (Heikes et al., 2002). It is worth noting that the aqueous OH reaction can occur in the ocean and within clouds, fog, raindrops, and even haze (Galbally et al., 2002; Heikes et al., 2002; Millet et al., 2008). Compared with other sinks we have discussed, aqueous OH oxidation is a much smaller sink (Galbally et al., 2002; Heikes et al., 2002, Millet et al., 2008). We have summarized the estimated global CH₃OH sinks in Table 4-8.

Table 4-8. Estimated global CH₃OH sinks in Tg/yr.

Description	Estimated CH ₃ OH sinks Tg/year: value (range)			
	Ref 1	Ref 2	Ref 3	Ref 4
Gas-phase OH oxidation	69 (41 - 128)	100 (25 - 150)	88 (59 - 149)	108 (107 - 131)
Liquid-phase OH oxidation	5 (2 - 15)	10 (5 - 20)	<1 (0 - 10)	
Dry deposition to land	24 (11 - 43)	70 (35 - 210)	40 (24 - 70)	34 (28 - 48)
Wet deposition to land	11 (5 - 20)	5 (3 - 20)	13 (9 - 50)	3 (2.7 - 3.6)
Wet deposition to the ocean	6 (6)	5 (1 - 16)	101 (101)	
Dry deposition to the ocean	N/A	80 (60 - 150)		49 (48 - 56)

[1]. Galbally et al., 2002; [2]. Heikes et al., 2002; [3]. Millet et al., 2008; [4]. Stavrakou et al., 2011.

4.4. Methods

We use two methods to assess the biosignature potential of CH₃OH. We first introduce our one-dimensional photochemistry model in Chapter 4.4.1. Then, we describe our

transmission spectra model (SEAS) in Chapter 4.4.2.

4.4.1 Photochemistry Model

We use our photochemistry model (Hu et al., 2012) to calculate the CH₃OH mixing ratio as a function of vertical altitude in exoplanet atmospheres. Our one-dimensional photochemistry model (Hu et al., 2012) can simulate a wide variety of planetary atmosphere scenarios (e.g., oxidized, oxic, and reduced) by calculating the atmosphere's steady-state chemical composition. Our photochemistry model includes more than 800 chemical reactions, thermal escape of C, H, O, N, and S-bearing species, as well as UV photolysis of atmospheric molecules. Our photochemistry code also includes wet and dry depositions, surface emissions, and formation and deposition of sulfur-containing (both elemental sulfur and sulfuric acid) aerosols. We have validated our photochemistry model by simulating modern Earth's and Mars' atmospheric composition, matching observations of major trace gases in both scenarios. Our model uses the delta-Eddington two-stream method to calculate ultraviolet and visible radiation in the atmosphere. Our model also includes molecular absorption, Rayleigh scattering, and aerosol Mie scattering to compute the optical depth. For applications of our photochemistry model, see (Hu et al., 2012; Seager et al., 2013; Hu et al., 2013; Sousa-Silva et al., 2020; Zhan et al., 2021 and Huang et al., 2022).

In this work, we simulate an Earth-sized exoplanet with an H₂-dominated atmosphere orbiting an M dwarf star. We use the synthetic stellar radiation model of GJ 876 (Lloyd et al., 2016; France et al., 2016). We set the planet's surface temperature to 288 K and surface pressure to 1 bar. The planet's atmosphere consists of a lower convective layer and a higher radiative layer (Hu et al., 2012). We set the temperature of the convective layer to follow the dry adiabatic lapse rate. We assume the temperature to be constant (isothermal) in the radiative layer (Hu et al., 2012), given that we do not consider heating in the upper atmosphere. For more details of how we set our atmospheric profiles, see (Hu et al., 2012; Huang et al., 2022).

In our simulations, we include all the reactions mentioned in (Hu et al., 2012) except for reactions that involve more than two carbon atoms (C_{>2-chem}), HSO₂ thermal decay, and high-temperature reactions (Hu et al., 2012). Moreover, we set the surface deposition (including both rainout and dry deposition) of H₂, CO, CH₄, N₂, C₂H₂, C₂H₄, C₂H₆, and O₂ to zero to facilitate robust comparison with reference benchmark scenarios from (Hu et al., 2012). Such assumption corresponds to the situation where surface biology is not an efficient sink for these gases, which does not hold for modern Earth. However, our results are robust to this assumption of inefficient deposition of non-CH₃OH gases as the main removal mechanisms of CH₃OH are surface deposition and direct photolysis. Finally, we present our stellar radiation model, the atmospheric temperature-pressure profile, and the surface boundary conditions in Appendix J.

4.4.2 Transmission Spectra model and Simulated Observation

To assess the possibility of detecting CH₃OH in an H₂-dominated atmosphere, we simulate

transmission spectra using our 'Simulated Exoplanet Atmosphere Spectra' (SEAS) model (Zhan et al., 2021). We also simulate James Webb Space Telescope (JWST) observations with noise calculated from PandExo, a noise simulator based on Space Telescope Science Institute's (STScI) exposure time calculator (Batalha et al., 2017). We focus on H₂-dominated atmospheres, given their relatively large transit depth (Chapter 4.6.3). In this section, we briefly describe our spectral analysis. Please refer to (Zhan et al. 2021; Huang et al., 2022) for more details of our model.

We use our spectra model SEAS to simulate theoretical transmission spectra. SEAS takes the temperature-pressure profile and the mixing ratio profile from the photochemistry code as input and calculates the absorption of light along the limb path of each layer of the atmosphere (Zhan et al., 2021). In our model, we divide the atmosphere into layers, and the width of each layer is one atmospheric scale height. We assume that each layer of the atmosphere is in local thermodynamic equilibrium. We simulate transmission spectra at a spectral resolution of $R = 1000$ and use the HAPI package (Kochanov et al., 2016) to calculate molecular absorption cross-sections from the HITRAN database (Gordon et al., 2017; Zhan et al., 2021). We have validated our SEAS model by reproducing Earth's atmosphere spectra (Zhan et al., 2021). Note that SEAS currently does not include refraction. As a result, our model works best for M dwarf planets, where refraction has the least impact on observations (B  tr  mieux et al., 2014; Misra et al., 2014).

We evaluate the detectability of the atmosphere by using the criterion presented in (Seager et al., 2013; Batalha et al., 2017; Zhan et al., 2021 and Huang et al., 2022). Specifically, we estimate the observational uncertainties using the Pandexo JWST noise simulator (Batalha et al., 2017). We use both the Near InfraRed Spectrograph (NIRSpec) G140M, G235M, and G395M and the Mid-Infrared Instrument (MIRI) LRS observation modes. These two instruments have a combined spectral coverage of about 1 to 13 μm . Here, we consider a 5 M_{Earth} , 1.5 R_{Earth} super-Earth with an H₂-dominated atmosphere transiting an M5V star (GJ 876). We choose such a massive planet because a large planet is more likely to retain an H₂-dominated atmosphere than an Earth-sized planet. We project the results from our photochemistry model onto the super-Earth by keeping 'the mixing ratio as a function pressure' constant. For more details, see (Sousa-Silva et al., 2020). The planet's transit duration is roughly 3.2 hours. The distance to the star is 10 parsec. Here, we bin our spectral resolution to $R = 10$. We also include a ten ppm JWST systematic noise floor in our spectral analysis. Finally, we use a null-hypothesis test (e.g., Madhusudhan et al., 2009) to assess whether we can distinguish between an atmosphere with and without significant CH₃OH. We first compute the reduced chi-square statistics between our simulated observational data and the ground truth (i.e., no CH₃OH) model. Then we repeat this calculation between our data and a best fit flat-line model. We say CH₃OH is detectable if the ground truth model better explains our data. We set the significance threshold at 3σ (i.e., $p\text{-value} < 0.003$).

4.5 Results

We use our photochemistry model and the SEAS model to study the biosignature potential of CH₃OH. In short, we find that CH₃OH can theoretically accumulate to a detectable level on an exoplanet with an H₂-dominated atmosphere orbiting an M5V dwarf star. However,

the CH₃OH surface production flux required to reach its 10 ppm JWST detection threshold is unreasonably large. Currently, for exoplanets with CO₂- or N₂-dominated atmospheres, the atmospheric scale height is generally too small for atmosphere detection, so we leave that category to the discussion (Chapter 4.6.3). We note that while we have not yet discovered a terrestrial planet with an H₂-dominated atmosphere, several studies suggest the possibility of such planets (e.g., Elkins-Tanton et al., 2008; Owen et al., 2020; Lin et al., 2022). We detail our photochemical simulations in Chapter 4.5.1 and discuss the detectability of CH₃OH in Chapter 4.5.2.

4.5.1 Accumulation of CH₃OH on Exoplanets with H₂-dominated Atmospheres

We use our photochemistry model to study the possibility of CH₃OH accumulation in the atmosphere. We find that CH₃OH can accumulate to a detectable level on an exoplanet with an H₂-dominated atmosphere orbiting an M5V dwarf star similar to GJ 876 only when the CH₃OH surface production flux is unreasonably large. To be detectable by JWST, CH₃OH must reach an atmospheric concentration of 10 ppm (Chapter 4.5.2). The CH₃OH bioproduction flux required to reach the 10 ppm JWST detection threshold must be on the order of 10¹⁴ molecules cm⁻² s⁻¹ (~1.0×10⁶ Tg year⁻¹). This flux is roughly three times the annual O₂ production on Earth. 10 ppm CH₃OH implies 10¹⁸ mol of CH₃OH in the ocean-atmosphere system, assuming Henry's law equilibration between the atmosphere and ocean.

This carbon budget is potentially plausible from a planetary perspective. It is less than the surface (crust) carbon budget of the planet (~8.3×10²¹ mol) (Wood et al., 1996), and it is smaller than the amount of carbon life has fixed (mineralized) into continental sedimentary rocks (~10²¹ mol) throughout Earth's geological time (Galvez et al., 2020)¹⁰. However, we argue that the flux required to sustain 10 ppm of CH₃OH in the atmosphere is implausible from a biochemical perspective. Specifically, Earth's contemporary biosphere has about 2.0×10¹⁵ kg (~10¹⁷ mol) of carbon in total (Falkowski et al., 2000), approximately 10 times less than the carbon budget required to reach the 10¹⁸ mol of CH₃OH (see Chapter 4.6.6 for the discussion of the plausibility of high bioproduction fluxes of organic carbon gases). We plot the CH₃OH mixing ratio as a function of atmospheric pressure in Figure 4-4.

¹⁰ We assume the planet's total C reservoir is the same as Earth's.

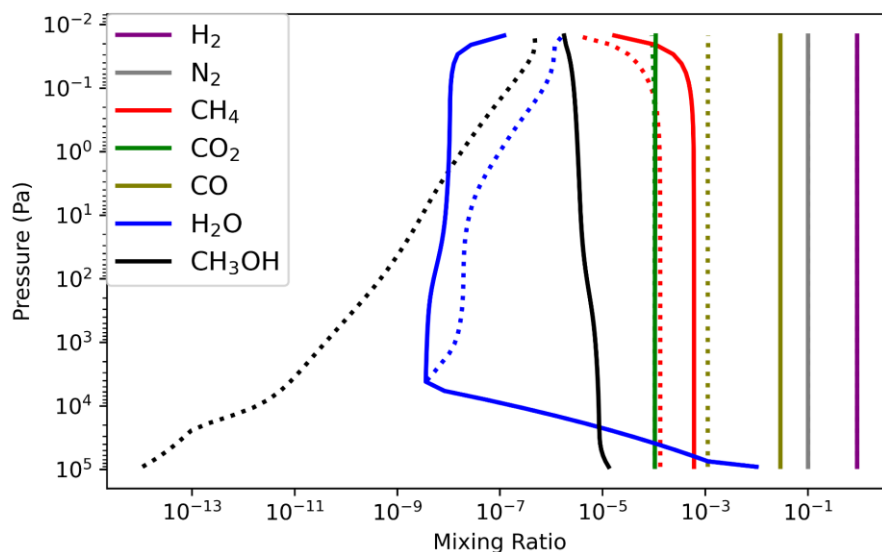


Figure 4-4. The volume mixing ratio of CH₃OH and other representative atmospheric species on an exoplanet with an H₂-dominated atmosphere orbiting an M5V dwarf star similar to GJ 876. The x-axis shows the mixing ratio, and the y-axis shows atmospheric pressure in Pa. Each color denotes one particular molecule. The dotted curves represent our base scenario, where CH₃OH surface production flux is zero. The solid curves represent our primary scenario, where the CH₃OH column-averaged mixing ratio is 10 ppm. In this case, CH₃OH surface production flux is 1.18×10^{14} molecule cm⁻² s⁻¹.

One of the reasons why CH₃OH is difficult to accumulate to its detectable level in the atmosphere is its high solubility in water. Due to CH₃OH's high water solubility, the dominant removal mechanism of CH₃OH on our simulated exoplanet is wet deposition (i.e., rainout), followed by dry deposition and photochemical loss. In contrast, the main CH₃OH removal pathway on Earth is photochemical oxidation (Chapter 4.3.1). The main reason for this difference is that the Sun is a G2V star, while our simulated exoplanet revolves around an M5V star that emits much less UV. In addition, we find that the top three CH₃OH photochemical removal pathways are direct photolysis, reaction with H radicals, and reaction with OH radicals. It is worth pointing out that we do not include atmospheric escape in our simulations. On Earth-sized exoplanets, gases such as H₂ can escape. However, we assume that the H₂ mixing ratio is constant in the atmosphere. We have summarized the main CH₃OH removal mechanisms and their respective fluxes in Table 4-9.

Table 4-9. The main CH₃OH removal mechanisms and their respective fluxes on our simulated exoplanet with an H₂-dominated atmosphere orbiting an M dwarf star similar to GJ 876.

CH ₃ OH removal mechanisms	Loss rate [molecule cm ⁻² s ⁻¹]
Wet deposition	8.7×10^{13}
Dry deposition	3.1×10^{13}
Photochemical loss (Total)	1.5×10^{10}
CH ₄ O → CH ₃ O + H	1.5×10^{10}

$\text{CH}_4\text{O} + \text{H} \rightarrow \text{CH}_3\text{O} + \text{H}_2$	2.1×10^6
$\text{CH}_4\text{O} + \text{OH} \rightarrow \text{CH}_3\text{O} + \text{H}_2\text{O}$	5.3×10^5

We show in Chapter 4.6.1 that the water solubility of CH_3OH is about 4 times higher than that of NH_3 . The higher water solubility of CH_3OH would naively suggest that CH_3OH is more susceptible to wet deposition than NH_3 , therefore, more difficult to accumulate in an H_2 -dominated atmosphere than NH_3 . However, this is not the case. The flux required for NH_3 to reach its detection limit (5 ppm) is on the order of 10^{16} molecule $\text{cm}^{-2} \text{s}^{-1}$, assuming efficient surface deposition of NH_3 (Huang et al., 2022). In contrast, for the more water-soluble CH_3OH , the production flux required to achieve the same atmospheric concentration (5 ppm) is approximately 2 orders of magnitude smaller, around 10^{14} molecule $\text{cm}^{-2} \text{s}^{-1}$. The reason for such discrepancy is that CH_3OH and NH_3 behave differently when dissolved in water. Once dissolved in water, CH_3OH does not dissociate, whereas NH_3 forms highly soluble NH_4^+ ions. Since NH_3 dissolves in water to form NH_4^+ ions, NH_3 's effective Henry's law constant at $T = 290 \text{ K}$ and $\text{pH} = 5$ ($\sim 1.5 \times 10^6 \text{ mol L}^{-1} \text{ atm}^{-1}$) is much larger than its standard Henry's law constant ($\sim 6.0 \times 10^2 \text{ mol L}^{-1} \text{ atm}^{-1}$) (Giorgi et al., 1985; R. Sander, 2015). The very high effective Henry's law constant of NH_3 translates into NH_3 's very high susceptibility to wet deposition and very high required production fluxes. Unlike NH_3 , CH_3OH does not dissociate in water (e.g., Brown et al., 2009). Therefore, CH_3OH 's effective Henry's law constant ($\sim 2.2 \times 10^2 \text{ mol L}^{-1} \text{ atm}^{-1}$) is roughly the same as its standard Henry's law constant ($\sim 2.1 \times 10^2 \text{ mol L}^{-1} \text{ atm}^{-1}$) (R. Sander, 2015). The effective Henry's law constant of CH_3OH is about 4 orders of magnitude lower than that of NH_3 , which in reality makes CH_3OH much less susceptible to wet deposition than NH_3 .

To verify the robustness of our CH_3OH simulation results, we conduct sensitivity tests on the temperature-pressure profile (i.e., the strength of the cold trap) and the eddy diffusion profile. We find that the column-averaged mixing ratio of CH_3OH remains roughly the same order of magnitude in our sensitivity tests (Table 4-10). Therefore, we conclude that our results are not sensitive to the variations in the eddy diffusion magnitude (\pm an order of magnitude) or the strength of the cold trap.

Table 4-10. Steady-state photochemical simulation outputs as a function of eddy diffusion magnitude and presence/absence of cold traps for exoplanets with H_2 -dominated atmospheres orbiting M dwarfs.

Variation in the eddy diffusion magnitude			
Eddy diffusion coefficient scaling factor	0.1	1	10
CH_3OH column-averaged mixing ratio	5.0 ppm	10.0 ppm	12.2 ppm
CH_3OH outgassing [molecule $\text{cm}^{-2} \text{s}^{-1}$]	1.2×10^{14}	1.2×10^{14}	1.2×10^{14}
Chemical production [molecule $\text{cm}^{-2} \text{s}^{-1}$]	1.3×10^9	5.7×10^9	9.8×10^9
Chemical loss [molecule $\text{cm}^{-2} \text{s}^{-1}$]	3.6×10^9	1.5×10^{10}	1.8×10^{10}
Dry deposition [molecule $\text{cm}^{-2} \text{s}^{-1}$]	3.5×10^{13}	3.1×10^{13}	2.9×10^{13}
Wet deposition [molecule $\text{cm}^{-2} \text{s}^{-1}$]	8.3×10^{13}	8.7×10^{13}	8.9×10^{13}
Variation in the temperature-pressure profile			
Presence of a cold trap	standard	reduced	
Temperature above tropopause [K]	160	220	
CH_3OH column-averaged mixing ratio	10.0 ppm	9.6 ppm	
CH_3OH outgassing [molecule $\text{cm}^{-2} \text{s}^{-1}$]	1.2×10^{14}	1.2×10^{14}	

Chemical production [molecule cm ⁻² s ⁻¹]	5.7×10^9	2.9×10^9
Chemical loss [molecule cm ⁻² s ⁻¹]	1.5×10^{10}	6.5×10^9
Dry deposition [molecule cm ⁻² s ⁻¹]	3.1×10^{13}	3.1×10^{13}
Wet deposition [molecule cm ⁻² s ⁻¹]	8.7×10^{13}	8.7×10^{13}

For the choice of eddy diffusion coefficient (K_{zz}), we have increased or decreased our existing eddy diffusion profile by one order of magnitude. We find that CH₃OH column-averaged mixing ratio is slightly higher in a more diffusive atmosphere, given the same surface production flux. As K_{zz} increases, more CH₃OH is transported to the upper atmosphere before being removed by wet or dry deposition. In essence, a larger K_{zz} suppresses the effectiveness of CH₃OH surface deposition, causing the atmospheric concentration of CH₃OH to increase. In addition, we test the effect of a cold trap on CH₃OH atmospheric concentration. A cold trap is a part of the upper atmosphere where the temperature is low enough to condense volatiles (Wordsworth et al., 2013, Wordsworth et al., 2014). To simulate a cold trap in an H₂-dominated atmosphere, we set the temperature above tropopause to 160 K. In contrast, to simulate an atmosphere with a reduced cold trap, we set the temperature above tropopause to 220 K (Appendix J). In this case, we assume that the planet has a relatively hot stratosphere due to UV absorbers in the atmosphere. We find that the presence of a cold trap does not affect CH₃OH surface deposition flux. We also find that a reduced cold trap makes CH₃OH photochemical production and loss slightly less efficient¹¹. Overall, CH₃OH atmospheric concentration remains roughly the same in this test.

In another work, we discussed the phenomenon of 'photochemical runaway' (Ranjan et al., 2022). Specifically, when the gas's production flux is large enough to saturate its photochemical sinks, it can rapidly accumulate to very high concentrations in the atmosphere (Ranjan et al., 2022). Some of the biosignature gases that can experience runaway are O₂, CO, and NH₃ (Zahnle 1986; Kasting 2014; Gregory et al. 2021; Ranjan et al., 2022). We run a series of simulations to see if CH₃OH will experience this 'runaway' effect. Like other gases (e.g., NH₃), CH₃OH runaway at biochemically plausible production fluxes requires inefficient surface deposition (Ranjan et al., 2022). If CH₃OH surface deposition is efficient, the CH₃OH column-averaged mixing ratio scales linearly with its surface production flux (Figure 4-5). The required CH₃OH surface production flux to reach 10,000 ppm (~1%) is about 1.2×10^{17} molecules cm⁻² s⁻¹ ($\sim 9.9 \times 10^8$ Tg year⁻¹), roughly 3000 times the annual O₂ production on Earth. CH₃OH does not experience runaway due to the presence of surface deposition.

¹¹ It is counter-intuitive that the photochemical reaction (i.e., production and loss) flux of CH₃OH decreases in a warmer atmosphere, and we do not fully understand why we observed such a decrease. The bottom line is that the strength of the cold trap does not affect our results.

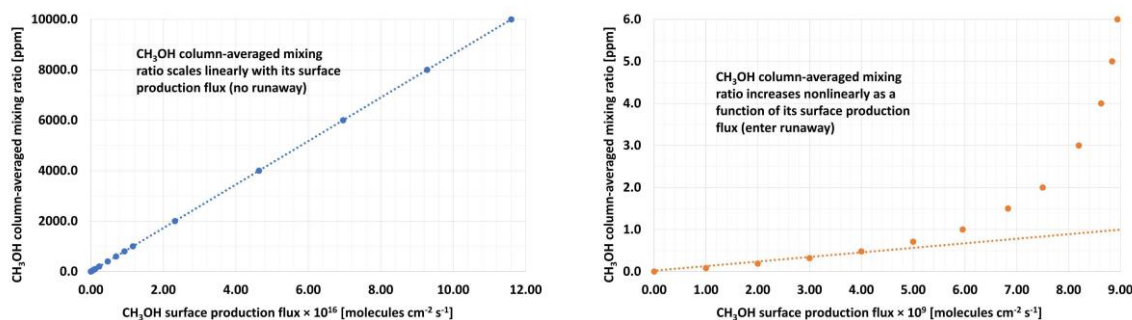


Figure 4-5. Accumulation of CH₃OH on an exoplanet with an H₂-dominated atmosphere orbiting an M5V dwarf star. The x-axis shows CH₃OH surface production flux in molecules cm⁻² s⁻¹, and the y-axis shows CH₃OH column-averaged mixing ratio in ppm. Note that each plot has a different x-axis scale. Left panel: Due to the presence of surface deposition (i.e., wet and dry deposition), CH₃OH does not go into a runaway, even at extremely high flux. Right panel: In the case where CH₃OH surface deposition is absent (i.e., no rainout or dry deposition), the column-averaged mixing ratio of CH₃OH increases nonlinearly as a function of its surface production flux. In this case, CH₃OH experiences runaway, and it can rapidly accumulate to high concentrations in the atmosphere.

If CH₃OH surface deposition is absent (i.e., no rainout or dry deposition), CH₃OH can experience photochemical runaway (Figure 4-5). This exception can only occur if CH₃OH bioproduction is robust enough to saturate its surface sinks. By saturation, we mean that life produces more CH₃OH than the surface sinks can remove at any given moment. In this case, we find that the critical flux required for CH₃OH to experience runaway is quite small, about 5.0×10^9 molecules cm⁻² s⁻¹ (~ 43 Tg year⁻¹), similar to the threshold for CO. This is because, like CO, the photochemical loss of CH₃OH is dominated by the reaction with OH and is therefore limited by the production rate of OH from H₂O photolysis (Kasting 1990; Ranjan et al., 2022). Consequently, CH₃OH and CO enter runaway at similar net surface production fluxes. Considering CH₃OH runaway, we estimate¹² that the required CH₃OH bioproduction flux to reach the 10 ppm JWST detection threshold should be approximately 9.0×10^9 molecules cm⁻² s⁻¹ (~ 77 Tg year⁻¹). This flux is roughly 8% of the annual CH₄ production on Earth. While CH₃OH runaway is theoretically possible and hugely beneficial for CH₃OH accumulation and detection, we currently do not know how likely it is to occur on an exoplanet. We include this particular case here for the completeness of this paper.

4.5.2 The Detectability of CH₃OH with James Webb Space Telescope

We assess the detectability of CH₃OH using our 'Simulated Exoplanet Atmosphere Spectra' (SEAS) model. For an exoplanet with an H₂-dominated atmosphere orbiting an M5V dwarf star, we find that only when the column-averaged mixing ratio of CH₃OH reaches at least 10 ppm can we detect it with JWST. To determine the detection threshold, we focus on CH₃OH's spectral feature around 3.4 μm and include a ten ppm JWST systematics noise floor.

¹² Our current photochemistry code has difficulty converging when simulating a 'runaway' species. That is why we can only provide an estimate here.

In Figure 4-6, we simulate transmission spectra of a hypothetical $5M_{\text{Earth}}$, $1.5R_{\text{Earth}}$ super-Earth with an H_2 -dominated atmosphere transiting an M5V dwarf star similar to GJ 876. Specifically, we compare a simulated transmission spectrum with 10 ppm of CH_3OH and one without CH_3OH .

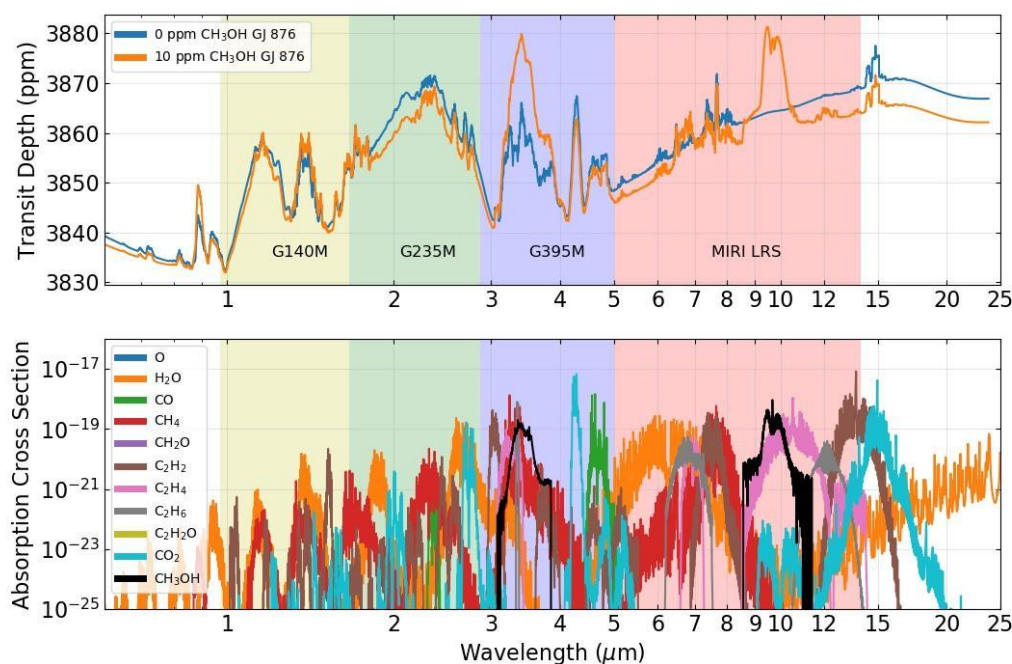


Figure 4-6. Upper panel: Simulated transmission spectra of a hypothetical $5M_{\text{Earth}}$, $1.5R_{\text{Earth}}$ super-Earth with an H_2 -dominated atmosphere transiting an M5V dwarf star similar to GJ 876. The x-axis shows wavelength (μm), and the y-axis shows transit depth (ppm). We simulate the spectra from 0.3 - 23 μm , covering the wavelength span of JWST NIRSpec and MIRI LRS. The yellow, green, and blue regions show the spectral coverage of G140M, G235M, and G395M, respectively, and the red region shows that of MIRI LRS. The orange curve shows the simulated spectrum with CH_3OH column-averaged mixing ratio equal to 10 ppm, and the blue curve shows the simulated spectrum with no CH_3OH . **Lower panel:** Comparison of CH_3OH absorption cross-sections with cross-sections of other molecules in the atmosphere such as H_2O , CH_4 , and CO_2 . Each color denotes one species. We omit H_2 because its absorption is mainly collision-induced.

When the CH_3OH column-averaged mixing ratio is below the 10 ppm threshold, its spectra features are not prominent. Since we assume that CH_3OH mainly comes from the surface, the atmospheric concentration of CH_3OH decreases with increasing altitude. As CH_3OH concentration increases, more CH_3OH can accumulate in the upper atmosphere, amplifying its spectral features. When the CH_3OH column-averaged mixing ratio reaches or exceeds 10 ppm, we can detect it by characterizing its 3.4 μm feature.

To further verify that the detection threshold of CH_3OH is 10 ppm on exoplanets with H_2 -dominated atmospheres, we simulate JWST observations with realistic noise calculated

from PandExo (Batalha et al., 2017). We also include a detection noise floor of 10 ppm. We compare a simulated JWST observation with 10 ppm of CH₃OH and one with no CH₃OH (Figure 4-7).

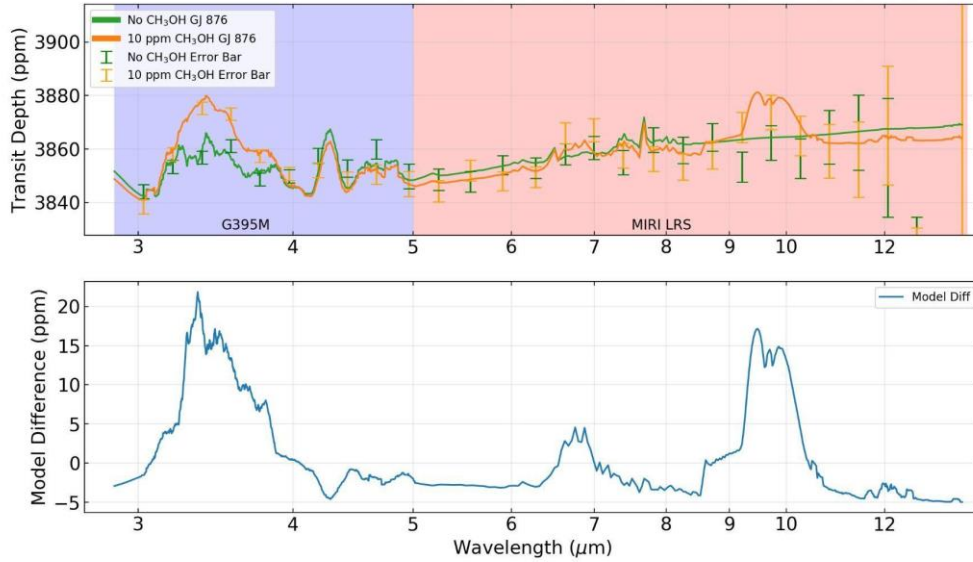


Figure 4-7. Upper panel: Simulated JWST observations of a hypothetical $5M_{\text{Earth}}$, $1.5R_{\text{Earth}}$ super-Earth with an H₂-dominated atmosphere transiting an M5V dwarf star similar to GJ 876. The x-axis shows wavelength (μm), and the y-axis shows transit depth (ppm). The simulated observations cover the wavelength range of NIRSpec G395M and MIRI LRS, as we only used CH₃OH's 3.4 μm , 6.9 μm , and 9.5 μm features for the detectability analysis. The orange curve shows the simulated observation with CH₃OH column-averaged mixing ratio equal to 10 ppm, and the green curve shows the simulated observation with no CH₃OH. The error bars are 95% confidence intervals. The total number of transits is 20 (i.e., 10 transits each for NIRSpec G395M and MIRI LRS), and the spectral resolution is $R = 10$. **Lower panel:** Model difference (ppm) between the two simulated observations. The blue curve shows CH₃OH's spectral features around 3.4 μm , 6.9 μm , and 9.5 μm . Negative values indicate that an increase in CH₃OH leads to a decrease in CO and CH₄ in the atmosphere.

We find that the simulated JWST observation with 10 ppm CH₃OH has two spectral features (i.e., 3.4 μm and 9.5 μm) about 10 - 20 ppm larger than the simulated observation without CH₃OH. The difference between the two models achieves statistical significance ($>3\sigma$), indicating a confident simulated detection of CH₃OH.

We have to point out that, even though the detection threshold of CH₃OH is about 10 ppm on exoplanets with H₂-dominated atmospheres, constraining the amount of CH₃OH in an exoplanet's atmosphere is challenging, which requires more transits and observation time. In addition, detection of CH₃OH on exoplanets with non-H₂-dominated atmospheres (e.g., CO₂- or N₂-dominated atmospheres) requires significantly more (>100) transits. That is because, for exoplanets with high molecular-weight atmospheres, the transit depth resulting from the small atmosphere scale height is too small compared to the assumed ten ppm

JWST systematic noise floor.

The atmosphere might have various species with overlapping spectral features, so we must investigate the distinguishability of CH₃OH from other atmospheric molecules. We compare the spectral absorbance of CH₃OH with various other species (Figure 4-8). One of the unique spectral features of alcohol molecules comes from the presence of hydroxyl groups (-OH). Therefore, we can use CH₃OH's spectral feature around 2.7 μm (O-H stretching) to distinguish CH₃OH from other molecules without OH groups (e.g., CH₄, CO₂, NH₃, and C₅H₈). To distinguish CH₃OH from H₂O, we can use CH₃OH's absorption band around 10 μm (C-O/C-C rovibrations) (Plyler 1952; Harrison et al., 2012). However, distinguishing CH₃OH from other alcohols (e.g., ethanol) can be challenging because of their similar OH features. It is worth noting that complex alcohols may have other spectral features not present in CH₃OH. Furthermore, a mixture of hydrocarbons and water (e.g., CH₄ and H₂O) may mimic CH₃OH's spectral features and be indistinguishable from CH₃OH (when observed at low resolutions). In the future, with the development and use of atmosphere retrieval algorithms such as Markov chain Monte Carlo (MCMC) (e.g., Benneke et al., 2012; de Wit 2015) or the Hamiltonian Monte Carlo (HMC) method (e.g., Neal 2011; Hoffman et al., 2014), we expect to be able to distinguish CH₃OH from other atmospheric species (e.g., major/trace gases and other alcohols) more accurately.

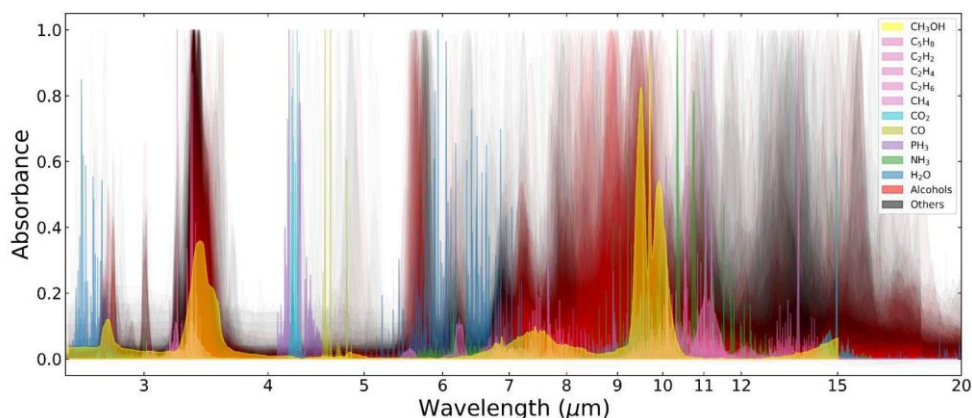


Figure 4-8. Spectral absorbance of CH₃OH (yellow) and various species, including 5 common atmospheric molecules (CH₄, CO₂, CO, NH₃, and H₂O), 3 simple hydrocarbons (C₂H₂, C₂H₄, and C₂H₆), 2 previously studied biosignature gases (C₅H₈ and PH₃), and other hydrocarbons (including alcohols) with fewer than seven carbon atoms and have spectral measurements. The x-axis shows wavelength (μm), and the y-axis shows absorbance (normalized to 1). Here we use spectral data from NIST rather than HITRAN. We use the HITRAN database for our previous detectability analysis (e.g., Zhan et al., 2021; Huang et al., 2022) because HITRAN data have higher resolutions and are more accurate than NIST data. However, to study CH₃OH distinguishability, we choose NIST data because of their broader spectral coverage than HITRAN. We normalize all absorbances to 1 to facilitate comparison. Thanks to the presence of the hydroxyl group, we can use CH₃OH's feature around 2.7 μm (O-H stretching) to distinguish CH₃OH from other molecules without OH groups. CH₃OH's broadband at around 10 μm (C-O stretching/vibrations) can be masked by other species.

4.6. Discussion

We first review alcohols' solubility in water in Chapter 4.6.1. We then examine the antifreeze properties of CH_3OH in Chapter 4.6.2. Next, we briefly discuss CH_3OH as a biosignature gas on exoplanets with CO_2 - and N_2 -dominated atmospheres in Chapter 4.6.3. Additionally, in Chapter 4.6.4, we explore how volatility impacts the biosignature potential of alcohols. We comment on CH_3OH and atmospheric hazes in Chapter 4.6.5. Finally, we discuss the plausibility of high bioproduction fluxes in Chapter 4.6.6.

4.6.1 Alcohols' Solubility in Water

Alcohols with less than five carbon atoms ($C \leq 4$) are very soluble in water since they can easily form hydrogen bonds with water molecules. Alcohols with longer hydrocarbon chains ($C \geq 5$) become less soluble in water due to the hydrophobic nature of the hydrocarbon chains.

We use Henry's law to study the solubility of chemicals in water: $H^{\text{CP}}_{(x)} = C_{(x)}/p$. Here $H^{\text{CP}}_{(x)}$ is Henry's law constant for a species X in $\text{mol Pa}^{-1}\text{m}^{-3}$. P is the partial pressure of that species in Pascal, and $C_{(x)}$ is the dissolved concentration (in mol m^{-3}) under the equilibrium condition. The larger H^{CP} , the more soluble the species is. Here we compare the solubility of 11 representative alcohols to 17 other molecules at 1 atm and 298 K (Figure 4-9). The list includes common atmospheric gases and potential biosignature gases. We collected the data from (R. Sander, 2015).

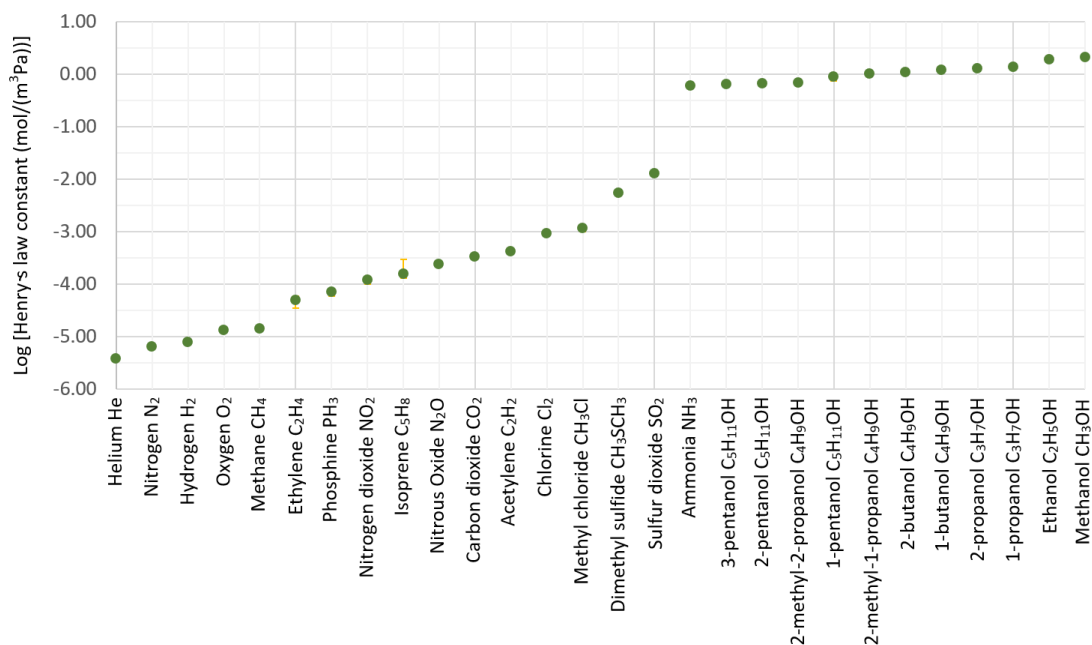


Figure 4-9. Solubility of various atmospheric gasses in water. The x-axis shows the chemical species' names, and the y-axis shows Henry's law constant on a log scale. Alcohols with less than five carbon atoms ($C \leq 4$) are very soluble in water. Methanol is the most water-soluble alcohol. CH_3OH is more soluble than NH_3 , one of the most soluble biosignature gas candidates studied (Huang et al., 2022).

Methanol is highly soluble in water. CH_3OH is so water-soluble that it can form a homogenous solution with water at any given concentration (i.e., miscible with water). CH_3OH is even more soluble than NH_3 , one of the most soluble biosignature gas candidates studied (Huang et al., 2022). Due to methanol's high water solubility, wet deposition (rainfall) can efficiently remove gaseous CH_3OH from the atmosphere.

4.6.2 CH_3OH as an Antifreeze

When CH_3OH gas dissolves in water, the solution's freezing point is lowered from the original value of 0°C of pure water. This phenomenon is called freezing-point depression. Freezing-point depression occurs when a small amount of solute (e.g., salt or, in this case, alcohol) dissolves in a solvent (e.g., water). Since CH_3OH is an antifreeze, a mixed solution of water and CH_3OH has a lower freezing point than pure water.

Here we approximate the ocean as a solvent composed of water by temporarily ignoring other solutes already dissolved in the ocean. We made this assumption to facilitate our study of the effect of dissolved CH_3OH on the ocean's freezing point. We can use a linear equation to estimate the extent of freezing-point depression (also known as 'Blagden's law'): $\Delta T_f = K_f \cdot i \cdot b$. Here ΔT is the change in freezing point in $^\circ\text{C}$. K_f is the cryoscopic constant of the solvent in $^\circ\text{C kg mol}^{-1}$. The parameter b is the molality (i.e., moles of solute/kg of solvent), and i is the solute's van't Hoff factor. The cryoscopic constant of water is $1.86^\circ\text{C kg mol}^{-1}$ (David R. Lide et al., 2005). Since CH_3OH does not dissociate in water, the van't Hoff factor of CH_3OH is 1. We assume the mass of the exoplanet's ocean is the same as that of the Earth's ocean, and therefore the mass of the ocean is about 1.4×10^{21} kg (David R. Lide et al., 2005). In this case, the molality of CH_3OH only depends on the planet's total CH_3OH reserve. We assume the planet's total C and O reservoirs are the same as Earth's. We also assume that H is abundant, given that the planet we are interested in has an H_2 -dominated atmosphere. Given that the mass of Earth is about 5.97×10^{24} kg, and there is about 446 ppm of C and 30.12% of O on Earth by mass (Morgan et al., 1980), the planet's total CH_3OH reserve is only limited by the planet's total C reservoir.

In an extreme situation where life converts roughly 0.1% of the planetary C reservoir ($\sim 2.7 \times 10^{18}$ kg) into dissolved CH_3OH , the molality of CH_3OH can reach up to 0.06 mol/kg. However, even with such an unrealistically large CH_3OH inventory (by comparison, Earth's biosphere has about 2.0×10^{15} kg of carbon (Falkowski et al., 2000)), the ocean's freezing point has dropped by only 0.1°C . Even though the above estimates are very rough, our calculations show that it is highly improbable for life to produce enough CH_3OH to have any noticeable effect on the ocean's freezing point. Overall, we argue that the antifreeze capability of CH_3OH should not affect planet habitability.

4.6.3 CH₃OH on Exoplanets with CO₂- or N₂-dominated Atmospheres Orbiting M Dwarfs

So far, our study on CH₃OH as a biosignature gas has been focused on exoplanets with H₂-dominated atmospheres. In contrast, most terrestrial exoplanets with high-molecular-weight atmospheres (i.e., CO₂- or N₂-dominated atmospheres) have signals that are too weak to be detected using JWST. Specifically, for exoplanets with CO₂- or N₂-dominated atmospheres, due to the large mean molecular weight of the atmospheres, the atmospheric scale height is much smaller than that of exoplanets with H₂-dominated atmospheres. Due to the small atmospheric scale height, the resulting transit depth is too small compared to the assumed 10 ppm JWST systematic noise floor. Hence, the detectability of CH₃OH on exoplanets with CO₂- or N₂-dominated atmospheres is very low, given the weak atmosphere signals. For this reason, we argue that, at present, CH₃OH is not a suitable biosignature gas on exoplanets with CO₂- or N₂-dominated atmospheres. However, there are some exceptions where detection of trace gasses (e.g., CH₃OH) is possible with JWST. One of those rare cases is for planets transiting TRAPPIST-1, a nearby ultra-cool M8V star. For more details, see (Zhan et al., 2021) and (Appendix I, Huang et al., 2022).

Even though CH₃OH is a poor biosignature gas in CO₂- or N₂-dominated atmospheres, it can still theoretically accumulate on exoplanets with CO₂- or N₂-dominated atmospheres orbiting M dwarfs. We use our photochemistry model (Chapter 4.4.1) to simulate CO₂- and N₂-dominated atmospheres to support this argument. We use the same simulation parameters (i.e., the stellar profile, the atmospheric T-P profile (Appendix J), the eddy diffusion profile, and the surface boundary conditions) as in (Huang et al., 2022) to simulate CO₂- and N₂-dominated atmospheres. We find that it is a bit easier for CH₃OH to accumulate in CO₂- or N₂-dominated atmospheres than in H₂-dominated ones. Specifically, given a fixed CH₃OH surface production flux, CH₃OH column-averaged mixing ratio is the highest in CO₂-dominated (oxidized) atmospheres and the lowest in H₂-dominated (reduced) atmospheres (see Table 4-11). We also observed this trend for another biosignature gas (NH₃) (Huang et al., 2022). The CH₃OH column-averaged mixing ratio is the highest in CO₂-dominated atmospheres because of its relatively low wet deposition rate. Wet deposition rate scales linearly with atmospheric water content, which is a function of temperature (Giorgi et al., 1985; Hu et al., 2012). The relatively high lapse rate of CO₂-dominated atmospheres suppresses temperature, reducing atmospheric water content and rainout, ultimately making CH₃OH easier to accumulate.

Table 4-11. Steady-state simulation outputs for exoplanets with H₂-dominated, CO₂-dominated, and N₂-dominated atmospheres orbiting M dwarf stars (M5V).

Atmospheric scenarios	H ₂ -dominated	CO ₂ -dominated	N ₂ -dominated
CH ₃ OH outgassing [molecule/(cm ² s)]	1.2×10^{13}	1.2×10^{13}	1.2×10^{13}
CH ₃ OH column-averaged mixing ratio	1.0 ppm	3.9 ppm	3.0 ppm
Chemical production [molecule/(cm ² s)]	2.8×10^9	2.1×10^3	1.8×10^{10}
Chemical loss [molecule/(cm ² s)]	8.2×10^9	3.5×10^7	4.8×10^{10}
Dry deposition [molecule/(cm ² s)]	3.1×10^{12}	9.3×10^{12}	7.6×10^{12}
Wet deposition [molecule/(cm ² s)]	8.9×10^{12}	2.7×10^{12}	4.4×10^{12}

4.6.4 Volatility of Alcohols and its Impact on Alcohols' Biosignature Potential

In addition to solubility (Chapter 4.6.1), a substance's volatility also has a profound impact on its biosignature potential. Simply put, the higher the volatility of a substance, the easier it is to evaporate and accumulate in the atmosphere. Beyond CH_3OH , we argue that alcohols with long carbon chains ($C > 4$) are poor biosignature gas candidates due to their relatively low volatility and high boiling points.

In general, alcohols are considered volatile at room temperature. However, alcohols are much less volatile than hydrocarbons (e.g., alkanes) with similar molecular weight. The reason is that alcohol molecules can form hydrogen bonds with each other. Hydrogen bonds are much stronger than van der Waals interactions between hydrocarbons. During evaporation, more energy is needed to break the hydrogen bonds and separate the alcohol molecules, significantly reducing the volatility. The volatility of alcohols depends on the length of the carbon chain and isomerism. Here we focus on monohydric alcohols (i.e., alcohol with one OH group). On the one hand, the volatility of alcohol decreases as the length of the carbon chain increases. When the carbon chain gets longer, the surface area of the molecule increases, which leads to an increase in the amount of van der Waals interactions and a decrease in volatility. On the other hand, when the OH group is at the center of the carbon chain, the molecule becomes more spherical, making the surface area smaller and volatility higher. In addition, when carbon chains surround the OH group, it is more challenging for alcohol to form a hydrogen bond, further increasing its volatility.

Volatility itself does not have a numerical value. We can use boiling point to help us compare the volatility of different substances: the higher the boiling point, the lower the volatility of the substance. In Figure 4-10, we plot the boiling points of 8 representative alcohols and 9 other hydrocarbons. The figure shows that the boiling point of alcohol is much higher than that of the corresponding hydrocarbon (e.g., methanol vs. ethane). Furthermore, the boiling point of alcohol increases as the length of the carbon chain increases (e.g., methanol vs. n-butanol). In addition, OH's position in the molecule affects the boiling point of alcohol (e.g., n-butanol vs. tert-butanol). All in all, given that alcohols with long carbon chains have low volatility and tend to be liquid at room temperatures, we consider them to be poor biosignature gas candidates.

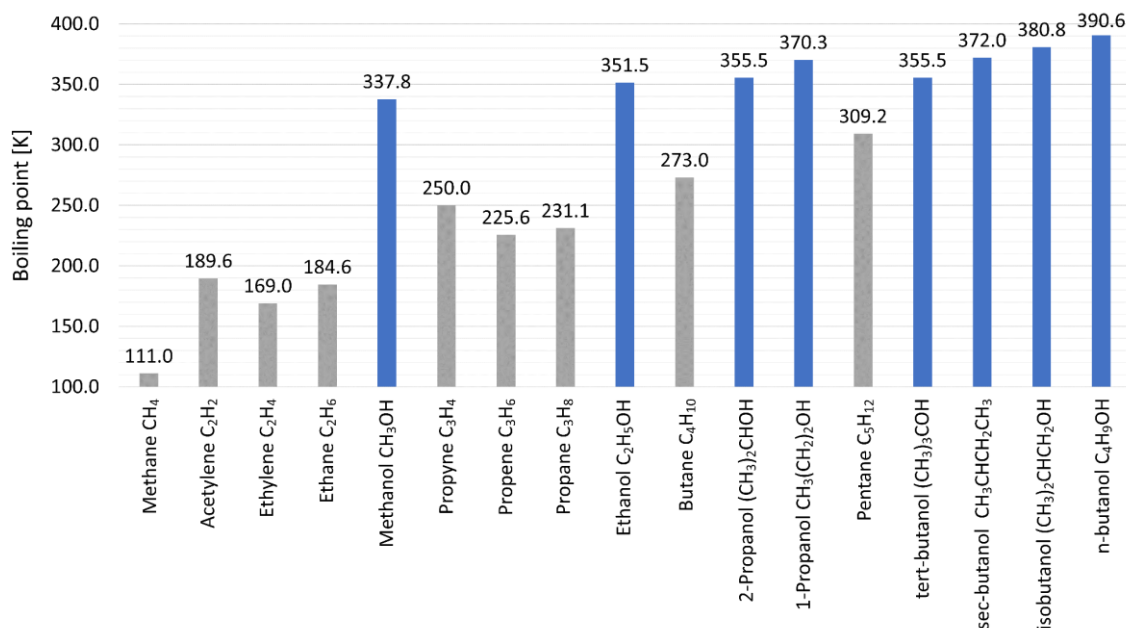


Figure 4-10. The boiling points of 8 representative alcohols and 9 other hydrocarbons. The x-axis shows the species' names, and the y-axis shows the boiling point in K. We arrange the x-axis in ascending order of molecular weight. The blue bars represent alcohols, and the gray bars represent other hydrocarbons. We collect the data from NIST.

4.6.5 CH₃OH and Atmospheric Hazes

On Earth, volatile organic compounds (VOCs) such as methanol and formaldehyde have been known to contribute to the formation of organic aerosols and hazes (e.g., Han et al., 2017; Sheng et al., 2018; Wei et al., 2018; Hui et al., 2019; Xue et al., 2020). In Earth's oxidizing atmosphere, CH₃OH can react with OH, O, and H radicals to give various products, such as CH₃O, CH₂OH, and CH₃ radicals (Chapter 4.3.1). These products can further react with nitrogen oxides (NO_x) and sulfur oxides (SO_x) in the atmosphere to yield complex molecular species and fine airborne particles that act as nucleation precursors. When mixed with other air pollutants and dust, these nucleation precursors can form aerosol particles (e.g., PM_{2.5}), promoting haze formation.

In contrast, we know very little about whether or how CH₃OH induces organic haze on an exoplanet. Unlike organic hazes that have been studied in detail (e.g., Domagal-Goldman et al., 2011; Arney et al., 2018), there are very few theoretical or experimental studies on CH₃OH-induced hazes in an H₂-dominated atmosphere. Some papers speculate that with the help of photochemistry, CH₃OH may facilitate organic haze formation, but the mechanism needs to be further studied (Arney et al., 2018; Moran et al., 2020). Given the limited information, we suspect CH₃OH might have minimal effect on haze formation in an H₂-dominated, reducing atmosphere. In a recent publication (Moran et al., 2020), researchers used high-resolution mass spectrometry to measure the chemical properties of photochemical hazes generated in the laboratory. They find that most haze particles (general formulae: C_xH_yN_zO_w) produced in an H₂-dominated atmosphere at 300K are polar (Moran

et al., 2020). In theory, these solid haze particles can dissolve in polar solvents such as H₂O and CH₃OH. Their solubility in polar solvents makes them susceptible to atmospheric precipitation. In another study (Liu et al., 2019), the authors identified a new catalytic reaction between CH₃OH and SO₃ that converts CH₃OH into methyl hydrogen sulfate (CH₄O₄S). This reaction can be catalyzed by H₂O, sulfuric acid (H₂SO₄), or dimethylamine ((CH₃)₂NH). The CH₄O₄S produced is much less volatile than CH₃OH and is a poor haze-forming agent due to its relatively weak nucleation ability (Liu et al., 2019). Therefore, a high concentration of atmospheric CH₃OH might lower aerosol particles' generation rate and negatively affect haze formation.

4.6.6 Plausibility of High Bioproduction Fluxes

The biological surface flux of CH₃OH needed for CH₃OH to accumulate to detectable atmosphere levels is likely biologically unattainable (10^{14} molecules cm⁻² s⁻¹, or about 3 times the annual O₂ production on Earth). While mathematically possible, such high biological fluxes of organic carbon gases result in a massive waste of carbon—the main building block for life. The biological production of organic carbon gases is predominantly a result of biological activity that is not tied directly to energy metabolism and biomass build-up. Therefore, if organic carbon gases are produced in very high amounts, their production also has to provide a significant evolutionary gain to offset the enormous expense in used energy and carbon.

Gases that are instead a waste product of primary energy metabolism or biomass build-up are much more likely to be produced by life in significant amounts (i.e., with high fluxes). In prior work, we have given an example of NH₃ as a biosignature gas that can accumulate on exoplanets with H₂-dominated atmospheres if life is a net source of NH₃ and produces enough NH₃ to saturate the surface sinks (Huang et al., 2022). NH₃ is a readily available source of nitrogen for biomass build-up. Therefore, its release into the atmosphere in huge quantities might be considered 'wasteful'. However, in our proposed example, the production of NH₃ is a result of theoretical primary energy metabolism on the 'cold Haber World' (Seager et al., 2013a). In the 'cold Haber World' scenario, we assume life has evolved the catalytic machinery to break the N₂ triple bond and extract energy by fixing atmospheric H₂ and N₂ into NH₃ (Seager et al., 2013a; Huang et al., 2022), thus tying the release of NH₃ to the net energy gain. While large NH₃ biological surface fluxes (10^{10} molecules cm⁻² s⁻¹ for an NH₃-saturated surface and 10^{15} molecules cm⁻² s⁻¹ for an NH₃-unsaturated surface) are required for atmospheric NH₃ to accumulate to detectable levels in the cold Haber World scenario (Huang et al., 2022), we argue, based on the primary energy metabolism argument, that it is biologically plausible. Such energy gain is not readily available for organic carbon gases scenarios, such as CH₃OH or carbonyls (Zhan et al., 2022). For example, one way to gain energy by producing methanol is to partially oxidize CH₄ to CH₃OH with atmospheric O₂. Such a process is unlikely to happen in the H₂-rich anoxic atmospheres because of the lack of O₂.

4.7. Summary

In this paper, we examine the biosignature potential of CH₃OH in detail. We use a variety of approaches, from comparing Henry's law constants for different atmospheric species to our one-dimensional photochemistry model and our transmission spectra (SEAS) model.

Methanol (CH₃OH) has many advantages as a biosignature gas candidate. First, CH₃OH's hydroxyl group (OH) has a unique spectral feature compared to other anticipated gases in rocky exoplanets atmospheres. Second, there are no significant known abiotic CH₃OH sources on terrestrial planets in the solar system. Third, life on Earth produces CH₃OH in large quantities.

However, despite CH₃OH's advantages, we consider CH₃OH a poor biosignature gas in terrestrial exoplanet atmospheres due to the enormous production flux required to reach its detection limit. CH₃OH's high water solubility makes it very difficult to accumulate in the atmosphere. For the highly favorable planetary scenario of an exoplanet with an H₂-dominated atmosphere orbiting an M5V dwarf star, we find that only when the column-averaged mixing ratio of CH₃OH reaches at least 10 ppm can we detect it with JWST. CH₃OH bioproduction flux required to reach the 10 ppm JWST detection threshold must be on the order of 10¹⁴ molecules cm⁻² s⁻¹, which is roughly three times the annual O₂ production on Earth. Considering that such an enormous flux of CH₃OH is essentially a massive “waste” of organic carbon - a major building block of life, we think this flux, while mathematically possible, is likely biologically unattainable.

We also find that, due to the presence of surface deposition, CH₃OH does not experience runaway, even at extremely high flux. CH₃OH runaway can only occur in the exceptional case with no CH₃OH surface deposition (i.e., no rainout or dry deposition). This exception happens only if CH₃OH bioproduction is robust enough to saturate its surface sinks. Considering CH₃OH runaway, we estimate that the required CH₃OH bioproduction flux to reach the 10 ppm JWST detection threshold is approximately 9×10⁹ molecules cm⁻² s⁻¹ (~ 77 Tg year⁻¹), which is about 8% of the annual CH₄ production on Earth. Beyond CH₃OH, we argue that alcohols with long carbon chains (C > 4) are poor biosignature gas candidates due to their high water solubility and relatively low volatility.

Finally, although CH₃OH can theoretically accumulate on exoplanets with CO₂- or N₂-dominated atmospheres, such planets' small atmospheric scale height and weak atmosphere signals put them out of reach for near-term observations. We hope that as telescope technology improves, potential biosignature gases (e.g., CH₃OH) that are not yet readily observable with the JWST can one day be observed and more thoroughly studied.

We are very grateful to the Heising-Simons Foundation (grant number #2018-1104) and NASA (grant numbers 80NSSC19K0471 and NNX15AC86G) for supporting our project.

Appendix J. Photochemical Simulation Parameters

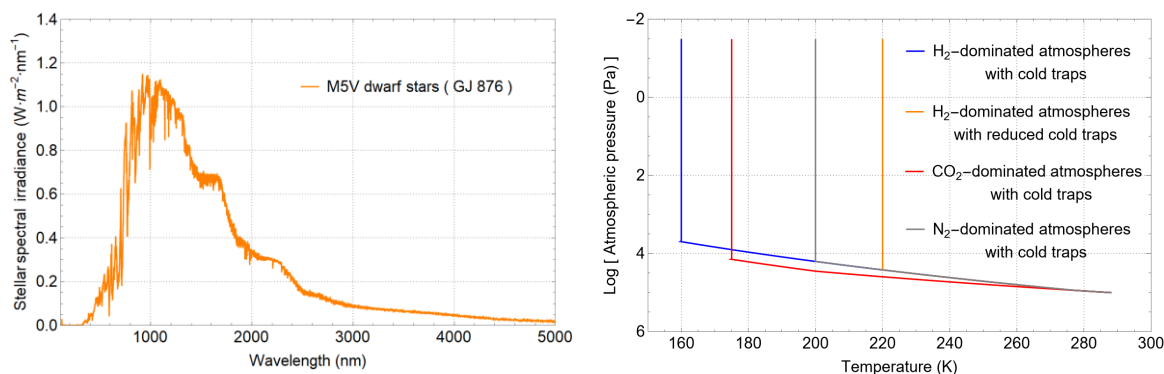


Figure 4-11. **Left panel:** The synthetic stellar radiation model of GJ 876 (Lloyd et al., 2016; France et al., 2016). The y-axis shows spectral irradiance in $\text{W m}^{-2} \text{nm}^{-1}$, and the x-axis shows wavelength in nm. **Right panel:** The temperature-pressure profiles of the simulated exoplanets with H_2 -dominated, CO_2 -dominated, and N_2 -dominated atmospheres. The y-axis shows atmospheric pressure (Pa) on a log scale, and the x-axis shows temperature in Kelvin (K).

Our photochemistry model demarcates chemical species into four types: type “X”, for species for which the full photochemical transport equation is solved, type “F” for species assumed to be in photochemical equilibrium (i.e., for which transport is neglected), type “C” for chemically inert species which are assumed not to react or transport and type “A” for aerosol species. In addition, for the lower boundary condition, we can either specify a fixed surface mixing ratio (type “1”) or a fixed emission/deposition velocity (type “2”) (Hu et al., 2012).

Table 4-12. Surface boundary conditions for exoplanets with H_2 -dominated atmospheres.

Name	Type	Initial Mixing Ratio	Upper Boundary Flux Beside Escape (Upwards) [molecule/(cm^2s)]	Lower Boundary Type	Dry Deposition Velocity [cm/s]	Lower Boundary Flux (Upwards) [molecule/(cm^2s)]
H	X	0	0	2	1	0
H_2	C	0.9	0	1	0	0.9
O	X	0	0	2	1	0
O(1D)	X	0	0	2	0	0
O_2	X	0	0	2	0	0
O_3	X	0	0	2	0	0
OH	X	0	0	2	1	0
HO_2	X	0	0	2	1	0
H_2O	X	2.00×10^{-6}	0	1	0	1.00×10^{-2}
H_2O_2	X	0	0	2	0.5	0
CO_2	X	0	0	2	1.00×10^{-4}	3.00×10^{11}
CO	X	0	0	2	1.00×10^{-8}	0
CH_2O	X	0	0	2	0.1	0
CHO	X	0	0	2	0.1	0
C	X	0	0	2	0	0
CH	X	0	0	2	0	0
CH_2	X	0	0	2	0	0

CH ₂₁	X	0	0	2	0	0
CH ₃	X	0	0	2	0	0
CH ₄	X	0	0	2	0	3.00×10^8
CH ₃ O	X	0	0	2	0.1	0
CH ₄ O	X	0	0	2	0.1	1.20×10^{13}
CH ₂ O ₂	X	0	0	2	0.1	0
CH ₃ O ₂	X	0	0	2	0	0
CH ₄ O ₂	X	0	0	2	0.1	0
C ₂	X	0	0	2	0	0
C ₂ H	X	0	0	2	0	0
C ₂ H ₂	X	0	0	2	0	0
C ₂ H ₃	X	0	0	2	0	0
C ₂ H ₄	X	0	0	2	0	0
C ₂ H ₅	X	0	0	2	0	0
C ₂ H ₆	X	0	0	2	1.00×10^{-5}	0
C ₂ HO	X	0	0	2	0	0
C ₂ H ₂ O	X	0	0	2	0.1	0
C ₂ H ₃ O	X	0	0	2	0.1	0
C ₂ H ₄ O	X	0	0	2	0.1	0
C ₂ H ₅ O	X	0	0	2	0.1	0
N ₂	C	0.1	0	1	0	0.1
S	X	0	0	2	0	0
S ₂	X	0	0	2	0	0
S ₃	X	0	0	2	0	0
S ₄	X	0	0	2	0	0
SO	X	0	0	2	0	0
SO ₂	X	0	0	2	1	3.00×10^9
SO ₂₁	X	0	0	2	0	0
SO ₂₃	X	0	0	2	0	0
SO ₃	X	0	0	2	0	0
H ₂ S	X	0	0	2	0.015	3.00×10^8
HS	X	0	0	2	0	0
HSO	X	0	0	2	0	0
HSO ₂	X	0	0	2	0	0
HSO ₃	X	0	0	2	0	0
H ₂ SO ₄	X	0	0	2	1	0
H ₂ SO ₄ A	A	0	0	2	0.2	0
S ₈	X	0	0	2	0	0
S ₈ A	A	0	0	2	0.2	0
CHO ₂	X	0	0	2	0.1	0
N	X	0	0	2	0	0
NH ₃	X	0	0	2	1	0
NH ₂	X	0	0	2	0	0
NH	X	0	0	2	0	0
N ₂ O	X	0	0	2	0	0
NO	X	0	0	2	0.02	0
NO ₂	X	0	0	2	0.02	0
NO ₃	X	0	0	2	1	0
N ₂ O ₅	X	0	0	2	4	0
HNO	X	0	0	2	0	0
HNO ₂	X	0	0	2	0.5	0
HNO ₃	X	0	0	2	4	0

HNO ₄	X	0	0	2	4	0
HCN	X	0	0	2	0.01	0
CN	X	0	0	2	0.01	0
CNO	X	0	0	2	0	0
HCNO	X	0	0	2	0	0
CH ₃ NO ₂	X	0	0	2	0.01	0
CH ₃ NO ₃	X	0	0	2	0.01	0
CH ₅ N	X	0	0	2	0	0
C ₂ H ₂ N	X	0	0	2	0	0
C ₂ H ₅ N	X	0	0	2	0	0
N ₂ H ₂	X	0	0	2	0	0
N ₂ H ₃	X	0	0	2	0	0
N ₂ H ₄	X	0	0	2	0	0
OCS	X	0	0	2	0.01	0
CS	X	0	0	2	0.01	0
CH ₃ S	X	0	0	2	0.01	0
CH ₄ S	X	0	0	2	0.01	0

Table 4-13. Surface boundary conditions for exoplanets with CO₂-dominated atmospheres.

Name	Type	Initial Mixing Ratio	Upper Boundary Flux Beside Escape (Upwards) [molecule/(cm ² s)]	Lower Boundary Type	Dry Deposition Velocity [cm/s]	Lower Boundary Flux (Upwards) [molecule/(cm ² s)]
H	X	0	0	2	1	0
H ₂	X	1.60×10^{-3}	0	2	0	3.00×10^{10}
O	X	0	0	2	1	0
O(1D)	X	0	0	2	0	0
O ₂	X	0	0	2	0	0
O ₃	X	0	0	2	0.4	0
OH	X	0	0	2	1	0
HO ₂	X	0	0	2	1	0
H ₂ O	X	2.00×10^{-6}	0	1	0	0.01
H ₂ O ₂	X	0	0	2	0.5	0
CO ₂	X	0.9	0	1	0	0.9
CO	X	0	0	2	1.00×10^{-8}	0
CH ₂ O	X	0	0	2	0.1	0
CHO	X	0	0	2	0.1	0
C	X	0	0	2	0	0
CH	X	0	0	2	0	0
CH ₂	X	0	0	2	0	0
CH ₂₁	X	0	0	2	0	0
CH ₃	X	0	0	2	0	0
CH ₄	X	0	0	2	0	3.00×10^8
CH ₃ O	X	0	0	2	0.1	0
CH ₄ O	X	0	0	2	0.1	1.20×10^{13}
CH ₂ O ₂	X	0	0	2	0.1	0
CH ₃ O ₂	X	0	0	2	0.1	0
CH ₄ O ₂	X	0	0	2	0	0
C ₂	X	0	0	2	0.1	0
C ₂ H	X	0	0	2	0	0
C ₂ H ₂	X	0	0	2	0	0

C ₂ H ₃	X	0	0	2	0	0
C ₂ H ₄	X	0	0	2	0	0
C ₂ H ₅	X	0	0	2	0	0
C ₂ H ₆	X	0	0	2	0	0
C ₂ HO	X	0	0	2	1.00×10^{-5}	0
C ₂ H ₂ O	X	0	0	2	0	0
C ₂ H ₃ O	X	0	0	2	0.1	0
C ₂ H ₄ O	X	0	0	2	0.1	0
C ₂ H ₅ O	X	0	0	2	0.1	0
N ₂	X	0	0	2	0.1	0
S	X	0	0	2	0	0
S ₂	X	0	0	2	0	0
S ₃	X	0	0	2	0	0
S ₄	X	0	0	2	0	0
SO	X	0	0	2	0	0
SO ₂	X	0	0	2	1	3.00×10^9
SO ₂₁	X	0	0	2	0	0
SO ₂₃	X	0	0	2	0	0
SO ₃	X	0	0	2	1	0
H ₂ S	X	0	0	2	0.015	3.00×10^8
HS	X	0	0	2	0	0
HSO	X	0	0	2	0	0
HSO ₂	X	0	0	2	0	0
HSO ₃	X	0	0	2	0.1	0
H ₂ SO ₄	X	0	0	2	1	0
H ₂ SO ₄ A	A	0	0	2	0.2	0
S ₈	X	0	0	2	0	0
S ₈ A	A	0	0	2	0.2	0
CHO ₂	C	0.1	0	1	0	0.1
N	X	0	0	2	0	0
NH ₃	X	0	0	2	1	0
NH ₂	X	0	0	2	0	0
NH	X	0	0	2	0	0
N ₂ O	X	0	0	2	0	0
NO	X	0	0	2	0.02	0
NO ₂	X	0	0	2	0.02	0
NO ₃	X	0	0	2	1	0
N ₂ O ₅	X	0	0	2	4	0
HNO	X	0	0	2	0	0
HNO ₂	X	0	0	2	0.5	0
HNO ₃	X	0	0	2	4	0
HNO ₄	X	0	0	2	4	0
HCN	X	0	0	2	0.01	0
CN	X	0	0	2	0.01	0
CNO	X	0	0	2	0	0
HCNO	X	0	0	2	0	0
CH ₃ NO ₂	X	0	0	2	0.01	0
CH ₃ NO ₃	X	0	0	2	0.01	0
CH ₅ N	X	0	0	2	0	0
C ₂ H ₂ N	X	0	0	2	0	0
C ₂ H ₅ N	X	0	0	2	0	0
N ₂ H ₂	X	0	0	2	0	0

N ₂ H ₃	X	0	0	2	0	0
N ₂ H ₄	X	0	0	2	0	0
OCS	X	0	0	2	0.01	0
CS	X	0	0	2	0.01	0
CH ₃ S	X	0	0	2	0.01	0
CH ₄ S	X	0	0	2	0.01	0

Table 4-14. Surface boundary conditions for exoplanets with N₂-dominated atmospheres.

Name	Type	Initial Mixing Ratio	Upper Boundary Flux Beside Escape (Upwards) [molecule/(cm ² s)]	Lower Boundary Type	Dry Deposition Velocity [cm/s]	Lower Boundary Flux (Upwards) [molecule/(cm ² s)]
H	X	0	0	2	1	0
H ₂	X	0	0	2	0	3.00×10^{10}
O	X	0	0	2	1	0
O(1D)	X	0	0	2	0	0
O ₂	X	0	0	2	0	0
O ₃	X	0	0	2	0.4	0
OH	X	0	0	2	1	0
HO ₂	X	0	0	2	1	0
H ₂ O	X	2.00×10^{-6}	0	1	0	1.00×10^{-2}
H ₂ O ₂	X	0	0	2	0.5	0
CO ₂	X	0	0	2	1.00×10^{-4}	3.00×10^{11}
CO	X	0	0	2	1.00×10^{-8}	0
CH ₂ O	X	0	0	2	0.1	0
CHO	X	0	0	2	0.1	0
C	X	0	0	2	0	0
CH	X	0	0	2	0	0
CH ₂	X	0	0	2	0	0
CH ₂₁	X	0	0	2	0	0
CH ₃	X	0	0	2	0	0
CH ₄	X	0	0	2	0	3.00×10^8
CH ₃ O	X	0	0	2	0.1	0
CH ₄ O	X	0	0	2	0.1	1.20×10^{13}
CH ₂ O ₂	X	0	0	2	0.1	0
CH ₃ O ₂	X	0	0	2	0.1	0
CH ₄ O ₂	X	0	0	2	0.1	0
C ₂	X	0	0	2	0.1	0
C ₂ H	X	0	0	2	0	0
C ₂ H ₂	X	0	0	2	0	0
C ₂ H ₃	X	0	0	2	0	0
C ₂ H ₄	X	0	0	2	0	0
C ₂ H ₅	X	0	0	2	0	0
C ₂ H ₆	X	0	0	2	0	0
C ₂ HO	X	0	0	2	1.00×10^{-5}	0
C ₂ H ₂ O	X	0	0	2	0.1	0
C ₂ H ₃ O	X	0	0	2	0.1	0
C ₂ H ₄ O	X	0	0	2	0.1	0
C ₂ H ₅ O	X	0	0	2	0.1	0
N ₂	X	0	0	2	0.1	0
S	C	1	0	1	0	1

S ₂	X	0	0	2	0	0
S ₃	X	0	0	2	0	0
S ₄	X	0	0	2	0	0
SO	X	0	0	2	0	0
SO ₂	X	0	0	2	0	0
SO ₂₁	X	0	0	2	1	3.00 × 10 ⁹
SO ₂₃	X	0	0	2	0	0
SO ₃	X	0	0	2	0	0
H ₂ S	X	0	0	2	1	0
HS	X	0	0	2	0.015	3.00 × 10 ⁸
HSO	X	0	0	2	0	0
HSO ₂	X	0	0	2	0	0
HSO ₃	X	0	0	2	0	0
H ₂ SO ₄	X	0	0	2	0.1	0
H ₂ SO ₄ A	X	0	0	2	1	0
S ₈	A	0	0	2	0.2	0
S ₈ A	X	0	0	2	0	0
CHO ₂	A	0	0	2	0.2	0
N	X	0	0	2	0	0
NH ₃	X	0	0	2	1	0
NH ₂	X	0	0	2	0	0
NH	X	0	0	2	0	0
N ₂ O	X	0	0	2	0	0
NO	X	0	0	2	0.02	0
NO ₂	X	0	0	2	0.02	0
NO ₃	X	0	0	2	1	0
N ₂ O ₅	X	0	0	2	4	0
HNO	X	0	0	2	0	0
HNO ₂	X	0	0	2	0.5	0
HNO ₃	X	0	0	2	4	0
HNO ₄	X	0	0	2	4	0
HCN	X	0	0	2	0.01	0
CN	X	0	0	2	0.01	0
CNO	X	0	0	2	0	0
HCNO	X	0	0	2	0	0
CH ₃ NO ₂	X	0	0	2	0.01	0
CH ₃ NO ₃	X	0	0	2	0.01	0
CH ₅ N	X	0	0	2	0	0
C ₂ H ₂ N	X	0	0	2	0	0
C ₂ H ₅ N	X	0	0	2	0	0
N ₂ H ₂	X	0	0	2	0	0
N ₂ H ₃	X	0	0	2	0	0
N ₂ H ₄	X	0	0	2	0	0
OCS	X	0	0	2	0.01	0
CS	X	0	0	2	0.01	0
CH ₃ S	X	0	0	2	0.01	0
CH ₄ S	X	0	0	2	0.01	0

Chapter 5

Assessment of Hydrogen Chloride as a Bioindicator on Exoplanets with H₂-dominated Atmospheres

The results presented in this chapter will be published in a paper currently in preparation. It is best to treat all the results as preliminary. The final published paper may differ from the content of this chapter. I would like to thank Prof. Sara Seager, Dr. Sukrit Ranjan, and Dr. Janusz J. Petkowski for their assistance and support in this project.

Abstract

As more and more exoplanets have been discovered in recent years, the search for biosignature gases is becoming one of the crucial ways to find extraterrestrial life. In the atmosphere, some biosignature gases do not survive photochemical destruction. We can only infer the presence of these biosignature gases by detecting their photochemical products, which we call bioindicators. In this paper, we carefully examine the bioindicator potential of HCl. HCl has many advantages of being a potential bioindicator in an H₂-dominated atmosphere, one of which is that there are very few abiotic sources of HCl, with the only exception being volcanic activity. However, despite HCl's advantages, we believe that HCl is not a suitable bioindicator because it cannot accumulate to detectable levels in the atmosphere. Through my simplified chloride steady-state chemical model, we find that even if life on such a planet produces CH₃Cl at a flux of 3.5×10^{13} molecules cm⁻² s⁻¹, the same as Earth's gross oxygen production flux, there is still less than 10 ppb of HCl in the atmosphere, far from being detectable by JWST. The extremely high water solubility of HCl means that wet deposition can efficiently remove it from the atmosphere, preventing HCl from accumulating to detectable levels in the atmosphere.

5.1 Introduction

With the development of telescopes, more and more exoplanets have been discovered in recent years. In March 2022, NASA announced that the number of confirmed exoplanets had passed 5000. Looking for biosignature gases in exoplanets' atmospheres is expected to become one of the crucial ways to find extraterrestrial life. Biosignature gases are gases produced by living organisms that can accumulate in the atmosphere. To date, many gases have been proposed as biosignature gases, including methane (CH₄) (Leger et al., 1996; Des Marais et al., 2002; Kaltenegger et al., 2007; Dlugokencky et al., 2011), ammonia (NH₃) (Seager et al., 2013; Huang et al., 2022) and isoprene (C₅H₈) (Zhan et al., 2021) to mention a few. The most widely known biosignature gas has to be O₂ (e.g., Jeans, 1930; Meadows et al., 2018). However, some biosignature gases do not survive photochemical destruction. These biosignature gases themselves cannot accumulate to detectable levels in the atmosphere. We can only infer the presence of biosignature gases by detecting their photochemical products. We refer to the final products of the chemical reactions of

biosignature gases as bioindicators (Seager et al., 2013).

We are motivated to study hydrogen chloride (HCl) because of its many advantages as a bioindicator in H₂-dominated atmospheres. In highly reducing atmospheres, many gases are converted to their most hydrogenated (i.e., reduced) form: dimethyl sulfide (DMS) will be turned into H₂S and CH₄; N₂O will be turned into H₂O and N₂ (Seager et al., 2013). Since the most reduced form of Cl element is HCl, atmospheric methyl chloride (CH₃Cl) and chlorine (Cl₂) gas will end up as HCl in H₂-dominated atmospheres. In addition, there are very few abiotic sources of HCl, with the only exception being volcanic activity (see Chapter 5.2). The high water solubility of HCl (see Chapter 5.5.1) means that only when life converts enough non-volatile forms of Cl into HCl gas can HCl accumulate in the atmosphere to detectable levels. (Seager et al., 2013) very briefly mentions HCl as a potential bioindicator. In this work, we will take a closer look at the bioindicator potential of HCl.

We first discuss chlorine's abundance, distribution, and circulation on Earth (Chapter 5.2). We introduce our research methods in Chapter 5.3. We present our results in Chapter 5.4 and Chapter 5.5. Finally, we conclude our paper with a summary (Chapter 5.6).

5.2 The Abundance, Distribution, and Circulation of Chlorine on Earth

Chlorine (Cl) is a member of the halogen group with an atomic number of 17 and an atomic weight of about 35.45. At room temperature and pressure, chlorine is a greenish-yellow gas ($T_{\text{melt}} \cong -101.5^{\circ}\text{C}$; $T_{\text{boil}} \cong -34.0^{\circ}\text{C}$; density $\cong 3.2 \text{ g/L}$) (David R. Lide et al., 2005). Chlorine is a strong oxidizing agent and is highly reactive. Chlorine can react (i.e., combine) with almost all elements to form Cl-containing compounds. Due to its high reactivity, chlorine as a free element (i.e., Cl₂ gas) does not exist in nature. Instead, chlorine is predominantly found on Earth as chlorides (e.g., dissolved Cl⁻ ions or chloride salts) (Greenwood et al., 1997; David R. Lide et al., 2005). In this section, we will discuss the abundance and distribution of chlorine on Earth in Chapter 5.2.1 and review Earth's chlorine cycle in Chapter 5.2.2.

5.2.1 Abundance and Distribution of Chlorine on Earth

Chlorine is very abundant on Earth. Of the 94 naturally-occurring elements, chlorine ranks in the top 20 in terms of abundance (Graedel et al., 1996; Öberg 2002; Sharp et al., 2013; Atashgahi et al., 2018; Svensson et al., 2021). So far, there is no consensus on the exact value of the total amount of chlorine on Earth, with estimates ranging from a low of about $1 \times 10^{12} \text{ Tg}$ to a high of about $2 \times 10^{13} \text{ Tg}$ ($\text{Tg} = 10^{12} \text{ g}$, Graedel et al., 1996; Sharp et al., 2013). It is worth noting that chlorine is not evenly distributed on Earth but concentrated in its three major reservoirs: the mantle, the crust, and the ocean (Graedel et al., 1996; Sharp et al., 2013; Svensson et al., 2021). Specifically, nearly all of Earth's chlorine (> 99%) is locked up in the mantle. Chlorine in the mantle hardly participates in Earth's chlorine cycle, the only way being through volcanism (Graedel et al., 1996). Chlorine stored in the crust also has little involvement in the chlorine cycle. Crustal chlorine can only participate in cycling via weathering (Graedel et al., 1996). In contrast, chlorine in the oceans can easily

circulate between the hydrosphere, the atmosphere, and the biosphere. Although oceanic chlorine represents only a tiny fraction ($< 0.1\%$) of the Earth's total chlorine reserves, it plays a vital role in the chlorine cycle thanks to its high accessibility and mobility (Graedel et al., 1996). In addition to the three main reservoirs mentioned above, other chlorine reservoirs include freshwater (e.g., lakes and rivers), the pedosphere (e.g., soil, sediment, and litter), the atmosphere (troposphere and stratosphere), the cryosphere (e.g., glaciers and ice caps), and the biosphere (Graedel et al., 1996; Sharp et al., 2013; Atashgahi et al., 2018; Svensson et al., 2021). We have not found any papers showing the presence of chlorine in Earth's core, so we do not consider the core a chlorine reservoir. In the following paragraphs, we will go over each reservoir one by one.

The largest chlorine reservoir on Earth is the mantle, which holds more than 250 times more chlorine than all other reservoirs combined (Graedel et al., 1996; Svensson et al., 2021). Since the 1970s, many researchers have tried to estimate the amount of chlorine in Earth's mantle (e.g., Schilling et al., 1978; Dreibus et al., 1987; Graedel et al., 1996; Burgess et al., 2002; Sharp et al., 2013; Svensson et al., 2021). Because each makes different assumptions, their estimates vary widely, from approximately 1.0×10^{11} Tg to roughly 2.2×10^{13} Tg (Graedel et al., 1996; Sharp et al., 2013; Svensson et al., 2021). Here we use the estimate of 2.2×10^{13} Tg from (Graedel et al., 1996) and (Svensson et al., 2021), where the authors assume the same chlorine-to-silicon ratio in the mantle as in meteorites (Cameron 1968; Graedel et al., 1996; Svensson et al., 2021). The crust is the second-largest chlorine reservoir on Earth after the mantle (Graedel et al., 1996; Sharp et al., 2013; Svensson et al., 2021). Crustal chlorine is mainly concentrated in evaporites and sedimentary salt beds (Graedel et al., 1996; Sharp et al., 2013). Unlike chlorine in the mantle, crustal chlorine is accessible to humans (Graedel et al., 1996). Estimates of chlorine abundance in the crust are relatively consistent, around 6.0×10^{10} Tg (Graedel et al., 1996; Sharp et al., 2013; Svensson et al., 2021).

The oceans are not only Earth's third-largest chlorine reservoir but also the primary repository for chlorine in the hydrosphere (Graedel et al., 1996). Chlorine exists in the oceans primarily as dissolved chloride ions (Cl^-). The abundance of oceanic chlorine can be easily estimated from the Cl concentration in the ocean. Given that the average concentration of Cl is roughly 19.4 g/L (Graedel et al., 1996; David R. Lide et al., 2005; Svensson et al., 2021), there should be about 2.6×10^{10} Tg of chlorine in the oceans (Graedel et al., 1996; Svensson et al., 2021). While the oceans store less than half the amount of chlorine as the crust, it is the source of most chlorine in Earth's chlorine cycle (Graedel et al., 1996, see Chapter 5.2.2 for more details). Compared to the oceans (saltwater), freshwater is a much smaller chlorine reservoir. Freshwater on Earth includes surface water (e.g., rivers and lakes) and groundwater (e.g., water stored in soils and aquifers) (Graedel et al., 1996). Rivers and lakes together contain approximately 1×10^{17} L of water (Gleick et al., 1993; Graedel et al., 1996), while soils and aquifers store roughly 80 times as much (Graedel et al., 1993; Graedel et al., 1996). It is estimated that the average chlorine concentration in rivers is about 5.8 mg/L, while the typical chlorine concentration for groundwater is roughly 40 mg/L (Freeze et al., 1979; Graedel et al., 1996). Therefore, freshwater (i.e., surface water and groundwater combined) contains roughly 3.2×10^5 Tg of chlorine, which is about five orders of magnitude lower than the chlorine abundance in the oceans (Graedel et al., 1996; Svensson et al., 2021).

There is also considerable chlorine in the pedosphere (Graedel et al., 1996; Svensson et al., 2021). The amount of chlorine stored in the pedosphere is roughly an order of magnitude lower than in freshwater (Graedel et al., 1996; Svensson et al., 2021). Unlike oceans or freshwater, where chlorine exists almost exclusively as Cl^- ions, chlorine in the pedosphere can exist as inorganic chlorides or as chlorinated organic species (i.e., organic chlorine ' Cl_{org} ') (Graedel et al., 1996; Svensson et al., 2021). Due to the diversity and complexity of chlorine compounds (particularly Cl_{org}), an accurate estimate of the total chlorine abundance in the pedosphere is very challenging (Graedel et al., 1996; Svensson et al., 2021). So far, we still know very little about Cl_{org} in soils (Svensson et al., 2021). Most research on pedospheric Cl_{org} has focused on anthropogenic chlorinated wastes and pollutants, such as dichlorodiphenyltrichloroethanes (DDTs) (Jonsson 1994; Pöykiö et al., 2008; Tagliabue et al., 2020; Svensson et al., 2021). For a long time, people believed that Cl_{org} , in general, were xenobiotic (i.e., not naturally occurring), persistent (i.e., non-biodegradable), and toxic (e.g., Kühn et al., 1977; Keller 1989). Because of this, the contribution of Cl_{org} to the total chlorine abundance in the pedosphere is often overlooked (e.g., Graedel et al., 1996). However, these stereotypes about Cl_{org} have been proven wrong (Öberg 2002). In general, soils contain as much Cl_{org} as inorganic chlorides and even more in some types of soils (Redon et al., 2011; Gustavsson et al., 2012; Redon et al., 2013; Svensson et al., 2021). Specifically, the average mass fraction of inorganic chlorides in soils is about 0.01% (Graedel et al., 1996), while Cl_{org} 's concentration can reach 0.5% in soils rich in organic matter (e.g., humus) (Redon et al. 2011; Svensson et al., 2021). Overall, it has been estimated that there is about 4.8×10^4 Tg of chlorine in the pedosphere in total, assuming equal amounts of inorganic chlorides and Cl_{org} (Graedel et al., 1996; Svensson et al., 2021).

The biosphere is a relatively small chlorine reservoir, storing about 50 times less chlorine than the pedosphere (Svensson et al., 2021). Chlorine in the biosphere is mainly concentrated in terrestrial biomass, especially in plants (Tröjbom et al., 2010; Svensson et al., 2021). Growing plants absorb large amounts of Cl^- from the soils. Some of the absorbed Cl^- ions can accumulate in roots, bark, or leaves, and some can be converted into Cl_{org} (Svensson et al., 2021). Cl^- concentrations vary in different parts of the plant, with fresh leaves generally having the highest concentrations (Svensson et al., 2021). On average, the Cl^- concentration in a growing plant is about 1 milligram per gram of dry matter (i.e., mg/g d.m.) (Svensson et al., 2021). Plants will show deficiency symptoms when Cl^- concentrations fall below 0.1 mg/g d.m., whereas toxicity will occur if Cl^- concentrations exceed 4 mg/g d.m. (White et al., 2001; Marschner 2011; Svensson et al., 2021). In contrast, plant Cl_{org} content is more challenging to estimate. One reason is the wide variety of organic chlorines found in plants. For example, in terrestrial vascular plants, hundreds of organic chlorines have been identified (Gribble 2009; Svensson et al., 2021). Some of these compounds are short-lived, such as chlorinated auxins (Engvild 1994; Walter et al., 2020), while others have relatively long environmental half-lives, such as chlorinated fatty acids (Björn 1999; Dembitsky et al., 2002; Mu et al., 2004). Another reason is the lack of experimental data. Only a few plants, such as spruce and beech, have available Cl_{org} measurements (Svensson et al., 2021). In all, we still know very little about Cl_{org} in plants. The current best estimate of plant Cl_{org} content is between 0.01 and 0.1 mg/g d.m. (Öberg et al., 2005; Svensson et al., 2021). Given that the global plant biomass is about 9×10^5 Tg

(Bar-On et al., 2018), it is estimated that there is approximately 900 Tg of chlorine in the biosphere (Svensson et al., 2021).

The atmosphere (the troposphere and stratosphere combined) is a minor chlorine reservoir (Graedel et al., 1996; Svensson et al., 2021). There is roughly 160 times less chlorine in the atmosphere than in the biosphere (Svensson et al., 2021). There are three primary sources of chlorine in the atmosphere: hydrogen chloride (HCl), methyl chloride (CH₃Cl), and sea salt aerosols (Graedel et al., 1996; Svensson et al., 2021). There are significant regional and elevational (i.e., altitude) variations in the atmospheric concentrations of HCl (Graedel et al., 1996). HCl concentrations in or near urban areas are significantly higher than those in remote regions. Specifically, HCl concentrations in urban areas can reach up to 3000 ppt, while near the surface in remote areas, HCl concentrations are typically below 300 ppt (Graedel et al., 1996). The atmospheric concentration of HCl also decreases with increasing altitude. The average concentration of HCl in the atmospheric boundary layer (i.e., within a few hundred meters above the surface) is approximately 200 ppt (Graedel et al., 1996). Above the boundary layer (i.e., in the free troposphere), the concentration of HCl decreases rapidly to below 100 ppt (Graedel et al., 1996). Overall, the contribution of HCl to the atmospheric chlorine content is estimated to be about 0.6 Tg (Graedel et al., 1996). CH₃Cl is another major reactive Cl-containing species in the atmosphere. Given that the average atmospheric concentration of CH₃Cl is roughly 620 ppt (Graedel et al., 1996), its contribution to the atmospheric chlorine content is approximately 3.7 Tg (Graedel et al., 1996). Sea salt aerosols are another vital source of atmospheric chlorine. Most sea salt aerosols are injected into the lower troposphere and rapidly redeposit back into the sea (Graedel et al., 1996). The production of sea salt aerosols depends on numerous factors, such as wave action, wind speed, and water temperature (Graedel et al., 1996; Christiansen et al., 2019; Nielsen et al., 2020). Atmospheric concentrations of sea salt aerosols vary widely (Graedel et al., 1996). Given that the typical concentrations of sea salt aerosols average around 100 nM/m³ (Graedel et al., 1995; Graedel et al., 1996), their contribution to the atmospheric chlorine content is estimated to be about 1 Tg (Graedel et al., 1996). Stratospheric chlorine has a relatively small contribution to the overall atmospheric chlorine abundance (Graedel et al., 1996; Svensson et al., 2021). Most Cl-containing compounds in the stratosphere are of anthropogenic origin (Graedel et al., 1996). It is estimated that approximately 0.4 Tg of chlorine is currently in the stratosphere (Graedel et al., 1996; Svensson et al., 2021). In all, there is approximately 5.3 Tg of chlorine in the troposphere (0.6 Tg from HCl, 3.7 Tg from CH₃Cl, and 1 Tg from sea salt aerosols) and roughly 0.4 Tg of chlorine in the stratosphere, for a total of about 5.7 Tg of chlorine in the Earth's atmosphere (Graedel et al., 1996; Svensson et al., 2021).

Finally, the cryosphere is a tiny chlorine reservoir (Graedel et al., 1996). The cryosphere stores very little chlorine, mainly because when snow or rain (with dissolved Cl⁻ ions) falls on glaciers or ice, most of the dissolved chlorine is eluted to the surrounding environment (Graedel et al., 1996). It is estimated that the cryosphere stores only about 5×10^{-4} Tg of chlorine (Graedel et al., 1996). We summarize all the chlorine reservoirs discussed in this section in Figure 5-1 below. It is worth pointing out that the chlorine abundance of each reservoir is not static but constantly changing.

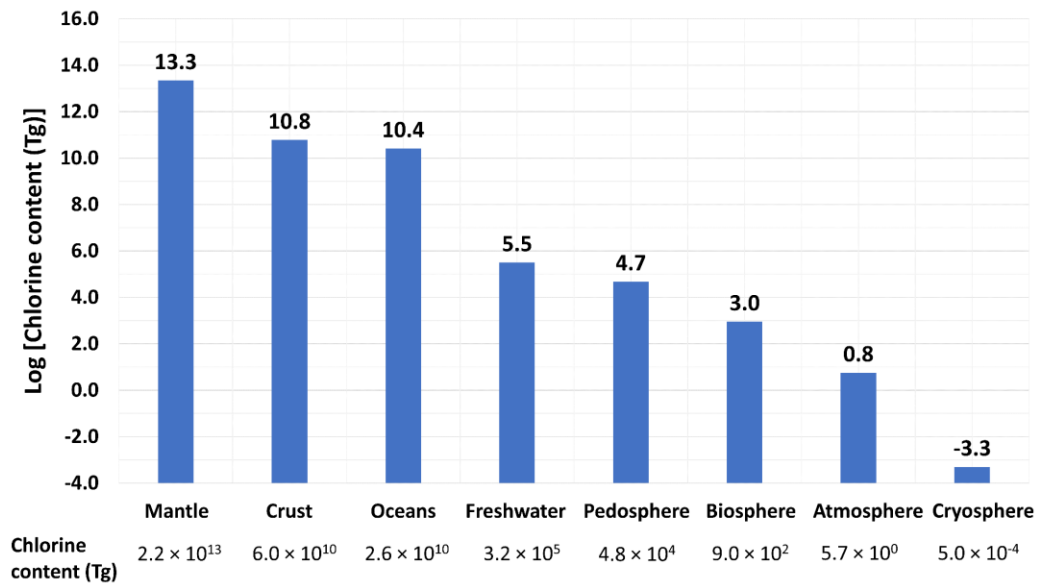


Figure 5-1. Chlorine reservoirs on Earth. The y-axis shows the estimated chlorine content of each reservoir (Tg) on a log scale. The x-axis shows the names of the reservoirs. Chlorine is not evenly distributed on Earth but is concentrated in its three major reservoirs: the mantle, the crust, and the oceans. Data from Graedel et al., 1996 and Svensson et al., 2021.

5.2.2 Overview of Earth's Natural Chlorine Cycle

Earth's chlorine cycle generally consists of three components: abiotic transformations of chlorine, microbial metabolism of inorganic and organic chlorine, and anthropogenic activities (Atashgahi et al., 2018). From a mass perspective, chlorine transfer between the oceans and the atmosphere (troposphere) dominates Earth's chlorine cycle (Graedel et al., 1996; Svensson et al., 2021). Specifically, the injection of sea salt aerosols from the oceans to the atmosphere is the most significant inter-reservoir chlorine flux on Earth, followed by the return of chlorine to the oceans via surface deposition (i.e., wet and dry deposition) (Graedel et al., 1996; Svensson et al., 2021). Over the past decades, people have tried to study Earth's chlorine cycle from different perspectives (e.g., from biological to geochemical), and many review articles have covered these topics (e.g., Neilson 1990; Chaudhry et al., 1991; Hardman 1991; Häggblom 1992; Graedel et al., 1996; Bhatt et al., 2007; Atashgahi et al., 2018; Svensson et al., 2021). In the following paragraphs, we will discuss the natural transfer of chlorine between different reservoirs in more detail.

We start with chlorine fluxes from the oceans to the atmosphere. The dominant natural source of atmospheric chlorine is the injection of sea salt aerosols from the oceans (Graedel et al., 1996). It is estimated that the oceans can deliver approximately 5.97×10^3 Tg of chlorine per year to the atmosphere through sea salt injection (Graedel et al., 1995; Graedel et al., 1996). However, most sea salt aerosols only stay briefly in the lower troposphere before quickly depositing back into the oceans (Graedel et al., 1996). Due to the short atmospheric lifetime of sea salt aerosols, despite the enormous flux, sea salt aerosols represent only a small fraction of the total atmospheric chlorine reserve (Chapter 5.2.1). In

the atmosphere above the oceans (sometimes called the 'marine boundary layer'), some sea salt aerosols can undergo acidification (by naturally derived acids) and be converted to HCl gas (Martens et al., 1973; Brimblecombe et al., 1988; Keene et al., 1990; Graedel et al., 1996). It is estimated that the production flux of HCl through dechlorination of sea salt aerosols is around 25 Tg/year (Graedel et al., 1996). It is worth noting that this dechlorination process can also yield other reactive inorganic Cl-compounds such as HClO and ClNO₂ (Graedel et al., 1995; Graedel et al., 1996; Vogt et al., 1996), albeit their production fluxes are minimal. In addition to inorganic Cl-compounds, the oceans also emit a variety of chlorinated organic species (Cl_{org}) into the atmosphere (Grimvall et al., 1995; Graedel et al., 1996). Among these naturally occurring Cl_{org}, CH₃Cl accounts for the vast majority (Graedel et al., 1996; Atashgahi et al., 2018). CH₃Cl can be produced by marine plants (e.g., seaweeds and phytoplankton) and unicellular marine eukaryotes (Scarratt et al., 1998; Atashgahi et al., 2018). The CH₃Cl flux from the oceans to the atmosphere is estimated to be only about 2 Tg/year (Tait et al., 1994; Graedel et al., 1996). Combining the contributions of sea salt aerosols, HCl, and CH₃Cl, the total chlorine flux from the oceans to the atmosphere should be around 6.0×10^3 Tg/year (Graedel et al., 1996).

Next, we discuss chlorine fluxes coming out of the atmosphere. The dominant removal mechanism of atmospheric chlorine is surface deposition, including wet and dry deposition (Graedel et al., 1996; Svensson et al., 2021). In general, chlorine surface deposition is higher in densely vegetated areas than in open areas due to interception by vegetation (e.g., leaves and tree canopies) (Svensson et al., 2021). To estimate chlorine surface deposition flux, we can roughly divide the Earth's surface into two categories: oceans and land (the sum of pedosphere and cryosphere). The wet deposition flux of atmospheric chlorine to land is easy to estimate (Graedel et al., 1996; Svensson et al., 2021). Earth's average annual rainfall is about 5.1×10^5 km³, of which roughly 1.1×10^5 km³ falls on land (Lvovitch et al., 1973; Jaeger 1983; Graedel et al., 1996). Since the average concentration of chlorine in precipitation is about 5 mM (millimoles per liter) (Graedel et al., 1995; Graedel et al., 1996), the wet deposition flux of chlorine to land is about 20 Tg/year (Graedel et al., 1996). The dry deposition flux of chlorine to land depends on various factors, such as air temperature and the presence of plants, to name a few. (Svensson et al., 2012) estimates that dry deposition of chlorine accounts for 15% to 73% of total chlorine deposition on Earth. For simplicity, we assume that chlorine's dry and wet deposition flux to land are the same. Therefore, the total deposition flux of chlorine to land is approximately 40 Tg/year (Graedel et al., 1996). Given that the cryosphere covers about 13% of the Earth's land area (Bolch et al., 2021), we estimate the total deposition flux of chlorine to the cryosphere to be about 5.2 Tg/year, and the total deposition flux of chlorine to the pedosphere to be about 34.8 Tg/year. Chlorine deposition flux from the atmosphere to the oceans is enormous, comparable to that of sea salt injection (Graedel et al., 1996). We estimate that the chlorine deposition flux to the oceans should be at least 5.96×10^3 Tg/year, balancing the chlorine flux from the oceans and ensuring that the atmospheric chlorine abundance remains relatively stable (Graedel et al., 1996). It is estimated that 80% of the chlorine deposition flux to the oceans ($\sim 4.8 \times 10^3$ Tg/year) is due to the gravitational settling (dry deposition) of sea salt aerosols and Cl-containing particulates, while 20% ($\sim 1.2 \times 10^3$ Tg/year) is due to precipitation (wet deposition) (Erickson et al., 1988; Graedel et al., 1996). Overall, we estimate chlorine's total surface deposition flux (deposition to land + deposition to oceans) to be about 6.0×10^3 Tg/year.

There are two caveats to our analysis above. First, our estimate is likely to be a lower bound since almost all the studies we have found so far focus only on inorganic chlorines. However, precipitation also contains a certain amount of organic chlorines (Cl_{org}) (Enell et al., 1991; Grimvall et al., 1991; Laniewski et al., 1995; Svensson et al., 2021). Some of the Cl_{org} that have been identified include industrial pollutants (e.g., pesticides and flame retardants) and chloroacetic acids, among others (Frank 1991; Reimann et al., 1996; Stringer et al., 2001). Unfortunately, studies on Cl_{org} in precipitation are still scarce, and we know very little about their origins and geographical distributions (Svensson et al., 2021). Second, in this work, we study the atmosphere as a whole (i.e., a single layer). In reality, chlorine transfer can also occur between the troposphere and the stratosphere (Graedel et al., 1996). Thanks to turbulent mixing, some tropospheric chlorine species with relatively long atmospheric lifetimes can be transferred upwards into the stratosphere (Graedel et al., 1996). CH_3Cl emitted from the oceans and terrestrial ecosystems is one of the few Cl -compounds that can survive the journey to the stratosphere. CH_3Cl is one of the dominant sources of stratospheric chlorine (Graedel et al., 1996). The chlorine flux between the troposphere and the stratosphere is estimated to be about 0.06 Tg/year (0.03 Tg/year from the troposphere to the stratosphere and 0.03 Tg/year from the stratosphere to the troposphere) (Graedel et al., 1993; Graedel et al., 1996).

In addition to the oceans and the atmosphere, the pedosphere is also actively involved in Earth's chlorine cycle. The pedosphere can release chlorine into the atmosphere through mineral aerosol injection or biomass burning (Graedel et al., 1996). In arid regions of the world, strong winds can blow large amounts of soil dust into the atmosphere (Graedel et al., 1996). Mineral aerosols formed from these soil dust usually contain considerable amounts of chlorine (Talbot et al., 1986; Graedel et al., 1996), and they can travel thousands of miles by winds before being removed by surface deposition (Swap et al., 1992; Andreae et al., 1996; Graedel et al., 1996). Therefore, mineral aerosols are one of the essential sources of particulate chlorides in the continental boundary layer (i.e., the lower troposphere above the continents) (Graedel et al., 1996). It is estimated that the pedosphere can deliver approximately 15 Tg/year of chlorine to the atmosphere through mineral aerosol injection (Graedel et al., 1996). The amount of chlorine emitted from biomass burning is very limited. Note that our discussion here focuses only on natural combustion (i.e., excluding combustion due to anthropogenic activities). It is estimated that approximately 70% - 85% of the chlorine contained in biomass can be released during the combustion process (Andreae et al., 1996; Graedel et al., 1996; McKenzie et al., 1996). Of these released chlorines, more than 90% are inorganic chlorines (e.g., HCl), less than 3% are CH_3Cl , and the rest are other chlorinated organic species (Graedel et al., 1996). It is estimated that biomass burning can release roughly 3 Tg/year of chlorine (inorganic Cl + Cl_{org}) into the atmosphere (Andreae 1993; Andreae et al., 1996; Graedel et al., 1996). The pedosphere also loses chlorine to freshwater. Earlier in this section, we estimate that approximately 34.8 Tg of atmospheric chlorine is deposited onto continents through surface deposition each year. However, the pedosphere (i.e., soil) is not good at absorbing deposited chlorine (Graedel et al., 1996). Except for a small fraction that is incorporated into minerals (e.g., as evaporites) (Stallard et al., 1981; Graedel et al., 1996), most atmospheric chlorine deposited on land passes through watersheds and ends up in surface waters (Feth 1981; Graedel et al., 1996). (Graedel et al., 1996) estimates that the flux of precipitation passthrough is about 34

Tg/year. Mineral dissolution is another pathway through which the pedosphere transfers chlorine into freshwater (Graedel et al., 1996). Many naturally occurring chloride minerals are highly soluble in water (Chapter 5.5.3). The mineral dissolution flux is estimated to be about 11 Tg/year (Graedel et al., 1996). Overall, the pedosphere transfers an estimated 45 Tg/year of chlorine to freshwater (Graedel et al., 1996). So far, we have not found any papers that show chlorine transfer between the pedosphere and Earth's crust.

People have long believed that almost all chlorine in freshwater comes from the atmosphere (Graedel et al., 1996; Svensson et al., 2021). However, the vast majority of riverine chlorine comes from the crust, specifically from the weathering of chlorine-bearing minerals in shales and sandstone (Eriksson 1960; Graedel et al., 1996; Schlesinger et al., 2013; Svensson et al., 2021). Mineral-rich hot springs in volcanic regions are also essential sources of riverine chlorine (Stallard et al., 1981; Berner et al., 1987; Graedel et al., 1996). Overall, the weathering of Earth's crust is estimated to provide freshwater with approximately 175 Tg of chlorine per year (Graedel et al., 1996). At the same time, freshwater is constantly transferring chlorine to the oceans. It is estimated that the average annual flux of river water to the oceans is about 3.8×10^{16} L/year, and that of groundwater to the oceans is roughly 2.2×10^{15} L/year (Berner et al., 1987; Graedel et al., 1996). Given that a typical chlorine concentration in freshwater is about 7 mg/L (Smith et al., 1987), the estimated chlorine transfer flux from freshwater to the oceans is approximately 220 Tg/year (Graedel et al., 1996). Chlorine can also be transferred from the oceans to the crust and from the cryosphere to the oceans. The former is due to diagenesis of oceanic chlorine, with an estimated flux of about 17 Tg/year (Graedel et al., 1996). The latter is due to the elution of cryospheric chlorine, with an estimated flux of only about 6 Tg/year (Graedel et al., 1996).

There is also chlorine transfer from the mantle to the atmosphere. On Earth, volcanoes emit various chlorine-containing compounds into the atmosphere (Gribble 1992; Graedel et al., 1996). About one-third of the volcanic chlorine is thought to be directly extracted from the mantle, and the rest is thought to be due to seawater entering into magma chambers (also known as 'magma intrusion') (Graedel et al., 1996). Among the chlorine-containing compounds produced during volcanic eruptions, HCl predominates (Gribble 1992; Graedel et al., 1996). The emission fluxes of other chlorine-containing gases are negligibly small (Symonds et al., 1988; Graedel et al., 1996). Due to the sporadic nature of volcanic eruptions and uncertainty about eruption intensity, there is considerable variability in the estimates of volcanic HCl fluxes, ranging from about 0.4 Tg/year to roughly 11 Tg/year (Symonds et al., 1988; Graedel et al., 1996). We use their average of 6 Tg/year (2 Tg/year from mantle extraction and 4 Tg/year from magma intrusion) as our volcanic HCl flux estimate. Note that there is a discrepancy between how we and (Graedel et al., 1996) treat magma intrusion. In (Graedel et al., 1996), magma intrusion is considered part of the chlorine transfer from the oceans to the atmosphere. Here, we consider magma intrusion as part of volcanism. Due to the high water solubility of HCl (Chapter 5.5.1), most of the volcanic HCl redeposits back to the surface shortly after the eruption (Tabazadeh et al., 1993; Graedel et al., 1996).

To wrap up our review, we need to talk about the role of the biosphere in Earth's chlorine cycle. Earlier in this section, when discussing chlorine transfer from the oceans to the

atmosphere, we mention that the marine biosphere can produce a variety of organic chlorines, of which CH₃Cl dominates, with an estimated emission flux of about 2 Tg/year (Tait et al., 1994; Grimvall et al., 1995; Graedel et al., 1996; Scarratt et al., 1998; Atashgahi et al., 2018). Estimating chlorine production flux from the terrestrial biosphere is challenging, partly because we still know very little about the abundance and distribution of chlorine within the terrestrial biosphere (Chapter 5.2.1). Achieving a reliable estimate of chlorine bioproduction flux involves the integration of extensive (long-term, preferably global) observations and rigorous modeling. (Graedel et al., 1996) estimates the terrestrial CH₃Cl bioproduction flux to be about 0.5 Tg/year. Here, we arbitrarily assume that the combined bioproduction flux of all other chlorine species is roughly equal to that of CH₃Cl. Therefore, we estimate that the overall terrestrial chlorine bioproduction flux should be at least 1 Tg/year. We want to emphasize that this estimate should be viewed as a lower limit. We summarize all our discussions of Earth's natural chlorine cycle in Figure 5-2.

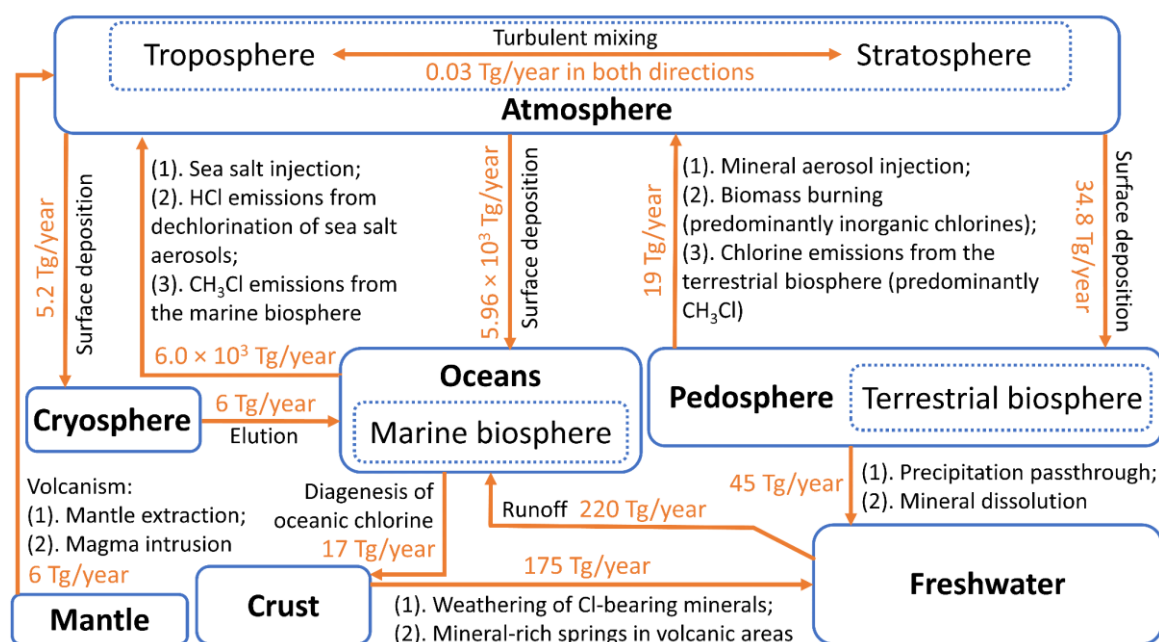


Figure 5-2. An overview of Earth's natural chlorine cycle. Earth's major chlorine reservoirs are shown in blue boxes. Orange arrows indicate how chlorine is transferred between different reservoirs. The unit of chlorine flux is Tg/year. From a mass perspective, chlorine transfer between the oceans and the atmosphere dominates Earth's chlorine cycle (Graedel et al., 1996; Svensson et al., 2021). Here we would like to emphasize that our quantitative estimates are still preliminary and may contain some uncertainties.

5.3 Methods

We use two methods to study HCl as a bioindicator in H₂-dominated atmospheres. First, we present my simplified chlorine steady-state chemical model (Chapter 5.3.1). We then introduce our one-dimensional photochemistry model in Chapter 5.3.2.

5.3.1 Simplified Chlorine Steady-State Chemical Model

I developed and used a simplified chlorine steady-state chemical model to study whether HCl can be a good bioindicator in an H₂-dominated atmosphere. This model does not require complex computational simulations. As a result, my simplified chlorine chemical model is much simpler and less time-consuming to run than our full-fledged photochemistry model. For details of my simplified chlorine steady-state chemical model and how I used it to draw a preliminary conclusion, please see Chapter 2.2.

5.3.2 Photochemistry Model - Chlorine Chemical Network

In addition to my simplified chlorine chemical model, we would like to use our photochemistry model to verify whether HCl is a good bioindicator in an H₂-dominated atmosphere. Currently, there are more than 800 chemical reactions in our photochemistry model (Hu et al., 2012), and we include all of them in our simulations except high-temperature reactions, HSO₂ thermal decay, and reactions that involve more than two carbon atoms (C_{>2-chem}). However, one of the limitations of our current photochemistry code is that it does not have Cl-chemistry. To properly simulate an exoplanet with robust chlorine bioproduction, as a first step, we need to collect all relevant chlorine reactions and encode them into our model. The chlorine reactions we are looking for must satisfy the following two conditions. First, the reactions must be able to take place within the atmospheric temperature range we are simulating (i.e., between 160 K and 290 K). Reactions that can only occur at high temperatures (e.g., high-temperature thermal decomposition reactions) or low temperatures (i.e., cryogenic reactions) are excluded. Second, since we are simulating an exoplanet with a reducing H₂-dominated atmosphere, we exclude those reactions in which the reactants are oxidized chlorine compounds (e.g., reactions involving ClO₂ or ClO₄). We thoroughly searched the NIST database and the JPL database for chlorine reactions. Overall, we add 12 new Cl-containing chemical species and a chlorine chemical network consisting of 92 chemical reactions to our existing photochemical model. We present our current collection results in Appendix K.

5.4 Results

I developed a simplified chloride steady-state chemical model to study the possibility of HCl accumulation in the atmosphere. Through our calculations, we find that HCl is unable to accumulate to detectable levels on an exoplanet with an H₂-dominated atmosphere orbiting an M5V dwarf star similar to GJ 876. Specifically, we find that even if life on such a planet produces CH₃Cl at a flux of 3.5×10^{13} molecules cm⁻² s⁻¹, the same as Earth's gross oxygen production flux, there is still less than 10 ppb of HCl in the atmosphere, far from being detectable by JWST. In the following paragraphs, I will explain in detail how I came to this conclusion. I will also explain the approximations I made throughout my calculations and how these approximations affect my calculations and overall conclusion.

First, let's quickly review the basic idea behind our model. On our hypothetical planet, we assume that life does not directly produce HCl gas but instead produces CH₃Cl. We think that the biological production of CH₃Cl might be due to: signaling, stress, or other

biological/physiological reasons (e.g., see Segura et al., 2005; Hu et al., 2012). So far, we have not found any known references claiming that bioproduction of CH_3Cl is tied to energy extraction or biomass buildup. In a high-reducing H_2 -dominated atmosphere, CH_3Cl is photochemically converted to HCl through this reaction: $\text{CH}_3\text{Cl} + \text{H} \rightarrow \text{CH}_3 + \text{HCl}$. Following the method we outlined in Chapter 2.2, we first need to run a baseline scenario and extract the number density of oxygen radicals ($[\text{O}]$), hydrogen radicals ($[\text{H}]$), hydroxyl radicals ($[\text{OH}]$), and water vapor ($[\text{H}_2\text{O}]$) from it. As a reminder, in our baseline scenario, we simulate an exoplanet with an H_2 -dominated atmosphere (just like what we did in Chapter 4). Except, in this case, we turn the production of CH_3OH off. The figure below shows the mixing ratio profiles of the major chemical species in the atmosphere (the left panel) and the number density of O, H, OH, and H_2O as a function of altitude (the right panel) (Figure 5-3).

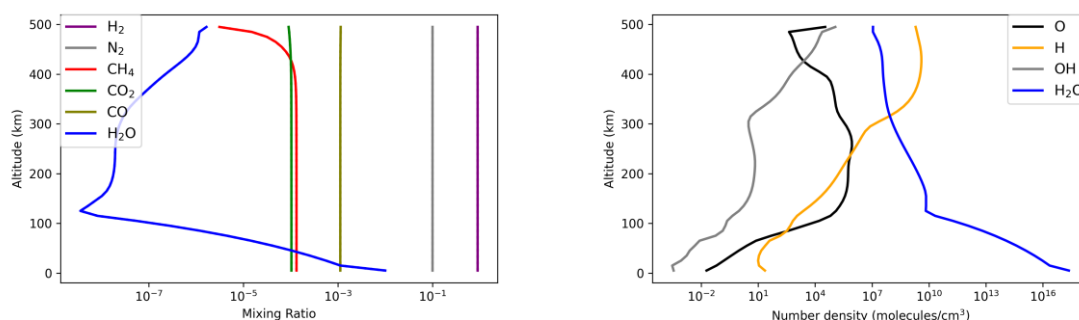


Figure 5-3. Left panel: The volume mixing ratio of several major chemical species on an exoplanet with an H_2 -dominated atmosphere orbiting an M5V dwarf star similar to GJ 876. The x-axis shows the mixing ratio, and the y-axis shows altitude in km. **Right panel:** The number density of O, H, OH, and H_2O as a function of altitude in the atmosphere. The x-axis shows the number density in molecules cm^{-3} , and the y-axis shows altitude in km. Each color denotes one particular chemical species.

To calculate the rainout rate of HCl ($k_R(z)$), we need to get the temperature-dependent Henry's law equation for HCl ($H'(T)$), the number density of water ($[\text{H}_2\text{O}]$), and atmospheric temperature as a function of altitude ($T(z)$). We can get $[\text{H}_2\text{O}]$ and $T(z)$ from our baseline scenario. I found in the NIST database the temperature-dependent Henry's law equation for HCl : $H(T) = (2.0 \times 10^6) \cdot \text{Exp}[(9.0 \times 10^3) \cdot ((1/T) - (1/298.15))]$. Here, I want to point out that, although NIST says that this expression already takes into account the dissociation of HCl in solution, it does not explicitly state that it is HCl 's effective Henry's law equation. Therefore, by using this solubility expression, we may slightly underestimate the wet deposition flux of HCl . The figure below shows the temperature as a function of altitude (the left panel) and my calculated rainout rate for HCl (the right panel) (Figure 5-4).

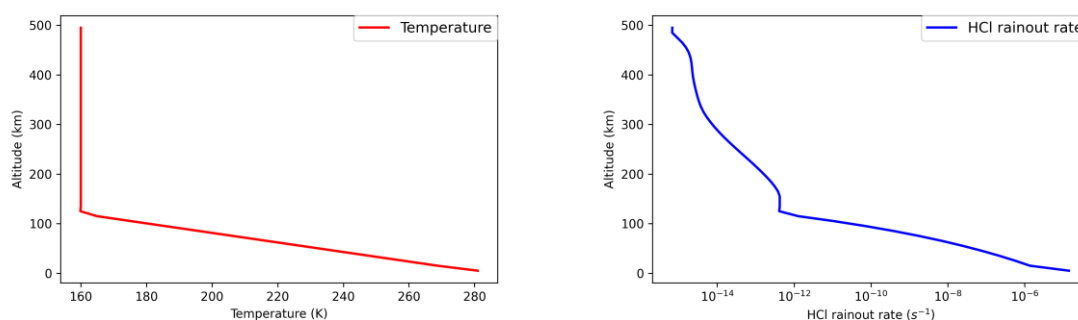


Figure 5-4. **Left panel:** The atmospheric temperature as a function of altitude. The x-axis shows the temperature in Kelvin, and the y-axis shows altitude in km. **Right panel:** my calculated rainout rate for HCl as a function of altitude. The x-axis shows the HCl rainout rate in s^{-1} , and the y-axis shows altitude in km.

The shape of the rainout rate of HCl is very similar to that of $[H_2O]$. The reason is that the rainout rate is a function of water density in the atmosphere (Equation 2-3): the higher the concentration of water vapor (i.e., the more humid), the bigger the rainout rate. Since most of the water vapor is concentrated at low altitudes, the rainout rate of HCl decreases with increasing altitude. As we mentioned in Chapter 2, to get the HCl rainout flux (in molecules $cm^{-2} s^{-1}$), we need to multiply $K_R(z)$ by the number density of HCl ($[HCl]$, in molecules cm^{-3}) and the width of each atmospheric bin ($width_{bin}$, in cm). Our simulated atmosphere has a total of 50 layers, and each layer's width (i.e., height) is the same, which is 1000000 cm (or 10 km). Compared to the wet deposition flux, the dry deposition flux of HCl is much easier to estimate. It has been reported that HCl's dry deposition velocity to the land is between 1 cm/s and 2 cm/s (Ramsay et al., 2018). Here, we take their average value of 1.5 cm/s as the dry deposition velocity value for HCl in our model. HCl can react with O, H, and OH radicals in the atmosphere, and we summarize their reactions in the table below (Table 5-1).

Table 5-1. Photochemical reactions between HCl and O, H and OH in the atmosphere. The reaction rate constant has a unit of $cm^3 molecule^{-1} s^{-1}$.

	Reactants	Products	Reaction rate constant (k)	Source	Valid temperature range [K]
F1	H + HCl	H ₂ + Cl	$2.41 \times 10^{-12} (T/298)^{1.44} \text{Exp}(-1240/T)$	NIST	200 - 1200
F2	OH + HCl	H ₂ O + Cl	$1.8 \times 10^{-12} \text{exp}(-250/T)$	JPL 19-5	138 - 1060
F3	O + HCl	OH + Cl	$1.0 \times 10^{-11} \text{exp}(-3300/T)$	JPL 19-5	293 - 3197

Once we have the reaction rate constant and the valid temperature range for each reaction, we can simplify our model. First, we can safely omit the reaction between HCl and O (i.e., Forward reaction 3, or 'Reaction F3'). The reaction between HCl and O can only occur above 293 K. However, the temperature of our simulated atmosphere is below 280 K. Therefore, this reaction is unlikely to occur in our simulated atmosphere. Even if it did happen, the reaction would be negligibly slow. To further simplify our calculations, we can also ignore the reactions between HCl and H and between HCl and OH. The rationale behind this is that while these two reactions (Reaction F1 and F2) are taking place, their

reverse reactions (Reaction R1 and R2) are also taking place simultaneously and at a similar rate (Table 5-2).

Table 5-2. Photochemical reverse reactions of reforming HCl in the atmosphere. The reaction rate constant has a unit of $\text{cm}^3 \text{ molecule}^{-1} \text{ s}^{-1}$.

	Reactants	Products	Reaction rate constant (k)	Source	Valid Temperature Range [K]
R1	$\text{H}_2 + \text{Cl}$	$\text{H} + \text{HCl}$	$3.9 \times 10^{-11} \exp(-2309.9/T)$	NIST	200 - 310
R2	$\text{H}_2\text{O} + \text{Cl}$	$\text{OH} + \text{HCl}$	$2.63 \times 10^{-12} (T/298)^{1.67} \exp(-7679.4/T)$	NIST	200 - 3000

Therefore, by omitting these two HCl photochemical reactions (Reaction F1 and F2), we might underestimate the photochemical removal flux of HCl, thereby making it easier for HCl to accumulate on our simulated exoplanet with an H_2 -dominated atmosphere. Next, we need to estimate the photolysis flux of HCl. In a UV environment, HCl undergoes photolysis and generates H radicals and Cl radicals ($\text{HCl} \rightarrow \text{H} + \text{Cl}$). The wavelengths of photons that HCl can absorb are between 135 nm and 230 nm (JPL 19-5). The quantum yield is taken to be 1. As we discussed in Chapter 2, we can calculate the photolysis rate of HCl as a function of altitude ($J(z)$) using Equation 2-4. The figure below shows the absorption cross sections of HCl and CH_3Cl at 298 K (the left panel) and my calculated photolysis rate for HCl (the right panel) (Figure 5-5).

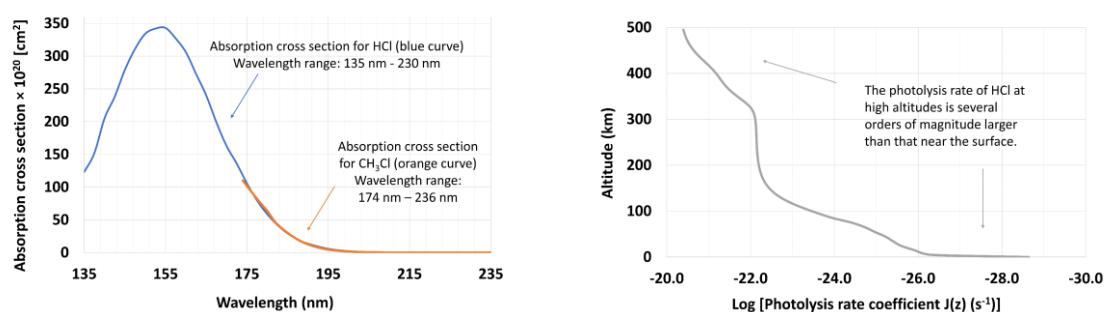


Figure 5-5. **Left panel:** The absorption cross sections of HCl and CH_3Cl at 298 K. The x-axis shows wavelength in nm, and the y-axis shows the absorption cross-sections in $\times 10^{20} \text{ cm}^2$. **Right panel:** my calculated photolysis rate coefficient for HCl ($J(z)$). The y-axis shows altitude in km, and the x-axis shows the photolysis rate coefficient (s^{-1}) on a log scale.

To get the photolysis flux of HCl (in molecules $\text{cm}^{-2} \text{ s}^{-1}$), we need to multiply $J(z)$ by the number density of HCl ($[\text{HCl}]$, in molecules cm^{-3}) and the width of each atmospheric bin ($\text{width}_{\text{bin}}$, in cm). The photolysis rate of HCl ($J(z)$) is several orders of magnitude smaller than the rainout rate of HCl ($K_R(z)$) (Figure 5-4), suggesting that in the atmosphere, the primary removal mechanism for HCl is wet deposition. Such a conclusion is expected, given HCl's extremely high water solubility. Another observation is that the photolysis rate increases with altitude. UV radiation is progressively attenuated as it penetrates the atmosphere. Therefore, the amount of UV at the top of the atmosphere is much greater than that near the surface. Here, we would like to point out that our method for estimating the

HCl photolysis flux is sensitive to $\text{width}_{\text{bin}}$. The wider the bin, the less the number of atmospheric layers, and the more UV penetrates the atmosphere, resulting in a larger photolysis flux.

Finally, we need to estimate the production flux of HCl from CH_3Cl . The reaction ($\text{CH}_3\text{Cl} + \text{H} \rightarrow \text{CH}_3 + \text{HCl}$) has a reaction rate of $9.3 \times 10^{-16} \text{ cm}^3 \text{ molecule}^{-1} \text{ s}^{-1}$. This reaction rate was measured experimentally at 298 K (Triebert et al., 1995). Unfortunately, there is no information on how the reaction rate varies with temperature. Therefore, following how we handle similar chemicals in our photochemistry code, we assume that the reaction rate is constant within our temperature range. This assumption would cause us to overestimate the conversion rate from CH_3Cl to HCl, making it easier for HCl to accumulate in our simulated atmosphere.

To calculate the production flux of HCl (in molecules $\text{cm}^{-2} \text{ s}^{-1}$), we need to multiply the reaction rate constant (k) by the number density of H (in molecules cm^{-3}), the number density of CH_3Cl , and the width of each atmospheric bin (in cm): Production flux = $k \cdot [\text{H}] \cdot [\text{CH}_3\text{Cl}] \cdot \text{width}_{\text{bin}}$. To estimate the number density of CH_3Cl , we need to repeat all the above calculations for CH_3Cl . As we mentioned in Chapter 2, the production flux of CH_3Cl is the input to our model. For CH_3Cl , we only consider three of its dominant removal pathways: wet deposition, dry deposition, and direct photolysis. To estimate the wet deposition flux of CH_3Cl , we have to get the temperature-dependent Henry's law constant for CH_3Cl , which I found in NIST: $H(T) = (1.3 \times 10^{-1}) \cdot \text{Exp}[(3.30 \times 10^3) \cdot ((1/T) - (1/298.15))]$. We want to point out that this is the physical Henry's law constant for CH_3Cl . However, since CH_3Cl does not dissociate in water, we think CH_3Cl 's physical Henry's law constant should be an acceptable approximation. We have already shown the absorption cross sections of CH_3Cl in Figure 5-5. An interesting point worth noting is that the absorption cross-section curve of CH_3Cl looks the same as that of HCl from 174 nm onwards. As a result, CH_3Cl 's photolysis flux is smaller than HCl's due to CH_3Cl 's narrower photolysis window.

To estimate the dry deposition flux of CH_3Cl , we need to estimate its dry deposition velocity (in cm/s). So far, we have not found any known literature claiming that CH_3Cl has a non-zero dry deposition velocity. Therefore, we have to assume CH_3Cl 's dry deposition velocity is 0 in our simplified model. Even if CH_3Cl could slowly deposit onto the ground, the flux would be too small to affect our results. At this point, we have obtained all the parameters we need to calculate the concentration of HCl using Equation 2-6. We assume that life on such a planet produces CH_3Cl at a flux of $3.5 \times 10^{13} \text{ molecules cm}^{-2} \text{ s}^{-1}$, the same as Earth's gross oxygen production flux. In this case, we calculate the number density of HCl to be about $7 \times 10^{11} \text{ molecules cm}^{-3}$ (or a volume mixing ratio of roughly 5 ppb), which will not be detectable with JWST given any reasonable (or realistic) number of transits. We conclude that HCl is not a suitable bioindicator because it cannot accumulate in the atmosphere. This result is expected. The extremely high water solubility of HCl means that wet deposition can efficiently remove it from the atmosphere, preventing HCl from accumulating to detectable levels. Another minor reason is that the conversion from CH_3Cl to HCl is not very efficient. We consider our conclusion to be robust. In our model, we underestimate the removal flux of CH_3Cl (in other words, overestimate the production flux of HCl) and slightly underestimate the overall removal flux of HCl. As a result, the case we

study here represents the most favorable scenario for HCl accumulation, yet HCl fails to accumulate to detectable levels even in this optimum scenario. In reality, we believe HCl will be even less likely to accumulate to detectable levels in the atmosphere.

5.5 Discussion

We first review the solubility of chlorine-containing gas molecules in Chapter 5.5.1. We then discuss the acidity of chlorine-containing acids in Chapter 5.5.2. Finally, we explore naturally occurring chloride minerals and their properties in Chapter 5.5.3.

5.5.1 Solubility of Chlorine-containing Gas Molecules

Among the nine chlorine-containing gas molecules we study in this section, HCl has the highest water solubility. HCl is highly soluble in water, even more so than NH_3 , one of the most soluble biosignature gas candidates studied (Huang et al., 2022). Chlorine dioxide (ClO_2), the most stable oxide of chlorine, is also very soluble in water, especially in cold water ($< 5^\circ\text{C}$) (Vogt et al., 2010). As members of chloroalkanes, molecules such as methyl chloride (CH_3Cl) and chloroform (CHCl_3) are only slightly soluble in water. This is because chloroalkanes cannot form hydrogen bonds with water. Although chlorine (Cl_2) is a nonpolar molecule, it is still sparingly soluble due to Cl_2 's ability to react with water (i.e., disproportionation). Carbon tetrachloride (CCl_4) is insoluble in water because it is neither a polar molecule nor reacts with water.

We can compare the solubility of different gases in water by using Henry's law constants: $H^{\text{CP}}_{(x)} = C_{(x)}/p$. Here $H^{\text{CP}}_{(x)}$ is Henry's law constant for a species X in $\text{mol m}^{-3} \text{ Pa}^{-1}$. $C_{(x)}$ is the dissolved concentration in mol m^{-3} , and p is the partial pressure of that species at equilibrium. The SI unit for p is Pascal. The larger Henry's law constant, the more soluble the gas is. Here we compare the solubility of 9 representative chlorine-containing gas molecules to 19 other molecules' at 298 K and 1 atm. (Figure 5-6). This list includes common atmospheric gases (e.g., oxygen (O_2)), four fluorine/bromine-bearing species (e.g., methyl fluoride (CH_3F)), and potential biosignature gases (e.g., isoprene (C_5H_8)) (R. Sander, 2015).

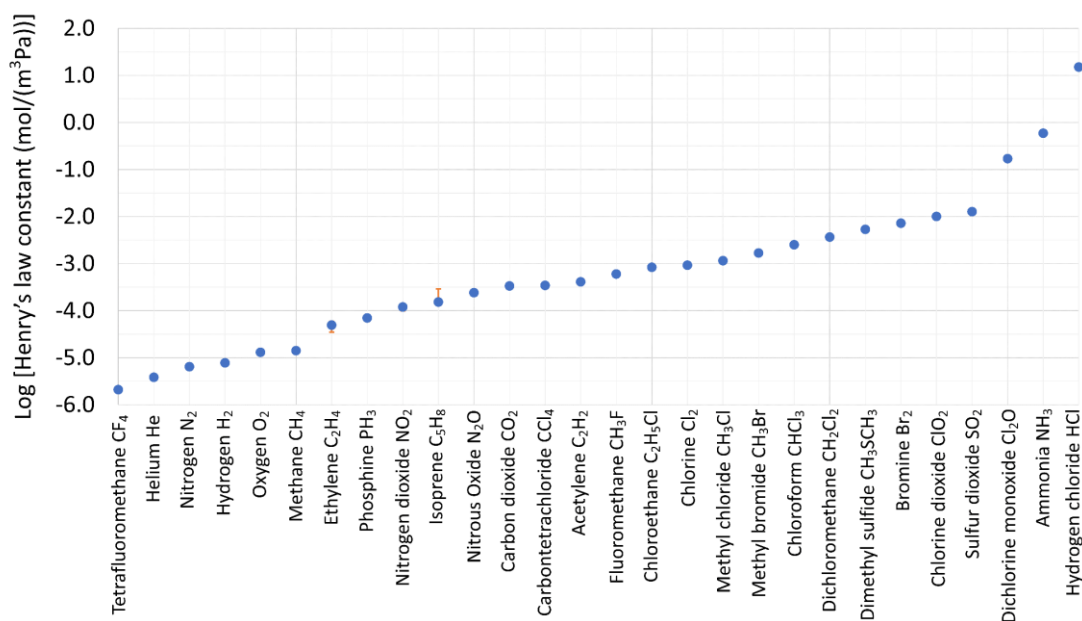


Figure 5-6. The water solubility of various species. The x-axis shows the names of the chemical species, and the y-axis shows Henry's law constant on a log scale. HCl is highly soluble in water, even more so than NH₃, one of the most soluble biosignature gas candidates studied (Huang et al., 2022). Both Cl₂O and ClO₂ are also very soluble in water. Chloroalkanes, in general, are only slightly soluble in water because they cannot form hydrogen bonds with water. Despite being a nonpolar molecule, Cl₂ is still sparingly soluble because it disproportionates in water. CCl₄ is insoluble because it is neither a polar molecule nor reacts with water.

The high water solubility of HCl means that wet deposition (rainfall) can efficiently remove it from the atmosphere. Therefore, without robust biological chlorine production, abiotically produced HCl cannot accumulate to detectable levels in the atmosphere on its own.

5.5.2 Acidity of Chlorine-containing Acids

There are five common chlorine-containing acids: hydrochloric acid (HCl), hypochlorous acid (HClO), chlorous acid (HClO₂), chloric acid (HClO₃), and perchloric acid (HClO₄). Among these five acids: HClO and HClO₂ are weak acids, while HCl, HClO₃, and HClO₄ are strong acids. Strong acids ionize completely (i.e., give off H⁺) in water, while weak acids only ionize partially. We use pK_a (the negative log of the acid dissociation constant) to measure the acidity of an acid. The stronger the acid, the more negative the pK_a is. Here we compare the acidity of HCl, HClO, HClO₂, HClO₃, and HClO₄ to that of 12 other common acids at 25°C (Figure 5-7). For polyprotic acids, we use pK_a to refer to the first deprotonation (i.e., pK_{a1}).

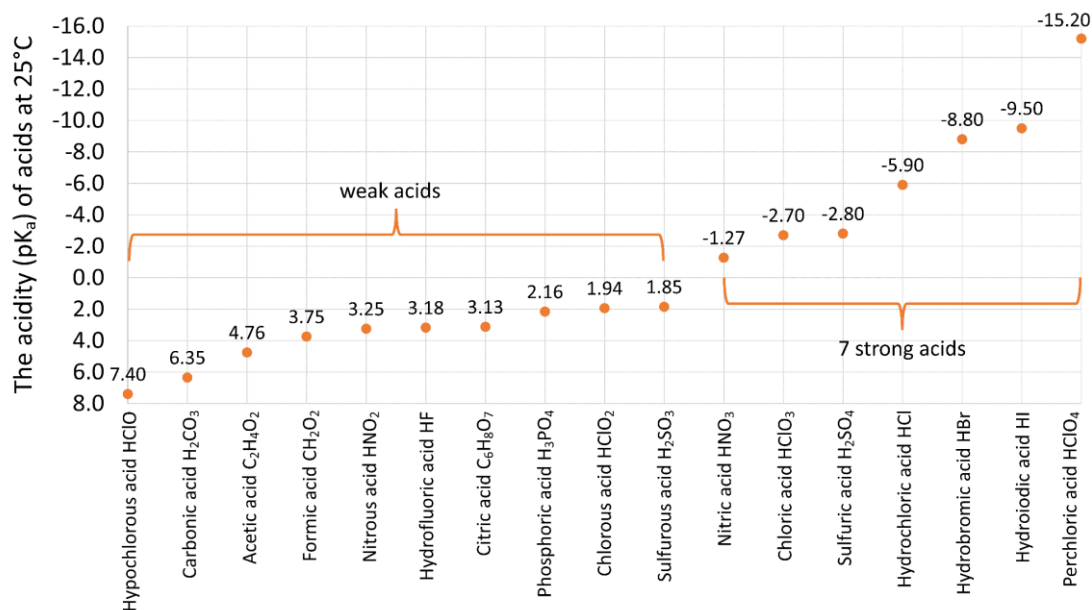


Figure 5-7. The acidity of various acids. The x-axis shows the chemical species' names, and the y-axis shows acids' acidity (pK_a) at 25°C. HCl, HClO₃, and HClO₄ are strong acids, while HClO and HClO₂ are weak acids. Reference: For HCl, HBr, HI, and HClO₄: (Trummal et al., 2016); For HF, HNO₃, and HClO₃: (Perrin et al., 1967); For H₂SO₄: (Kotrlý et al., 1985); For all other acids: (David R. Lide et al., 2005).

Among HCl, HClO, HClO₂, HClO₃, and HClO₄, only HCl and HClO can be directly generated by dissolving chlorine-containing gas molecules in water. HCl gas dissolves in water to form HCl acid. Cl₂ gas can react with H₂O to yield HCl and HClO (Cl₂ + H₂O ⇌ HCl + HClO). In addition, the dissolving of Cl₂O in water also produces HClO (Cl₂O + H₂O ⇌ 2HClO). HClO₂, HClO₃, and HClO₄ can be generated indirectly through chemical reactions (e.g., Hong et al., 1968; Ni et al., 1998; Horváth et al., 2003; Holleman 2019). It is worth emphasizing that not all chlorine-containing gases dissolve in water to form acids. Chlorine dioxide (ClO₂) does not hydrolyze in water, despite its high water solubility (Chapter 5.5.1). Similarly, chloroalkanes do not react with water and remain as dissolved gases in solution.

5.5.3 Naturally Occurring Chloride Minerals

As we mentioned in Chapter 5.2.1, the crust is the second-largest chlorine reservoir on Earth (Graedel et al., 1996; Sharp et al., 2013; Svensson et al., 2021). In the crust, chlorine can form rich and diverse minerals with various elements such as calcium (Ca), sodium (Na), potassium (K), and magnesium (Mg). One of the best-known naturally occurring chloride minerals is halite (also known as 'rock salt'), a colorless or white crystal. Halite is nothing but the mineral form of sodium chloride (NaCl). The number of chloride minerals currently recognized by the International Mineralogical Association (IMA) is around 400 (Siivola et al., 2007; Warr 2021; Pasero et al., 2022). We list some simple chloride minerals and their respective physical properties in Table 5-3. We collected the data from the

Handbook of Mineralogy (Anthony et al., 1997).

Table 5-3. Some simple naturally occurring chloride minerals (Anthony et al., 1997).

Name of the mineral	Chemical formula	Color	Density [g cm ⁻³]	Note
Halite	NaCl	Colourless/White	2.17	Water-soluble
Sylvite	KCl	Grey/White	1.99	Water-soluble
Molysite	FeCl ₃	Brown-red	2.90	Highly deliquescent
Tolbachite	CuCl ₂	Golden-brown	3.42	Soluble/Hygroscopic
Scacchite	MnCl ₂	Brown-red	2.98	Soluble/Deliquescent
Cotunnite	PbCl ₂	Pale yellow/green	5.80	Slightly soluble
Rorisite	CaFCl	Colorless	2.78	Soluble/Hygroscopic
Sinjarite	CaCl ₂ ·2H ₂ O	Pale pink	1.66	Highly hygroscopic
Antarcticite	CaCl ₂ ·6H ₂ O	Colourless/White	1.72	Highly hygroscopic
Eriochalcite	CuCl ₂ ·2H ₂ O	Greenish blue	2.47	Water-soluble
Bischofite	MgCl ₂ ·6H ₂ O	Colourless/White	1.60	Soluble/Deliquescent
Chloraluminite	AlCl ₃ ·6H ₂ O	Colourless/White	1.64	Soluble/ Deliquescent

Chloride minerals come in many colors (depending on which element chloride binds to) and have a wide range of densities. What most chloride minerals have in common is their relatively high water solubility. Some chloride minerals, such as antarcticite (CaCl₂·6H₂O), are hygroscopic and can absorb moisture from the air. Other chloride minerals, such as molysite (FeCl₃), are deliquescent. Deliquescent minerals can keep absorbing moisture until they dissolve themselves in the absorbed water and form a solution. Due to their relatively high water solubility, most chloride minerals are found in arid or volcanically active regions. Specifically, chloride minerals like halite (NaCl), sylvite (KCl), bischofite (MgCl₂·6H₂O), and antarcticite (CaCl₂·6H₂O) are precipitates from saline brines or groundwater (Anthony et al., 1997). On the other hand, chloride minerals represented by molysite (FeCl₃), scacchite (MnCl₂), cotunnite (PbCl₂), and chloraluminite (AlCl₃·6H₂O) are the products of volcanic or fumarolic activities (Anthony et al., 1997).

5.6 Summary

In this chapter, we carefully examine the bioindicator potential of HCl. I use a variety of approaches, ranging from Henry's law equation to my simplified chloride steady-state chemical model.

In the atmosphere, some biosignature gases do not survive photochemical destruction. We can only infer the presence of these biosignature gases by detecting their photochemical products, which we call bioindicators. HCl has many advantages of being a potential bioindicator in an H₂-dominated atmosphere. First, many gases are converted to their most hydrogenated form in highly reducing atmospheres. Since the most reduced form of Cl element is HCl, methyl chloride (CH₃Cl) gas should end up as HCl. Second, there are very few abiotic sources of HCl, with the only exception being volcanic activity.

However, despite HCl's advantages, we believe that HCl is not a suitable bioindicator because it cannot accumulate to detectable levels on an exoplanet with an H₂-dominated atmosphere orbiting an M5V dwarf star similar to GJ 876. Through my model, we find that even if life on such a planet produces CH₃Cl at a flux of 3.5×10^{13} molecules cm⁻² s⁻¹, the same as Earth's gross oxygen production flux, there is still less than 10 ppb of HCl in the atmosphere, far from being detectable by JWST. The extremely high water solubility of HCl means that wet deposition can efficiently remove it from the atmosphere, preventing HCl from accumulating to detectable levels in the atmosphere.

In this paper, I also provide a comprehensive literature review on the abundance, distribution, and circulation of chlorine on Earth. In the future, we would like to upgrade our existing photochemistry code by adding a comprehensive Cl-reaction network. We plan to run our photochemistry code and quantitatively confirm my simplified chloride chemical model results.

We are very thankful to the Heising-Simons Foundation (grant number #2018-1104) and NASA (grant numbers 80NSSC19K0471 and NNX15AC86G) for their support of our project.

Appendix K. Chlorine Chemical Reaction Network for the Photochemistry Model

Table 5-4. New chlorine species to be added to the photochemical model.

	Chemical formula	Name	Type	Standard Number	Molecular Mass [amu]
1	HCl	Hydrogen chloride	X	112	36
2	Cl ₂	Chlorine gas	X	113	71
3	CH ₃ Cl	Methyl chloride (Chloromethane)	X	114	50
4	CH ₂ Cl ₂	Dichloromethane	X	115	85
5	CHCl ₃	Chloroform (Trichloromethane)	X	116	119
6	CCl ₄	Tetrachloromethane	X	117	154
7	HOCl	Hypochlorous acid	X	118	52
8	Cl	Chlorine radical	X	119	35
9	CH ₂ Cl	Chloromethyl radical	X	120	49
10	CHCl ₂	Dichloromethyl radical	X	121	84
11	ClO	Chlorine monoxide radical	X	122	51
12	CCl ₃	Trichloromethyl radical	X	123	118

Table 5-5. HCl reactions to be added to the photochemical model.

	Reactants	Products	Rate expression	Source	Temp range [K]
1		O(3P) + HCl	1.8×10^{-11}	JPL 19-5	199 – 379
2	O(1D) + HCl	H + ClO	3.3×10^{-11}	JPL 19-5	199 – 379
3		Cl + OH	9.9×10^{-11}	JPL 19-5	199 – 379

4	O + HCl	OH + Cl	$1.0 \times 10^{-11} \exp(-3300/T)$	JPL 19-5	293 – 3197
5	OH + HCl	H ₂ O + Cl	$1.8 \times 10^{-12} \exp(-250/T)$	JPL 19-5	138 – 1060
6	C ₂ H ₃ + HCl	C ₂ H ₄ + ·Cl	$8.7 \times 10^{-13} \exp(-99.8/T)$	NIST	203 - 343
7	HCl + ·CH ₂	·CH ₃ + ·Cl	$2.82 \times 10^{-12} \exp(-436.6/T)$	NIST	296 - 670
8	HCl + ·Cl	Cl ₂ + H·	$1.66 \times 10^{-7} \exp(-23934.2/T)$	NIST	250 - 730
9	HCl + H·	H ₂ + ·Cl	$2.41 \times 10^{-12} (T/298)^{1.44} \exp(-1240/T)$	NIST	200 - 1200
10	·CH ₂ Cl + HCl	CH ₃ Cl + ·Cl	$2.39 \times 10^{-13} (T/298)^{1.57} \exp(-2100/T)$	NIST	200 - 3000
11	HS + ·Cl	HCl + S	1.1×10^{-10}	NIST	296
12	HNO ₃ + ·Cl	HCl + NO ₃	2.0×10^{-16}	NIST	298
13	·OH + ClO	HCl + O ₂	1.2×10^{-12}	NIST	298
14	HO ₂ + ClO	HCl + O ₃	2.01×10^{-14}	NIST	298
15	·C ₂ H ₅ + ·Cl	C ₂ H ₄ + HCl	3.01×10^{-10}	NIST	298
16	H ₂ + ClO	·OH + HCl	4.98×10^{-16}	NIST	294
17	CH ₃ Cl + H·	·CH ₃ + HCl	9.3×10^{-16}	NIST	298
18	Cl ₂ O + H·	HCl + ClO	4.1×10^{-11}	NIST	300
19	HO ₂ + Cl	HCl + O ₂	$1.4 \times 10^{-11} \exp(270/T)$	JPL 19-5	226 – 420
20		OH + ClO	$3.6 \times 10^{-11} \exp(-375/T)$	JPL 19-5	226 – 420
21	Cl + H ₂	HCl + H	$3.05 \times 10^{-11} \exp(-2270/T)$	JPL 19-5	199 – 3000
22		HCl + HO ₂	$1.1 \times 10^{-11} \exp(-980/T)$	JPL 19-5	265 – 424
23	Cl + H ₂ O ₂	HCl + CH ₃	$7.1 \times 10^{-12} \exp(-1270/T)$	JPL 19-5	181 – 1550
24	Cl + C ₂ H ₆	HCl + C ₂ H ₅	$7.2 \times 10^{-11} \exp(-70/T)$	JPL 19-5	48 – 1400
25	Cl + CH ₃ Cl	HCl + CH ₂ Cl	$2.03 \times 10^{-11} \exp(-1110/T)$	JPL 19-5	233 – 843
26	Cl + CH ₂ Cl ₂	HCl + CHCl ₂	$7.4 \times 10^{-12} \exp(-910/T)$	JPL 19-5	273 – 790
27	Cl + CHCl ₃	HCl + CCl ₃	$3.3 \times 10^{-12} \exp(-990/T)$	JPL 19-5	220 – 1010
28	Cl + H ₂ S	HCl + SH	$3.4 \times 10^{-11} \exp(225/T)$	JPL 19-5	202 – 914
29	CHCl ₃ + ·Cl	·CCl ₃ + HCl	$4.9 \times 10^{-12} \exp(-1240/T)$	NIST	240 - 330
30	CCl ₄ + H·	·CCl ₃ + HCl	$1.36 \times 10^{-10} \exp(-2937/T)$	NIST	297 - 904
31	CH ₂ O + ·Cl	HCO + HCl	$8.2 \times 10^{-11} \exp(-34/T)$	NIST	200 - 500
32	H ₂ S + ·Cl	HCl + SH	$3.7 \times 10^{-11} \exp(208.1/T)$	NIST	200 - 430
33	H ₂ O ₂ + ·Cl	HO ₂ + HCl	$1.1 \times 10^{-11} \exp(-980.2/T)$	NIST	260 - 430
34	HO ₂ + ·Cl	HCl + O ₂	$1.8 \times 10^{-11} \exp(169.6/T)$	NIST	250 - 420
35	·CH ₃ + ·Cl	HCl + ·CH ₂	$3.65 \times 10^{-11} \exp(-4150/T)$	NIST	296 - 670
36	H ₂ + ·Cl	HCl + H·	$3.9 \times 10^{-11} \exp(-2309.9/T)$	NIST	200 - 310
37	CH ₂ Cl ₂ + ·Cl	CHCl ₂ + HCl	$2.8 \times 10^{-11} \exp(-1300/T)$	NIST	270 - 370
38	CH ₃ Cl + ·Cl	·CH ₂ Cl + HCl	$3.3 \times 10^{-11} \exp(-1250/T)$	NIST	233 - 322
39	Cl ₂ + H·	HCl + ·Cl	$1.43 \times 10^{-10} \exp(-590.5/T)$	NIST	250 - 730
40	·NH ₂ + ClO	HCl + HNO	$1.0 \times 10^{-10} (T/298)^{-1.08} \exp(-128.7/T)$	NIST	200 - 2500
41	H ₂ O + ·Cl	·OH + HCl	$2.63 \times 10^{-12} (T/298)^{1.67} \exp(-7679.4/T)$	NIST	200 - 3000
42	NH ₃ + ·Cl	HCl + ·NH ₂	$9.11 \times 10^{-19} (T/298)^{2.47} \exp(-726.4/T)$	NIST	200 - 2000
43	HOCl + ·Cl	HCl + ClO	$6.92 \times 10^{-15} (T/298)^{4.07} \exp(169.6/T)$	NIST	220 - 2000

44	$\cdot\text{OH} + \text{Cl}_2$		$6.76 \times 10^{-13} (\text{T}/298)^{1.39} \exp(176.8/\text{T})$	NIST	200 - 3000
45	$\text{C}_2\text{H}_6 + \cdot\text{Cl}$	$\cdot\text{C}_2\text{H}_5 + \text{HCl}$	$3.9 \times 10^{-11} (\text{T}/298)^{0.70} \exp(117/\text{T})$	NIST	203 - 1400
46	$\text{CH}_4 + \cdot\text{Cl}$	$\cdot\text{CH}_3 + \text{HCl}$	$8.24 \times 10^{-13} (\text{T}/298)^{2.49} \exp(-609.1/\text{T})$	NIST	200 - 1104

Table 5-6. CH_3Cl reactions to be added to the photochemical model.

	Reactants	Products	Rate expression	Source	Temp range [K]
47	$\text{O}(1\text{D}) + \text{CH}_3\text{Cl}$	$\cdot\text{OH} + \cdot\text{CH}_2\text{Cl}$	3.4×10^{-10}	NIST	300
48	$\text{CH}_3\text{Cl} + \cdot\text{OH}$	$\cdot\text{CH}_2\text{Cl} + \text{H}_2\text{O}$	$3.8 \times 10^{-12} \exp(-1340/\text{T})$	NIST	240 - 300
49	$\text{CH}_3\text{Cl} + \cdot\text{Cl}$	$\cdot\text{CH}_3 + \text{Cl}_2$	$2.06 \times 10^{-11} (\text{T}/298)^{1.63} \exp(-12780/\text{T})$	NIST	200 - 3000
50	$\cdot\text{CH}_3 + \cdot\text{Cl}$	CH_3Cl	6.0×10^{-11}	NIST	202 - 298
51	$\cdot\text{CH}_3 + \text{Cl}_2$	$\text{CH}_3\text{Cl} + \cdot\text{Cl}$	$1.67 \times 10^{-13} (\text{T}/298)^{2.52} \exp(663.9/\text{T})$	NIST	188 - 500

Table 5-7. Cl_2 reactions to be added to the photochemical model.

	Reactants	Products	Rate expression	Source	Temp range [K]
52	$\text{O}(1\text{D}) + \text{Cl}_2$	$\text{ClO} + \cdot\text{Cl}$	1.99×10^{-10}	NIST	298
53	$\text{Cl}_2 + \text{O}\cdot$	$\text{ClO} + \cdot\text{Cl}$	$4.17 \times 10^{-12} \exp(-1370/\text{T})$	NIST	174 - 602
54	$\cdot\text{OH} + \text{Cl}_2$	$\text{HOCl} + \cdot\text{Cl}$	$3.6 \times 10^{-12} \exp(-1200/\text{T})$	NIST	230 - 360
55	$\cdot\text{CH}_2\text{Cl} + \text{Cl}_2$	$\text{CH}_2\text{Cl}_2 + \cdot\text{Cl}$	$2.93 \times 10^{-13} (\text{T}/298)^{1.45} \exp(-42.1/\text{T})$	NIST	295 - 873
56	$\text{CHCl}_2 + \text{Cl}_2$	$\text{CHCl}_3 + \cdot\text{Cl}$	$6.74 \times 10^{-14} (\text{T}/298)^{1.60} \exp(-370/\text{T})$	NIST	200 - 3000
57	$\cdot\text{CCl}_3 + \text{Cl}_2$	$\text{CCl}_4 + \cdot\text{Cl}$	$1.42 \times 10^{-13} (\text{T}/298)^{1.52} \exp(-550/\text{T})$	NIST	200 - 3000
58	$\text{Cl}_2\text{O} + \text{ClO}$	$\text{O}_2 + \text{Cl}_2 + \cdot\text{Cl}$	1.08×10^{-15}	NIST	298
59	$\cdot\text{Cl} + \cdot\text{Cl}$	Cl_2	$6.15 \times 10^{-34} \exp(906/\text{T})$	NIST	195 - 520
60	$\text{ClO} + \cdot\text{Cl}$	$\text{Cl}_2 + \text{O}\cdot$	$1.74 \times 10^{-12} \exp(-4589.9/\text{T})$	NIST	174 - 602
61	$\text{ClO} + \text{ClO}$	$\text{O}_2 + \text{Cl}_2$	$1.0 \times 10^{-12} \exp(-1590/\text{T})$	NIST	260 - 390
62	$\text{Cl}_2\text{O} + \cdot\text{Cl}$	$\text{Cl}_2 + \text{ClO}$	$6.2 \times 10^{-11} \exp(130/\text{T})$	NIST	230 - 380
63	$\text{CH}_2\text{Cl}_2 + \cdot\text{Cl}$	$\cdot\text{CH}_2\text{Cl} + \text{Cl}_2$	$2.34 \times 10^{-11} (\text{T}/298)^{1.23} \exp(-10960/\text{T})$	NIST	200 - 3000
64	$\text{CHCl}_3 + \cdot\text{Cl}$	$\text{CHCl}_2 + \text{Cl}_2$	$5.25 \times 10^{-11} (\text{T}/298)^{0.97} \exp(-9200/\text{T})$	NIST	200 - 3000

Table 5-8. CH_2Cl_2 reactions to be added to the photochemical model.

	Reactants	Products	Rate expression	Source	Temp range [K]
65	$\text{OH} + \text{CH}_2\text{Cl}_2$	$\text{CHCl}_2 + \text{H}_2\text{O}$	$1.92 \times 10^{-12} \exp(-880/\text{T})$	JPL 19-5	219 - 955

Table 5-9. CHCl_3 reactions to be added to the photochemical model.

	Reactants	Products	Rate expression	Source	Temp range [K]
66	CHCl ₃ + ·OH	·CCl ₃ + H ₂ O	9.3x10 ⁻¹³ exp(-660.1/T)	NIST	240 - 300
67	CHCl ₃ + H·	·CCl ₃ + H ₂ O	8.05x10 ⁻¹³ (T/298) ^{2.85} exp(-913/T)	NIST	200 - 5000
68	·CCl ₃ + H ₂ S	CHCl ₃ + SH	1.18x10 ⁻³⁸ (T/298) ^{3.50} exp(-4820.9/T)	NIST	200 - 2000
69	·CCl ₃ + H ₂ O	CHCl ₃ + ·OH	4.72x10 ⁻³⁹ (T/298) ^{3.73} exp(-23203.4/T)	NIST	200 - 2000

Table 5-10. Cl₂O reactions to be added to the photochemical model.

	Reactants	Products	Rate expression	Source	Temp range [K]
70	Cl ₂ O + O·	ClO + ClO	2.7x10 ⁻¹¹ exp(-530/T)	NIST	230 - 380
71	Cl ₂ O	ClO + ·Cl	1.34x10 ⁻⁵ (T/298) ^{-4.76} exp(-17298/T)	NIST	150 - 2000
72	·OH + Cl ₂ O	HOCl + ClO	1.78x10 ⁻¹² (T/298) ^{1.39} exp(415.1/T)	NIST	200 - 3000
73	ClO + ·Cl	Cl ₂ O	6.78x10 ⁻¹¹ (T/298) ^{0.07} exp(-93.8/T)	NIST	150 - 2000
74	HOCl + ClO	·OH + Cl ₂ O	5.49x10 ⁻¹³ (T/298) ^{1.77} exp(-9386/T)	NIST	200 - 3000

Table 5-11. CCl₄ reactions to be added to the photochemical model.

	Reactants	Products	Rate expression	Source	Temp range [K]
75	CCl ₄ + O·	·CCl ₃ + ClO	3.32x10 ⁻¹⁴ exp(-2259.9/T)	NIST	270 - 380
76	CCl ₄ + ·OH	·CCl ₃ + HOCl	1.0x10 ⁻¹² exp(-2259.9/T)	NIST	250 - 300
77	·CCl ₃ + ·Cl	CCl ₄	6.51x10 ⁻¹¹	NIST	298

Table 5-12. HOCl reactions to be added to the photochemical model.

	Reactants	Products	Rate expression	Source	Temp range [K]
78	HOCl + O·	·OH + ClO	1.7x10 ⁻¹³	NIST	210 - 300
79	·OH + HOCl	H ₂ O + ClO	3.01x10 ⁻¹² exp(-500.3/T)	NIST	200 - 300
80	HOCl + H·	H ₂ + ClO	9.18x10 ⁻¹⁶ (T/298) ^{4.89} exp(-214.1/T)	NIST	220 - 2000
81	H ₂ O ₂ + ClO	HO ₂ + HOCl	5.06x10 ⁻¹³	NIST	298
82	H ₂ + ClO	HOCl + H·	1.1x10 ⁻²⁰	NIST	298
83	HO ₂ + ClO	O ₂ + HOCl	4.8x10 ⁻¹³ exp(700/T)	NIST	200 - 300
84	·NH ₂ + ClO	HOCl + NH	2.11x10 ⁻¹⁶ (T/298) ^{5.11} exp(-1035.5/T)	NIST	200 - 2500
85	NH ₃ + ClO	HOCl + ·NH ₂	1.87x10 ⁻²⁴ (T/298) ^{3.85} exp(-4344.2/T)	NIST	200 - 2000
86	CH ₂ O + ClO	HCO + HOCl	9.12x10 ⁻¹² (T/298) ^{0.60} exp(-3015.2/T)	NIST	200 - 2000

Table 5-13. Cl radical reactions to be added to the photochemical model.

	Reactants	Products	Rate expression	Source	Temp range [K]
87	HO ₂ + ·Cl	·OH + ClO	6.3x10 ⁻¹¹ exp(-570.1/T)	NIST	230 - 420
88	ClO + N	NO + ·Cl	4.98x10 ⁻¹⁴	NIST	298
89	·CCl + N	CN + ·Cl	5.71x10 ⁻¹³	NIST	298
90	CHCl ₂ + N	HCN + ·Cl + ·Cl	1.98x10 ⁻¹¹	NIST	298
91	·OH + ClO	HO ₂ + ·Cl	1.9x10 ⁻¹¹	NIST	298
92	ClO + O·	O ₂ + ·Cl	2.5x10 ⁻¹¹ exp(109.4/T)	NIST	220 - 390

Chapter 6

Summary and Future Work

The question of whether there is life similar to ours on other planets has been motivating people to create new tools and models to study the universe. Perhaps, one of the most impactful breakthroughs of the past few decades was the discovery in 1995 of a Jupiter-mass exoplanet orbiting a main-sequence star (51 Pegasi) by two astronomers, Michel Mayor and Didier Queloz. Their discovery marked the birth of an entirely new field of study, 'exoplanet research.' Exoplanets, sometimes referred to as 'extrasolar planets,' are planets that orbit stars outside the solar system. Over the past decade, hundreds of new exoplanets have been discovered every year, thanks to advances in telescope technology.

In Chapter 1, I briefly describe what exoplanets are and how we can discover them. In brief, we can roughly group the exoplanets into four categories. Terrestrial planets are rocky exoplanets with Earth-like masses and possibly iron-rich cores. Super-Earths are much more massive than Earth but smaller than Uranus or Neptune. Neptune-like exoplanets typically have thick H₂/He-dominated atmospheres similar to Neptune's and may have liquid oceans and ice deep in the atmospheres. Finally, gas giants are gas-dominated planets with a size similar to or much larger than Saturn or Jupiter. In this chapter, I also provide a general overview of four techniques that astronomers commonly use to discover and study exoplanets: the transit method, the radial velocity method, microlensing, and direct imaging. Each technique has its own advantages and disadvantages. In recent years, more and more exoplanets have been discovered through the transit method. A transit occurs whenever an exoplanet passes in front of its host star. During transit, some of the light from the star is absorbed by the exoplanet's atmosphere, giving us clues about the atmosphere's chemical compositions. In this chapter, I also introduce biosignature gases. Biosignature gases are gases produced by living organisms that can accumulate to detectable levels in the atmosphere. Once detected, it can be attributed to signs of life on the planet. I stress that, to be a good biosignature gas, a chemical must be detectable (i.e., it must be able to accumulate in the atmosphere) and distinguishable (i.e., we can distinguish it from other gases). So far, only a few molecules have been studied as potential biosignature gases, such as oxygen (O₂), methane (CH₄), methyl chloride (CH₃Cl), nitrous oxide (N₂O), methanethiol (CH₃SH), DMS ((CH₃)₂S), among others. In a recent paper published by our group (Seager et al., 2016), we propose that we should systematically evaluate All Small Molecules (ASM) as possible biosignature gases. Inspired by this idea, in recent years, our group has studied some new and even exotic biosignature gases, such as phosphine (PH₃) (Sousa-Silva et al., 2020), isoprene (C₅H₈) (Zhan et al., 2021), and ammonia (NH₃) (Huang et al., 2022), to name a few.

In Chapter 2, I comprehensively review the various methods I have used in my research. Specifically, I focus on the following three methods: Henry's law equation and Henry's law constants, my simplified chlorine steady-state chemical model, and our comprehensive photochemistry model. In our study, we find that the solubility of a chemical species can profoundly affect whether it can accumulate in the atmosphere. The more water-soluble a chemical is, the easier it is to dissolve in cloud droplets and rainwater, making it difficult

for the chemical species to accumulate to detectable levels in the atmosphere. We usually use Henry's law to describe the solubility of a substance. There are many types (i.e., variants) of Henry's law constants, the most common of which is the physical Henry's law constant (HCP) with a unit of $\text{mol Pa}^{-1}\text{m}^{-3}$. In our research, we often compare Henry's law constants of the biosignature gas candidates we want to study with those of some common atmospheric gases. In this way, we can intuitively feel the impact of wet deposition on the biosignature gas and make preliminary predictions about whether it can accumulate in the atmosphere. Henry's law constant is also a function of temperature, which can be approximated by the van't Hoff equation. Next, I take a closer look at my simplified chloride steady-state chemical model. I developed a simplified chloride steady-state chemical model to study whether hydrogen chloride (HCl) is a good bioindicator in an H_2 -dominated atmosphere. Thanks to this simplified model, we can have a rough idea of whether HCl gas would accumulate to detectable levels in an H_2 -dominated atmosphere without running our complicated photochemistry code. I have to make two assumptions for my simplified chloride steady-state chemical model to work. First, I assume that HCl and CH_3Cl are trace gases in the atmosphere, and their respective production flux is small. Therefore, their presence does not affect the concentration of other major chemical species in the atmosphere. Second, I assume that HCl and CH_3Cl are well-mixed in the atmosphere, and their concentrations do not change with height. Since HCl is in a steady state in the atmosphere, its production flux must equal its total removal flux. I consider three removal pathways for HCl: wet deposition, dry deposition, and photochemical destruction, each of which can be estimated using equations. In my model, I assume that life does not directly produce HCl gas but produces CH_3Cl , which is later photochemically converted to HCl in a high-reducing H_2 -dominated atmosphere through this reaction: $\text{CH}_3\text{Cl} + \text{H} \rightarrow \text{CH}_3 + \text{HCl}$. Hence, the production flux of HCl is equal to the reaction flux between CH_3Cl and H. Overall, we can write a balanced equation where the only unknown is the bioproduction flux of CH_3Cl , and we can use the equation to solve for the concentration of HCl in the atmosphere.

In Chapter 2, I also introduce our photochemistry code in detail. In our research, we often use our one-dimensional photochemistry model (Hu et al., 2012) to calculate the mixing ratio of the biosignature gas we want to study as a function of vertical altitude in an exoplanet atmosphere. The most prominent feature of our photochemistry code is that it is very flexible: we can use it to simulate different planets with different atmospheres orbiting a wide variety of host stars. In our research, we often use GJ 876 as the host star for our simulated exoplanets because GJ 876 has the lowest near-ultraviolet (NUV) and far-ultraviolet (FUV) output of all the available stars. We have three benchmark scenarios: CO_2 -dominated highly oxidizing atmospheres, N_2 -dominated weakly oxidizing atmospheres, and H_2 -dominated reducing atmospheres. We have a different temperature-pressure profile and an eddy diffusion profile for each scenario. For each of the scenarios we study, we set the planet's surface pressure to 1 bar and temperature to 288 K. We divide the atmosphere into two layers: a lower convective layer and a higher radiative layer (Hu et al., 2012). We set the temperature of the convective layer to follow the dry adiabatic lapse rate. We set the temperature above tropopause to 160K, 200K, and 175K for the H_2 -dominated, N_2 -dominated, and CO_2 -dominated atmosphere. Since we do not consider heating in the upper atmosphere, we assume the temperature to be constant (isothermal) in the radiative layer (Hu et al., 2012). In our model, the vertical mixing processes are

parameterized by the atmosphere's eddy diffusion coefficient (k_{zz}). The choice of K_{zz} can impact whether the biosignature gas can accumulate in the atmosphere because photochemistry is most important in the upper atmosphere layers, whereas we assume that most biosignature gases are primarily produced at the planet's surface. The larger K_{zz} , the more likely the biosignature gas will be transported to the upper atmosphere before being removed by wet or dry deposition. K_{zz} is measured or inferred for solar system planets but is not known for exoplanets. In our studies, we often use the known Earth's eddy diffusion profile and scale it up to approximate the eddy diffusion profile of our simulated exoplanets. Currently, our photochemistry code includes more than 800 reactions and 111 species. In our simulations, we include all the reactions mentioned in (Hu et al., 2012) except for reactions that involve more than two carbon atoms ($C_{>2}$ -chem), HSO_2 thermal decay, and high-temperature reactions (Hu et al., 2012). Moreover, we set the surface deposition (including rainout and dry deposition) of H_2 , CO , CH_4 , N_2 , C_2H_2 , C_2H_4 , C_2H_6 , and O_2 to zero to facilitate robust comparison with reference benchmark scenarios from (Hu et al., 2012).

In Chapter 3, I examine the potential of NH_3 as a biosignature gas. I am motivated to study the biosignature potential of NH_3 since NH_3 plays a significant role in biochemistry. Due to its high bio-usability, plants and various microorganisms can easily absorb NH_3 . NH_3 is an ideal nitrogen source for life on Earth since it can be integrated into various amino acids and other organic molecules without life having to break the strong N_2 triple bond. Additionally, some life can use NH_3 as an energy source by oxidizing NH_3 . Furthermore, NH_3 stands out from all the previously studied biosignature gases because NH_3 has a very high solubility in water. NH_3 's high water solubility means the atmospheric accumulation of NH_3 is highly dependent on planetary conditions such as whether life produces a substantial amount of NH_3 and whether there are active NH_3 -removal sinks on the surface (including land and ocean). To study NH_3 as a potential biosignature gas, I use various approaches, ranging from comparing Henry's law constants for different atmospheric gases to our simplified ocean- NH_3 interaction model to applications of our comprehensive photochemistry code and transmission spectra model. In brief, NH_3 in a terrestrial planet's atmosphere is generally a good biosignature gas, primarily because terrestrial planets have no significant known abiotic NH_3 source. However, the conditions required for NH_3 to accumulate in the atmosphere are stringent. NH_3 's high water solubility and high bio-usability likely prevent NH_3 from accumulating in the atmosphere to detectable levels unless life is a net source of NH_3 and produces enough NH_3 to saturate the surface sinks. Only then can NH_3 accumulate in the atmosphere with a reasonable surface production flux. Specifically, for the highly favorable planetary scenario of terrestrial planets with H_2 -dominated atmospheres orbiting M dwarf stars (M5V), we find a minimum of about 5 ppm column-averaged mixing ratio is needed for NH_3 to be detectable with JWST, considering a 10 ppm JWST systematic noise floor. When the surface is saturated with NH_3 (i.e., there are no NH_3 -removal reactions on the surface), the required biological surface flux to reach 5 ppm is on the order of 10^{10} molecules $\text{cm}^{-2} \text{s}^{-1}$, comparable to the terrestrial biological production of CH_4 . However, when the surface is unsaturated with NH_3 , due to additional sinks present on the surface, life would have to produce NH_3 at surface flux levels on the order of 10^{15} molecules $\text{cm}^{-2} \text{s}^{-1}$ ($\sim 4.5 \times 10^6 \text{ Tg year}^{-1}$). This value is roughly 20,000 times greater than the biological production of NH_3 on Earth and about 10,000 times greater than Earth's CH_4 biological production. Additionally, volatile amines share NH_3 's weaknesses

and strengths as a biosignature since volatile amines have similar solubilities and reactivities to NH_3 . Finally, to establish NH_3 as a biosignature gas, we must rule out mini-Neptunes with deep atmospheres, where temperatures and pressures are high enough for NH_3 's atmospheric production.

In Chapter 4, I examine the biosignature potential of CH_3OH in detail. CH_3OH is an important precursor molecule for life's biochemistry, as it is the building block of a diverse set of biochemicals such as acetic acid, methylamines, and methyl esters, to name a few. In the atmosphere, CH_3OH is a significant source of formaldehyde (CH_2O) and carbon monoxide (CO) (Tie et al., 2003; Solomon et al., 2005; Millet et al., 2008; Hu et al., 2011). CH_3OH has many advantages as a biosignature gas candidate. First, CH_3OH 's hydroxyl group (OH) has a unique spectral feature compared to other anticipated gases in rocky exoplanets' atmospheres. Second, there are no significant known abiotic CH_3OH sources on terrestrial planets in the solar system. Due to CH_3OH 's high water solubility, the limited amount of abiotic CH_3OH produced can be easily removed by rain, making it extremely difficult to accumulate. Third, life on Earth produces CH_3OH in large quantities. In this chapter, I use a variety of approaches, from comparing Henry's law constants for different atmospheric species to our one-dimensional photochemistry model and our transmission spectra (SEAS) model. Despite CH_3OH 's advantages, we consider CH_3OH a poor biosignature gas in terrestrial exoplanet atmospheres due to the enormous production flux required to reach its detection limit. For the highly favorable planetary scenario of an exoplanet with an H_2 -dominated atmosphere orbiting an M5V dwarf star, we find that only when the column-averaged mixing ratio of CH_3OH reaches at least 10 ppm can we detect it with JWST. CH_3OH bioproduction flux required to reach the 10 ppm JWST detection threshold must be on the order of 10^{14} molecules $\text{cm}^{-2} \text{s}^{-1}$, which is roughly three times the annual O_2 production on Earth. Considering that such an enormous flux of CH_3OH is essentially a massive "waste" of organic carbon - a major building block of life, we think this flux, while mathematically possible, is likely biologically unattainable. We also find that, due to the presence of surface deposition, CH_3OH does not experience runaway, even at extremely high flux. CH_3OH runaway can only occur in the exceptional case with no CH_3OH surface deposition (i.e., no rainout or dry deposition). This exception happens only if CH_3OH bioproduction is robust enough to saturate its surface sinks. Considering CH_3OH runaway, we estimate that the required CH_3OH bioproduction flux to reach the 10 ppm JWST detection threshold is approximately 9×10^9 molecules $\text{cm}^{-2} \text{s}^{-1}$ ($\sim 77 \text{ Tg year}^{-1}$), which is about 8% of the annual CH_4 production on Earth. Beyond CH_3OH , we argue that alcohols with long carbon chains ($\text{C} > 4$) are poor biosignature gas candidates due to their high water solubility and relatively low volatility. Finally, although CH_3OH can theoretically accumulate on exoplanets with CO_2 - or N_2 -dominated atmospheres, such planets' small atmospheric scale height and weak atmosphere signals put them out of reach for near-term observations. We hope that as telescope technology improves, potential biosignature gases (e.g., CH_3OH) that are not yet readily observable with the JWST can one day be observed and more thoroughly studied.

In Chapter 5, I carefully examine the bioindicator potential of HCl . In the atmosphere, some biosignature gases do not survive photochemical destruction. These biosignature gases themselves cannot accumulate to detectable levels in the atmosphere. We can only infer the presence of biosignature gases by detecting their photochemical products. We refer to the

final products of the chemical reactions of biosignature gases as bioindicators (Seager et al., 2013). I am motivated to study hydrogen chloride (HCl) for its many advantages as a bioindicator in H₂-dominated atmospheres. In highly reducing atmospheres, many gases are converted to their most hydrogenated (i.e., reduced) form: dimethyl sulfide (DMS) will be turned into H₂S and CH₄; N₂O will be turned into H₂O and N₂ (Seager et al., 2013). Since the most reduced form of Cl element is HCl, atmospheric methyl chloride (CH₃Cl) and chlorine (Cl₂) gas will end up as HCl in H₂-dominated atmospheres. In addition, there are very few abiotic sources of HCl, the only exception being volcanic activity. The high water solubility of HCl means that only when life converts enough non-volatile forms of Cl into HCl gas can HCl accumulate in the atmosphere to detectable levels. I developed a simplified chloride steady-state chemical model to study whether hydrogen chloride (HCl) is a good bioindicator in an H₂-dominated atmosphere. Despite HCl's advantages, I believe that HCl is not a suitable bioindicator because it cannot accumulate to detectable levels on an exoplanet with an H₂-dominated atmosphere orbiting an M5V dwarf star similar to GJ 876. Through my model, I find that even if life on such a planet produces CH₃Cl at a flux of 3.5×10^{13} molecules cm⁻² s⁻¹, the same as Earth's gross oxygen production flux, there is still less than 10 ppb of HCl in the atmosphere, far from being detectable by JWST. The extremely high water solubility of HCl means that wet deposition can efficiently remove it from the atmosphere, preventing HCl from accumulating to detectable levels in the atmosphere.

In Chapter 5, I also provide a comprehensive literature review on the abundance, distribution, and circulation of chlorine on Earth. Chlorine is very abundant on Earth. Of the 94 naturally-occurring elements, chlorine ranks in the top 20 in terms of abundance (Graedel et al., 1996; Öberg 2002; Sharp et al., 2013; Atashgahi et al., 2018; Svensson et al., 2021). So far, there is no consensus on the exact value of the total amount of chlorine on Earth, with estimates ranging from a low of about 1×10^{12} Tg to a high of about 2×10^{13} Tg (Graedel et al., 1996; Sharp et al., 2013). Chlorine is not evenly distributed on Earth but concentrated in its three major reservoirs: the mantle, the crust, and the ocean (Graedel et al., 1996; Sharp et al., 2013; Svensson et al., 2021). Specifically, nearly all of Earth's chlorine (> 99%) is locked up in the mantle. Chlorine in the mantle hardly participates in Earth's chlorine cycle, the only way being through volcanism (Graedel et al., 1996). Crustal chlorine can only participate in cycling via weathering (Graedel et al., 1996). Even though oceanic chlorine represents only a tiny fraction (< 0.1%) of the Earth's total chlorine reserves, it plays a vital role in the chlorine cycle thanks to its high accessibility and mobility (Graedel et al., 1996). In addition to the three main reservoirs mentioned above, other chlorine reservoirs include freshwater (e.g., lakes and rivers), the pedosphere (e.g., soil, sediment, and litter), the atmosphere (troposphere and stratosphere), the cryosphere (e.g., glaciers and ice caps), and the biosphere (Graedel et al., 1996; Sharp et al., 2013; Atashgahi et al., 2018; Svensson et al., 2021). Earth has a very complex chlorine cycle. From a mass perspective, chlorine transfer between the oceans and the atmosphere (troposphere) dominates Earth's chlorine cycle (Graedel et al., 1996; Svensson et al., 2021). Specifically, the injection of sea salt aerosols from the oceans to the atmosphere is the most significant inter-reservoir chlorine flux on Earth, followed by the return of chlorine to the oceans via surface deposition (i.e., wet and dry deposition) (Graedel et al., 1996; Svensson et al., 2021). In this chapter, I also review the solubility of chlorine-containing gas molecules (e.g., methyl chloride (CH₃Cl), chloroform (CHCl₃), and carbon tetrachloride

(CCl_4)), discuss the acidity of chlorine-containing acids (e.g., hydrochloric acid (HCl), hypochlorous acid (HClO), and chlorous acid (HClO_2)), and explore naturally occurring chloride minerals and their properties (e.g., halite (NaCl), sylvite (KCl), and molysite (FeCl_3)).

Overall, this thesis summarizes my work in identifying and characterizing potential biosignature gases. My research is highly interdisciplinary, which includes chemistry, atmospheric science, astrobiology, geology, and computational simulation, to name a few. My thesis aims to improve our understanding of biosignature gases and provide more diverse research methods and a more comprehensive framework for future work. One of my priorities in the near future is to complete and publish my HCl paper. To accomplish this task, I have to run our photochemistry code and quantitatively confirm the results from my simplified chlorine chemical model. To properly simulate an exoplanet with robust chlorine bioproduction, as a first step, we need to collect all relevant chlorine reactions and encode them into our model. The chlorine reactions we are looking for must satisfy the following two conditions. First, the reactions must be able to take place within the atmospheric temperature range we are simulating (i.e., between 160 K and 290 K). Reactions that can only occur at high temperatures (e.g., high-temperature thermal decomposition reactions) or low temperatures (i.e., cryogenic reactions) are excluded. Second, since we are simulating an exoplanet with a reducing H_2 -dominated atmosphere, we exclude those reactions in which the reactants are oxidized chlorine compounds (e.g., reactions involving ClO_2 or ClO_4). We have currently identified 92 potential chemical reactions that meet our requirements. The next step is to read the literature for these reactions to ensure that all the reaction rates are correct and up-to-date. Next, we must properly encode all these reactions into our existing model and ensure our photochemistry model still works. Our current photochemistry model is not perfect, and there are many areas that we can improve. For example, we can check and revise the existing reaction network. All the reactions were collected and compiled in 2012. Over the past decade, the reaction rates of many reactions have been revised or corrected. Many of these updates have not yet been incorporated into our photochemistry code. Another area we can improve on our photochemistry model is to make it more self-consistent (i.e., smarter). Currently, there is no feedback loop between our temperature-pressure and atmospheric composition profile. Therefore, when our simulated scenario deviates significantly from the initial condition we prescribed, our code might start to produce some errors. If our code could autonomously update its parameters (e.g., T-P profile) on the fly, our code could simulate a broader range of atmospheric scenarios than it currently can. Our model currently doesn't include high-energy electrons or protons. Therefore, we might slightly underestimate the overall removal flux of chemicals in the atmosphere. We can get more accurate results by having high-energy electrons or protons in our future simulations. In our studies, we often use the known Earth's eddy diffusion profile and scale it up to approximate the eddy diffusion profile of our simulated exoplanets. We want to point out that this approximation is not physically accurate for exoplanets. The Earth's diffusion profile takes this shape because of the absorption of UV by O_3 . The eddy diffusion profiles will likely have different shapes on exoplanets without ozone layers. In the future, we can try to develop an analytical method to better estimate the K_{zz} profiles. Currently, we do not include atmospheric escape in our simulations. On Earth-sized exoplanets, gases such as H_2 can escape. However, we assume that the H_2 mixing ratio is constant in the atmosphere. We can improve our future simulation results by

considering atmospheric escape (especially H_2). In the long run, my future research is full of possibilities. There are many new projects I can do in the future. I have a lot of knowledge and experience in experimental science. Two of the three experiments I participated in during my Ph.D. have been published (Seager et al., 2020; Zhan et al., 2021), and one is currently in prep. In the future, I hope to be able to participate in more cool scientific experiments if I have the opportunity. At present, JWST has just started its science operation. I am very proud to be a member of the JWST GTO team. I hope to be more involved in JWST research projects in the future. Planetary science is an interdisciplinary science that includes physics, astronomy, biology, and chemistry, to name a few. I hope my interdisciplinary strengths will bring my unique contribution to planetary research. In the long run, through my hard work and dedication, I hope to leave my own footprint in the field of planetary science.

List of Figures

Figures in Chapter 2:

Figure 2-1. The effect of temperature on Henry's law constant.	24
Figure 2-2. The synthetic stellar spectrum input of our photochemistry mode	29
Figure 2-3. The temperature-pressure profiles of the simulated exoplanets with H ₂ -dominated, CO ₂ -dominated, and N ₂ -dominated atmospheres.	31
Figure 2-4. The eddy diffusion profile of the simulated exoplanets with H ₂ -dominated atmospheres.	32
Figure 2-5. The eddy diffusion profile of the simulated exoplanets with N ₂ -dominated atmospheres.	32
Figure 2-6. The eddy diffusion profile of the exoplanets with CO ₂ -dominated atmospheres.	33

Figures in Chapter 3:

Figure 3-1. Interconversions between the main nitrogen species.	39
Figure 3-2. Biological production of six different gases in Tg year ⁻¹ .	40
Figure 3-3. Equilibrium volume mixing ratio of NH ₃ as a function of the planet's total NH ₃ reserve and ocean pH.	50
Figure 3-4. Simulated spectra of an exoplanet with an H ₂ -dominated atmosphere transiting an M5V star for a range of NH ₃ column-averaged mixing ratios.	51
Figure 3-5. Simulated JWST exoplanet atmosphere observation for a 10 M _{Earth} , 1.75 R _{Earth} super-Earth with an H ₂ -dominated atmosphere transiting an M5V star.	53
Figure 3-6. Comparison between 20 and 200 transits for simulated JWST exoplanet atmosphere observations for a 10 M _{Earth} , 1.75 R _{Earth} super-Earth with H ₂ -dominated atmosphere transiting an M5V star.	54
Figure 3-7. The volume mixing ratio of various atmospheric species on planets with H ₂ -dominated, CO ₂ -dominated, and N ₂ -dominated atmospheres orbiting active M dwarfs.	56
Figure 3-8. The solubility of common molecules on a log scale.	58
Figure 3-9. A simplified NH ₃ land-ocean transport cycle.	59
Figure 3-10. Spectral features of primary, secondary and tertiary amines in NIST.	62
Figure 3-11. The synthetic stellar spectrum input of our photochemistry model.	65
Figure 3-12. The temperature-pressure profiles of the simulated exoplanets with H ₂ -dominated, CO ₂ -dominated, and N ₂ -dominated atmospheres.	65
Figure 3-13. The eddy diffusion profiles of the simulated exoplanets with H ₂ -dominated, CO ₂ -dominated, and N ₂ -dominated atmospheres.	66
Figure 3-14. IR absorbance spectra of primary amines.	75
Figure 3-15. IR absorbance spectra of secondary amines.	76
Figure 3-16. IR absorbance spectra of tertiary amines.	76
Figure 3-17. The temperature-pressure profiles of the simulated exoplanets with 'standard' and 'reduced' cold traps.	78
Figure 3-18. The volume mixing ratio of NH ₃ on planets with H ₂ -dominated atmospheres orbiting active M dwarfs.	81

Figures in Chapter 4:

Figure 4-1. Average atmospheric CH ₃ OH concentrations over/in some representative regions.	86
Figure 4-2. A simplified schematic diagram of the global CH ₃ OH biogeochemical cycle.	88
Figure 4-3. Through the action of pectin methylesterase (PME), pectin demethylation produces CH ₃ OH as a by-product.	89
Figure 4-4. The volume mixing ratio of CH ₃ OH and other representative atmospheric species on an exoplanet with an H ₂ -dominated atmosphere orbiting an M5V dwarf star similar to GJ 876.	98
Figure 4-5. Accumulation of CH ₃ OH on an exoplanet with an H ₂ -dominated atmosphere orbiting an M5V dwarf star.	101
Figure 4-6. Simulated transmission spectra of a hypothetical 5M _{Earth} , 1.5R _{Earth} super-Earth with an H ₂ -dominated atmosphere transiting an M5V dwarf star similar to GJ 876.	102
Figure 4-7. Simulated JWST observations of a hypothetical 5M _{Earth} , 1.5R _{Earth} super-Earth with an H ₂ -dominated atmosphere transiting an M5V dwarf star similar to GJ 876.	103
Figure 4-8. Spectral absorbance of CH ₃ OH and various species.	104
Figure 4-9. Solubility of various atmospheric gasses in water.	105
Figure 4-10. The boiling points of 8 representative alcohols and 9 other hydrocarbons.	109
Figure 4-11. The synthetic stellar radiation model of GJ 876 and The temperature-pressure profiles of the simulated exoplanets with H ₂ -dominated, CO ₂ -dominated, and N ₂ -dominated atmospheres.	112
 <u>Figures in Chapter 5:</u>	
Figure 5-1. Chlorine reservoirs on Earth.	124
Figure 5-2. An overview of Earth's natural chlorine cycle.	128
Figure 5-3. The volume mixing ratio of several major chemical species on an exoplanet with an H ₂ -dominated atmosphere and The number density of O, H, OH, and H ₂ O as a function of altitude in the atmosphere.	130
Figure 5-4. The atmospheric temperature as a function of altitude and my calculated rainout rate for HCl as a function of altitude.	131
Figure 5-5. The absorption cross sections of HCl and CH ₃ Cl at 298 K, and my calculated photolysis rate coefficient for HCl (J(z)).	132
Figure 5-6. The water solubility of various species.	135
Figure 5-7. The acidity of various acids.	136

List of Tables

Tables in Chapter 1:

Table 1-1. Different types of exoplanets and their respective characteristics.	14
Table 1-2. Advantages and disadvantages of each detection method.	15
Table 1-3. Some biosignature gases that people have studied.	16
Table 1-4. Phosphine, isoprene, and ammonia as biosignature gases.	17

Tables in Chapter 2:

Table 2-1. Henry's law constants for some representative gases in water.	23
Table 2-2. Some representative stars and their respective spectral types.	28
Table 2-3. Atmospheric compositions of our three benchmark scenarios.	29

Tables in Chapter 3:

Table 3-1. Major anthropogenic NH ₃ sources and their estimated flux.	37
Table 3-2. A summary of global anthropogenic NH ₃ emission estimates.	38
Table 3-3. NH ₃ -producing reactions. The reaction rates are in units of cm ³ molecule ⁻¹ s ⁻¹ .	41
Table 3-4. Reactions between NH ₃ and H, O and OH radicals in the atmosphere. The reaction rates have units of cm ³ molecule ⁻¹ s ⁻¹ .	42
Table 3-5. Photolysis reactions of NH ₃ .	42
Table 3-6. NH ₃ -removing reactions. The reaction rates are in units of cm ³ molecule ⁻¹ s ⁻¹ .	43
Table 3-7. Henry's law constant for some representative gases in water.	49
Table 3-8. Simulated mixing ratios and surface fluxes for exoplanets with H ₂ -dominated, CO ₂ -dominated, and N ₂ -dominated atmospheres orbiting M dwarf stars.	55
Table 3-9. Naturally occurring NH ₄ -containing minerals.	61
Table 3-10. Surface boundary conditions for exoplanets with CO ₂ -dominated atmospheres.	67
Table 3-11. Surface boundary conditions for exoplanets with H ₂ -dominated atmospheres.	69
Table 3-12. Surface boundary conditions for exoplanets with N ₂ -dominated atmospheres.	71
Table 3-13. The pK _a values of some representative amines at 25°C.	73
Table 3-14. Reactions between life produced volatile amines and OH radicals. Reaction rates are at 298 K. Second-order reactions have units of [cm ³ molecule ⁻¹ s ⁻¹].	73
Table 3-15. Reactions between life produced volatile amines and O radicals. Reaction rates are at 298 K. Second-order reactions have units of [cm ³ molecule ⁻¹ s ⁻¹].	74
Table 3-16. Primary (15), Secondary (9) and Tertiary (2) Amines in NIST.	74
Table 3-17. The top three photochemical removal mechanisms for NH ₃ on exoplanets with H ₂ -dominated, CO ₂ -dominated, and N ₂ -dominated atmospheres orbiting M dwarf stars (M5V).	77
Table 3-18. Simulated mixing ratios and reaction rates for exoplanets with H ₂ -dominated atmospheres orbiting M dwarf stars (M5V).	78
Table 3-19. Steady-state simulation outputs as a function of eddy diffusion magnitude, NH ₃ surface flux, and presence/absence of wet and dry deposition of NH ₃ for exoplanets with H ₂ -dominated atmospheres orbiting M dwarf stars (M5V).	79

Tables in Chapter 4:

Table 4-1. Estimates of the global CH ₃ OH emission flux.	87
Table 4-2. Estimated global CH ₃ OH sources in Tg/yr.	88
Table 4-3. CH ₃ OH-producing reactions in the atmosphere.	90
Table 4-4. CH ₃ OH photochemical oxidation by OH.	91
Table 4-5. CH ₃ OH removal reactions in the atmosphere.	92
Table 4-6. Photolysis reactions of CH ₃ OH.	92
Table 4-7. Thermal decomposition of CH ₃ OH (NIST).	93
Table 4-8. Estimated global CH ₃ OH sinks in Tg/yr.	94
Table 4-9. The main CH ₃ OH removal mechanisms and their respective fluxes on our simulated exoplanet with an H ₂ -dominated atmosphere orbiting an M dwarf star similar to GJ 876.	98
Table 4-10. Steady-state photochemical simulation outputs as a function of eddy diffusion magnitude and presence/absence of cold traps for exoplanets with H ₂ -dominated atmospheres orbiting M dwarfs.	99
Table 4-11. Steady-state simulation outputs for exoplanets with H ₂ -dominated, CO ₂ -dominated, and N ₂ -dominated atmospheres orbiting M dwarf stars.	107
Table 4-12. Surface boundary conditions for exoplanets with H ₂ -dominated atmospheres.	112
Table 4-13. Surface boundary conditions for exoplanets with CO ₂ -dominated atmospheres.	114
Table 4-14. Surface boundary conditions for exoplanets with N ₂ -dominated atmospheres.	116

Tables in Chapter 5:

Table 5-1. Photochemical reactions between HCl and O, H and OH in the atmosphere.	131
Table 5-2. Photochemical reverse reactions of reforming HCl in the atmosphere.	132
Table 5-3. Some simple naturally occurring chloride minerals.	137
Table 5-4. New chlorine species to be added to the photochemical model.	138
Table 5-5. HCl reactions to be added to the photochemical model.	138
Table 5-6. CH ₃ Cl reactions to be added to the photochemical model.	140
Table 5-7. Cl ₂ reactions to be added to the photochemical model.	140
Table 5-8. CH ₂ Cl ₂ reactions to be added to the photochemical model.	140
Table 5-9. CHCl ₃ reactions to be added to the photochemical model.	140
Table 5-10. Cl ₂ O reactions to be added to the photochemical model.	141
Table 5-11. CCl ₄ reactions to be added to the photochemical model.	141
Table 5-12. HOCl reactions to be added to the photochemical model.	141
Table 5-13. Cl radical reactions to be added to the photochemical model.	142

Bibliography

1. Amante, C. & Eakins, B. W. ETOPO1 1 Arc-Minute Global Relief Model: Procedures, Data Sources and Analysis. NOAA Tech. Memo. NESDIS NGDC-24 19 (2009) doi:10.1594/PANGAEA.769615.
2. Andreae, M. O. The influence of tropical biomass burning on climate and the atmospheric chemistry, in " Biogeochemistry of Global Change: Radiatively Active Trace Gases" RS Oreland, ed. RS Orel. 113–150 (1993).
3. Andreae, M. O. et al. Methyl halide emissions from savanna fires in southern Africa. *J. Geophys. Res. Atmos.* 101, 23603–23613 (1996).
4. Andreae, M. O. & Merlet, P. Emission of trace gases and aerosols from biomass burning. *Global Biogeochem. Cycles* 15, 955–966 (2001).
5. Anthony, J. W. Handbook of mineralogy. Vol. 3: Halides, hydroxides and oxides. (Mineral Data Pub., 1997).
6. Ardaseva, A. et al. Lightning Chemistry on Earth-like Exoplanets. arXiv 470, 187–196 (2017).
7. Arney, G. N. et al. Pale orange dots: The impact of organic haze on the habitability and detectability of earthlike exoplanets. arXiv 836, 49 (2017).
8. Arney, G., Domagal-Goldman, S. D. & Meadows, V. S. Organic haze as a biosignature in anoxic Earth-like atmospheres. *Astrobiology* 18, 311–329 (2017).
9. Atashgahi, S. et al. Microbial synthesis and transformation of inorganic and organic chlorine compounds. *Front. Microbiol.* 3079 (2018).
10. Atkinson, R. et al. Evaluated kinetic and photochemical data for atmospheric chemistry: Volume II—gas phase reactions of organic species. *Atmos. Chem. Phys.* 6, 3625–4055 (2006).
11. Barker, J. F., Hubbard, C. E., Lemon, L. A. & Voro, K. A. The influence of methanol in gasoline fuels on the formation of dissolved plumes, and the fate and natural remediation of methanol and BTEX dissolved in groundwater. *Hydrocarb. Contam. Soils Groundwater.* Lewis Publ. New York (1992).
12. Bar-On, Y. M., Phillips, R. & Milo, R. The biomass distribution on Earth. *Proc. Natl. Acad. Sci. U. S. A.* 115, 6506–6511 (2018).
13. Basch, H., Mogi, K., Musaev, D. G. & Morokuma, K. Mechanism of the methane→methanol conversion reaction catalyzed by methane monooxygenase: a density functional study. *J. Am. Chem. Soc.* 121, 7249–7256 (1999).
14. Batalha, N. E. et al. PandExo: A community tool for transiting exoplanet science with jwst & hst. arXiv 129, 64501 (2017).
15. Battersby, C. et al. The origins space telescope. *Nat. Astron.* 2, 596–599 (2018).
16. Behera, S. N., Sharma, M., Aneja, V. P. & Balasubramanian, R. Ammonia in the atmosphere: A review on emission sources, atmospheric chemistry and deposition on terrestrial bodies. *Environ. Sci. Pollut. Res.* 20, 8092–8131 (2013).
17. Benneke, B. & Seager, S. Atmospheric retrieval for super-Earths: uniquely constraining the atmospheric composition with transmission spectroscopy. *Astrophys. J.* 753, 100 (2012).
18. Bernath, P. F. Atmospheric chemistry experiment (ACE): Mission overview. *Opt. InfoBase Conf. Pap.* 32, (2005).
19. Berner, E. K. & Berner, R. A. Global water cycle: geochemistry and environment. Prentice-Hall, Inc., Englewood Cliffs New Jersey. 1987. 397 (1987).

20. Bétrémieux, Y. & Kaltenecker, L. Impact of atmospheric refraction: how deeply can we probe exo-Earth's atmospheres during primary eclipse observations? *Astrophys. J.* 791, 7 (2014).
21. Bhatt, P., Kumar, M. S., Mudliar, S. & Chakrabarti, T. Biodegradation of chlorinated compounds—a review. *Crit. Rev. Environ. Sci. Technol.* 37, 165–198 (2007).
22. Birnbaum, G., Borysow, A. & Orton, G. S. Collision-induced absorption of H₂-H₂ and H₂-He in the rotational and fundamental bands for planetary applications. *Icarus* 123, 4–22 (1996).
23. Björn, H. Uptake, turnover and distribution of chlorinated fatty acids in aquatic biota. (1999).
24. Bolch, T. & Christiansen, H. H. Mountains, lowlands, and coasts: The physiography of cold landscapes. in *Snow and Ice-Related Hazards, Risks, and Disasters* 199–213 (Elsevier, 2021).
25. Bouwman, A. F., Boumans, L. J. M. & Batjes, N. H. Estimation of global NH₃ volatilization loss from synthetic fertilizers and animal manure applied to arable lands and grasslands. *Global Biogeochem. Cycles* 16, 1–8 (2002).
26. Bouwman, A. F. et al. A global high-resolution emission inventory for ammonia. *Global Biogeochem. Cycles* 11, 561–587 (1997).
27. Brasseur, G. P. & Jacob, D. J. *Modeling of Atmospheric Chemistry*. Modeling of Atmospheric Chemistry (Cambridge University Press, 2017). doi:10.1017/9781316544754.
28. Brimblecombe, P. & Clegg, S. L. The solubility and behaviour of acid gases in the marine aerosol. *J. Atmos. Chem.* 7, 1–18 (1988).
29. Brown, T. L. *Chemistry: the central science*. (Pearson Education, 2009).
30. Burgess, B. K. & Lowe, D. J. Mechanism of molybdenum nitrogenase. *Chem. Rev.* 96, 2983–3011 (1996).
31. Burkholder, J. B. et al. Chemical kinetics and photochemical data for use in atmospheric studies; evaluation number 19. (2020).
32. Burton, G. R., Chan, W. F., Cooper, G. & Biron, C. E. Absolute oscillator strengths for photoabsorption (6–360 eV) and ionic photofragmentation (10–80 eV) of methanol. *Chem. Phys.* 167, 349–367 (1992).
33. Byrne, N. et al. Presence and activity of anaerobic ammonium-oxidizing bacteria at deep-sea hydrothermal vents. *ISME J.* 3, 117–123 (2009).
34. Cameron, A. G. W. *Origin and Distribution of the Elements*. vol. 30 (Pergamon, 1968).
35. Caranto, J. D. & Lancaster, K. M. Nitric oxide is an obligate bacterial nitrification intermediate produced by hydroxylamine oxidoreductase. *Proc. Natl. Acad. Sci. U. S. A.* 114, 8217–8222 (2017).
36. Catling, D. C. & Kasting, J. F. *Atmospheric evolution on inhabited and lifeless worlds*. (Cambridge University Press, 2017).
37. Chaudhry, G. R. & Chapalamadugu, S. Biodegradation of halogenated organic compounds. *Microbiol. Rev.* 55, 59–79 (1991).
38. Cheng, B., Bahou, M., Lee, Y. & Lee, L. C. Absorption cross sections and solar photodissociation rates of deuterated isotopomers of methanol. *J. Geophys. Res. Sp. Phys.* 107, SIA-7 (2002).
39. Christiansen, S., Salter, M. E., Gorokhova, E., Nguyen, Q. T. & Bilde, M. Sea spray aerosol formation: Laboratory results on the role of air entrainment, water temperature, and phytoplankton biomass. *Environ. Sci. Technol.* 53, 13107–13116 (2019).
40. Cockell, C. S. Carbon biochemistry and the ultraviolet radiation environments of F, G,

- and K main sequence stars. *Icarus* 141, 399–407 (1999).
41. Cohen, E. R. et al. Quantities, units and symbols in physical chemistry. (International Union of Pure and Applied Chemistry, The Royal Society of ..., 2007).
 42. Cottrell, T. L. The strengths of chemical bonds. (Butterworths Scientific Publications, 1958).
 43. Crutzen, P. J. & Andreae, M. O. Biomass burning in the tropics: Impact on atmospheric chemistry and biogeochemical cycles. *Science* (80-.). 250, 1669–1678 (1990).
 44. Daims, H. et al. Complete nitrification by *Nitrospira* bacteria. *Nature* 528, 504–509 (2015).
 45. Daines, S. J., Mills, B. J. W. & Lenton, T. M. Atmospheric oxygen regulation at low Proterozoic levels by incomplete oxidative weathering of sedimentary organic carbon. *Nat. Commun.* 8, 1–11 (2017).
 46. De Wit, J. Maps and masses of transiting exoplanets: towards new insights into atmospheric and interior properties of planets. *arXiv Prepr. arXiv1509.01493* (2015).
 47. Dembitsky, V. M. & Srebnik, M. Natural halogenated fatty acids: their analogues and derivatives. *Prog. Lipid Res.* 41, 315–367 (2002).
 48. Dentener, F. J. & Crutzen, P. J. A three-dimensional model of the global ammonia cycle. *J. Atmos. Chem.* 19, 331–369 (1994).
 49. Des Marais, D. J. et al. Erratum: Remote sensing of planetary properties and biosignatures on extrasolar terrestrial planets (*Astrobiology* (2002) 2: 2 (153-181)). *Astrobiology* 3, 216 (2003).
 50. Devol, A. H. Nitrogen cycle: Solution to a marine mystery. *Nature* 422, 575–576 (2003).
 51. Dillon, T. J., Hölscher, D., Sivakumaran, V., Horowitz, A. & Crowley, J. N. Kinetics of the reactions of HO with methanol (210–351 K) and with ethanol (216–368 K). *Phys. Chem. Chem. Phys.* 7, 349–355 (2005).
 52. Dlugokencky, E. J., Nisbet, E. G., Fisher, R. & Lowry, D. Global atmospheric methane: Budget, changes and dangers. *Philos. Trans. R. Soc. A Math. Phys. Eng. Sci.* 369, 2058–2072 (2011).
 53. Domagal-Goldman, S. D., Meadows, V. S., Claire, M. W. & Kasting, J. F. Using biogenic sulfur gases as remotely detectable biosignatures on anoxic planets. *Astrobiology* 11, 419–441 (2011).
 54. Dong, Y. et al. Anthropogenic emissions and distribution of ammonia over the Yangtze River Delta. *Huanjing Kexue Xuebao / Acta Sci. Circumstantiae* 29, 1611–1617 (2009).
 55. Earnshaw, A. & Greenwood, N. N. *Chemistry of the Elements*. vol. 60 (Butterworth-Heinemann Oxford, 1997).
 56. Elderfield, H. & Schultz, A. Mid-ocean ridge hydrothermal fluxes and the chemical composition of the ocean. *Annu. Rev. Earth Planet. Sci.* 24, 191–224 (1996).
 57. Elkins-Tanton, L. T. & Seager, S. Ranges of atmospheric mass and composition of super-Earth exoplanets. *Astrophys. J.* 685, 1237 (2008).
 58. Enell, M. & Wennberg, L. Distribution of halogenated organic compounds (AOX)–Swedish transport to surrounding sea areas and mass balance studies in five drainage systems. *Water Sci. Technol.* 24, 385–395 (1991).
 59. Engvild, K. C. The chloroindole auxins of pea, strong plant growth hormones or endogenous herbicides. (1994).
 60. Erickson III, D. J. & Duce, R. A. On the global flux of atmospheric sea salt. *J. Geophys. Res. Ocean.* 93, 14079–14088 (1988).

61. Eriksson, E. The yearly circulation of chloride and sulfur in nature; meteorological, geochemical and pedological implications. Part II. *Tellus* 12, 64–109 (1960).
62. Falkowski, P. et al. The global carbon cycle: a test of our knowledge of earth as a system. *Science* (80-.). 290, 291–296 (2000).
63. Fall, R. & Benson, A. A. Leaf methanol—the simplest natural product from plants. *Trends Plant Sci.* 1, 296–301 (1996).
64. Fauchez, T. J. et al. Impact of clouds and hazes on the simulated JWST transmission spectra of habitable zone planets in the TRAPPIST-1 system. *Astrophys. J.* 887, 194 (2019).
65. Feth, J. H. Chloride in natural continental water; a review. (1981).
66. Fleischmann, E. M. The measurement and penetration of ultraviolet radiation into tropical marine water. *Limnol. Oceanogr.* 34, 1623–1629 (1989).
67. France, K. et al. the Muscles Treasury Survey. I. Motivation and Overview. *Astrophys. J.* 820, 89 (2016).
68. Frank, H. Airborne chlorocarbons, photooxidants, and forest decline. *Ambio* 13–18 (1991).
69. Freeze, R. A. & Cherry, J. A. *Groundwater.* (1979).
70. Gaillard, F. et al. The Diverse Planetary Ingassing/Outgassing Paths Produced over Billions of Years of Magmatic Activity. *Space Sci. Rev.* 217, 1–54 (2021).
71. Gaillard, F. & Scaillet, B. A theoretical framework for volcanic degassing chemistry in a comparative planetology perspective and implications for planetary atmospheres. *Earth Planet. Sci. Lett.* 403, 307–316 (2014).
72. Galbally, I. E. & Kirstine, W. The production of methanol by flowering plants and the global cycle of methanol. *J. Atmos. Chem.* 43, 195–229 (2002).
73. Galloway, J. N. The Global Nitrogen Cycle. *Treatise on Geochemistry* 8–9, 557–583 (2003).
74. Galvez, M. E., Fischer, W. W., Jaccard, S. L. & Eglinton, T. I. Materials and pathways of the organic carbon cycle through time. *Nat. Geosci.* 13, 535–546 (2020).
75. Gamsjäger, H., Lorimer, J. W., Salomon, M., Shaw, D. G. & Tomkins, R. P. T. The IUPAC-NIST solubility data series: A guide to preparation and use of compilations and evaluations. *J. Phys. Chem. Ref. data* 39, 23101 (2010).
76. Gamsjäger, H., Lorimer, J. W., Scharlin, P. & Shaw, D. G. Glossary of terms related to solubility (IUPAC Recommendations 2008). *Pure Appl. Chem.* 80, 233–276 (2008).
77. Gaudi, B. S. et al. The Habitable Exoplanet Observatory (HabEx) Mission Concept Study Interim Report. *arXiv Prepr. arXiv1809.09674* (2018).
78. Ge, S. et al. Abundant NH₃ in China Enhances Atmospheric HONO Production by Promoting the Heterogeneous Reaction of SO₂ with NO₂. *Environ. Sci. Technol.* 53, 14339–14347 (2019).
79. Giorgi, F. & Chameides, W. L. The rainout parameterization in a photochemical model. *J. Geophysical Res.* 90, 7872–7880 (1985).
80. Gleick, P. H. *Water in crisis.* Pacific Inst. Stud. Dev., Environ. Secur. Stock. Env. Institute, Oxford Univ. Press. 473p 9, 761–1051 (1993).
81. Glindemann, D., De Graaf, R. M. & Schwartz, A. W. Chemical reduction of phosphate on the primitive Earth. *Orig. Life Evol. Biosph.* 29, 555–561 (1999).
82. Glindemann, D., Edwards, M. & Schrems, O. Phosphine and methylphosphine production by simulated lightning - A study for the volatile phosphorus cycle and cloud formation in the earth atmosphere. *Atmos. Environ.* 38, 6867–6874 (2004).
83. Goldblatt, C., Lenton, T. M. & Watson, A. J. Bistability of atmospheric oxygen and the

- Great Oxidation. *Nature* 443, 683–686 (2006).
84. Gordon, I. E. et al. The HITRAN2016 molecular spectroscopic database. *J. Quant. Spectrosc. Radiat. Transf.* 203, 3–69 (2017).
85. Graedel, T. E. & Keene, W. C. Tropospheric budget of reactive chlorine. *Global Biogeochem. Cycles* 9, 47–77 (1995).
86. Graedel, T. E. & Crutzen, P. J. *Atmospheric change: an earth system perspective*. (1993).
87. Graedel, T. E. & Keene, W. C. The budget and cycle of Earth's natural chlorine. *Pure Appl. Chem.* 68, 1689–1697 (1996).
88. Greaves, J. S. et al. Phosphine gas in the cloud decks of Venus. *Nat. Astron.* (2020) doi:10.1038/s41550-020-1174-4.
89. Gregory, B. S., Claire, M. W. & Rugheimer, S. Photochemical modelling of atmospheric oxygen levels confirms two stable states. *Earth Planet. Sci. Lett.* 561, 116818 (2021).
90. Gribble, G. W. *Naturally occurring organohalogen compounds—a comprehensive update*. vol. 91 (Springer Science & Business Media, 2009).
91. Gribble, G. W. *Naturally occurring organohalogen compounds—a survey*. *J. Nat. Prod.* 55, 1353–1395 (1992).
92. Grimvall, A., Boren, H., Jonsson, S., Karlsson, S. & Sävenhed, R. Organohalogens of natural and industrial origin in large recipients of bleach-plant effluents. *Water Sci. Technol.* 24, 373–383 (1991).
93. Grimvall, A. & De Leer, E. W. B. *Naturally-produced organohalogens*. vol. 1 (Springer Science & Business Media, 1995).
94. Guenther, A. et al. Estimates of global terrestrial isoprene emissions using MEGAN (Model of Emissions of Gases and Aerosols from Nature). *Atmos. Chem. Phys.* 6, 3181–3210 (2006).
95. Guenther, A. et al. A global model of natural volatile organic compound emissions. *J. Geophys. Res. Atmos.* 100, 8873–8892 (1995).
96. Gustavsson, M. et al. Organic matter chlorination rates in different boreal soils: the role of soil organic matter content. *Environ. Sci. Technol.* 46, 1504–1510 (2012).
97. Guzmán-Marmolejo, A. & Segura, A. Methane in the solar system. *Boletín la Soc. Geológica Mex.* 67, 377–385 (2015).
98. Hägele, J., Lorenz, K., Rhäsa, D. & Zellner, R. Rate constants and CH₃O product yield of the reaction OH+ CH₃OH→ products. *Berichte der Bunsengesellschaft für Phys. Chemie* 87, 1023–1026 (1983).
99. Häggblom, M. M. Microbial breakdown of halogenated aromatic pesticides and related compounds. *FEMS Microbiol. Rev.* 9, 29–71 (1992).
100. Han, D. et al. Volatile organic compounds (VOCs) during non-haze and haze days in Shanghai: characterization and secondary organic aerosol (SOA) formation. *Environ. Sci. Pollut. Res.* 24, 18619–18629 (2017).
101. Hanson, R. S. & Hanson, T. E. Methanotrophic bacteria. *Microbiol. Rev.* 60, 439–471 (1996).
102. Hardman, D. J. Biotransformation of halogenated compounds. *Crit. Rev. Biotechnol.* 11, 1–40 (1991).
103. Harrison, J. J., Allen, N. D. C. & Bernath, P. F. Infrared absorption cross sections for methanol. *J. Quant. Spectrosc. Radiat. Transf.* 113, 2189–2196 (2012).
104. Hawtof, R. et al. Catalyst-free, highly selective synthesis of ammonia from nitrogen

- and water by a plasma electrolytic system. *Asian J. Chem.* 31, eaat5778 (2019).
105. He, C. et al. Haze formation in warm H₂-rich exoplanet atmospheres. *arXiv* 1–8 (2020) doi:10.3847/psj/abb1a4.
106. He, J., Rakov, V., Wang, D. & Wang, P. K. Lightning physics and effects. *Atmospheric Research* vols 129–130 (Cambridge University Press, 2013).
107. Heikes, B. G. et al. Atmospheric methanol budget and ocean implication. *Global Biogeochem. Cycles* 16, 80–81 (2002).
108. Hess, W. P. & Tully, F. P. Hydrogen-atom abstraction from methanol by hydroxyl radical. *J. Phys. Chem.* 93, 1944–1947 (1989).
109. Hoffman, M. D. & Gelman, A. The No-U-Turn sampler: adaptively setting path lengths in Hamiltonian Monte Carlo. *J. Mach. Learn. Res.* 15, 1593–1623 (2014).
110. Holleman, A. F. *Lehrbuch der anorganischen Chemie.* (Walter de Gruyter GmbH & Co KG, 2019).
111. Holloway, J. A. M. & Dahlgren, R. A. Nitrogen in rock: Occurrences and biogeochemical implications. *Global Biogeochem. Cycles* 16, 65-1-65–17 (2002).
112. Hong, C. C. & Rapson, W. H. Kinetics of disproportionation of chlorous acid. *Can. J. Chem.* 46, 2053–2060 (1968).
113. Horvath, A. K., Nagypal, I., Peintler, G., Epstein, I. R. & Kustin, K. Kinetics and mechanism of the decomposition of chlorous acid. *J. Phys. Chem. A* 107, 6966–6973 (2003).
114. HOU, X. & YU, X. An ammonia emissions inventory for agricultural sources in Hefei, China. *Atmos. Ocean. Sci. Lett.* 13, 260–267 (2020).
115. Hu, L. et al. Sources and seasonality of atmospheric methanol based on tall tower measurements in the US Upper Midwest. *Atmos. Chem. Phys.* 11, 11145–11156 (2011).
116. Hu, R. & Seager, S. Photochemistry in terrestrial exoplanet atmospheres. III. Photochemistry and thermochemistry in thick atmospheres on super earths and mini neptunes. *Astrophys. J.* 784, 63 (2014).
117. Hu, R., Seager, S. & Bains, W. Photochemistry in terrestrial exoplanet atmospheres. I. Photochemistry model and benchmark cases. *Astrophys. J.* 761, (2012).
118. Hu, R., Seager, S. & Bains, W. Photochemistry in terrestrial exoplanet atmospheres. II. H₂S and SO₂ photochemistry in anoxic atmospheres. *Astrophys. J.* 769, 166 (2013).
119. Huang, J., Seager, S., Petkowski, J. J., Ranjan, S. & Zhan, Z. Assessment of Ammonia as a Biosignature Gas in Exoplanet Atmospheres. *Astrobiology* 22, 171–191 (2022).
120. Hui, L. et al. VOC characteristics, sources and contributions to SOA formation during haze events in Wuhan, Central China. *Sci. Total Environ.* 650, 2624–2639 (2019).
121. Jacob, D. J. Chemistry of OH in remote clouds and its role in the production of formic acid and peroxy monosulfate. *J. Geophys. Res. Atmos.* 91, 9807–9826 (1986).
122. Jaeger, L. Monthly and areal patterns of mean global precipitation. in *Variations in the global water budget* 129–140 (Springer, 1983).
123. Jeans, J. *The universe around us.* (1930).
124. Jetten, M. S. M. et al. Biochemistry and molecular biology of anammox bacteria biochemistry and molecular biology of anammox bacteria M.S.M. Jetten et al. *Crit. Rev. Biochem. Mol. Biol.* 44, 65–84 (2009).
125. Jiménez, E., Gilles, M. K. & Ravishankara, A. R. Kinetics of the reactions of the hydroxyl radical with CH₃OH and C₂H₅OH between 235 and 360 K. *J. Photochem. Photobiol. A Chem.* 157, 237–245 (2003).
126. Johns, M. et al. Giant Magellan Telescope: overview. in *Ground-based and Airborne*

- Telescopes IV vol. 8444 84441H (International Society for Optics and Photonics, 2012).
127. Johnson, B. & Goldblatt, C. The nitrogen budget of Earth. *Earth-Science Rev.* 148, 150–173 (2015).
128. Jonsson, P. Large-scale changes of contaminants in Baltic Sea sediments during the twentieth century. (1994).
129. Kaltenecker, L., Traub, W. A. & Jucks, K. W. Spectral Evolution of an Earth-like Planet. *Astrophys. J.* 658, 598–616 (2007).
130. Karl, T. et al. Exchange processes of volatile organic compounds above a tropical rain forest: Implications for modeling tropospheric chemistry above dense vegetation. *J. Geophys. Res. Atmos.* 109, (2004).
131. Kartal, B., Keltjens, J. T. & Jetten, M. S. M. Metabolism and Genomics of Anammox Bacteria. *Nitrification* 179–200 (2014) doi:10.1128/9781555817145.ch8.
132. Kartal, B. et al. Molecular mechanism of anaerobic ammonium oxidation. *Nature* 479, 127–130 (2011).
133. Kasting, J. F. Stability of ammonia in the primitive terrestrial atmosphere. *J. Geophys. Res. Ocean.* 87, 3091–3098 (1982).
134. Kasting, J. F. Atmospheric composition of Hadean–early Archean Earth: The importance of CO. *Geol. Soc. Am. Spec. Pap.* 504, 19–28 (2014).
135. Kasting, J. F. Runaway and moist greenhouse atmospheres and the evolution of Earth and Venus. *Icarus* 74, 472–494 (1988).
136. Kasting, J. F. Bolide impacts and the oxidation state of carbon in the Earth’s early atmosphere. *Orig. Life Evol. Biosph.* 20, 199–231 (1990).
137. Keene, W. C. et al. The geochemical cycling of reactive chlorine through the marine troposphere. *Global Biogeochem. Cycles* 4, 407–430 (1990).
138. KELLER, M. AOX-Belastung von Oberflächengewässern im Jahr 1987. *Vom Wasser* 72, 199–210 (1989).
139. Kiene, R. P. Microbial sources and sinks for methylated sulfur compounds in the marine environment. *Microb. growth C1 Compd.* 7, 15–33 (1993).
140. Kochanov, R. V et al. HITRAN Application Programming Interface (HAPI): A comprehensive approach to working with spectroscopic data. *J. Quant. Spectrosc. Radiat. Transf.* 177, 15–30 (2016).
141. Korhonen, H., Carslaw, K. S., Spracklen, D. V., Mann, G. W. & Woodhouse, M. T. Influence of oceanic dimethyl sulfide emissions on cloud condensation nuclei concentrations and seasonality over the remote Southern Hemisphere oceans: A global model study. *J. Geophys. Res. Atmos.* 113, (2008).
142. Körner, E., von Dahl, C. C., Bonaventure, G. & Baldwin, I. T. Pectin methylesterase Na PME1 contributes to the emission of methanol during insect herbivory and to the elicitation of defence responses in *Nicotiana attenuata*. *J. Exp. Bot.* 60, 2631–2640 (2009).
143. Kotrlý, S. & Sucha, L. Handbook of chemical equilibria in analytical chemistry. (1985).
144. Kraft, B., Strous, M. & Tegetmeyer, H. E. Microbial nitrate respiration - Genes, enzymes and environmental distribution. *J. Biotechnol.* 155, 104–117 (2011).
145. Kuhn, W. UNTERSUCHUNGEN ZUR BESTIMMUNG DES ORGANISCH GEBUNDENEN CHLORS MIT HILFE EINES NEUARTIGEN ANREICHERUNGSVERFAHRENS. (1977).
146. Kuypers, M. M. M., Marchant, H. K. & Kartal, B. The microbial nitrogen-cycling network. *Nat. Rev. Microbiol.* 16, 263 (2018).

147. Lam, P. & Kuypers, M. M. M. Microbial Nitrogen Cycling Processes in Oxygen Minimum Zones. *Ann. Rev. Mar. Sci.* 3, 317–345 (2011).
148. Lamarque, J. F. et al. Global and regional evolution of short-lived radiatively-active gases and aerosols in the Representative Concentration Pathways. *Clim. Change* 109, 191–212 (2011).
149. Laniewski, K., Borén, H., Grimvall, A., Jonsson, S. & Sydow, L. von. Chemical characterisation of adsorbable organic halogens (AOX) in precipitation. in *Naturally-Produced Organohalogenes* 113–129 (Springer, 1995).
150. Léger, A. et al. Could we search for primitive life on extrasolar planets in the near future? *Icarus* 123, 249–255 (1996).
151. Lehninger, A. L., Nelson, D. L. & Cox, M. M. Integration and hormonal regulation of mammalian metabolism. *Princ. Biochem.* 2nd ed. Worth Publ. New York, NY 736–787 (1993).
152. Lide, D. R. CRC handbook of chemistry and physics, internet version 2005. (2005).
153. Lin, Z., Seager, S., Ranjan, S., Kozakis, T. & Kaltenecker, L. H₂-dominated Atmosphere as an Indicator of Second-generation Rocky White Dwarf Exoplanets. *Astrophys. J. Lett.* 925, L10 (2022).
154. Lincowski, A. P. et al. Evolved Climates and Observational Discriminants for the TRAPPIST-1 Planetary System. *Astrophys. J.* 867, 76 (2018).
155. Liu, L. et al. Unexpected quenching effect on new particle formation from the atmospheric reaction of methanol with SO₃. *Proc. Natl. Acad. Sci.* 116, 24966–24971 (2019).
156. Liu, M. et al. Ammonia emission control in China would mitigate haze pollution and nitrogen deposition, but worsen acid rain. *Proc. Natl. Acad. Sci. U. S. A.* 116, 7760–7765 (2019).
157. Loftus, K., Wordsworth, R. D. & Morley, C. V. Sulfate Aerosol Hazes and SO₂ Gas as Constraints on Rocky Exoplanets' Surface Liquid Water. *arXiv* 887, 231 (2019).
158. Lustig-Yaeger, J., Meadows, V. S. & Lincowski, A. P. The detectability and characterization of the TRAPPIST-1 exoplanet atmospheres with JWST. *Astron. J.* 158, 27 (2019).
159. Lvovitch, M. I. The global water balance. *Eos, Trans. Am. Geophys. Union* 54, 28–53 (1973).
160. Madhusudhan, N. & Seager, S. A temperature and abundance retrieval method for exoplanet atmospheres. *Astrophys. J.* 707, 24 (2009).
161. Manabe, S. & Wetherald, R. T. Thermal Equilibrium of the Atmosphere with a Given Distribution of Relative Humidity. *J. Atmos. Sci.* 24, 241–259 (1967).
162. Mancinelli, R. L. & McKay, C. P. The evolution of nitrogen cycling. *Orig. Life Evol. Biosph.* 18, 311–325 (1988).
163. Manion, J. A. et al. NIST Chemical Kinetics Database, NIST Standard Reference Database 17, Version 7.0 (Web Version), Release 1.6. 8, Data version 2015.09, National Institute of Standards and Technology, Gaithersburg, Maryland, 20899-8320. Web address <http://kinetics.nist.gov> (2015).
164. Mao, H., Talbot, R., Nielsen, C. & Sive, B. Controls on methanol and acetone in marine and continental atmospheres. *Geophys. Res. Lett.* 33, (2006).
165. Marchant, H. K., Lavik, G., Holtappels, M. & Kuypers, M. M. M. The fate of nitrate in intertidal permeable sediments. *PLoS One* 9, e104517 (2014).
166. Marschner, H. Marschner's mineral nutrition of higher plants. (Academic press, 2011).

167. Martens, C. S., Wesolowski, J. J., Harriss, R. C. & Kaifer, R. Chlorine loss from Puerto Rican and San Francisco Bay area marine aerosols. *J. Geophys. Res.* 78, 8778–8792 (1973).
168. Martin, R. S., Mather, T. A. & Pyle, D. M. Volcanic emissions and the early Earth atmosphere. *Geochim. Cosmochim. Acta* 71, 3673–3685 (2007).
169. Mather, T. A. et al. Nitric acid from volcanoes. *Earth Planet. Sci. Lett.* 218, 17–30 (2004).
170. McCarren, J. et al. Microbial community transcriptomes reveal microbes and metabolic pathways associated with dissolved organic matter turnover in the sea. *Proc. Natl. Acad. Sci.* 107, 16420–16427 (2010).
171. McCormick, M. P., Thomason, L. W. & Trepte, C. R. Atmospheric effects of the Mt Pinatubo eruption. *Nature* 373, 399–404 (1995).
172. McDermott, J. M., Sylva, S. P., Ono, S., German, C. R. & Seewald, J. S. Geochemistry of fluids from Earth’s deepest ridge-crest hot-springs: Piccard hydrothermal field, Mid-Cayman Rise. *Geochim. Cosmochim. Acta* 228, 95–118 (2018).
173. McKenzie, L. M., Hao, W. M., Richards, G. N. & Ward, D. E. Measurement and modeling of air toxins from smoldering combustion of biomass. *Environ. Sci. Technol.* 29, 2047–2054 (1995).
174. McKenzie, L. M., Ward, D. E. & Hao, W. M. Chlorine and bromine in the biomass of tropical and temperate ecosystems. *Biomass Burn. Glob. Chang.* 1, 241–248 (1996).
175. Meadows, V. S. et al. Exoplanet Biosignatures: Understanding Oxygen as a Biosignature in the Context of Its Environment. *Astrobiology* 18, 630–662 (2018).
176. Mikhail, S., Barry, P. H. & Sverjensky, D. A. The relationship between mantle pH and the deep nitrogen cycle. *Geochim. Cosmochim. Acta* 209, 149–160 (2017).
177. Mikhail, S. & Sverjensky, D. A. Nitrogen speciation in upper mantle fluids and the origin of Earth’s nitrogen-rich atmosphere. *Nat. Geosci.* 7, 816–819 (2014).
178. Millet, D. B. et al. New constraints on terrestrial and oceanic sources of atmospheric methanol. *Atmos. Chem. Phys.* 8, 6887–6905 (2008).
179. Misra, A., Meadows, V. & Crisp, D. The effects of refraction on transit transmission spectroscopy: application to Earth-like exoplanets. *Astrophys. J.* 792, 61 (2014).
180. Möller, D. M. Chemistry of the climate system. *Chemistry of the Climate System* (Walter de Gruyter GmbH & Co KG, 2014). doi:10.1515/9783110331943.
181. Moran, S. E. et al. Chemistry of temperate super-Earth and mini-Neptune atmospheric hazes from laboratory experiments. *Planet. Sci. J.* 1, 17 (2020).
182. Morgan, J. W. & Anders, E. Chemical composition of earth, Venus, and Mercury. *Proc. Natl. Acad. Sci.* 77, 6973–6977 (1980).
183. Moss, R. H. et al. The next generation of scenarios for climate change research and assessment. *Nature* 463, 747–756 (2010).
184. Mu, H., Ewald, G., Nilsson, E., Sundin, P. & Wesén, C. Fate of chlorinated fatty acids in migrating sockeye salmon and their transfer to arctic grayling. *Environ. Sci. Technol.* 38, 5548–5554 (2004).
185. Navarro-González, R., McKay, C. P. & Mvondo, D. N. A possible nitrogen crisis for Archaean life due to reduced nitrogen fixation by lightning. *Nature* 412, 61–64 (2001).
186. Neal, R. M. MCMC using Hamiltonian dynamics. *Handb. markov Chain monte carlo* 2, 2 (2011).
187. Nee, J. B., Suto, M. & Lee, L. C. Photoexcitation processes of CH₃OH: Rydberg states and photofragment fluorescence. *Chem. Phys.* 98, 147–155 (1985).

188. Neilson, A. H. The biodegradation of halogenated organic compounds. *J. Appl. Bacteriol.* 69, 445–470 (1990).
189. Neufeld, J. D. et al. Stable-isotope probing implicates *Methylophaga* spp and novel Gammaproteobacteria in marine methanol and methylamine metabolism. *ISME J.* 1, 480–491 (2007).
190. Nguyen, D. A., Iwaniw, M. A. & Fogler, H. S. Kinetics and mechanism of the reaction between ammonium and nitrite ions: Experimental and theoretical studies. *Chem. Eng. Sci.* 58, 4351–4362 (2003).
191. Ni, Y. & Yin, G. Disproportionation of chlorous acid at a strong acidity. *Ind. Eng. Chem. Res.* 37, 2367–2372 (1998).
192. Nielsen, L. S. & Bilde, M. Exploring controlling factors for sea spray aerosol production: temperature, inorganic ions and organic surfactants. *Tellus B Chem. Phys. Meteorol.* 72, 1–10 (2020).
193. Öberg, G. The natural chlorine cycle—fitting the scattered pieces. *Appl. Microbiol. Biotechnol.* 58, 565–581 (2002).
194. Öberg, G., Holm, M., Sandén, P., Svensson, T. & Parikka, M. The role of organic-matter-bound chlorine in the chlorine cycle: a case study of the Stubbetorp catchment, Sweden. *Biogeochemistry* 75, 241–269 (2005).
195. Olivier, J. G. J., Bouwman, A. F., Van Der Hoek, K. W. & Berdowski, J. J. M. Global air emission inventories for anthropogenic sources of NO(x), NH₃ and N₂O in 1990. *Environ. Pollut.* 102, 135–148 (1998).
196. Owen, J. E., Shaikhislamov, I. F., Lammer, H., Fossati, L. & Khodachenko, M. L. Hydrogen dominated atmospheres on terrestrial mass planets: evidence, origin and evolution. *Space Sci. Rev.* 216, 1–24 (2020).
197. P, D. *CRC Handbook of Chemistry and Physics. Journal of Molecular Structure* vol. 268 (CRC press, 1992).
198. P. Loyd, R. O. et al. The MUSCLES Treasury Survey. III. X-ray to infrared spectra of 11 M and K stars hosting planets. *Astrophys. J.* 824, 102 (2016).
199. Perrin, D. D. Dissociation constants of inorganic acids and bases in aqueous solution. *Pure Appl. Chem.* 20, 133–236 (1969).
200. Plyler, E. K. Infrared spectra of methanol, ethanol, and n-propanol. *J. Res. Natl. Bur. Stand* 48, 281–286 (1952).
201. Pöykiö, R., Nurmesniemi, H. & Kivilinna, V.-A. EOX concentrations in sediment in the part of the Bothnian Bay affected by effluents from the pulp and paper mills at Kemi, Northern Finland. *Environ. Monit. Assess.* 139, 183–194 (2008).
202. Preisler, A. et al. Biological and chemical sulfide oxidation in a Beggiatoa inhabited marine sediment. *ISME J.* 1, 341–353 (2007).
203. Rakov, V. A. & Uman, M. A. *Lightning: physics and effects.* (Cambridge university press, 2003).
204. Ranjan, S. et al. Photochemistry of anoxic abiotic habitable planet atmospheres: impact of new H₂O cross-sections. *arXiv* (2020) doi:10.3847/1538-4357/ab9363.
205. Ranjan, S. et al. Photochemical Runaway in Exoplanet Atmospheres: Implications for Biosignatures. *Nat. Astron.* (2022).
206. Ranjan, S., Todd, Z. R., Rimmer, P. B., Sasselov, D. D. & Babbin, A. R. Nitrogen oxide concentrations in natural waters on early earth. *arXiv* 20, 2021–2039 (2019).
207. Ranjan, S., Wordsworth, R. & Sasselov, D. D. The surface UV environment on planets orbiting M dwarfs: implications for prebiotic chemistry and the need for experimental

- follow-up. *Astrophys. J.* 843, 110 (2017).
208. Rascio, N. & La Rocca, N. Biological nitrogen fixation. *Encycl. Ecol.* 264–279 (2018) doi:10.1016/B978-0-444-63768-0.00685-5.
209. Redon, P.-O. et al. Chloride and organic chlorine in forest soils: storage, residence times, and influence of ecological conditions. *Environ. Sci. Technol.* 45, 7202–7208 (2011).
210. Redon, P.-O., Jolivet, C., Saby, N., Abdelouas, A. & Thiry, Y. Occurrence of natural organic chlorine in soils for different land uses. *Biogeochemistry* 114, 413–419 (2013).
211. Reimann, S., Grob, K. & Frank, H. Chloroacetic acids in rainwater. *Environ. Sci. Technol.* 30, 2340–2344 (1996).
212. Ridgway, J., Appleton, J. D. & Levinson, A. A. Ammonium geochemistry in mineral exploration—a comparison of results from the American cordilleras and the southwest Pacific. *Appl. Geochemistry* 5, 475–489 (1990).
213. Ringwood, A. E. *Origin of the Earth and Moon*. New York Springer-Verlag (1979).
214. Roberge, A., Fischer, D. & Peterson, B. The Large UV/Optical/Infrared Surveyor (LUVOIR): Telling the Story of Life in the Universe. *Baas* 51, 199 (2019).
215. Rugheimer, S. & Kaltenegger, L. Spectra of Earth-like planets through geological evolution around FGKM stars. *Astrophys. J.* 854, 19 (2018).
216. Sagan, C. & Chyba, C. The early faint sun paradox: Organic shielding of ultraviolet-labile greenhouse gases. *Science* (80-.). 276, 1217–1221 (1997).
217. Sander, R. Compilation of Henry’s law constants (version 4.0) for water as solvent. *Atmos. Chem. Phys.* 15, 4399–4981 (2015).
218. Scarratt, M. G. & Moore, R. M. Production of methyl bromide and methyl chloride in laboratory cultures of marine phytoplankton II. *Mar. Chem.* 59, 311–320 (1998).
219. Schaefer, L. & Fegley, B. Atmospheric composition of Hadean-early Archean Earth: The importance of CO: Comment. *Spec. Pap. Geol. Soc. Am.* 504, 29–31 (2014).
220. Schimel, J. P. & Bennett, J. Nitrogen mineralization: Challenges of a changing paradigm. *Ecology* 85, 591–602 (2004).
221. Schlesinger, W. H. & Hartley, A. E. A global budget for atmospheric NH₃. *Biogeochemistry* 15, 191–211 (1992).
222. Schlesinger, W. H. & Bernhardt, E. S. *Biogeochemistry: an analysis of global change*. (Academic press, 2013).
223. Schrauzer, G. N., Strampach, N., Hui, L. N., Palmer, M. R. & Salehi, J. Nitrogen photoreduction on desert sands under sterile conditions. *Proc. Natl. Acad. Sci.* 80, 3873–3876 (1983).
224. Seager, S., Bains, W. & Hu, R. Biosignature gases in H₂-Dominated atmospheres on rocky exoplanets. *Astrophys. J.* 777, (2013).
225. Seager, S., Bains, W. & Petkowski, J. J. Toward a List of Molecules as Potential Biosignature Gases for the Search for Life on Exoplanets and Applications to Terrestrial Biochemistry. *Astrobiology* 16, 465–485 (2016).
226. Seager, S., Huang, J., Petkowski, J. J. & Pajusalu, M. Laboratory studies on the viability of life in H₂-dominated exoplanet atmospheres. *Nat. Astron.* 4, 802–806 (2020).
227. Seager, S., Bains, W. & Hu, R. A biomass-based model to estimate the plausibility of exoplanet biosignature gases. *Astrophys. J.* 775, 104 (2013).
228. Seager, S. et al. The Venusian lower atmosphere haze as a depot for desiccated microbial life: a proposed life cycle for persistence of the venusian aerial biosphere. *Astrobiology* (2020).
229. Seager, S., Schrenk, M. & Bains, W. An astrophysical view of Earth-based metabolic

- biosignature gases. *Astrobiology* 12, 61–82 (2012).
230. Segura, A. et al. Biosignatures from Earth-like planets around M dwarfs. *Astrobiology* 5, 706–725 (2005).
231. Seinfeld, J. & Pandis, S. *Atmospheric Chemistry and Physics*. 1997. New York (2008).
232. Sharp, Z. D. & Draper, D. S. The chlorine abundance of Earth: implications for a habitable planet. *Earth Planet. Sci. Lett.* 369, 71–77 (2013).
233. Sheng, J. et al. Characterizing the level, photochemical reactivity, emission, and source contribution of the volatile organic compounds based on PTR-TOF-MS during winter haze period in Beijing, China. *Atmos. Res.* 212, 54–63 (2018).
234. Shi, Q., Davidovits, P., Jayne, J. T., Worsnop, D. R. & Kolb, C. E. Uptake of gas-phase ammonia. 1: Uptake by aqueous surfaces as a function of pH. *J. Phys. Chem. A* 103, 8812–8823 (1999).
235. Sigurdsson, H., Houghton, B., McNutt, S., Rymer, H. & Stix, J. *The Encyclopedia of Volcanoes*. The Encyclopedia of Volcanoes (Elsevier, 2015). doi:10.1016/c2015-0-00175-7.
236. Siivola, J. & Schmid, R. Recommendations by the IUGS Subcommittee on the Systematics of Metamorphic Rocks: List of mineral abbreviations. Web version 01.02. 07. (2007).
237. Singh, H. B. et al. Analysis of the atmospheric distribution, sources, and sinks of oxygenated volatile organic chemicals based on measurements over the Pacific during TRACE-P. *J. Geophys. Res. Atmos.* 109, (2004).
238. Skidmore, W. Thirty Meter Telescope Detailed Science Case: 2015. *Res. Astron. Astrophys.* 15, 1945–2140 (2015).
239. Smirnov, A., Hausner, D., Laffers, R., Strongin, D. R. & Schoonen, M. A. A. Abiotic ammonium formation in the presence of Ni-Fe metals and alloys and its implications for the Hadean nitrogen cycle. *Geochem. Trans.* 9, 1–20 (2008).
240. Smith, R. A., Alexander, R. B. & Wolman, M. G. Water-quality trends in the nation's rivers. *Science* (80-.). 235, 1607–1615 (1987).
241. Söderlund, R. & Svensson, B. H. The Global Nitrogen Cycle. *Ecol. Bull.* 23–73 (1976).
242. Solomon, S. J., Custer, T., Schade, G., Soares Dias, A. P. & Burrows, J. Atmospheric methanol measurement using selective catalytic methanol to formaldehyde conversion. *Atmos. Chem. Phys.* 5, 2787–2796 (2005).
243. Sousa-Silva, C. et al. Phosphine as a biosignature gas in exoplanet atmospheres. *Astrobiology* 20, 235–268 (2019).
244. Stallard, R. F. & Edmond, J. M. Geochemistry of the Amazon: 1. Precipitation chemistry and the marine contribution to the dissolved load at the time of peak discharge. *J. Geophys. Res. Ocean.* 86, 9844–9858 (1981).
245. Stavrakou, T. et al. First space-based derivation of the global atmospheric methanol emission fluxes. *Atmos. Chem. Phys.* 11, 4873–4898 (2011).
246. Stevenson, D. P. *The Strengths of Chemical Bonds*. Journal of the American Chemical Society vol. 77 (Butterworths Scientific Publications, 1955).
247. Stief, P. et al. Dissimilatory nitrate reduction by *Aspergillus terreus* isolated from the seasonal oxygen minimum zone in the Arabian Sea. *BMC Microbiol.* 14, 35 (2014).
248. Stringer, R. & Johnston, P. *Chlorine and the environment: an overview of the chlorine industry*. (2001).
249. Strous, M. et al. Deciphering the evolution and metabolism of an anammox bacterium

- from a community genome. *Nature* 440, 790–794 (2006).
250. Stüeken, E. E., Buick, R., Guy, B. M. & Koehler, M. C. Isotopic evidence for biological nitrogen fixation by molybdenum-nitrogenase from 3.2 Gyr. *Nature* 520, 666–669 (2015).
251. Sugiyama, M., Stone, P. H. & Emanuel, K. A. The role of relative humidity in radiative-convective equilibrium. *J. Atmos. Sci.* 62, 2001–2011 (2005).
252. Sutton, M. A. et al. Towards a climate-dependent paradigm of ammonia emission and deposition. *Philos. Trans. R. Soc. B Biol. Sci.* 368, 20130166 (2013).
253. Svensson, T., Kylin, H., Montelius, M., Sandén, P. & Bastviken, D. Chlorine cycling and the fate of Cl in terrestrial environments. *Environ. Sci. Pollut. Res.* 28, 7691–7709 (2021).
254. Svensson, T., Lovett, G. M. & Likens, G. E. Is chloride a conservative ion in forest ecosystems? *Biogeochemistry* 107, 125–134 (2012).
255. Swap, R., Garstang, M., Greco, S., Talbot, R. & Kållberg, P. Saharan dust in the Amazon Basin. *Tellus B* 44, 133–149 (1992).
256. Symonds, R. B. WI Rose MH Reed. Contrib. Cl-and F-bearing gases to Atmos. by volcanoes, *Nat.* 334, 415–418 (1988).
257. Tabazadeh, A. & Turco, R. P. Stratospheric chlorine injection by volcanic eruptions: HCl scavenging and implications for ozone. *Science* (80-.). 260, 1082–1086 (1993).
258. Tagliabue, M., Grande, M., Perucchini, S., Bellettato, M. & Montanari, E. Removal of chlorinated pesticide contamination by soil washing with sole water. *SN Appl. Sci.* 2, 1–4 (2020).
259. Tait, V. K., Moore, R. M. & Tokarczyk, R. Measurements of methyl chloride in the northwest Atlantic. *J. Geophys. Res. Ocean.* 99, 7821–7833 (1994).
260. Talbot, R. W. et al. Distribution and geochemistry of aerosols in the tropical North Atlantic troposphere: Relationship to Saharan dust. *J. Geophys. Res. Atmos.* 91, 5173–5182 (1986).
261. Tamai, R. & Spyromilio, J. European Extremely Large Telescope: progress report. in *Ground-based and Airborne Telescopes V* vol. 9145 91451E (International Society for Optics and Photonics, 2014).
262. Tian, H. et al. Global methane and nitrous oxide emissions from terrestrial ecosystems due to multiple environmental changes. *Ecosyst. Heal. Sustain.* 1, 1–20 (2015).
263. Tie, X., Guenther, A. & Holland, E. Biogenic methanol and its impacts on tropospheric oxidants. *Geophys. Res. Lett.* 30, (2003).
264. Tjihuis, L., Van Loosdrecht, M. C. M. & Heijnen, J. J. A thermodynamically based correlation for maintenance gibbs energy requirements in aerobic and anaerobic chemotrophic growth. *Biotechnol. Bioeng.* 42, 509–519 (1993).
265. Tröjbom, M. & Grolander, S. Chemical conditions in present and future ecosystems in Forsmark-implications for selected radionuclides in the safety assessment SR-Site. (2010).
266. Trummal, A., Lipping, L., Kaljurand, I., Koppel, I. A. & Leito, I. Acidity of strong acids in water and dimethyl sulfoxide. *J. Phys. Chem. A* 120, 3663–3669 (2016).
267. Uematsu, M. et al. Enhancement of primary productivity in the western North Pacific caused by the eruption of the Miyake-jima volcano. *Geophys. Res. Lett.* 31, (2004).
268. Van Damme, M. et al. Industrial and agricultural ammonia point sources exposed. *Nature* 564, 99–103 (2018).
269. van Niftrik, L. & Jetten, M. S. M. Anaerobic Ammonium-Oxidizing Bacteria: Unique Microorganisms with Exceptional Properties. *Microbiol. Mol. Biol. Rev.* 76, 585–596

- (2012).
270. Vogt, H. et al. Chlorine Oxides and Chlorine Oxygen Acids. *Ullmann's Encyclopedia of Industrial Chemistry* (2010) doi:https://doi.org/10.1002/14356007.a06_483.pub2.
271. Vogt, R., Crutzen, P. J. & Sander, R. A mechanism for halogen release from sea-salt aerosol in the remote marine boundary layer. *Nature* 383, 327–330 (1996).
272. Walter, A., Caputi, L., O'Connor, S., van Pée, K.-H. & Ludwig-Müller, J. Chlorinated auxins—how does *Arabidopsis Thaliana* deal with them? *Int. J. Mol. Sci.* 21, 2567 (2020).
273. Wang, J. et al. Fast sulfate formation from oxidation of SO₂ by NO₂ and HONO observed in Beijing haze. *Nat. Commun.* 11, 1–7 (2020).
274. Warr, L. N. IMA–CNMNC approved mineral symbols. *Mineral. Mag.* 85, 291–320 (2021).
275. Wei, L. F. et al. Gas-to-particle conversion of atmospheric ammonia and sampling artifacts of ammonium in spring of Beijing. *Sci. China Earth Sci.* 58, 345–355 (2015).
276. Wei, W., Li, Y., Wang, Y., Cheng, S. & Wang, L. Characteristics of VOCs during haze and non-haze days in Beijing, China: Concentration, chemical degradation and regional transport impact. *Atmos. Environ.* 194, 134–145 (2018).
277. Wendeborn, S. The Chemistry, Biology, and Modulation of Ammonium Nitrification in Soil. *Angew. Chemie - Int. Ed.* 59, 2182–2202 (2020).
278. White, P. J. & Broadley, M. R. Chloride in soils and its uptake and movement within the plant: a review. *Ann. Bot.* 88, 967–988 (2001).
279. Wood, B. J., Pawley, A. & Frost, D. R. Water and carbon in the Earth's mantle. *Philos. Trans. R. Soc. London. Ser. A Math. Phys. Eng. Sci.* 354, 1495–1511 (1996).
280. Wordsworth, R. D. & Pierrehumbert, R. T. Water loss from terrestrial planets with CO₂-rich atmospheres. *Astrophys. J.* 778, 154 (2013).
281. Wordsworth, R. & Pierrehumbert, R. Abiotic Oxygen-dominated Atmospheres on Terrestrial Habitable Zone Planets. *Astrophys. J.* 785, L20 (2014).
282. Xue, Y. et al. Origin and transformation of ambient volatile organic compounds during a dust-to-haze episode in northwest China. *Atmos. Chem. Phys.* 20, 5425–5436 (2020).
283. Yang, C. et al. Progress in deaminase materials for reducing haze formation. *New Chem. Mater.* 44, 1–3 (2016).
284. Ye, X. et al. Important role of ammonia on haze formation in Shanghai. *Environ. Res. Lett.* 6, 24019 (2011).
285. Yeung, L. Y. et al. In Situ Quantification of Biological N₂ Production Using Naturally Occurring ¹⁵N/¹⁵N. *Environ. Sci. Technol.* 53, 5168–5175 (2019).
286. Yokouchi, Y., Takenaka, A., Miyazaki, Y., Kawamura, K. & Hiura, T. Emission of methyl chloride from a fern growing in subtropical, temperate, and cool-temperate climate zones. *J. Geophys. Res. G Biogeosciences* 120, 1142–1149 (2015).
287. Yurimoto, H., Kato, N. & Sakai, Y. Assimilation, dissimilation, and detoxification of formaldehyde, a central metabolic intermediate of methylotrophic metabolism. *Chem. Rec.* 5, 367–375 (2005).
288. Zahnle, K., Claire, M. & Catling, D. The loss of mass-independent fractionation in sulfur due to a Palaeoproterozoic collapse of atmospheric methane. *Geobiology* 4, 271–283 (2006).
289. Zahnle, K. J. Photochemistry of methane and the formation of hydrocyanic acid (HCN) in the Earth's early atmosphere. *J. Geophys. Res. Atmos.* 91, 2819–2834 (1986).
290. Zhan, Z., Huang, J., Seager, S., Petkowski, J. J. & Ranjan, S. Organic Carbonyls Are Poor Biosignature Gases in Exoplanet Atmospheres but May Generate Significant CO.

Astrophys. J. 930, 133 (2022).

291. Zhan, Z. et al. Assessment of Isoprene as a Possible Biosignature Gas in Exoplanets with Anoxic Atmospheres. *Astrobiology* (2021).

292. Zhu, L. et al. Sources and Impacts of Atmospheric NH₃: Current Understanding and Frontiers for Modeling, Measurements, and Remote Sensing in North America. *Curr. Pollut. Reports* 1, 95–116 (2015).